CONVECTIVE HEAT TRANSFER IN A MOVING BED WITH SPECIAL REFERENCE TO MELTING

by
William Roger Wilson
Department of Chemical Engineering

THESIS
660·465
WIL

A thesis submitted to
The University of Aston in Birmingham
for the degree of
Doctor of Philosophy

12 FEB 73 158538

September 1972

SUMMARY

Previous workers have been unable to correlate data on forced convection melting of metals or organic solids in packed beds in the accepted manner of heat transfer factor or Nusselt number against Reynolds number. It was recognised that melting in a tower furnace was restricted to a short zone at the bottom so, to simplify the problem, Akers[2] simulated the upper zone under moving bed conditions. His heat transfer coefficients and those of Norton[26] were as much as an order of magnitude less than those obtained by other workers using fixed beds. It was considered that this discrepancy had to be explained before proceeding to the analysis of melting beds. The present work has shown that it stemmed from two main causes: dislocations of the bed near the walls permitted bypassing of the fluid in the regions of high voidage; with long beds the terminal temperature differences tended to zero so measurement errors became unusually significant. By operation with vessel to particle diameter ratios not less than 13 and by selection of conditions to prevent small terminal differences, data have been obtained for 6, 9 and 12 mm diameter glass ballotini heated by air which are in close agreement with published fixed bed results. They are correlated by:

$$Nu = 0.183 \times Re^{0.834} \text{ for } 95 < Re < 1662.$$

A previous model of adiabatic moving bed heat transfer with intra-particle temperature distribution has been extended to the non-adiabatic case. A new digital computer approach to solution of the model has shown that a previous hybrid-analogue computer method was unstable. Digital numerical integration has been used for analysis of experimental results and for prediction of general parameters which will greatly simplify the design of moving beds.

ACKNOWLEDGEMENTS

Help was received in a variety of ways from many people during the period that this work was carried out but none of it would have been possible without the initial invitation from Professor G.V. Jeffreys to join the Chemical Engineering research school and the financial support of both the Science Research Council and the University of Aston in Birmingham.

I wish to express my sincere thanks to my supervisor Dr. B. Gay for his guidance and encouragement throughout. The value of the interest shown and assistance rendered by Professor G.V. Jeffreys, other members of the academic staff, fellow research students, clerical staff and Mr. N. Roberts and his technical staff should also not be underestimated.

Since leaving Aston a number of people have helped to overcome the problems of completing the work away from the university: my fiancée, my parents, Mr. P. Preece, Dr. B. Gay and particularly Mr. M.A. Slatter.

The endless encouragement of my parents throughout my life is probably the greatest single factor in the development of my academic and industrial career. Tribute must also be paid to my fiancée, Gillian, without whom the work might not have been completed on time. I am very grateful for their support, patience and understanding which was forthcoming even at times of extreme stress.

I am pleased that my present employers, Alcan International Limited: Banbury, have shown interest in the project and I trust that my thesis and experience will be of value to them. I wish to

thank the girls of the Typing Pool and Print Room at Banbury for the cheerful way in which they undertook the task of typing and duplicating the thesis in the short time available.

CONTENTS

Page

Page

SECTION 1

INTRODUCTION

SECTION 1 - INTRODUCTION

While the object of the present work was to obtain reliable data for the design of packed bed melting equipment, the results are likely to be applicable to a wide range of processes involving both fixed and moving beds with heat or mass transfer or both, with and without chemical reaction. The following list illustrates the scope.

MOVING BEDS

(1) Heat Transfer

Cooling of coal briquettes, lime, cement and magnesia after roasting; superheating steam, inert gases and corrosive materials; preheating air for high temperature combustion; preheating ferrous charges to arc furnaces; melting aluminium, copper, zinc, lead, antimony and steel prior to casting.

(2) Chemical Reaction

Roasting sodium bicarbonate to carbonate, gypsum to semi-hydrate, ammonium polyuranate to uranium dioxide and phosphate rock to phosphorus; reduction of uranium trioxide to dioxide with hydrogen; thermal and catalytic cracking of hydrocarbons and subsequent burning of carbon off the catalyst; calcination of limestone; producer gas and water gas generation; coal carbonization; high pressure gasification of coal; blast furnace reduction of iron, nickel and lead ores; mineral wool production; copper matte extraction from sulphide ores; coal briquetting.

(3) Mass Transfer

Absorption of hydrocarbon vapours and subsequent recovery;

separation of methane and hydrogen sulphide from hydrogen; drying.

FIXED BEDS

(1) Heat Transfer

Waste heat recovery in regenerators; cooling of nuclear reactor fuel elements; heating of helium and cesium mixtures to high temperatures for magneto-hydro-dynamic power generation.

(2) Chemical Reaction

Catalysis; nitric oxide formation.

(3) Mass Transfer

Absorption; chromatography; distillation; drying; leaching.

With such a wide range of application, fluid to particle heat transfer in packed beds is obviously worthy of further study.

SECTION 2

LITERATURE SURVEY

SECTION 2 - LITERATURE SURVEY

2.1 Melting Beds

2.1.1 Metallurgical aspects

Although Ross[1] provided the initial stimulus for the work at Aston[2], the industrial significance of melting in moving beds was demonstrated by work carried out in the British Gas Industry on non-ferrous metals.

Until the late 1950's there were three basic types of furnace suitable for melting non-ferrous metals, both scrap and ingot:

(1) Reverberatory

Originally solid fuel fired (either coke or anthracite) but by then usually by liquid or gaseous fuels.

(2) Crucible

Same fuels as reverberatory furnaces.

(3) Electric

Usually induction heated.

Induction furnaces offered thermal efficiencies of up to 80% compared with only 30% and 15% for reverberatory and crucible furnaces respectively[3]. However, fuel and capital costs favoured the latter two except where the charged metal was likely to suffer serious oxidation by combustion gases.

The thermal efficiencies with liquid and gaseous fuels in similar furnaces were not significantly different but the price differential between manufactured towns gas and oil was heavily weighted in favour of the latter. The same was true of other heating processes, both industrial and domestic. Not surprisingly,

the gas industry was continually losing ground. However, the introduction of the Lurgi process for the high pressure gasification of coal[4,5] and later the application of the I.C.I. synthesis gas process to towns gas production[6] provided contact with the chemical industry and demonstrated the great advantages of continuous, counter-current processing. This principle was soon applied to the problem of melting non-ferrous metals, particularly aluminium, in the hope that the lost customers could be regained.

The objective was the development of processes with higher melting rates than reverberatory and crucible furnaces for a given size and capital cost and operation at much higher thermal efficiencies. It was further hoped that the processes would overcome several other problems inherent in conventional furnaces:

(1) Metal Loss by Oxidation

The oxidation of copper can be reduced by substoichiometric operation of burners but this is not possible with aluminium as reaction with water vapour in the products of combustion also occurs:

$$4Al + 3O_2 \rightarrow 2Al_2O_3$$
$$2Al + 3H_2O \rightarrow Al_2O_3 + 3H_2$$

However, it was felt that oxidation could be minimised if time of contact with combustion gases was reduced and overheating of metal avoided.

(2) Hydrogen Pick-up

The solubility of hydrogen in molten aluminium increases rapidly with temperature[7] and on subsequent solidification, "pin-hole" porosity occurs. Thus melt temperature and time of

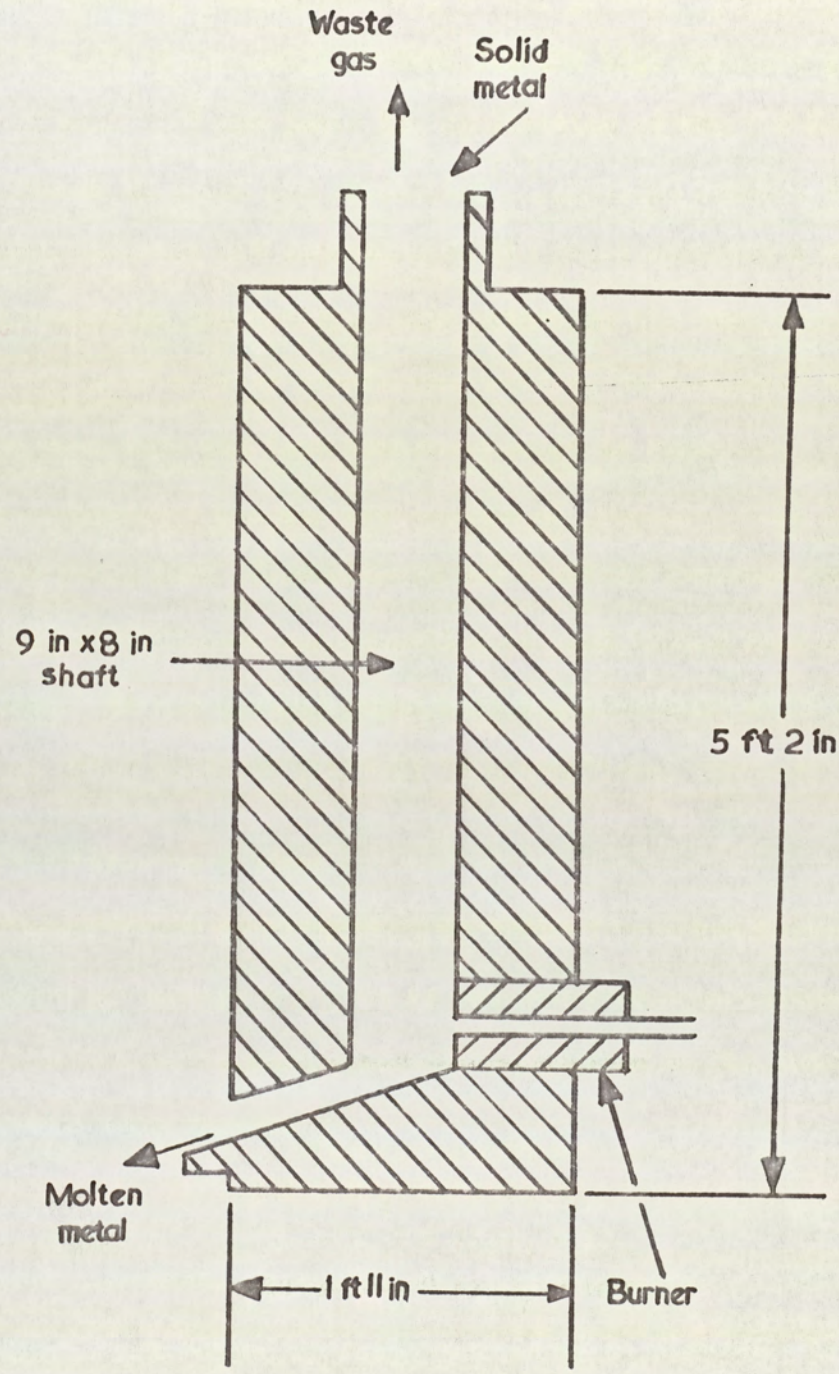

FIGURE 2:1 WATSON & GLEN'S TOWER MELTER

contact with combustion gases must be kept to a minimum.

(3) "On-Stream" Time Delay

The normal practice of holding large quantities of melt at casting temperature outside normal working hours or when casting operations are delayed is conducted at zero thermal efficiency. With rapid start-up and shut-down molten metal would be available "on tap" and holding would become unnecessary. This would lead to additional benefits of improvement in working conditions as would the low exhaust gas temperatures obtained at high efficiency.

The first step towards the ultimate goal was taken by Lawrie and Ayres[8]. Initially they used a reverberatory furnace in which the convective heat transfer was increased by impingement of flame gases on the charge. The fuel efficiency was claimed to be 44%.

They later constructed a furnace as an inclined refractory tunnel with a burner firing through it from the lower end and metal charged in counter-current[9]. Thus the convective component was increased yet again but the inclined tunnel did not make full use of the packed bed principle, i.e. bypassing of gas in the space between the roof and the charge occurred.

Watson and Glen[10] carried out a comparative study of radiation and convection melting. After preliminary trials, they built a convection melter as shown in Figure 2:1, which operated at thermal efficiencies between 50 and 75% and melting rates from 5 to 22 lb/min. They used aluminium ingots of nominal 99.5% purity weighing from 0.25 to 2.3 lb. The metal loss was measured in only one run and a figure of 0.5% obtained, although in their preliminary work with LM6 alloy (10-13% silicon) losses as high as 2.7% were recorded. At high gas rates, burning of aluminium occurred which

was attributed to uneven movement of ingots down the stack and consequent local overheating. This condition was avoided if the melting rate did not exceed 11 lb/min. This corresponded to a specific throughput of 1 320 lb/h ft^2 whereas for a conventional reverberatory furnace 50 lb/h ft^2 is reasonable.

Qualitative measurements of hydrogen content of the melt were made by solidification under reduced pressure and only slight pick-up was indicated, probably because the pouring temperature was never more than 75 deg C above the melting point. In the preliminary work the bed was supported on a grate which resulted in superheats of between 100 and 200 deg C but accumulation of dross tended to impede the melt flow and cause burning of the metal.

A significant feature of convection melting was the rapid start-up and shut-down. Metal started to pour within 30 seconds of lighting the burners and stopped within one minute of extinguishing them.

Glen[11] extended the work using essentially the equipment as illustrated in Figure 2:1 but with a wider range of operating variables viz. ingot and stack diameters, ingot to stack diameter ratio, type of metal, type of grate and hearth angle. He found that melting rates of 20 lb/min (2 400 lb/h ft^2) were possible provided the bed could be kept moving and burning avoided. Rodding of the bed was often necessary to maintain movement but was less acute with small ingots.

Oxidation loss with aluminium of 99.5% purity ranged from 0.4 to 3.6% but no attempt was made to correlate it with surface area to volume ratio or other variables so it is difficult to draw any

conclusions. Brass was melted to investigate selective oxidation with alloys and the zinc content was found to have been reduced from 39.0 to 36.2%.

The increased residence time of the melt due to decreasing the hearth angle from 32° to 20° to the horizontal did not affect the superheat of the metal. Over a wide range of heat inputs, the melt temperature remained between 10 and 20 deg C above the melting point. Superheats of up to 300 deg C were achieved by supporting the ingots on beds of coke or refractory but these became blocked with oxide. A water cooled grate was more satisfactory giving superheats of about 140 deg C but the coolant absorbed 13% of the heat input. The variation in melt temperature with each of the three supports was unacceptable, being as much as ± 50 deg C. Martins and Glen[12] later increased the residence time by use of an extended hearth over which filmwise flow of melt occurred. Superheat was said to be substantial and related to the hearth length and angle of declination.

Watson and Glen[10] and Glen[11] classified three common requirements of the metallurgical industry:

(1) Production at regular, frequent intervals of identical batches of molten metal from pre-alloyed stock in quantities up to a few pounds, e.g. die-casting, preparation of individual shots.

(2) Production of larger batches of varying weight at irregular intervals possibly from pre-alloyed stock.

E.g. for casting of single items directly or for transfer to crucible holding furnaces prior to casting.

(3) Continuous bulk production for continuous casting processes or distribution to holding furnaces:

(a) From pre-alloyed stock.

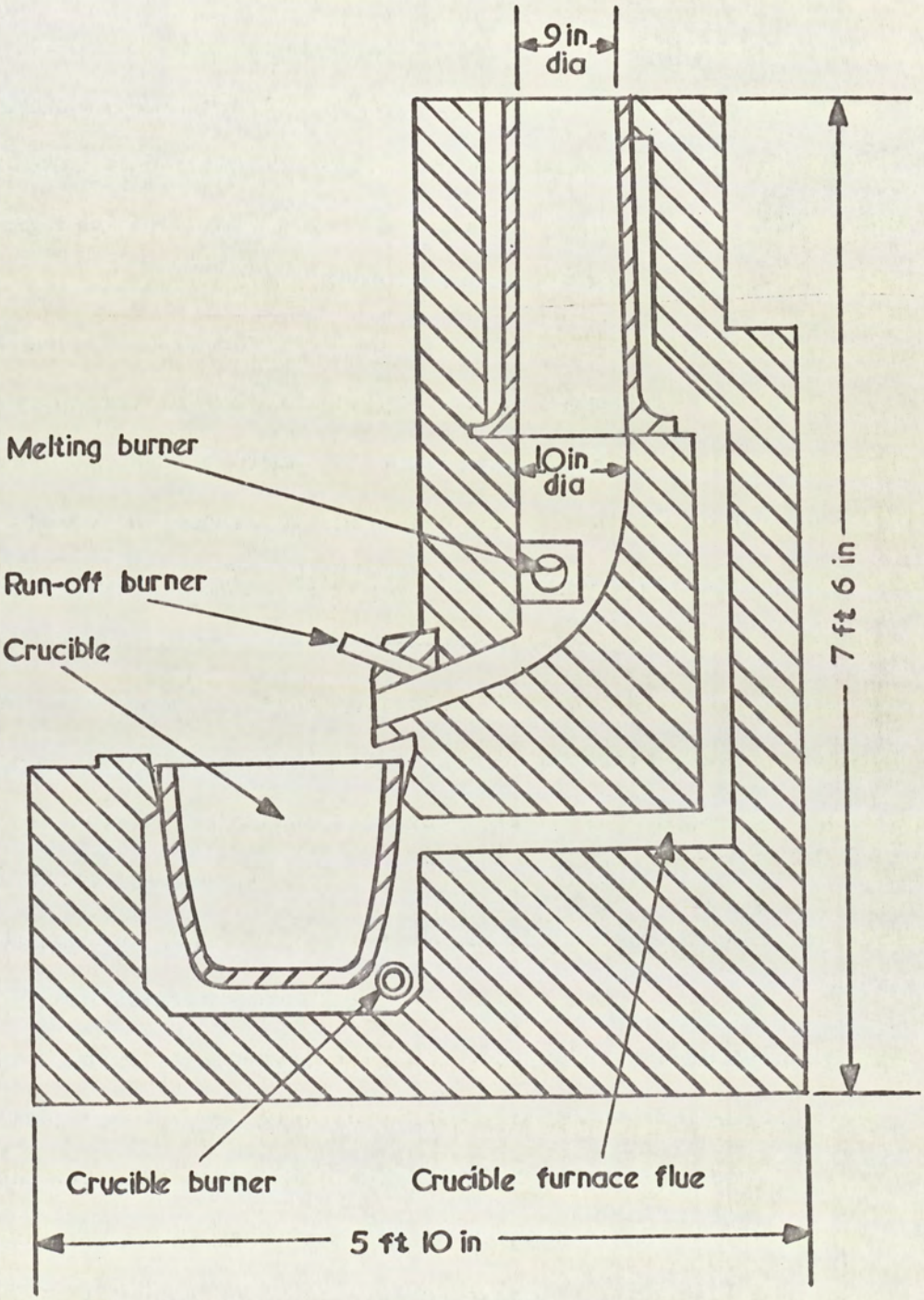

FIGURE 2:2 KNIGHT ET AL.'S TOWER WITH SUPERHEATING CRUCIBLE

(b) From variable stock, including scrap, requiring composition adjustments, degassing and cleaning.

They recognised that their radiation method had certain advantages of convenience and simplicity for die-casting operations but that it could not be expected to approach the thermal efficiency of the packed bed, forced convection, counterflow method. They felt that the latter offered the best basis for the design of a continuous melter of flexible performance and high efficiency.

Subsequent development of forced convection melting was not specifically concerned with die-casting requirements except where they could be met by the second and third classifications, i.e. by bale-out or pressurized syphoning[13] from holding furnaces. Work was also directed towards the problems of maintaining bed movement, raising superheat and determining melt loss.

Knight et al[14] applied the results of Watson and Glen's research to the development of commercial furnaces for both aluminium and copper. Their aluminium melter took the form of a combined tower furnace for melting and crucible holder for superheating, see Figure 2:2. The overall thermal efficiency was about 30% but the tower itself operated at about 50%. This relatively low efficiency was mainly attributable to low values of shaft to ingot diameter ratio and consequent wall effects and the small specific surface area of the large ingots (0.75 to 6.75 lb).

The melt loss was never more than 0.9% and the dross contained between 85 and 90% free metal. After eight hours continuous operation the build up of dross on the hearth had become significant but it was felt that the hearth design could be improved to eliminate this feature.

The small ingots and some types of foundry scrap tended to

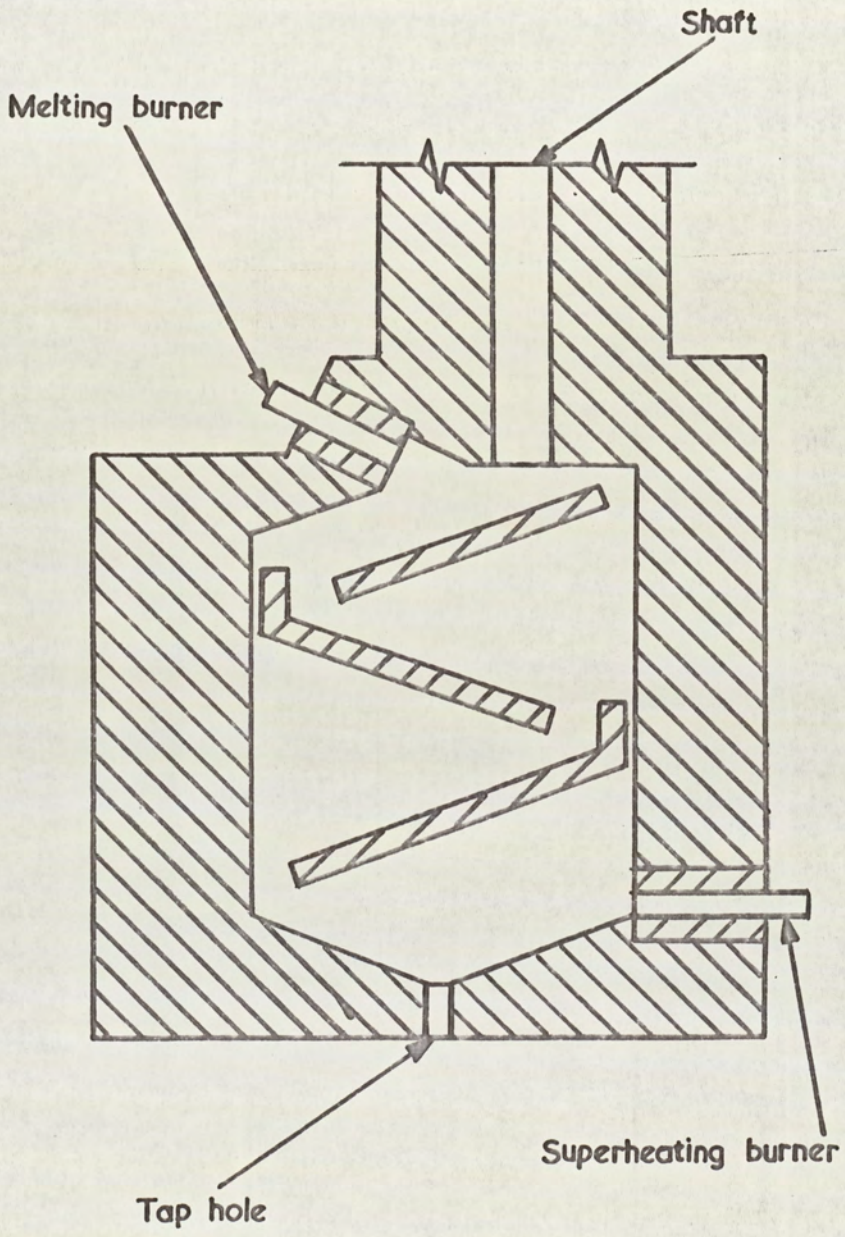

FIGURE 2:3 CASCADING HEARTH SUPERHEATER

bridge across the tower with consequent burning of the metal as reported by Watson and Glen[10] and Glen[11]. The taper of the circular cross-section shaft was from only 9 in at the top to 10 in over a height of 30 in.

The particular size of ingots and melting rate specified for the copper melter prevented true packed bed operation. A tower was designed with a trapezoidal cross-section just greater than that of the ingots so that they were fed endwise, one at a time. Consequently, the thermal efficiency, including superheating from the melting point of 1 083°C to 1 200°C, was only 20%. Superheating was accomplished during the flow of melt across the hearth. In later developments[15,16] the inclined hearth was suspended in a superheat chamber. Cascading multiple hearths were also used as shown in Figure 2:3.

Knight et al[14] made important observations of the different mechanisms of melting of aluminium and copper. Although pure aluminium melts at 658°C, alloys soften over wide ranges of temperature from as low as 525°C up to final melting points close to that of the pure metal. Feedstocks of both pure aluminium and its alloys have refractory outer skins of oxide which contain the molten metal during melting until punctured, either from outside by other feedstock or from within due to the weight of melt. Copper behaves quite differently. It wastes away from the outside in a similar manner to ice. Even if oxidation occurs, the oxide is soluble in the molten copper. Thus the melt is quickly removed from the melting zone. It seems possible that softening over wide temperature ranges and retention of melt within oxide skins both contribute towards the problems of tower blockages with aluminium

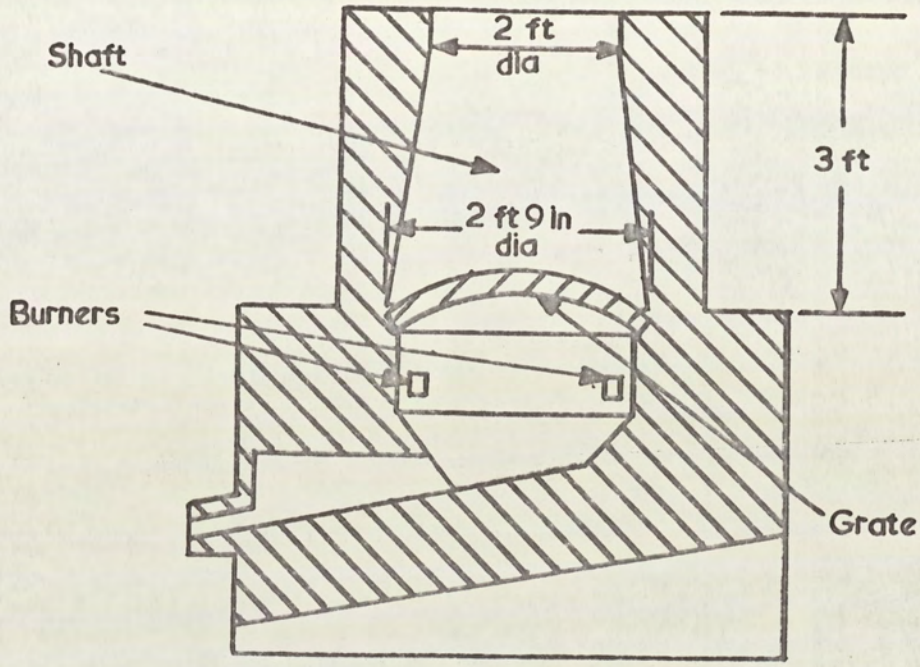

FIGURE 2:4 GAS COUNCIL BULK MELTER : INITIAL DESIGN

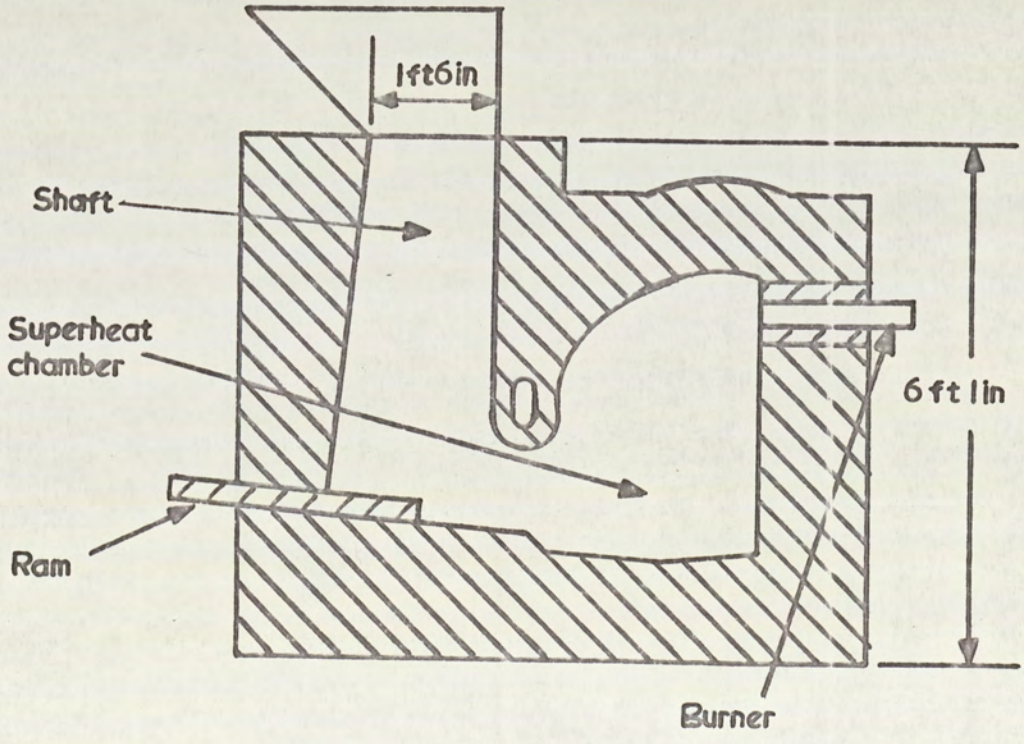

FIGURE 2:5 GAS COUNCIL BULK MELTER : FINAL DESIGN

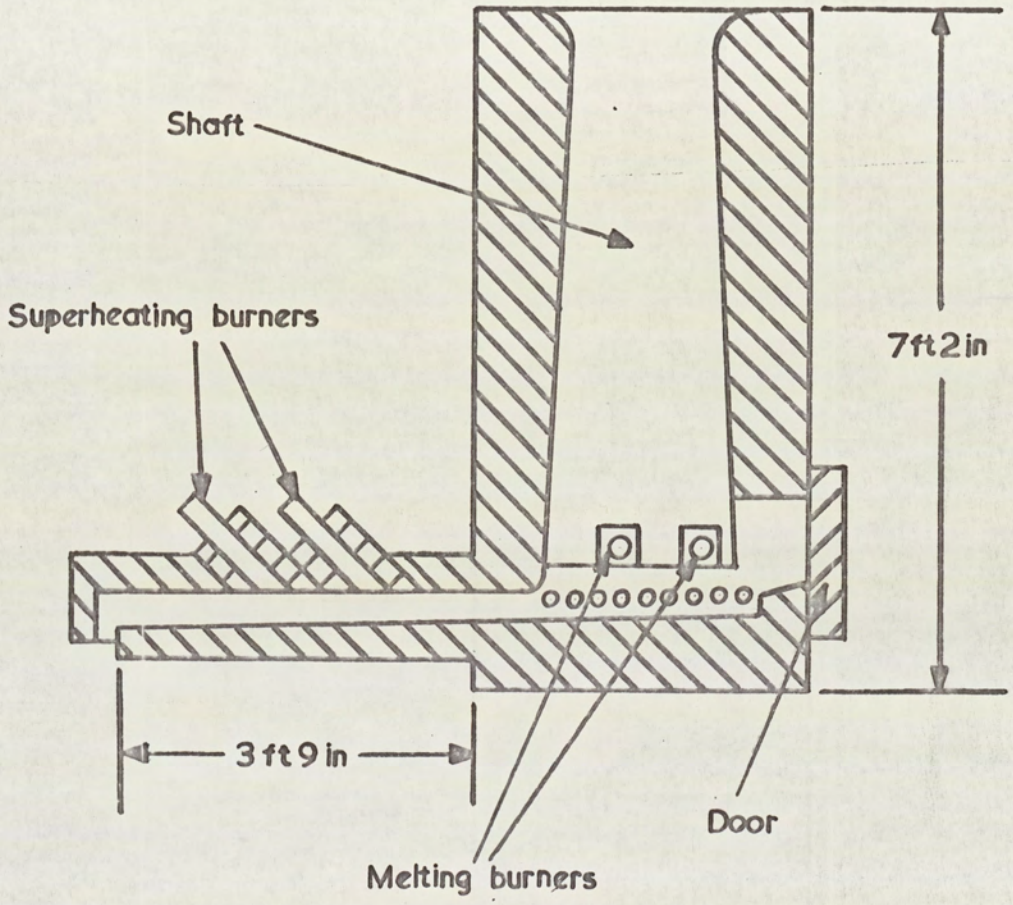

FIGURE 2:6 EASTERN GAS BOARD BULK MELTER

and its alloys.

The development of a bulk tower melter of 1.5 ton/h throughput for The Gas Council was carried out under contract by The Power Gas Corporation Limited[13]. Figure 2:4 represents the original conception of the furnace. Preliminary results suggested it was capable of operating at thermal efficiences of 59% with 100°C of superheat and oxidation losses of between 2 and 3%[7]. However, the mechanism of aluminium melting observed by Knight et al[14] seems to have been such a problem that the design had to be changed drastically before satisfactory movement of charge was achieved. In the final patented design[17] shown in Figure 2:5, it can be seen that there was a tower in which the charge was preheated until it became plastic, a reverberatory chamber in which melting and superheating took place and a ram for transfer between the two compartments.

Bulk melter development was also undertaken by the Eastern Gas Board and a furnace of 1.5 ton/h nominal throughput was built[18]. It featured a bar grate suspended only a few inches above the hearth and a shaft tapering from 1.56 ft^2 rectangular cross-section area at the top to 3 ft^2 at the bottom over a height of 6 ft, see Figure 2:6. The highest melting rate achieved was 1.7 ton/h at 63% efficiency but performance was generally lower than this at about 1 ton/h and 50%. Metal movement was satisfactory with little tendency to bridging so melt loss was only 1%. Temperatures of up to 750°C were obtained with the 4-ft long superheater.

The work in the British gas industry highlighted the poor thermal performance of conventional melting furnaces and showed how forced convection could be used to reduce both fuel and capital costs considerably. Although most of the research and development

effort was directed towards the melting of aluminium and its alloys there still seem to be problems which must be overcome before the process can be accepted by the metallurgical industry. The greatest one is that of bed movement. It is difficult to draw conclusions from the scanty, and often contradictory, published data but there is evidence that certain types of charge will not flow smoothly and consequent oxidation losses can be high. The data on melt losses even when movement is satisfactory are insufficient, particularly with regard to scrap. A comprehensive study of the effects of particle and shaft size and geometry, alloy composition and firing rate on movement, melt loss and thermal efficiency is still required. It may be that the problem of bed movement is insurmountable and some compromise between radiation and convection must be reached such as the inclined refractory tunnels of Lawrie and Ayres[9] and Keating[19].

However, tower furnaces seem particularly well suited to melting copper and the technique is already used industrially[20].

While the work on non-ferrous metal melting is quite recent, the technique of melting in a moving bed is many hundreds of years old. The production of iron in blast furnaces involves essentially the same heat transfer process although there are the added complications of mixed charge materials, chemical reaction and mass transfer. The foundry cupola is essentially similar but fed with scrap ferrous metal rather than iron ore. Heat is usually generated by combustion of coke within the furnace burden but gas fired installations have been reported[21,22]. In such cases, theoretical analysis should be much simpler as chemical reaction and mass transfer are less important.

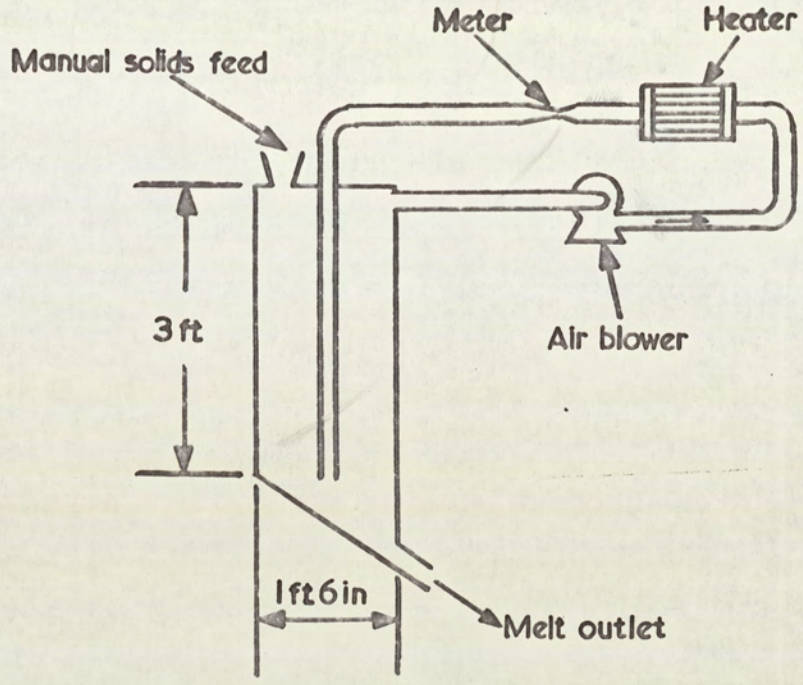

FIGURE 2:7 ORGANIC SOLIDS MELTER : ROSS

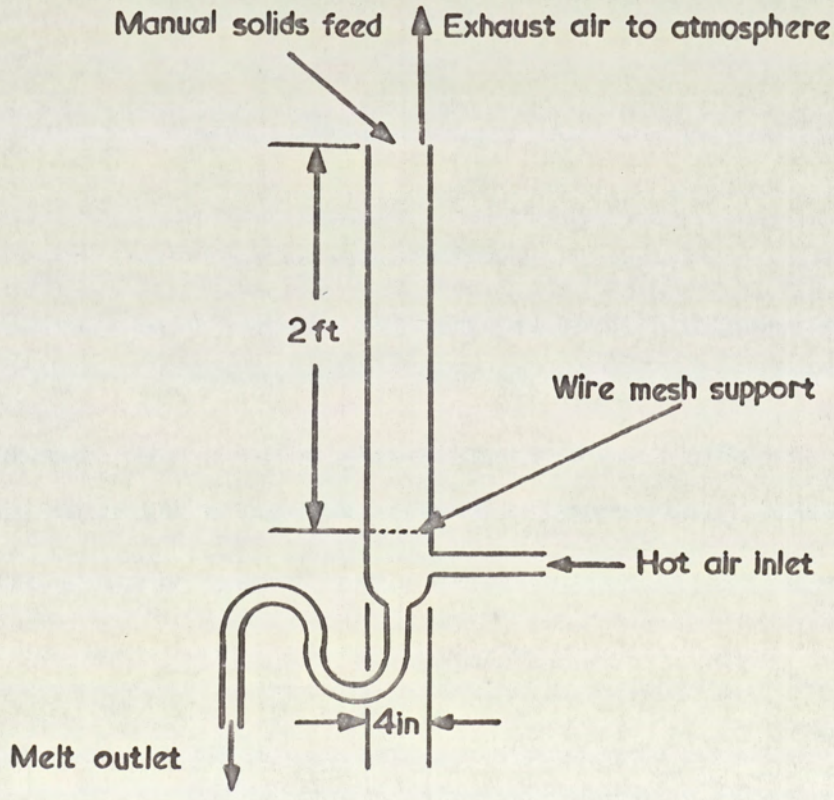

FIGURE 2:8 ORGANIC SOLIDS MELTER : AKERS

2.1.2 Heat transfer studies

Ross[1] appears to have carried out the first fundamental study of heat transfer in melting, packed beds. Using the apparatus illustrated in Figure 2:7 he melted spheres and cubes of naphthalene, cetylalcohol, lauric acid, phenol and paraffin wax.

He considered that it would be sufficient to suppose that at any point in the bed the solids would be covered with a draining film of melt.

As the specific surface area for heat transfer a changed during melting, his results were expressed in terms of the product of the overall heat transfer coefficient U and a, given by:

$$U.a = \frac{M[\lambda + c_s(T_M - T_{si})]}{A_x.L.\Delta T_{lm}} \quad \ldots . \quad (2:1)$$

The results were satisfactorily correlated by:

$$U.a = 0.15\left(\frac{G_f}{d_p}\right)^{0.66}, \frac{Btu}{hft^3\ deg\ F} \quad \ldots . \quad (2:2)$$

for: $10^2 < \frac{G_f}{d_p} < 10^5 \frac{lb}{hft^3}$

but in the range:

$$10^5 < \frac{G_f}{d_p} < 10^7 \frac{lb}{hft^3}$$

U.a seemed to be approaching various maxima. As heat transfer coefficients are inversely proportional to film thickness, Ross argued that increasing the gas rate, and therefore the melting rate, increased the gas film coefficient but reduced that of the melt film. This he expressed by:

$$h_f.a = C_1.G_f^{m_1} \quad \ldots\ (2:3)$$

$$h_M.a = C_2.G_f^{-m_2} \quad \ldots\ (2:4)$$

As gas and melt film coefficients are related by:

$$\frac{1}{U.a} = \frac{1}{h_f.a} + \frac{1}{h_M.a} \quad \ldots\ (2:5)$$

then at low gas rates:

$$\frac{1}{U.a} \simeq \frac{1}{h_f.a} \quad \ldots\ (2:6)$$

and, therefore:

$$h_f.a \simeq 0.15\left(\frac{G_f}{d_p}\right)^{0.66} \quad \ldots\ (2:7)$$

but at higher rates the effect of the melt film becomes increasingly significant.

Ross pointed out that flooding of the column and bed fluidization would occur before the maximum values of U.a were achieved so he developed a somewhat arbitrary design method which takes account of melt properties and enables the calculation of an overall coefficient of 80% of the maximum and the corresponding G_f/d_p. A better approach to the problem might be consideration of flooding and fluidization to determine limiting values of G_f first and then calculation of melting rates.

Following the work of Ross[1], Akers[2] constructed a tower melter as shown in Figure 2:8. Introduction of hot gas into the column through a central downcomer was not employed as it was felt that heat transfer from the surface of the pipe and gas bypassing through the region of high voidage around the downcomer could have occurred in Ross's equipment. The beds were supported on wire mesh

to eliminate errors of bed height determination. No heat transfer results were obtained due to problems of bed "hang-up" which stemmed from transport of melt droplets up the bed and subsequent solidification. An important qualitative conclusion was that there was a clear distinction between melting and preheating zones which suggested that Ross was not justified in treating the whole bed as the region of melting.

Hills[23] also reported "hang-up" or "scaffold" formation in beds of Wood's metal (also known as cerrobend; melting point 70°C; composition Bi 50%, Pb 27%, Sn 13%, Cd 10%) spheres melted by hot nitrogen. He concluded that the problem was due to heat losses at the walls and could be avoided by efficient insulation or provision of a heating jacket. The lower specific gravities of organic solids compared with that of Wood's metal (about 1 compared with 9.38) probably magnified the effects encountered by Akers.

After consulting the literature on gas-solid heat transfer in packed beds, Watson and Glen[10] tried to correlate their results in terms of j_H factors and Reynolds numbers, expecting a relationship of the form:

$$j_H = C_3 . Re^{m_3} \quad \ldots . \quad (2:8)$$

where m_3 is usually negative and fractional. From (2:8) it may be shown that:

$$h_f = C_4 . v^{(1 + m_3)} . d_p^{m_3} \quad \ldots . \quad (2:9)$$

where h_f is given by:

$$\frac{1}{U} = \frac{1}{h_f} + \frac{1}{h_M} + \frac{d_p}{C_5 . k_s} \quad \ldots . \quad (2:10)$$

where C_5 is a geometric factor for conduction in the solid. They

considered that the melt film and solid metal resistances were negligible so:

$$\frac{1}{U} = \frac{1}{h_f} \quad \ldots\ldots\ldots\ldots \quad (2:11)$$

However, no trend could be distinguished from a plot of:

j_H v.Re

although:

h_f v.V, with particle size as parameter, indicated that m_3 was positive, i.e. contrary to expectations, heat transfer coefficient increased with increasing particle size.

Although they had treated the whole bed as the melting region in a similar manner to Ross[1], they had observed experimentally that melting was restricted to a 4-in. deep zone. Also there were deficiencies in the total heat balances of up to 23% which were attributed partly to wall losses but mainly to combustion gas escaping through the tap hole. Recalculation of the results on a two zone basis did not alter them significantly and the index m_3 was still positive.

Other factors which probably contributed to the poor degree of correlation are the small values of shaft to particle diameter ratio (2.69 to 5.57), consequent wall effects and perhaps significant radiative components, the narrow range of gas flow rates (550 to 2,000 ft^3/h) due to problems of burner turn-down ratio and the small number of results (only 10).

Glen[11] extended the range of gas flow rates slightly and more than doubled the number of results but the conclusions remained much the same. He provided a flow diagram of the two zone

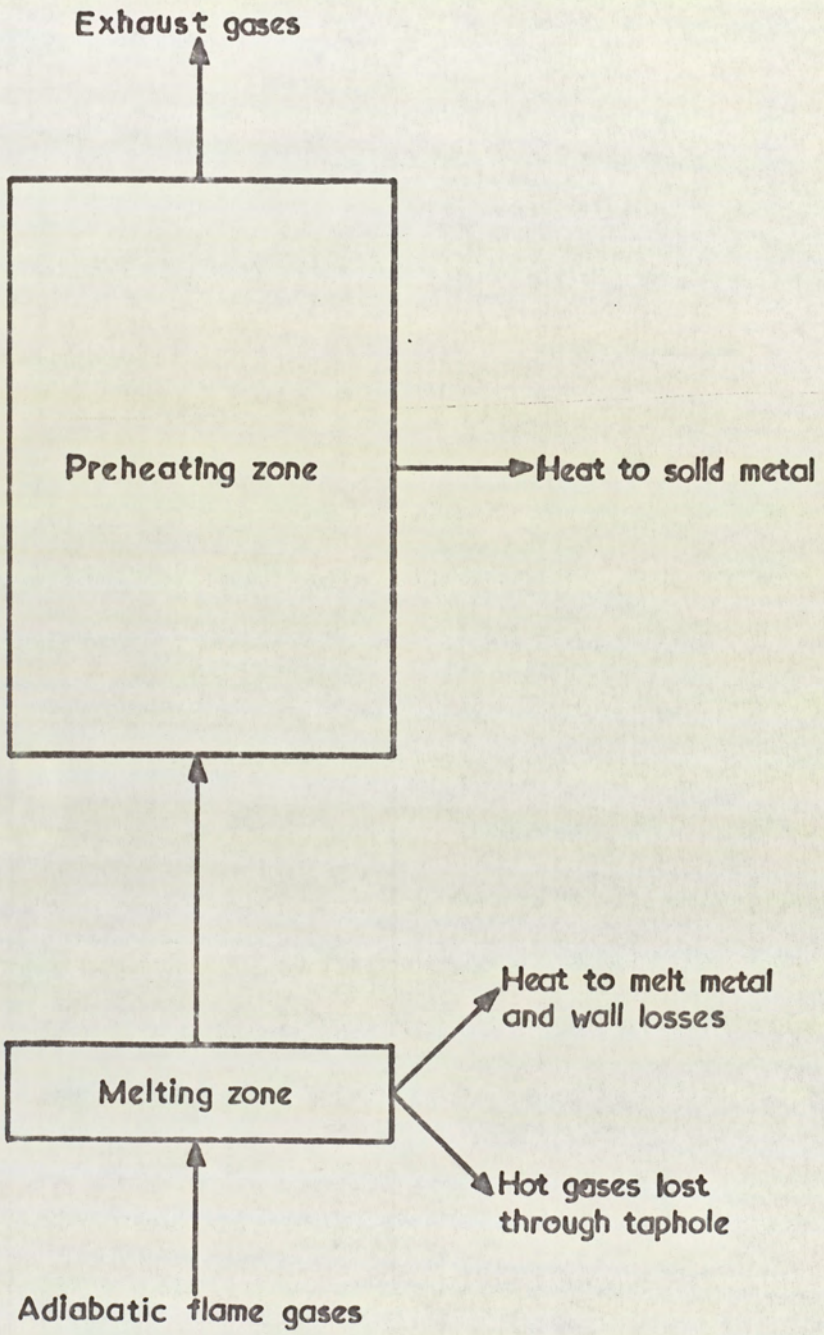

FIGURE 2:9 FLOW DIAGRAM FOR GLEN'S TWO-ZONE MODEL

calculations, see Figure 2:9. It can be seen that all the combustion gas is considered to pass through the melting zone, then the flow splits, some being lost through the tap hole and the remainder passing up through the preheating zone. This seems inconsistent with the design of the tower (see Figure 2:1) and the depth assigned to the melting zone. The centre line of the burner inlet was between 3.75 and 8 in. above the hearth so either all the gas did not pass through the melting zone or the zone depth was greater than 4 in. or both.

Using a graphical method, Glen[11] correlated both his own results for the preheating zone and those of Watson and Glen[10] by:

$$h_f = 0.00039.V.d_p^{0.2} + 1.18 \quad \ldots \quad (2:12)$$

where units are h_f, Btu/h ft^2 deg F;

V, ft/h

d_p, ft

In the present work, their results have been re-analysed by a statistical least mean squares technique and the following correlation obtained in the same units:

$$h_f = 0.015.V^{0.69}.d_p^{0.35} \quad \ldots \quad (2:13)$$

The melting zone coefficients were calculated on the basis that the surface area for heat transfer was the same as in the preheating zone but the values obtained were as much as four times greater than the corresponding preheat coefficients. The likely explanation is that the surface area does increase on melting and the effect seems to be proportional to ingot size, as one might expect.

Even with the two zone analysis there are deficiencies in the heat balances of between 1.1 and 7.7% which it has not been possible to explain[2,24].

The practical and theoretical problems involved in the study of the heat transfer processes occurring in melting, packed beds have been shown to be complex due to differences between the melting and preheating zones. It is reasonable to assume that the magnitude of the problems could be reduced if the melting and preheating zones could be separated. Accurate simulation of preheating should be quite simple but that of melting is probably impossible. However, an approximate method for the latter applied by Standish[25] was to study heat transfer in fixed beds irrigated by low melting point metals flowing countercurrent to hot gases.

The metals chosen were mercury and cerrobend and the gases were nitrogen, argon, carbon dioxide, acetylene and air. The bed materials were $\frac{1}{4}$ in. diameter steel, porcelain and carbon rings and porcelain saddles.

Standish recognised three important modes of heat transfer:

(1) Between the gas and the liquid metal.

(2) Between the packing and the liquid metal.

(3) Between the gas and the packing.

The first mechanism is one of direct transfer to the liquid metal and the net effect of the remaining two is an indirect transfer to the melt.

The rates of heat transfer to cerrobend with steel packing were found to be appreciably higher than with carbon or porcelain, whereas with mercury the influence of packing material was negligible. Standish observed that mercury tended to flow as

droplets due to its high surface tension so its area of contact with the packing was small. Consequently, the direct mode of heat transfer was predominant whereas with cerrobend both modes were important because rivulet and sheet flow occurred producing greater area of solid-liquid contact. The resistance to conduction through the steel packing was much less than for the other materials so indirect transfer was significant. Only with steel packing did the cerrobend results approach those of mercury.

Standish correlated his results by:

(1) Cerrobend and nitrogen, carbon and porcelain packing:

$$U.a = 8.2.Re^{0.9}.H_e^{0.41} \quad \ldots\ldots (2:14)$$

(2) Cerrobend and nitrogen, steel packing:

$$U.a = 15.6.Re^{0.9}.H_e^{0.41} \quad \ldots\ldots (2:15)$$

(3) All mercury results:

$$\frac{U.a}{k_f} = 1{,}450.Re^{0.89}.H_e^{0.40} \quad \ldots (2:16)$$

where U.a is expressed in Btu/h ft^3 deg F,

H_e is the liquid hold-up per unit volume of bed, k_f is expressed in Btu/h ft deg F.

Standish concluded that the melt heat transfer coefficients were 1.5 times higher than would be expected in the preheating zone of a blast furnace stack, although he gives no indication of how this conclusion was drawn. Glen[11] showed that the ratio of the coefficients in the two zones was dependent on ingot size. Perhaps Standish referred to $\frac{1}{4}$ in. diameter burden so 1.5 may be a conservative estimate.

TABLES 2:1, 2 AND 3. NORTON'S DATA

Table 2:1. Data as Presented by Norton

Gas	d_p in	G_f lb/h ft^2	U Btu/h ft^2 deg F
Air	5/16	938	4.3
	1/2	1180	4.5
Steam	5/16	740	5.0
	1/2	933	5.3
Methane	5/16	698	8.2
	1/2	880	8.7
Hydrogen	5/16	248	20
	1/2	312	22

Table 2:2. Data Converted to Dimensionless Groups

Gas	d_p in	Re	Nu
Air	5/16	280	3.2
	1/2	565	5.4
Steam	5/16	274	3.6
	1/2	555	6.1
Methane	5/16	306	2.3
	1/2	619	3.9
Hydrogen	5/16	155	2.5
	1/2	313	4.4

Table 2:3. Constants of Equation (2:18)

Gas	C_6	m_4
Air	0.0507	0.738
Steam	0.0535	0.750
Methane	0.0298	0.757
Hydrogen	0.0425	0.808

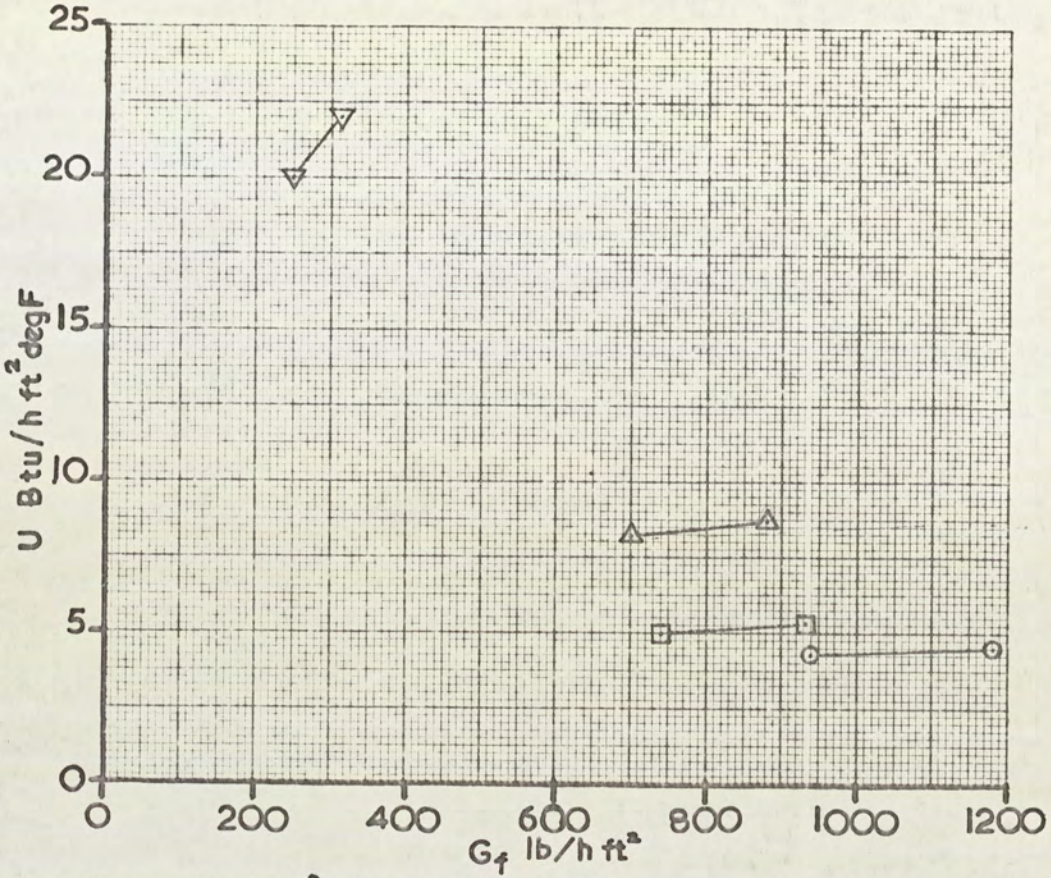

FIGURE 2:10 NORTON'S DATA: U v. G_f

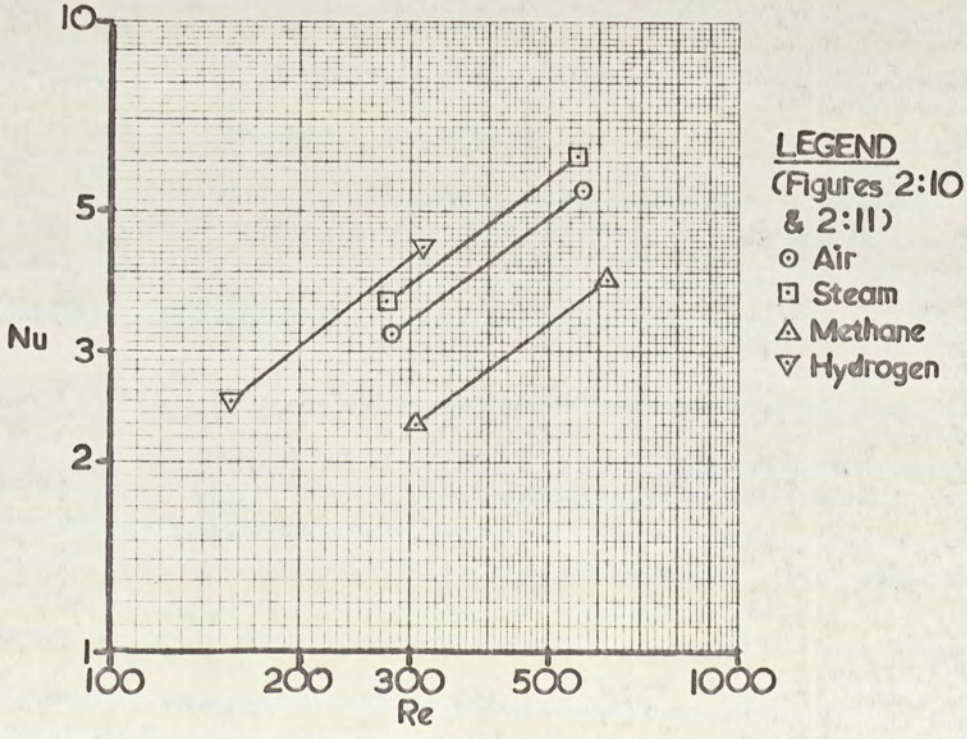

FIGURE 2:11 NORTON'S DATA: Nu v. Re

Simulation of the preheating zone has been carried out in two distinct ways: with moving packed beds and with stationary or fixed packed beds. Steady state results from the former are relatively simple to analyse but there are practical problems of producing the bed movement whereas the converse is true with unsteady state fixed bed operation. Much greater attention has been paid to fixed beds due to the simplicity of operation even with non-spherical particles which would be difficult to handle in small scale moving beds. Previous work using these techniques will now be reviewed.

2.2 Moving Beds

The first significant work was that of Norton[26] on pebble beds for preheating air prior to high temperature combustion. Norton provided limited data for 5/16 in and $\frac{1}{2}$ in diameter mullite, kaolin and alumina pebbles with air, steam, methane and hydrogen as shown in Table 2:1 and Figure 2:10. The gas flow rates represented maxima allowable before the onset of fluidisation. Heat transfer coefficients were calculated as for any two fluid heat exchanger:

$$U = \frac{Q}{a.A_x.L.\Delta T_m} \quad \ldots\ldots (2:17)$$

It can be seen that U increased as d_p and G_f increased but the most significant factor seems to have been the nature of the gas. It is not clear whether these were the only results obtained by Norton, but he reported no attempt at a correlation.

Bowers and Reintjes[27] tried to combine Norton's results with their own on calcination of anthracite briquettes, those of Kilpatrick et al[28] on a pebble bed heater for hydrocarbon

cracking and the fixed bed data of Gamson et al.[29] and Löf and Hawley[30]. This work has been extensively reviewed by Akers[2] and shown to be most unreliable.

In the present work, an attempt has been made to represent Norton's data by an equation of the form:

$$Nu = C_6.Re^m 4 \quad . \quad . \quad . \quad . \quad (2:18)$$

as shown in Table 2:2 and Figure 2:11. Although the results are still not consolidated onto one line, this does seem to be a better description than Figure 2:10. The constants of (2:18) are shown in Table 2:3.

Sissom and Jackson[31] investigated heat transfer between hot air and 0.027 in. diameter aluminium granules under moving bed conditions to obtain design data for gas turbine vehicle regenerators. The length of the test section was 13 in. but, depending on the relative flow rates of the two streams, much of that was ineffective,i.e. gas and solid temperatures approached each other in a short length above the gas inlet but thereafter were virtually coincident. The minimum effective length was only 0.048 in and the maximum seems to have been about 1.5 in. The lengths were determined from axial gas and solid termperature profiles obtained using 0.062 in diameter thermocouples. It was argued that under flow conditions these measured gas temperatures but, on stopping gas and solid streams simultaneously, they closely approximated to the solids temperatures. However, it was admitted that conduction from the column wall occurred.

As a means of obtaining fundamental data, Sissom and Jackson's method is open to serious criticism, although they achieved their object of demonstrating the compactness of granular aluminium

regenerators. Perhaps it is significant that they only provided a graphical representation of their results and reported that this was consistent with the correlation of Frantz[32].

$$Nu = 0.015\ Re^{1.6}\ Pr^{0.67} \quad . \ . \ . \ . \quad (2{:}19)$$

for: $8 < Re < 80$

This is hardly surprising as the temperature profiles predicted by (2:19) were plotted on top of the experimental profiles and probably used as a guide for selection of effective lengths. The asymptotic approach of the gas and solid temperatures was often determined from as few as three points.

Having established the existence of preheating zones in melting beds, Akers[2] proceeded to simulate them using hot air and moving beds of glass and ceramic spheres. These solids were chosen in preference to metals to provide a more rigorous test of a proposed mathematical model which took account of conduction within individual particles as well as forced convection at the surfaces of the particles. There was very wide scatter in his results which was improved only marginally after selection of data by error analysis.

The solids were fed into the bed through the gas outlet as shown in Figure 2:8 so it proved impossible to measure reliable gas temperatures at that point. It was necessary to calculate the probable gas outlet temperature from the heat balance, assuming the solids outlet temperature to be correct. However, the latter was subject to errors and doubts. First, it was not known whether the measured temperature was the mean, surface or some intermediate value. Secondly, due to low vessel to particle diameter ratios (between 6 and 16), it was likely that serious bypassing of gas in

the regions of high voidage at the walls and around the thermocouple probes occurred so the overall heat transfer rates were reduced. Thirdly, the solids outlet temperature was only measured on the column axis so radial variations could not be averaged.

Akers correlated his results by:

$$Nu = 0.002568\left(\frac{Re}{1-e}\right)^{1.29} \quad \ldots\ldots (2:20)$$

for:

$$518 < G_s < 4516 \quad lb/h\ ft^2$$

$$268 < G_f < 3471 \quad lb/h\ ft^2$$

$$170 < \frac{Re}{1-e} < 2600$$

2.3 Fixed Beds

The volume of work using fixed beds is considerable but may be classified according to the techniques employed:

(1) Step, sinusoidal and exponential inputs of gas temperature.

(2) Heat generation within individual spheres.

(3) Analogy with mass and momentum transfer. It is not proposed to deal with the theory upon which each of the methods is based but merely to indicate the experimental, practical and theoretical limitations and the published correlations.

2.3.1 Step input

This method is also known as the "single blow" technique and involves passing a fluid of constant inlet temperature through a fixed bed of solids initially at a uniform temperature. It is not necessary to measure solids temperatures during the experiment provided the initial condition is known. The temperature history of the fluid at the bed outlet is recorded and compared with theoretical curves first derived by Schumann[33] and later improved

and extended by Young[34] and Furnas[35]. A major assumption in the theoretical analysis is that the solids are of high thermal conductivity so that individual particles are at a uniform temperature at any instant, i.e. no intra-particle temperature distribution.

After unsuccessful attempts to determine heat transfer coefficients by direct measurement of gas and solids temperature differences under transient conditions[36], Furnas turned to using Schumann's curves and obtained the relationship[35]:

$$h_f.a = C_7.C_8.\frac{V^{0.7}\ T_{fm}^{0.3}}{d_p^{0.9}} \quad \ldots\ (2{:}21)$$

where C_7 is a coefficient characteristic of the bed material (different values for heating and cooling) and C_8 is a function of bed voidage. Materials used were cast iron spheres and crushed refractory, iron ore, limestone, coal and coke. The index of d_p for cooling coke was 1.3 not 0.9. Volumetric transfer coefficients were used due to doubts about particle surface areas and inter-particle contact areas for non-spherical particles.

Saunders and Ford[37] criticised the column material chosen by Furnas. It was "extra heavy" pipe of higher heat capacity and thermal conductivity than most of the bed materials so the wall heat losses were probably substantial. Attempts were made to heat the column and insulation before runs to the mean bed temperature achieved during the runs but the differences in the values of C_7 for heating and cooling suggest that this was unsuccessful. The closest agreement between the two values of C_7 occurred with the cast iron spheres, presumably because of the greater heat capacity than with the other bed materials. Kitaev et al.[38] considered

that the difference between heating and cooling results could have been due to residual temperature distributions within the particles at the start of the cooling cycles, particularly with coke. Having shown by using hydraulic analogues that the geometric factor for conduction in spherical solids, C_5, was 10, i.e:

$$\frac{1}{U} = \frac{1}{h_f} + \frac{d_p}{10\,k_s} \quad \ldots\ (2{:}10)$$

they took account of the finite thermal conductivity of the solids in calculating the true film coefficients from the experimental overall coefficients. They correlated Furnas's heating data for crushed solids by:

$$h_f.a = C_7.C_8.\frac{V^{0.9}T_{fm}^{0.3}}{d_p^{0.75}} \quad \ldots\ (2.22)$$

where the units are:

$h_f.a$, kcal/m^3 h deg K.

V, m/s superficial

T, ^oK

d_p, m

and considered that C_7 was virtually constant for all materials and equal to 160. They were very vague about the relationship between C_8 and the voidage and merely quoted:

$$C_8 = 0.5 \text{ for } e = 0.2$$

For cast iron spheres they gave:

$$h_f.a = 12\,\frac{V.T_{fm}^{0.3}}{d_p^{1.35}} \quad \ldots\ (2{:}23)$$

or:

$$h_f = \frac{2}{(1-e)}\,\frac{V.T_{fm}^{0.3}}{d_p^{0.35}} \quad \ldots\ (2{:}24)$$

in the same units as (2:22).

They seemed to suggest that the factor $T_{fm}^{0.3}$ was not a real effect, rather a result of the dependence of specific heat on temperature but did not elaborate on the matter.

As Furnas used particles from 0.4 to 7.3 cm in beds of 15 and 23 cm diameter, much of his work was subject to low $d_v:d_p$ ratios and consequent wall effects although Denton[39,40] believed that the supply of gas to and subsequent discharge from the beds through small central orifices would tend to offset these errors.

The approach of Saunders and Ford[37] to the selection of apparatus, analysis of results and subsequent use for design was different from that of other workers in that they established conditions of geometric similarity. They generalised the outlet gas temperature histories so that they would apply to other fixed bed equipment. The technique was essentially one of "scale-up" and did not require a specific knowledge of the heat transfer coefficients. However, they did compute the coefficients using their own modification of Schumann's curves and obtained the relationship:

$$h_f.a = 185 \frac{V}{d_p} \quad \ldots\ldots (2:25)$$

or:

$$h_f = \frac{185\ V}{6(1-e)} \quad \ldots\ldots (2:26)$$

for: $0.5 < V < 1.3$ m/s

in the same units as (2:22).

Akers[2] pointed out that, although their use of Schumann's solutions was simpler than that of Furnas, it bunched the curves together and made matching more difficult. Wall effects and

intra-particle temperature distributions are unlikely to have been very significant due to the small size of the spheres. They used steel, lead and glass balls in columns of 2, 4 and 8 in diameter with $d_v : d_p$ ratios not less than 32. Air inlet temperature was 100°C.

Löf and Hawley[30] obtained data on heating and subsequent cooling of beds of broken granitic gravel using Schumann's curves in the same manner as Furnas. Wall heat losses during the flow of hot air were compensated for by external heating but the results for bed cooling had to be discarded due to the heat input from the lagging. Particle diameters ranged from 0.3 to 1.3 in but gas velocities were low so conduction lag was possibly not significant. However, with a minimum $d_v : d_p$ of 7.5 there may have been important wall effects. They represented their results by:

$$h_f.a = 0.79 \left(\frac{G_f}{d_p} \right)^{0.7} \quad \ldots . \quad (2:27)$$

for: $58 < G_f < 322$

and air inlet temperatures between 100 and 250°F

where the units are:

$h_f.a$, Btu/h ft^3 deg F.

G_f, lb/h ft^2

d_p, ft

and showed that they were in reasonable agreement with Furnas's correlation but gave lower coefficients than Saunders and Ford's, a fact which they attributed to the greater active surface area of the spherical particles used by the latter.

Coppage and London[41] applied Schumann's curves to the transient heating of 0.08 in diameter lead shot by air in a

3 in diameter vessel. It seems that they overcame the problems of wall heat loss, wall voidage effects and particle conduction lag. Their results were correlated by:

$$Nu \frac{4e}{6(1-e)} = 0.21\left(\frac{Re.4}{6(1-e)}\right)^{0.6} \quad \ldots\ldots (2:28)$$

for: $$25 < \frac{Re.4}{6(1-e)} < 550$$

The voidage terms stemmed from their use of the mean hydraulic radius of the flow passages and desire to correlate data for woven wire mesh screens with that for spheres. For the spheres, e was 0.39. The inlet air temperature was only 20 deg F above ambient, presumably so that variations in the thermophysical properties were negligible.

Gliddon and Cranfield[42] obtained data for the cooling from 600°C of alkalised alumina in a bed of 214 mm diameter at a $d_v:d_p$ ratio of 178. No doubt some heat gain from the column walls occurred but this may not have manifested itself in the results as the outlet air temperature was measured on the bed axis. They correlated their data together with that of Littman et al.[43] by:

$$Nu = 0.36\, Re^{0.94} \quad \ldots\ldots (2:29)$$

for: $$2 < Re < 100$$

As the bed voidage ranged from 0.404 to 0.526, they tried to reduce the scatter of the results by using:

$$Nu \text{ v. } \frac{Re}{(1-e)}$$

but this was unsuccessful.

Kitaev et al[38] reported several Russian investigations.

Tsukhanova and Shapatina used a method similar to that of Saunders and Ford. They did not attempt to calculate heat transfer coefficients expecting that the scale-up procedure would be used in future applications. Their results are consequently not immediately suitable for moving bed problems. Chukhanov heated the container beforehand to the average expected gas temperature to minimise heat losses. His correlation was:

$$Nu = 0.24\ Re^{0.83} \quad \ldots\ (2{:}30)$$

for: $100 < Re < 140$

$d_v : d_p$ about 15

inlet air temperature about 230°C

His bed materials were steel spheres, damp coal, peat, bronze cylinders and chamotte fragments, all of 3.15 mm equivalent spherical diameter.

The accuracy of matching Schumann's curves was recently improved by Handley and Heggs[44] using an iterative numerical method. Their results for steel, lead and bronze spheres of $\frac{1}{8}$ in to $\frac{3}{8}$ in diameter were correlated by:

$$j_H \cdot Re \cdot e = 0.255\ Re^{0.665} \quad \ldots\ (2{:}31)$$

for: $100 < Re < 4000$

$0.36 < e < 0.39$

but there were slight deviations for $\frac{1}{8}$ in alumina and significant deviations for $\frac{1}{8}$ in to $\frac{3}{8}$ in lead and soda glass.

2.3.2 Sinusoidal input

This is usually referred to as the cyclic method. The mathematical analysis has the same starting point as Schumann's "single blow" technique but its relative simplicity makes it possible

to extend the basic model to include conduction within individual particles, axial conduction between particles and axial dispersion in the fluid phase.

The experimental procedure involves controlling the inlet fluid temperature sinusoidally and measuring either the phase lag or attenuation of the outlet temperature.

Meek[45] applied a simple mathematical model for analysis of his data but showed theoretically that intra-particle temperature distribution was insignificant for the 10 mm diameter steel ball bearings which he had used. He reduced the wall voidage effects considerably by setting the outer spheres in epoxy resin and measuring the air temperatures over the central portion of the conduit. He found that his own results and those of other workers were correlated best if the mean hydraulic radius were used:

$$e.j_H = 0.49\left(\frac{4.Re}{6(1-e)}\right)^{-0.38} \quad \ldots\ldots (2{:}32)$$

for: $$600 < \frac{4.Re}{6(1-e)} < 4000$$

At low Reynolds numbers, Littman et al.[43] reported that conduction in the solid phase and dispersion in the gas phase affect the frequency response to such an extent that the simple model is inadequate. They provided only graphical and tabular presentations of their data on heat transfer between air and copper, lead and glass spheres but they have been correlated together with the results of Gliddon and Cranfield[42] as mentioned in Section 2.3.1 by:

$$Nu = 0.36\, Re^{0.94} \quad \ldots\ldots (2{:}33)$$

for: $$2 < Re < 100$$

Lindauer[46] chose to correlate his data for small steel and tungsten spheres and air by a plot of:

$$e.j_H \text{ v. } Re$$

No expression was given but he also reported that:

$$h_f \propto \frac{G_f^{0.60}}{d_p^{0.44}} \quad \text{, for steel}$$

and:

$$h_f \propto \frac{G_f^{0.66}}{d_p^{0.44}} \quad \text{, for tungsten}$$

His model ignored axial dispersion in the gas phase and conduction within and between particles.

2.3.3 Exponential input

This is the most recent technique for investigation of fixed bed heat transfer and was developed jointly by the British Iron and Steel Research Association and the John Percy Group in Process Metallurgy, Imperial College. The work of Hills on melting beds, previously referred to in Section 2.1.2, formed part of the general programme of the same group.

Initially they were concerned with the overall heat and mass transfer and chemical reaction processes occurring in the iron blast furnace and a time lag simulation known as SCICE evolved (Stationary Charge In Controlled Environment). In this, the gas composition and temperature could be varied with time and the progress of a charge of typical burden down through the blast furnace simulated. The equipment could be operated at high temperatures just short of melting although Hills[23] did report work in Sweden which was intended to include the final physico-chemical changes.

The data from the original SCICE were mainly of a chemical nature[47] but, to improve existing mathematical models of blast furnace operation, heat transfer data were obtained by Bradshaw et al.[48] using air and nitrogen with steel and alumina spheres and haematite pellets. They used $d_v : d_p$ ratios of not less than 15 in a 40 cm diameter container so wall voidage effects were unlikely to be significant. Heat losses were minimised by controlled heating of the walls. They correlated their overall heat transfer coefficients by:

$$j_H = 0.492 \left(\frac{Re}{6(1-e)} \right)^{-0.382} \qquad \ldots\ldots\ldots\ldots (2:34)$$

for $35 < \frac{Re}{6(1-e)} < 610$

and $0.4 < e < 0.44$

As the transfer coefficients were noticeably higher for the steel balls than for the other materials they then included the effects of the solid thermal conductivity using the resistance equation:

$$\frac{1}{U} = \frac{1}{h_f} + \frac{d_p}{10 k_s} \qquad \ldots\ldots\ldots\ldots (2:10)$$

and obtained the expression:

$$j_H = 0.495 \left(\frac{Re}{6(1-e)} \right)^{-0.375} \qquad \ldots\ldots\ldots\ldots (2:35)$$

Although the axial gas turbulent thermal conductivity, k_{ef}, was mentioned in their theory, it is not clear whether the term:

$$\frac{k_{ef} \cdot 6(1-e)}{d_p (G_f c_f)^2}$$

was included in the right-hand side of (2:10).

They did not detect any relationship between transfer coefficients and temperature despite operating in the ranges 20-400°C, 20-800°C and 400-800°C.

2.3.4 Heat generation within individual particles

The present objective is the measurement of heat transfer coefficients between fluids and solid surfaces so the obvious approach might be the direct measurement of local fluid and solid temperatures. This was tried by Furnas[36] under unsteady state conditions but was most unsatisfactory so he had to turn to using Schumann's curves[33]. However, steady state can be achieved in a fixed packed bed by generating heat within individual spheres and continuously removing it by the flow of coolant.

Denton[39,40] inserted copper spheres containing electric heaters into random packed beds of similar sized glass spheres cooled by air. Solid-gas temperature differences were measured by soldering one junction of a thermocouple pair to the surface of a copper sphere and suspending the other in the air stream. Point heat transfer coefficients were determined and integrated over the whole sphere surface. Denton expressed his results by:

$$St = 0.72\ Re^{-0.30} \quad \ldots\ldots\ldots\ldots \quad (2{:}36)$$

for $500 < Re < 53000$

with the proviso that there were no wall voidage effects, a condition which was satisfied if:

$$d_v : d_p > 17.5$$

Wadsworth[49] carried out similar work but with a close regular packing arrangement which was designated by Martin et al.[50] as "rhombohedral No. 6 block passage" and had a voidage (defined for an infinite array) of 0.2595. Transfer coefficients were between 75 and 95% greater than those of Denton. Akers[2] suggested this might be due to conduction from the instrumented sphere to the adjacent wooden spheres. Some effect must have

been due to voidage as the packing used by Denton is unlikely to have been so close. If the results were plotted as:

$$St \text{ v. } \frac{Re}{(1-e)}$$

rather than:

$$St \text{ v. } Re$$

then the spacing of the correlating lines would not be as great.

Rowe and Claxton[51] reported heat and mass transfer data for spheres in arrays with voidage from 0.260 to 0.632 and also for isolated spheres. The fluids were air and water. A complex analysis of their own and other data produced:

$$Nu = C_9 + C_{10}.Pr^{\frac{1}{3}}.Re^{m_5} \quad \ldots\ldots\ldots\ldots \quad (2:37)$$

where

$$C_9 = \frac{2}{[1-(1-e)^{\frac{1}{3}}]}$$

$$C_{10} = \frac{2}{3.e}$$

$$\frac{(2-3m_5)}{(3m_5-1)} = 4.65\ Re^{-0.28}$$

It can be seen that the minimum value of Nusselt number must be 2, which is in accordance with the minimum possible theoretical value for a single sphere in an infinite stagnant medium. However, for multi-particle situations smaller values have been recorded and Cornish[52] showed on theoretical grounds that the Nusselt number should approach zero. This suggests that the analysis of Rowe and Claxton was perhaps unjustified.

Gillespie et al.[53] studied the effects of sphere position in randomly packed, air cooled beds and identified an entrance region, confined to the first two layers of the bed, in which the heat transfer coefficients were less than elsewhere. This they

attributed to the lower incident velocity and turbulence level. Also, they found that the coefficients were greater near the walls due to the greater flow rates in that region. They tried to relate the increase as the walls were approached to the velocity profiles published by Schwartz and Smith[54] but were unsuccessful. They used 12 in square cross section beds with $d_v:d_p$ of 12. They postulated a minimum rate of heat transfer by fitting the data to the equation:

$$Nu = C_{11} + C_{12} \cdot Re^{m}6 \quad \ldots\ldots\ldots \quad (2:38)$$

but found that the variance was least for:

$$C_{11} = 0$$

For the bulk of the bed:

$$Nu = C_{12} \cdot Re^{0.65} \quad \ldots\ldots\ldots \quad (2:39)$$

for $120 < Re < 1700$

where C_{12} ranged from 0.63 on the axis to 0.75 near the wall.

Baldwin et al.[55] performed essentially the same tests as Gillespie et al.[53] but used regular packing arrangements: dense cubic ($e = 0.26$) and regular cubic ($e = 0.48$). With $1^{15}/16$ in diameter spheres and pressurized water at 240°F they were able to work in the range of Reynolds numbers from 3000 to 70000. The entrance region was restricted to the first four layers for the regular cubic lattice but to only the first two for the closer packing. Remote from the entrance region their results were expressed by:

$$j_H = 0.99\ Re^{-0.33} \quad \ldots\ldots\ldots \quad (2:40)$$

for $e = 0.48$

$$j_H = 0.94\ Re^{-0.30} \quad \ldots\ldots\ldots \quad (2:41)$$

for $e = 0.26$

All of the above applications of the instrumented spheres technique involved placing electric resistance elements within the spheres. However, indirect methods of induction and dielectric heating have also been used, e.g. Eichorn and White[56] and Baumeister and Bennett[57]. Results in general agreement with other published data were reported.

2.3.5 Mass transfer

Gamson et al.[29] carried out early work on simultaneous heat and mass transfer in the constant drying rate period. They used shallow beds of spherical and cylindrical particles of diatomaceous earth soaked in distilled water. Although their $d_v : d_p$ ratios of not less than 16 were probably adequate, the entrance-exit effects of the shallow beds may have been significant with the larger particles (0.74 in d_p, 2.5 in depth). They represented their results by:

$$j_H = 1.064.Re^{-0.41} \quad \ldots\ldots\ldots \quad (2:42)$$

for $350 < Re < 4000$

and $$j_H = 18.1\ Re^{-1} \quad \ldots\ldots\ldots \quad (2:43)$$

for $Re < 40$

with a transition region in between. However, they did not report any data below a Reynolds number of 60 so (2:43) was rather unjustified. Wilke and Hougen[58] extended the work in the region $50 < Re < 250$ and obtained:

$$j_H = 1.96\ Re^{-0.51} \quad \ldots\ldots\ldots \quad (2:44)$$

for $50 < Re < 350$

Although (2:42) and (2:44) represented the data satisfactorily, Wilke and Hougen pointed out that there was a smooth transition from one to the other.

The mass transfer method could not be used at lower Reynolds numbers because the temperature difference at the bed outlet was too small to be measured accurately.

Recent work by Malling and Thodos[59] was directed towards the problems of entrance-exit effects. They found that three layers of inert plastic spheres at the entrance to the bed and two layers at the exit produced j_H factors 20% greater than in the previous work[29,58]. They also investigated the rôle of voidage by using distended beds of spheres and combined their results in the relationship:

$$j_H = 0.539\, e^{-1.19}\, Re^{-0.437} \quad \ldots\ldots \quad (2:45)$$

for $180 < Re < 8500$

After correcting for axial dispersion they gave:

$$j_H = 0.763\, e^{-1.19}\, Re^{-0.472} \quad \ldots\ldots \quad (2:46)$$

Chu et al.[60] showed that there were considerable variations among published mass transfer data for fixed and fluidized beds suggesting that there were differences in mechanism between the two types of system. Their own data for air and naphthalene expressed as:

$$j_D \text{ v. } Re$$

supported this view but inclusion of a voidage term in the Reynolds number produced a satisfactory correlation. Taking Gamson et al.'s[29] analogy between heat and mass transfer:

$$\frac{j_H}{j_D} = 1.076$$

their equations become:

$$j_H = 1.90 \left(\frac{Re}{1-e} \right)^{-0.44} \quad \ldots\ldots\ldots \quad (2:47)$$

for $30 < Re < 5000$

$$\text{and } j_H = 6.13 \left(\frac{Re}{1-e}\right)^{-0.78} \quad \ldots\ldots\ldots \quad (2:48)$$

for $1 < Re < 30$

Kitaev et al.[38] referred to the work of Fedorov on air drying of damp coal which was correlated by:

$$Nu = 0.23\ Re^{0.863} \quad \ldots\ldots\ldots \quad (2:49)$$

for $15 < Re < 160$

2.3.6 Momentum transfer

Although the analogy between heat and mass transfer has been substantiated for flow in numerous systems ranging from flat plates to packed beds, the analogy of either of these transfer processes with pressure drop is more limited. Hicks and Mandersloot[61] pointed out that heat and mass transfer rates are determined by the viscous losses associated with skin friction whereas pressure drop is also governed by the kinetic losses due to form drag.

Martin et al.[50] measured the pressure drops through regular arrangements of spheres and found that, even for the same lattice, widely differing friction factors could be obtained as the direction of flow was altered.

Meek[45] concluded that packing arrangements which produced increases in heat transfer entailed greater increases in friction and Handley and Heggs[44] suggested that the Chilton-Colburn analogy could not be applied to packed beds.

Contrary to most other opinions, Chu et al.[60] proposed the relationship:

$$j_H = \frac{f}{10} \quad \ldots\ldots\ldots\ldots \quad (2:50)$$

at the same $\frac{Re}{(1-e)}$.

2.4 General Correlations

One of the greatest problems in formulating a general correlation of the results is the various definitions of j_H factor, Reynolds number and Nusselt number used by different investigators. Simply because a particular form of correlation fits the results better than another is not definite proof of its value. It may just be that the sensitivity to a particular parameter is reduced. Random experimental error is inevitable. Systematic errors may remain undetected or unexplained and extrapolation will be most unreliable if observations are only made over small ranges of the variables.

Many investigations have been directed at solving particular, short term industrial problems, e.g. tower melting, blast furnace operation, catalytic cracking. No doubt they were reasonably reliable for interpolations and slight extrapolations of the systems for which they were originally conceived but, for an understanding of the fundamental process of heat transfer between solids and fluids in packed beds, they may just add to the general confusion. They are necessary in the interim period but overall progress would probably be faster if idealized systems were thoroughly investigated first.

Entrance, exit, wall voidage and wall heat loss effects should be eliminated or accounted for rigorously. Spherical, uniformly sized, non-porous particles should be employed so that doubts do not arise regarding point contact, active surface area or mean diameter definition. Where appropriate, intra-particle temperature distribution and axial dispersion should be accounted for.

In formulating a general representation of previous work, an

attempt will be made to adhere to the conditions suggested in the previous paragraph. The suggestions of Rowe[62] will also be borne in mind. Rowe gave an example illustrating how the indiscriminate use of dimensionless groups can lead to totally erroneous correlations. He reiterated the classification of Engel[63,64] for such groups:

(1) Those which can be derived from the fundamental equations of dynamics.

In packed bed systems the Reynolds number is likely to be the most useful although at very low flow rates the Péclet number might also be significant.

(2) Dimensionless ways of expressing experimental results.

e.g. Nusselt number.

(3) Dimensionless combinations of fluid properties.

e.g. Prandtl number.

(4) Geometric ratios.

e.g. $d_v : d_p$, voidage.

(5) Derived combinations of other groups.

e.g. Stanton number, heat transfer factor.

Rowe suggested that, ideally, only the first two categories should be used.

The most common relationships used by previous workers were:

j_H v. Re

St v. Re

Nu v. Re

Now

$$St = \frac{Nu}{Re.Pr} \quad , \quad j_H = St\ Pr^{\frac{2}{3}} = \frac{Nu}{Re.Pr}\ Pr^{\frac{2}{3}}$$

The only fluid used in the present work was air at no more than 150°C at the bed inlet so the Prandtl number was virtually constant for all runs.

Therefore:

$$Nu \text{ v. } Re$$

should suffice.

The effect of voidage has been referred to in many papers. Rowe suggested that a variable should only appear in one dimensionless group of any correlation. Admittedly d_p appears in both Nu and Re but the use of voidage in the manner[41]:

$$\frac{Nu.e}{(1-e)} \text{ v. } \frac{Re}{(1-e)}$$

seems rather extreme. One could use the interstitial loading rate, G_f/e, alone:

$$Nu \text{ v. } \frac{Re}{e}$$

or in combination with the characteristic dimension $\frac{d_p.e}{6(1-e)}$ as in fluid pressure drop work[93]:

$$j_H \text{ or } Nu \text{ v. } \frac{Re}{(1-e)}$$

A number of authors have attempted general correlations of published work, even including single sphere and fluidized bed results. The wide range of experimental and analytical techniques and the different errors involved probably accounts for much of the use of dimensionless groups from Engel's[63,64] fourth classification[51,65,66,67]. Despite the views of Cornish[52], the concept of minimum heat transfer rate has often been included[51,65,68].

Bird et al.[69] and Hougen et al.[70] both quoted the

correlations of Yoshida:

$$j_H = 0.91 \left(\frac{Re}{6(1-e)}\right)^{-0.51} \quad \ldots\ldots \quad (2:51)$$

for $\frac{Re}{6(1-e)} < 50$

and $$j_H = 0.61 \left(\frac{Re}{6(1-e)}\right)^{-0.41} \quad \ldots\ldots \quad (2:52)$$

for $\frac{Re}{6(1-e)} > 50$

Yeh[65] combined mass, heat and momentum transfer data to give:

$$Nu\, Pr^{-\frac{1}{3}} = 0.8\, Re^{0.65} \quad \ldots\ldots \quad (2:53)$$

for $50 < Re < 5000$

and $$Nu.Pr^{-\frac{1}{3}} = 1.91 \times 10^{(0.04\ Re)} \quad \ldots\ldots \quad (2:54)$$

for $0.5 < Re < 10$

with a smooth transition between the two.

Ranz[68] extended his semi-theoretical relationship for single spheres to packed beds and gave:

$$Nu = 2.0 + 0.6\ (9.1 \times Re)^{\frac{1}{2}}\, Pr^{\frac{1}{3}} \quad \ldots\ldots \quad (2:55)$$

for $80 < Re < 1000$.

Yagi and Muchi[67] reported comparable expressions involving voidage terms.

Kunii and Suzuki[71] developed a channelling model describing heat and mass transfer at low Reynolds numbers to reconcile the differences between the extrapolation of the Ranz equation and other published experimental data. They derived the expression:

$$Nu = \frac{Pe.d_p}{6(1-e)l} \quad \ldots\ldots \quad (2:56)$$

where l is the average channel length, approximately inversely proportional to d_p although the relationship was very ill-defined.

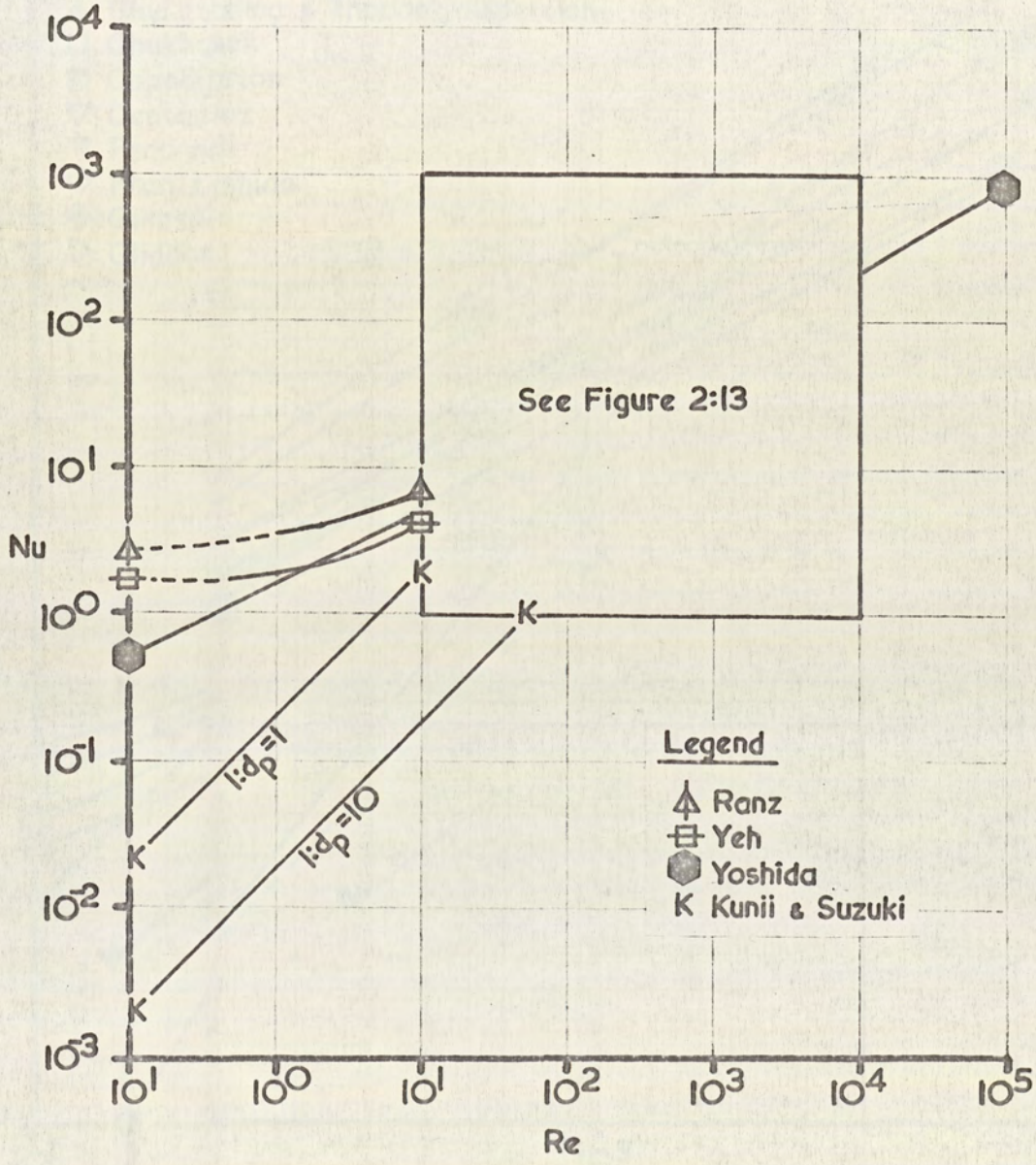

FIGURE 2:12 PREVIOUS PACKED BED HEAT TRANSFER DATA

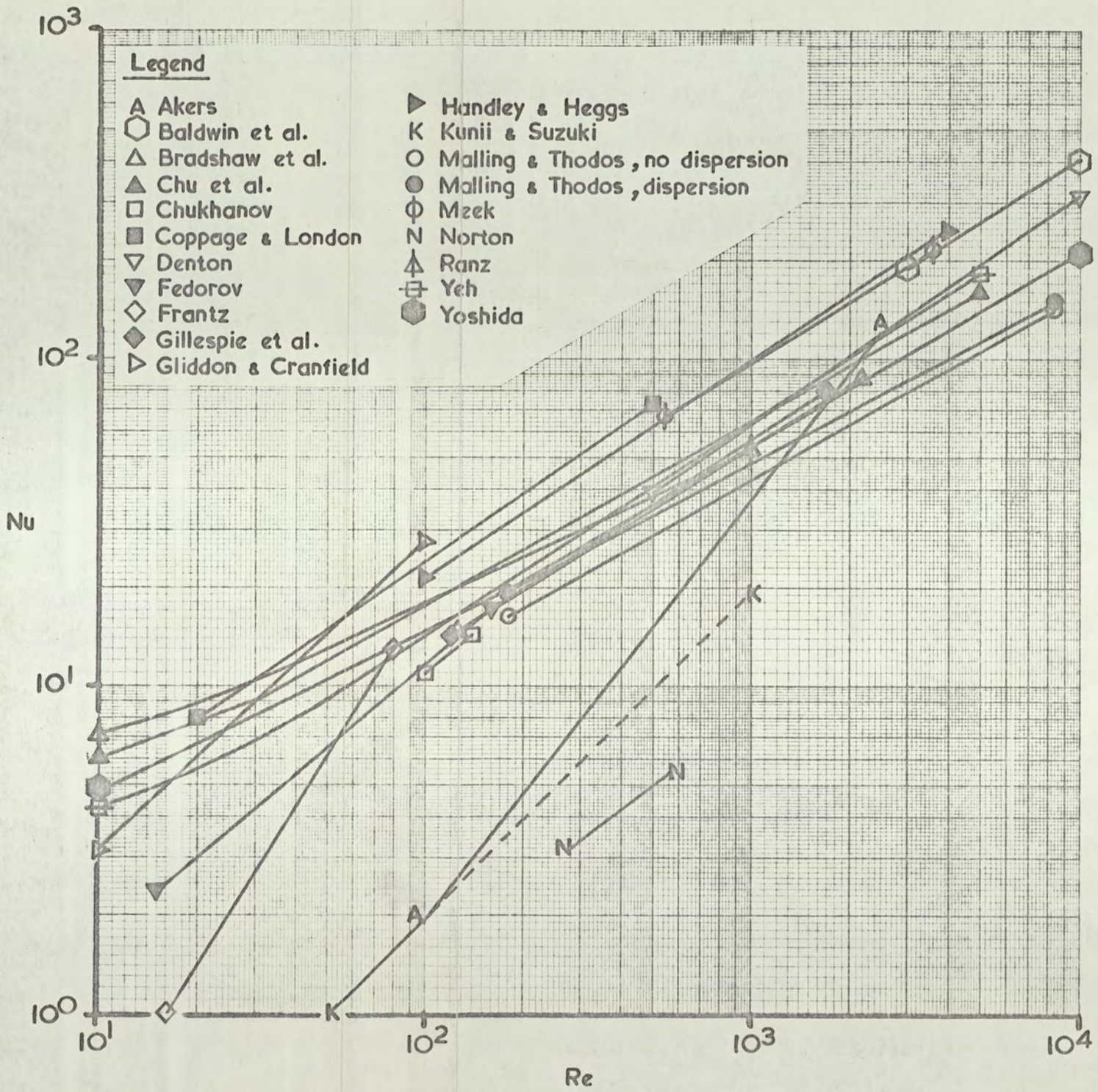

FIGURE 2:13 PREVIOUS PACKED BED HEAT TRANSFER DATA

Table 2:4. Summary of Previous Correlations (Air as Fluid)

Workers	Ref.	Equation Number	Correlation Constants		Reynolds Number Range
			C_6	m_4	
Akers	(2)	(2:20)	0.00496	1.29	100-2400
Baldwin et al.	(55)	(2:40)	0.875	0.67	3000-70000
Bradshaw et al.	(48)	(2:34)	0.708	0.625	125-2200
Chu et al.	(60)	(2:47) (2:48)	1.34 3.64	0.56 0.22	30-5000 1-30
Chukhanov	(38)	(2:30)	0.24	0.83	100-140
Coppage & London	(41)	(2:28)	0.509	0.69	20-500
Denton	(39) (40)	(2:36)	0.497	0.7	500-53000
Fedorov	(38)	(2:49)	0.23	0.863	15-160
Frantz	(32)	(2:19)	0.0117	1.6	8-80
Gillespie et al.	(53)	(2:39)	0.63	0.65	120-1700
Gliddon & Cranfield	(42)	(2:29)	0.36	0.94	2-100
Handley & Heggs	(44)	(2:31)	0.564	0.665	100-400
Kunii & Suzuki	(71)	(2:57)	0.0192 (1:dp=10) 0.192 (1:dp=1)	1.0 1.0	0.07-70 0.07-70

Table 2:4. (Continued)

Workers	Ref.	Equation Number	Correlation Constants		Reynolds Number Range
			C_6	m_4	
Malling & Thodos	(59)	(2:45)	0.875 (No dispersion)	0.563	180-8500
		(2:46)	1.24 (Dispersion)	0.528	180-8500
Meek	(45)	(2:32)	1.33	0.62	540-3600
Norton	(26)	(2:18)	0.0507	0.738	280-565
Ranz	(68)	(2:55)	$Nu=2.0+1.6xRe^{0.5}$		80-1000
Yeh	(65)	(2:53)	0.717	0.65	50-5000
		(2.54)	$Nu=1.69x10^{0.04xRe}$		0.5-10
Yoshida	(69)	(2:51)	1.546	0.49	$Re<180$
		(2:52)	0.912	0.59	$180<Re$

Notes:

(1) All correlations have been reduced to the form

$$Nu=f\ (Re)$$

and generally

$$Nu=C_6.Re^{m_4} \quad \text{.....(2:18)}$$

(2) Where appropriate, voidage taken as 0.4 and Prandtl number as 0.69.[73]

The equation was found to describe the available data on fluidized beds of small particles fairly well for:

$$\frac{l}{d_p} = 10$$

Péclet number was felt to be more appropriate in the region of interest than Reynolds number but for consistency with previous correlations (2:56) may be written as:

$$Nu = \frac{Re.Pr}{60(1-e)} \quad \ldots\ldots\ldots\ldots \quad (2:57)$$

for $0.05 < Re.Pr < 50$

Frantz[32] analysed published fluidized bed data and obtained:

$$Nu = 0.015\ Re^{1.6}\ Pr^{0.67} \quad \ldots\ldots\ldots \quad (2:58)$$

for $8 < Re < 80$

Barker[72] reviewed a great deal of data on fixed and moving beds but did not attempt a general correlation. The results were plotted in terms of:

$$j_H \text{ v. } Re$$

and showed considerable scatter. He pointed out that air had been the fluid in most investigations so the use of j_H was questionable.

A further attempt at unifying previous data is beyond the scope of the present work but a representation in terms of:

$$Nu \text{ v. } Re$$

is given in Figures 2:12 and 2:13 and Table 2:4. This includes general correlations and recent results not reviewed elsewhere.

Although there are discrepancies, the most significant feature is the position of the moving bed data. Norton's results[26]

are an order of magnitude lower than those obtained with fixed beds. Akers' results[2] intersect with the others but the Nusselt numbers are consistent only over a small range of Reynolds numbers. It is conceivable that heat transfer in moving beds could be slightly greater than in fixed due to the velocities of the solids and consequent higher relative Reynolds numbers but it seems unlikely that they could be lower. It is possible that the theoretical models of the moving beds were inadequate. Norton ignored the conduction lag in the particles so his data may have been subject to the same errors as that of Handley and Heggs[44] for glass and alumina. However, Akers[2] did include thermal conductivity. Only Malling and Thodos[59] have accounted for axial dispersion at the relevant Reynolds numbers but their correction was quite small. Radiation may have been significant in Norton's equipment but it would have enhanced the heat transfer.

Although Norton used $d_v:d_p$ ratios of not less than 38, with values between only 6 and 16 serious gas bypassing at the walls probably occurred in Akers' apparatus. The channelling model of Kunii and Suzuki[71] was intended to apply only at low Reynolds numbers. The ratio $1:d_p$ for particles of the sizes used by Akers and Norton would be between 0.1 and 2 so it is doubtful whether the model would have any relevance. However, if the wall effects are superimposed on the randomly distributed dispersion effects, it may be that the effective $1:d_p$ is much greater. Even in moving beds of high $d_v:d_p$ there may be dislocations of the matrix due to friction at the walls as reported by Brinn et al.[74] with sand at $d_v:d_p$ of about 30. It may be coincidence, but the extrapolation of Kunii and Suzuki's equation (2:57) for $1:d_p$ of 10 passes between the data of Akers and Norton.

2.5 Present Objectives

The literature survey demonstrated that the data obtained with fixed beds using a variety of measuring techniques are fairly consistent. The inclusion of fluidized bed results leads to complications but these need not concern us for the purpose of design of tower melting furnaces. However, it has not been possible to correlate melting bed data in the normally accepted manner:

i.e. j_H v. Re

St v. Re

Nu v. Re

and simulation of the preheating zone with moving beds has yielded heat transfer coefficients as much as an order of magnitude less than those in fixed beds.

The objective of the present work is to refine the techniques developed by Norton[26] and Akers[2] and determine whether or not there are significant differences between fixed and moving bed heat transfer.

SECTION 3

THEORY: MOVING BED HEAT TRANSFER

SECTION 3 - THEORY: MOVING BED HEAT TRANSFER

3.1 Choice of Model

Various models could be formulated but the simplest, and most commonly used by previous workers, is that suggested by Furnas[35] involving only forced convection heat transfer in an adiabatic enclosure with particles of infinite thermal conductivity. It has been shown in the preceding section that this model is adequate for small particles of high thermal conductivity but, for large ceramic solids, errors due to the temperature profile within individual particles (intra-particle temperature distribution) become significant.

At low Reynolds numbers, Littman et al.[43] showed that axial dispersion in the fluid and axial conduction between particles are also important. Only Malling and Thodos[59] have compared results from models with and without dispersion in the range of Reynolds number under investigation in the present work and they showed that the difference was small. In comparison with the gross discrepancies between fixed and moving beds reported in the literature, the dispersion correction is quite negligible.

Depending on the system under investigation, other factors may need to be included such as entrance-exit effects, non-uniform fluid and solid velocity and temperature profiles, wall heat losses, wall voidage effects and particle shape. It was felt that the simplest model which would adequately describe the beds used in the present work would be one involving intra-particle temperature distribution and wall heat losses. However, as Furnas's model is ideally suited to design work it was thought that it should be used in parallel with the more sophisticated analysis and an appraisal of its applicability made.

Whichever model is selected, there are two situations for which it must be solved:

(1) Prediction of gas and solid temperature distributions knowing all other bed parameters.

(2) Calculation of heat transfer coefficients from experimental data.

As examples of moving bed heat transfer in cocurrent flow (copper smelting[75], asbestos drying[38]) and for cooling of hot solids (dry quenching of coke[38] and preheating of combustion air[26]) have been reported, these cases will be dealt with also.

3.2 No Intra-Particle Temperature Distribution

The assumptions on which this model is based are:

(1) Individual solid particles are at a uniform temperature at a given position in the bed, i.e. infinite solid thermal conductivity.

(2) The particles are spherical.

(3) Point contact between particles.

(4) No radial temperature or velocity profiles in either the gas or solid streams.

(5) The bed operates at steady state with temperature dependent on position but not time.

(6) The thermophysical properties of the gas and solid are either independent of temperature or adequately represented by mean values obtained by integration with respect to temperature.

(7) No axial dispersion of heat in the gas phase.

(8) No axial conduction of heat between solid particles.

(9) The gas-solid heat transfer coefficient is independent of temperature, i.e. constant throughout the bed.

(10) The only mechanism of heat transfer between fluid and solids

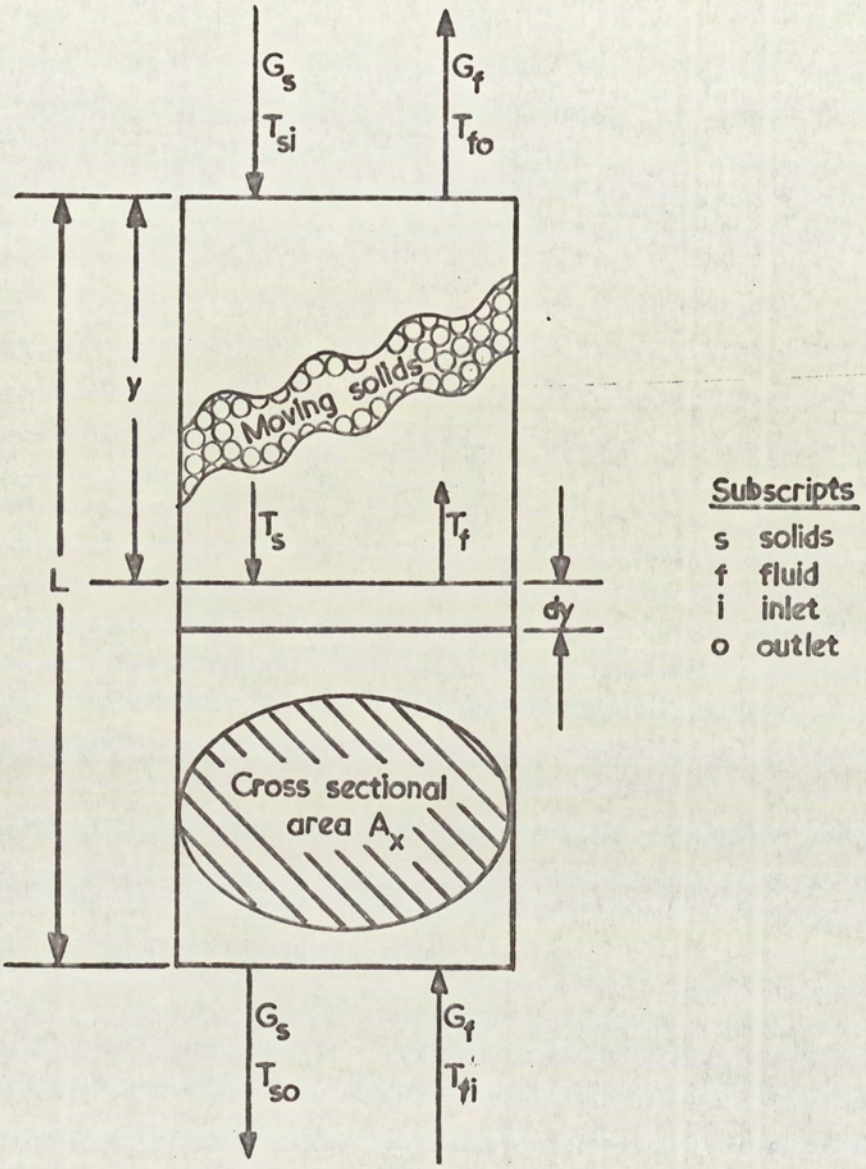

FIGURE 3:1 DIAGRAMMATIC MOVING BED HEAT EXCHANGER

is forced convection. There are no radiative components.
(11) There are no heat losses to the surroundings.

3.2.1 Basic equations

The transfer process may be represented by heat balances over the element of bed height dy and the boundary conditions, see Figure 3:1 :

$$G_f \cdot c_f \cdot A_x \cdot dT_f = h_f \cdot A_x \cdot dy \cdot a\,(T_f - T_s) \quad \ldots\ldots (3:1)$$

$$G_s \cdot c_s \cdot A_x \cdot dT_s = h_f \cdot A_x \cdot dy \cdot a\,(T_f - T_s) \quad \ldots\ldots (3:2)$$

At $y = 0$: $T_f = T_{fo}$, $T_s = T_{si}$

At $y = L$: $T_f = T_{fi}$, $T_s = T_{so}$

3.2.2 Prediction of gas and solid axial temperature distributions

Taking T_{si} as the datum temperature, the heat balance over the height from $y = 0$ to $y = y$ may be written

$$G_f \cdot c_f\,(T_f - T_{si}) = G_f \cdot c_f\,(T_{fo} - T_{si}) + G_s \cdot c_s\,(T_s - T_{si})$$

Rearranging

$$T_f = T_{fo} + \beta(T_s - T_{si}) \quad \ldots\ldots\ldots\ldots (3:3)$$

Where $\beta = \dfrac{G_s \cdot c_s}{G_f \cdot c_f}$

Substituting (3:3) in (3:2)

$$G_s \cdot c_s \cdot dT_s = h_f \cdot a \cdot dy\,[T_{fo} + \beta(T_s - T_{si}) - T_s]$$

Therefore

$$\int_{T_{si}}^{T_s} \frac{dT_s}{[T_{fo} + \beta(T_s - T_{si}) - T_s]} = \int_{0}^{y} \frac{h_f \cdot a \cdot dy}{G_s \cdot c_s}$$

for which the solution for $\beta < 1$ is

$$T_s = T_{si} + \frac{(T_{fo} - T_{si})(1 - \exp^{-m_7})}{(1-\beta)} \quad \ldots\ldots (3:4)$$

and, by substitution into (3:3)

$$T_f = T_{fo} + \frac{\beta(T_{fo}-T_{si})(1-\exp^{-m_7})}{(1-\beta)} \quad \ldots\ldots (3:5)$$

where

$$m_7 = \frac{h_f \cdot a \cdot y\ (1-\beta)}{G_s \cdot c_s}$$

a = specific surface area for heat transfer

$$= \frac{\text{surface area of solids}}{\text{volume of solids + voids}}$$

$$= \frac{\Pi \cdot d_p^{\,2}}{\frac{\Pi \cdot d_p^{\,3}}{6} \times \frac{1}{(1-e)}}$$

$$= \frac{6(1-e)}{d_p} \quad \ldots\ldots\ldots\ldots\ldots (3:6)$$

3.2.3 Analysis of experimental data

(3:1) and (3:2) may be rearranged:

$$\frac{dT_f}{(T_f-T_s)} = \frac{h_f \cdot a \cdot dy}{G_f \cdot c_f} \quad \ldots\ldots\ldots\ldots (3:7)$$

$$\frac{dT_s}{(T_f-T_s)} = \frac{h_f \cdot a \cdot dy}{G_s \cdot c_s} \quad \ldots\ldots\ldots\ldots (3:8)$$

For $\beta<1$, subtracting (3:7) from (3:8):

$$\frac{dT_s-dT_f}{(T_f-T_s)} = h_f \cdot a \cdot dy \left(\frac{1}{G_s \cdot c_s} - \frac{1}{G_f \cdot c_f}\right)$$

$$-\int_{T_{fo},\ T_{si}}^{T_{fi},\ T_{so}} \frac{d(T_f-T_s)}{(T_f-T_s)} = \frac{h_f \cdot a \cdot (1-\beta)}{G_f \cdot c_f \cdot \beta} \int_0^L dy$$

Which gives on integration

$$h_f = \frac{G_f \cdot c_f \cdot \beta}{a.L.(1-\beta)} \log_e \left(\frac{T_{fo}-T_{si}}{T_{fi}-T_{so}} \right) \quad \ldots\ldots\ldots (3:9)$$

3.2.4 Cocurrent flow

As the gas temperature decreases with distance down the bed, (3:1) becomes

$$G_f \cdot c_f \cdot dT_f = -h_f \cdot a \cdot dy \, (T_f - T_s)$$

with the boundary conditions

$$\text{At } y = 0: \; T_f = T_{fi}, \; T_s = T_{si}$$

$$\text{At } y = L: \; T_f = T_{fo}, \; T_s = T_{so}$$

The equations may be solved by the methods indicated in Sections 3.2.2 and 3.2.3. For all values of β:

$$T_s = T_{si} + \frac{(T_{fi}-T_{si})(1-\exp^{-m_8})}{(1+\beta)} \quad \ldots\ldots (3:10)$$

$$T_f = T_{fi} - \frac{\beta.(T_{fi}-T_{si})(1-\exp^{-m_8})}{(1+\beta)} \quad \ldots\ldots (3:11)$$

$$h_f = \frac{G_f \cdot c_f \cdot \beta}{a.L\,(1+\beta)} \log_e \left(\frac{T_{fi}-T_{si}}{T_{fo}-T_{so}} \right) \quad \ldots\ldots\ldots (3:12)$$

where

$$m_8 = \frac{h_f \cdot a \cdot y \, (1+\beta)}{G_s \cdot c_s}$$

3.2.5 Cooling of hot solids

This case may be dealt with either by restatement of the equations and rigorous solution or by similarity. The solutions developed so far are essentially those for any two-fluid heat exchanger so gas and solid may be interchanged. For $\beta<1$:

$$T_f = T_{fi} + \frac{(T_{so}-T_{fi})(1-\exp^{-m_9})}{(1-\beta)} \quad \ldots\ldots\ldots (3{:}13)$$

$$T_s = T_{so} + \frac{\beta(T_{so}-T_{fi})(1-\exp^{-m_9})}{(1-\beta)} \quad \ldots\ldots\ldots (3{:}14)$$

$$h_f = \frac{G_f \cdot c_f \cdot \beta}{a.L\,(1-\beta)} \log_e\left(\frac{T_{si}-T_{fo}}{T_{so}-T_{fi}}\right) \quad \ldots\ldots\ldots (3{:}15)$$

Where

$$m_9 = \frac{h_f \cdot a.(L-y)(1-\beta)}{G_s \cdot c_s}$$

3.3 Intra-Particle Temperature Distribution

The assumptions on which this model is based are exactly as set out in Section 3.2 except that the restriction to solids of infinite thermal conductivity is withdrawn and radial temperature profiles within individual particles are recognised.

3.3.1 Basic equations

The heat transferred from the gas stream to the surface of the particles is still represented by (3:1):

$$G_f \cdot c_f \cdot A_x \cdot dT_f = h_f \cdot A_x \cdot dy.a(T_f - T_5) \quad \ldots\ldots (3{:}16)$$

where T_5 is the particle surface temperature, but (3:2) is replaced by an expression for conduction through the solid surface

$$k_s \cdot \Pi \cdot d_p^2 \left(\frac{\partial T_5}{\partial r}\right)_{r=R} = h_f \cdot \Pi \cdot d_p^2 (T_f - T_5) \quad \ldots\ldots (3{:}17)$$

and by another for conduction within the particles

$$\frac{c_s \cdot \rho_s}{k_s} \frac{\partial T_s}{\partial t} = \frac{\partial^2 T_s}{\partial r^2} + \frac{2}{r}\frac{\partial T_s}{\partial r} \quad \ldots\ldots\ldots (3{:}18)$$

The boundary conditions of gas temperature remain as for the simple model but for the solid there is the added dependence on sphere radius.

3.3.2 Prediction of gas and solid axial temperature distributions

Lovell and Karnofsky[76] developed the Schmidt graphical method of solution of transient heat conduction problems for moving bed analysis. Although only approximate, it was an improvement over the simple model based on the assumption of infinite solid thermal conductivity. The method was superseded by an exact analytical solution formulated by Munro and Amundson[77] using Laplace transformation. Their solution for the gas temperature for β not equal to 1 is

$$\frac{T_f - T_{si}}{T_{fo} - T_{si}} = 1 + 6.\beta \sum_{j=1}^{j=\infty} \frac{1 - \exp^{-W_j^2 . z}}{(3\beta + W_j^2/Bi)^2 - 3(3\beta + W_j^2/Bi) + W_j^2(1 + 2/Bi)} \quad \ldots\ldots (3{:}19)$$

where $z = \dfrac{k_s(1-e)y}{G_s . c_s . R^2}$, the Fourier number, dimensionless,

$Bi = \dfrac{h_f . R}{k_s}$, the Biot number, dimensionless,

and W_j is the root of the transcendental equation

$$[(1-1/Bi)W_j^2 - 3\beta]\tan W_j + (3\beta + W_j^2/Bi)W_j = 0 \quad \ldots\ldots (3{:}20)$$

Timofeev[38] produced a solution of similar complexity. For $\beta < 1$ the solid surface temperature is given by

$$\frac{T_5 - T_{si}}{T_{fo} - T_{si}} = \frac{1}{1-\beta} + 2 \sum_{j=1}^{j=\infty} \frac{\sin W_j . \exp^{-W_j^2 z}}{f(W_j)} \quad \ldots\ldots (3{:}21)$$

where $f(W_j) = \dfrac{6\beta}{W_j^2}(\sin W_j - W_j \cos W_j) - \dfrac{W_j^2 - \frac{1}{2}W_j . \sin 2W_j}{\sin W_j - W_j \cos W_j}$

and Wj is the root of the transcendental equation

$$\frac{1}{Bi} = \frac{\tan W_j}{\tan W_j - W_j} - \frac{3\beta}{W_j^2} \qquad \ldots\ldots\ldots\ldots (3{:}22)$$

Kitaev et al.[38] have reduced the labour involved in applying Timofeev's solution by tabulating many of the roots of equation (3:22) and factors of f (W_j) and also representing the results graphically as

$$\frac{T_s - T_{si}}{T_{fo} - T_{si}} \quad \text{v.} \quad z$$

for the ranges

$$0.1 \leq \beta \leq 8.0$$
$$0.02 \leq Bi \leq \infty$$
$$0 \leq z \leq 2.0$$

Timofeev[38] also gave a simpler solution for the average solids temperature provided $z \geq 0.1$:

$$\frac{T_{sm} - T_{si}}{T_{fo} - T_{si}} = 1 - C_{11} \cdot \exp[-C_{12}(1-\beta)3.Bi.z] \qquad \ldots\ldots (3{:}23)$$

where C_{11} and C_{12} are functions of Bi and β and are expressed graphically.

The approach to the problem by Leung and Quon[78] was to transform the partial differential equation (3:18) into a set of ordinary differential equations using third order correct finite difference formulae. The ordinary equations were then solved either numerically using the Runge-Kutta-Gill[79] explicit finite difference method or by analogue computation. Although approximate, these techniques were considerably better than Lovell and Karnofsky's[76] graphical method and compared very well with the analytical solution of Munro and Amundson[77].

Akers'[2] analogue computer solution was similar to that of Leung and Quon[78] except that he used second order correct finite

differences. The program was checked against the results of Munro and Amundson[77] and Leung and Quon[78] for a problem originally posed by Lovell and Karnofsky[76]. That part of the program which accounted for solid phase conduction was checked against the analytical solution for heat transfer to a sphere in an infinite isothermal medium. Both checks demonstrated that the method was quite adequate. At Biot numbers less than 0.2, the stability of the circuit was very sensitive to the setting of the potentiometers but this was not regarded as a serious problem.

It was proposed that Akers'[2] solution should be used in the present work so the ordinary differential equations will now be derived and the method of implementation indicated.

The basic equations (3:16), (3:17) and (3:18) have been stated already and to those the following may be added:

(1) Due to symmetry, there will be a minimum temperature at the sphere centre for any position in the bed

$$\text{i.e.} \left(\frac{\partial T_s}{\partial r}\right)_{r=o} = 0 \quad \ldots\ldots\ldots\ldots\ldots\ldots \quad (3:24)$$

(2) Elapsed time and position in the bed are related by

$$G_s . A_x . t = y . A_x . \rho_s . (1-e)$$

$$\therefore t = \frac{y . \rho_s (1-e)}{G_s} \quad \ldots\ldots\ldots\ldots\ldots\ldots \quad (3:25)$$

It is convenient to use dimensionless variables to generalise the results and satisfy the amplitude scaling requirements of analogue computation:

(3) Dimensionless sphere radius variable x.

$$x = \frac{r}{R} \quad \ldots\ldots\ldots\ldots\ldots\ldots \quad (3:26)$$

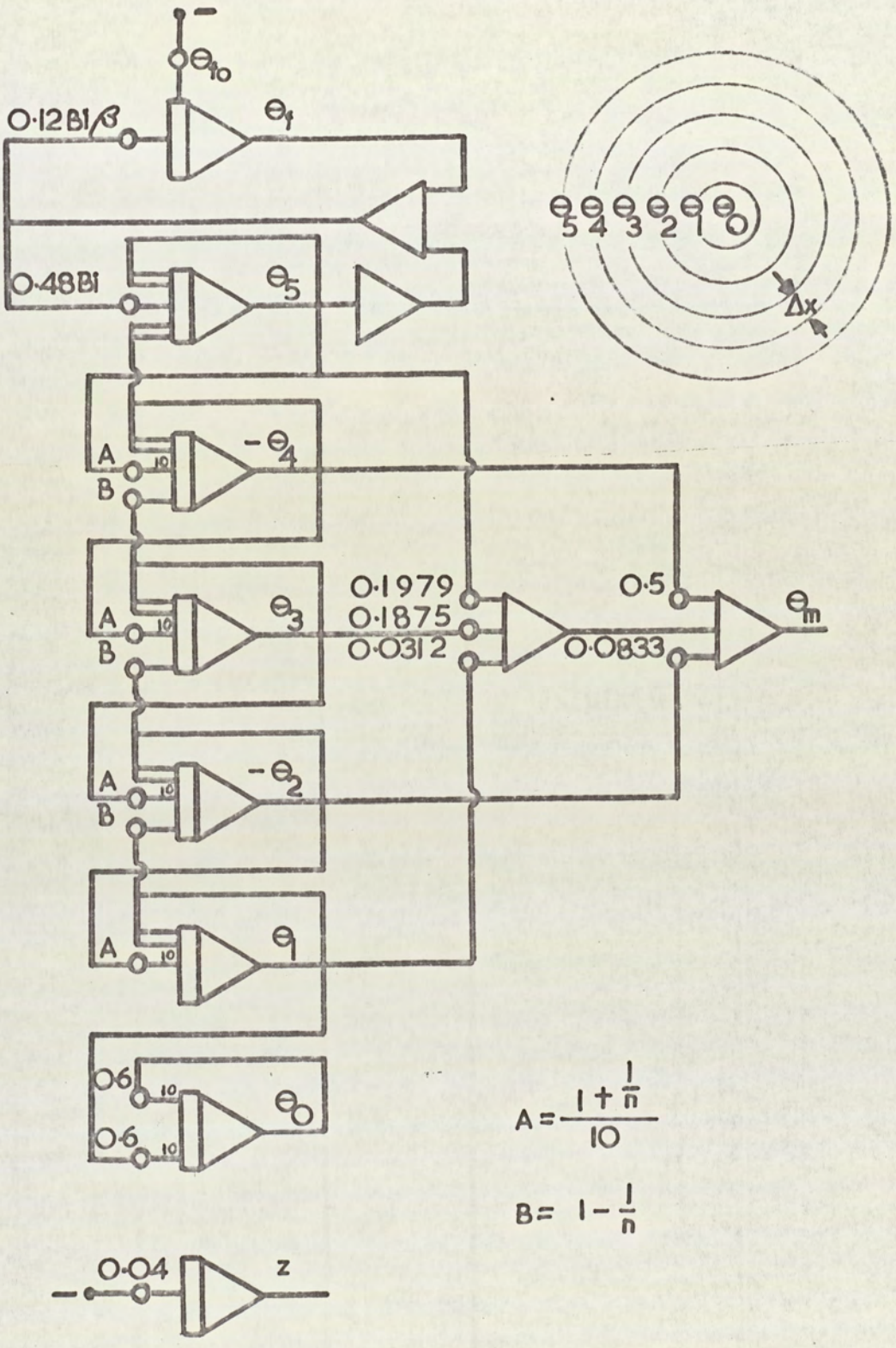

FIGURE 3:2 ANALOGUE COMPUTER CIRCUIT FOR PREDICTION OF FLUID AND SOLIDS TEMPERATURE DISTRIBUTIONS IN A MOVING BED HEAT EXCHANGER

(4) Dimensionless temperature variables θ.

$$\theta = \frac{T-T_{si}}{T_{fi}-T_{si}} \quad \ldots\ldots\ldots\ldots\ldots\ldots\ldots\ldots (3:27)$$

(5) Dimensionless bed length z (Fourier number).

$$z = \frac{k_s(1-e)y}{G_s.c_s.R^2} \quad \ldots\ldots\ldots\ldots\ldots\ldots\ldots\ldots (3:28)$$

Overall heat balance

The overall heat balance from y = 0 to y = L, equation (3:3), may be expressed in terms of dimensionless temperatures:

$$(T_{fi}-T_{fo}) = \beta(T_{so}-T_{si})$$

$$(\theta_{fi}-\theta_{fo}) = \beta(\theta_{so}-\theta_{si})$$

$$(1-\theta_{fo}) = \beta(\theta_{so}-0)$$

$$1-\theta_{fo}-\beta.\theta_{so} = 0 \quad \ldots\ldots\ldots\ldots\ldots\ldots\ldots\ldots (3:29)$$

Interior of the sphere

On substituting for t, r and T_s, rearranging and substituting z, (3:18) becomes

$$\frac{\partial\theta_s}{\partial z} = \frac{\partial^2\theta_s}{\partial x^2} + \frac{2}{x}\frac{\partial\theta_s}{\partial x} \quad \ldots\ldots\ldots\ldots\ldots\ldots\ldots\ldots (3:30)$$

If the spheres are considered to be made up of n spherical shells of thickness Δx, as shown in Figure 3:2, (3:30) may be reduced to a set of ordinary differential equations by use of Taylor series finite difference formulae:

$$\frac{\partial\theta_s}{\partial x} = \frac{\theta_{n+1} - \theta_{n-1}}{2.\Delta x} \quad \ldots\ldots\ldots\ldots\ldots\ldots\ldots\ldots (3:31)$$

$$\frac{\partial^2\theta_s}{\partial x^2} = \frac{\theta_{n+1} - 2.\theta_n + \theta_{n-1}}{(\Delta x)^2} \quad \ldots\ldots\ldots\ldots\ldots\ldots\ldots\ldots (3:32)$$

At the nodes between shells

$$x = n.\Delta x \quad \ldots\ldots\ldots\ldots\ldots\ldots\ldots\ldots\ldots\ldots (3:33)$$

On substitution, (3:30) becomes

$$\frac{d\theta_n}{dz} = \frac{\theta_{n+1}\left(1+\frac{1}{n}\right)-2.\theta_n+\theta_{n-1}\left(1-\frac{1}{n}\right)}{(\Delta x)^2} \quad \ldots\ldots\ldots\ldots (3:34)$$

At the sphere centre

(3:24) becomes

$$\left(\frac{\partial\theta_s}{\partial x}\right)_{x=o} = 0 \quad \ldots\ldots\ldots\ldots\ldots\ldots (3:35)$$

so, at x = 0, (3:30) becomes

$$\frac{\partial\theta_o}{\partial z} = \frac{\partial^2\theta_o}{\partial x^2} + \frac{2}{0}\,x^0 \quad \ldots\ldots\ldots\ldots\ldots\ldots (3:36)$$

i.e. indeterminate so L'Hôpital's rule must be applied. This may be stated as

If $\frac{f(x)}{g(x)}$ is indeterminate, then evaluate $\frac{f(x)}{g(x)}$ as $\frac{f'(x)}{g'(x)}$ or $\frac{f''(x)}{g''(x)}$ etc.

Now $f(x) = \frac{\partial\theta_s}{\partial x}$, $f'(x) = \frac{\partial^2\theta_s}{\partial x^2}$

and $g(x) = x$, $g'(x) = 1$

so (3:36) may be replaced by

$$\frac{\partial\theta_o}{\partial_z} = 3\,\frac{\partial^2\theta_o}{\partial x^2} \quad \ldots\ldots\ldots\ldots\ldots\ldots (3:37)$$

Substituting (3:32) gives

$$\frac{d\theta_o}{dz} = \frac{3(\theta_1-2.\theta_o+\theta_{-1})}{(\Delta x)^2}$$

But, by sphere symmetry,

$$\theta_1 = \theta_{-1}$$

so

$$\frac{d\theta_o}{dz} = \frac{6(\theta_1-\theta_o)}{(\Delta x)^2} \quad \ldots\ldots\ldots\ldots\ldots\ldots (3:38)$$

At the sphere surface

On substituting for r, T_f and T_s, (3:17) becomes

$$\frac{\partial\theta_5}{\partial x} = \frac{h_f.R}{k_s}(\theta_f-\theta_s)$$

$$= Bi\ (\theta_f-\theta_s)$$

Introducing the finite difference approximation:

$$\frac{\theta_i-\theta_4}{2.\Delta x} = Bi\ (\theta_f-\theta_s) \quad \ldots\ldots\ldots\ldots\ldots\ldots\ldots\ldots (3:39)$$

where θ_i is an imaginary solids temperature.

At the solid surface (3:34) becomes

$$\frac{d\theta_5}{dz} = \frac{\theta_i(1+\frac{1}{5})-2\theta_5+\theta_4(1-\frac{1}{5})}{(\Delta x)^2} \quad \ldots\ldots\ldots\ldots\ldots\ldots (3:40)$$

Eliminating θ_i between (3:39) and (3:40):

$$\frac{d\theta_5}{dz} = \frac{(1+\frac{1}{5})2.\Delta x.Bi(\theta_f-\theta_5)-2.\theta_5+2\theta_4}{(\Delta x)^2} \quad \ldots\ldots\ldots\ldots (3:41)$$

Throughout the sphere

Using a 6 point, closed end Newton-Coates quadrature[79], it is shown in Appendix 1.1 that the mean solid temperature is given by

$$\theta_{sm} = \frac{57.\theta_5}{288} + \frac{\theta_4}{2} + \frac{3.\theta_3}{16} + \frac{\theta_2}{12} + \frac{\theta_1}{32} \quad \ldots\ldots\ldots\ldots (3:42)$$

In the gas phase

On substituting for T_f, T_5 and a, rearranging and substituting z, (3:16) becomes

$$\frac{d\theta_f}{dz} = \frac{3.\beta Bi.(\Delta x)^2(\theta_f-\theta_5)}{(\Delta x)^2} \quad \ldots\ldots\ldots\ldots\ldots\ldots (3:43)$$

Position in the bed

This is effectively represented on the analogue computer by

machine time and may be monitored by continuously integrating a constant input of 1 machine unit, i.e.

$$\frac{dz}{dz} = 1 = \frac{(\Delta x)^2}{(\Delta x)^2} \quad \ldots\ldots\ldots\ldots\ldots\ldots\ldots\ldots\ldots\ldots (3{:}44)$$

Summary

The complete description of moving bed heat transfer involves the simultaneous solution of the following equations:

Overall heat balance: (3:29).

At the sphere centre (n = 0): (3:38).

Interior of the sphere (n = 1, 2, 3, 4): (3:34).

At the sphere surface (n = 5): (3:41).

Throughout the sphere: (3:42).

In the gas phase: (3:43).

Position in the bed: (3:44).

With the boundary conditions:

Initial: z = 0

$$\theta_s = \theta_{si} = \theta_n = 0, \text{ for } n = 0, 1, 2, 3, 4, 5$$

$$\theta_f = \theta_{fo}$$

Final: $z = z_L$

$$\theta_s = \theta_{so} = f(n)$$

$$\theta_f = \theta_{fi} = 1$$

Time scaling

All equations are of the form

$$\frac{d(T \text{ or } z)}{dz} = \frac{f(T \text{ or } z)}{(\Delta x)^2}$$

With inputs to the integrators of f(T or z), to generate T or z the integrator gains should be

$$\frac{1}{(\Delta x)^2} = 25.$$

This is physically too great for the machine but the problem may be conveniently time scaled by reducing the gains by the factor

$$(\Delta x)^2 = \frac{1}{25}$$

i.e. the calculation is slowed down 25 times. Thus the time for Z to grow from 0 to 1 machine unit is 25 s with integrator time constants of 1 s.

Amplitude scaling

The dimensionless temperatures have been defined such that they cannot exceed unity so further amplitude scaling is unnecessary.

The circuit

The analogue computer circuit is shown in Figure 3.2. The input parameters are Bi, β and θ_{fo}. The calculation starts at the top of the bed and follows the progress of a typical sphere down through the bed until the gas inlet point is reached where

$$\theta_f = \theta_{fi} = 1.$$

Thus the temperature distributions through the bed in the gas and solid phases are obtained and may be output to a digital voltmeter or a graph plotter.

3.3.3 Analysis of experimental data

It is clear that the analytical solutions described in the preceding section are unsuitable for the direct calculation of heat transfer coefficients from the measured variables of moving beds. Kitaev et al.'s[38] graphs enable the indirect use of Timofeev's solution but interpolation errors are inevitable and the small range of Z values (from 0 to maxima between 0.4 and 2.0, depending on the value of β) is a serious restriction.

The resistance equation (2:10) provides a very simple solution and has been employed by Kitaev et al.[38] and Bradshaw et al.[48].

The overall heat transfer coefficient may be calculated from the terminal temperatures using equation (3:9):

$$U = \frac{G_f . c_f . \beta}{a.L.(1-\beta)} \log_e \left(\frac{T_{fo} - T_{si}}{T_{fi} - T_{so}} \right) \quad \ldots\ldots\ldots\ldots\ldots (3:9)$$

Substitution in (3:45) then yields the true film coefficient:

$$\frac{1}{U} = \frac{1}{h_f} + \frac{d_p}{10.k_s} \quad \ldots\ldots\ldots\ldots\ldots\ldots\ldots (2:10)$$

$$h_f = \frac{10.U.k_s}{10.k_s - U.d_p} \quad \ldots\ldots\ldots\ldots\ldots\ldots\ldots (3:45)$$

Kitaev et al.[38] described the proof of (2:10) by hydraulic analogy for the case of a single sphere in an infinite isothermal medium. Bradshaw et al.[48] provided an analytical proof of it for step and exponential inputs to fixed beds. However, Wartmann and Mertes[80] suggested that for moving beds the constant C_5 in the conduction lag term was a function of Bi and β. They gave

$$8 < C_5 < 12$$

for $0.1 < Bi < 10$

$$0.1 < \beta < 2$$

and $C_5 = 10$

for $\beta = 1$

Analogue computer solutions are quite feasible, particularly if parallel logic facilities are available, and seem best suited to the present needs. They have the advantage of generating the temperature distributions, if these are required, and short computation time. It will be shown later that the incorporation of wall heat losses requires only trivial modifications to the circuitry.

The analogue computation of the gas film heat transfer coefficients from experimental data must be carried out iteratively.

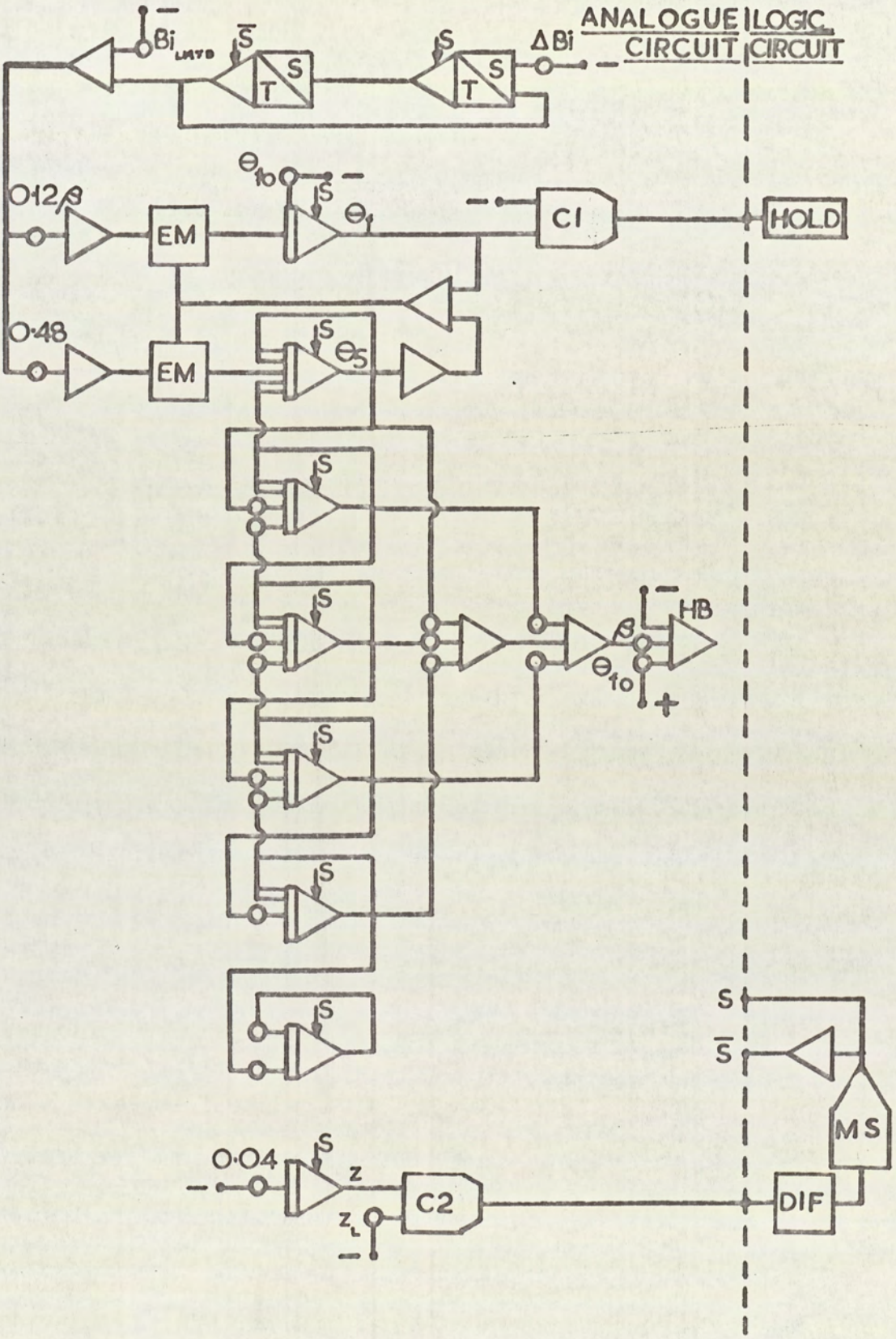

FIGURE 3:3 HYBRID-ANALOGUE COMPUTER CIRCUIT FOR ANALYSIS OF MOVING BED DATA

Equation (3:9) provides a first approximation to the coefficient which is an underestimate as it includes the conduction lag. If this value is input to the program, the temperatures will not have risen to the values appropriate to the bottom of the bed when that position is reached. The Biot number is then progressively increased and the calculation rerun until

$$\theta_f = \theta_{fi} = 1$$

at $z = z_L$

This may be done by manual control of the initial condition, operate and hold modes and incrementing of the Biot number potentiometer. This is particularly tedious and time consuming but the labour may be reduced considerably if a hybrid computer is available. Control may be effected automatically by logic signals which themselves are controlled by the state of the analogue computation. Such a circuit is shown in Figure 3:3. Control is accomplished in the following manner:

(1) Hold and subsequent reset follows from the test of bed length by comparator C2. This triggers the differentiator and, in turn, the monostable and thereby resets the calculation to Z = 0.

(2) Switching of the logic by the monostable reverses the rôles of the two track-store amplifiers and consequently increments the Biot number.

(3) After several iterations the correct Biot number is achieved and

$$\theta_f = \theta_{fi} = 1 \text{ at } z = z_L$$

θ_f trips comparator C1 and the final hold occurs. The accuracy of the solution can be checked by the output of the amplifier HB. If the heat balance is satisfied the output should be zero, as given by equation (3:29). As the rate of solution is no longer restricted

by human reactions, the calculation may be speeded up by as much as 100 times by decreasing the integrator time constants.

3.3.4 Cocurrent flow

As was pointed out in Section 3.2.4, the heat balance over the increment dy becomes

$$G_f \cdot c_f \cdot dT_f = -h_f \cdot a \cdot dy(T_f - T_s)$$

or, in dimesionless variables,

$$\frac{d\theta_f}{dz} = -\frac{3 \cdot \beta \cdot Bi \cdot (\Delta_x)^2 \cdot (\theta_f - \theta_5)}{(\Delta x)^2} \quad \ldots\ldots\ldots\ldots\ldots\ldots \quad (3:46)$$

with the boundary conditions

At $Z = 0$: $\theta_f = \theta_{fi} = 1$, $\theta_s = \theta_{si} = 0$

At $Z = z_L$: $\theta_f = \theta_{fo}$, $\theta_s = \theta_{so} = f(n)$

Thus the computation is run until

$$\theta_f = \theta_{fo}$$

rather than

$$\theta_f = \theta_{fi} = 1.$$

3.3.5 Cooling of hot solids

The heating model is equally applicable to cooling and, provided that the dimensionless temperatures are defined as before, it is not even necessary to modify the logic:

$$\theta = \frac{T - T_{si}}{T_{fi} - T_{si}} = \frac{T_{si} - T}{T_{si} - T_{fi}}$$

At $Z = 0$: $\theta_f = \theta_{fo}$, $\theta_s = \theta_{si} = 0$

At $Z = Z_L$: $\theta_f = \theta_{fi} = 1$, $\theta_s = \theta_{si} = f(n)$

Thus the boundary conditions are exactly as for heating.

The possibility of there being a temperature distribution in the solids at entry to the bed should not be overlooked but it does not introduce any real problems. It simply requires that initial

conditions be set on the sphere temperature integrators.

3.4 Non-Adiabatic Enclosure

The significance of wall heat losses will be discussed later. There are two situations requiring modelling:

(1) Determination of wall heat transfer coefficients using experimental data obtained from steady state, fixed beds.

(2) Incorporation of the heat losses into the moving bed model using the coefficients determined under steady state conditions.

In both situations it is assumed that the heat transfer to the column walls occurs solely by forced convection from the gas stream, i.e. conduction from the solids to the wall is negligible, and that the air remains well mixed at any given bed height, i.e. no radial temperature profiles in either the gas or solids. A further assumption is that the separate processes of forced convection at the inside surface, conduction through the wall and natural convection at the outside surface may be represented by an overall process involving the mean temperature difference between the ambient air and gas flowing through the bed.

3.4.1 Fixed beds

The heat balance over the element dy of a fixed bed at steady state is

$$G_f \cdot \frac{\Pi \cdot d_v^2}{4} \cdot c_f \cdot dT_f = U_w \cdot \Pi \cdot d_v \cdot dy (T_f - T_a) \quad \ldots\ldots\ldots (3:47)$$

where U_w is the overall wall heat transfer coefficient based on the inside surface area of the column.

$$\int_{T_{fo}}^{T_{fi}} \frac{dT_f}{(T_f - T_a)} = \int_0^L \frac{4 \cdot U_w \cdot dy}{d_v \cdot G_f \cdot c_f} \quad \ldots\ldots\ldots\ldots\ldots (3:48)$$

As the surroundings are effectively infinite, T_a is constant so (3:48) may be integrated to give

$$\left[\log_e(T_f-T_a)\right]_{T_{fo}}^{T_{fi}} = \frac{4.U_w.L}{d_v.G_f.c_f}$$

Whence

$$U_w = \frac{d_v.G_f.c_f}{4.L} \log_e\left(\frac{T_{fi}-T_a}{T_{fo}-T_a}\right) \quad \ldots\ldots\ldots\ldots (3:49)$$

Now, the total heat lost by the gas stream is

$$Q_w = G_f.c_f.A_x\,(T_{fi}-T_{fo}) \quad \ldots\ldots\ldots\ldots\ldots (3:50)$$

Eliminating $G_f.c_f$ between (3:49) and (3:50) gives

$$Q_w = U_w.\Pi.d_v.L.\Delta T_{lmw} \quad \ldots\ldots\ldots\ldots\ldots (3:51)$$

where

$$\Delta T_{lmw} = \frac{(T_{fi}-T_{fo})}{\log_e\left(\frac{T_{fi}-T_a}{T_{fo}-T_a}\right)} \quad \ldots\ldots\ldots\ldots (3:52)$$

3.4.2 Moving beds

Similarly, consider the heat balances over the element dy of the moving bed:

$$G_f.c_f.A_x.dT_f = h_f.A_x.a.dy\,(T_f-T_s) + U_w.\Pi.d_v.dy\,(T_f-T_a) \quad \ldots\ldots\ldots (3:53)$$

and

$$G_s.c_s.A_x.dT_s = h_f.A_x.a.dy\,(T_f-T_s) \quad \ldots\ldots\ldots\ldots (3:54)$$

and over the height from y = 0 to y = y:

$$G_f.c_f.A_x(T_f-T_{si}) = G_f.c_f.A_x(T_{fo}-T_{si}) + G_s.c_s.A_x(T_s-T_{si}) + U_w.\Pi.d_v.y(T_f-T_a)_m \quad \ldots\ldots\ldots (3:55)$$

where $(T_f-T_a)_m$ is the mean temperature difference between the gas stream and the ambient air over the height from y = 0 to y = y.

It seems unlikely that simple, analytical solutions to (3:53), (3:54) and (3:55) could be found which would be comparable with (3:9). In the present work, two approximate solutions were used, one based on (3:9) and another, more exact one, involving analogue computation.

3.4.3 Moving beds: No intra-particle temperature distribution: Logarithmic mean temperature difference solution

Equation (3:9) has been derived for an adiabatic exchanger:

$$h_f = \frac{G_f \cdot c_f \cdot}{a.L}\left(\frac{\beta}{1-\beta}\right)\log_e\left(\frac{T_{fo}-T_{si}}{T_{fi}-T_{so}}\right)$$

This may be re-expressed as

$$\log_e\left(\frac{T_{fo}-T_{si}}{T_{fi}-T_{so}}\right) = h_f.a.L\left(\frac{1}{G_s.c_s} - \frac{1}{G_f.c_f}\right)$$

Now the heat transfer rates are given by

$$Q_f = G_f.c_f.A_x\,(T_{fi}-T_{fo}) \quad \ldots\ldots\ldots\ldots\ldots\ldots \quad (3:56)$$

$$Q_s = G_s.c_s.A_x\,(T_{so}-T_{si}) \quad \ldots\ldots\ldots\ldots\ldots\ldots \quad (3:57)$$

Substituting

$$\log_e\left(\frac{T_{fo}-T_{si}}{T_{fi}-T_{so}}\right) = h_f.a.L\left(\frac{A_x.(T_{so}-T_{si})}{Q_s} - \frac{A_x\,(T_{fi}-T_{fo})}{Q_f}\right) \quad \ldots \quad (3,58)$$

For the adiabatic case

$$Q = Q_f = Q_s$$

$$\therefore Q = h_f.a.L.A_x\,\frac{[(T_{fo}-T_{si}) - (T_{fi}-T_{so})]}{\log_e\left(\frac{T_{fo}-T_{si}}{T_{fi}-T_{so}}\right)}$$

$$= h_f.a.L.A_x.\Delta T_{lm} \quad \ldots\ldots\ldots\ldots\ldots\ldots\ldots\ldots \quad (3:59)$$

For the non-adiabatic case, a first approximation to h_f may be obtained from (3:59) by using

$$Q = Q_s = Q_f - Q_w$$

where Q_w is given by (3:51) and (3:52).

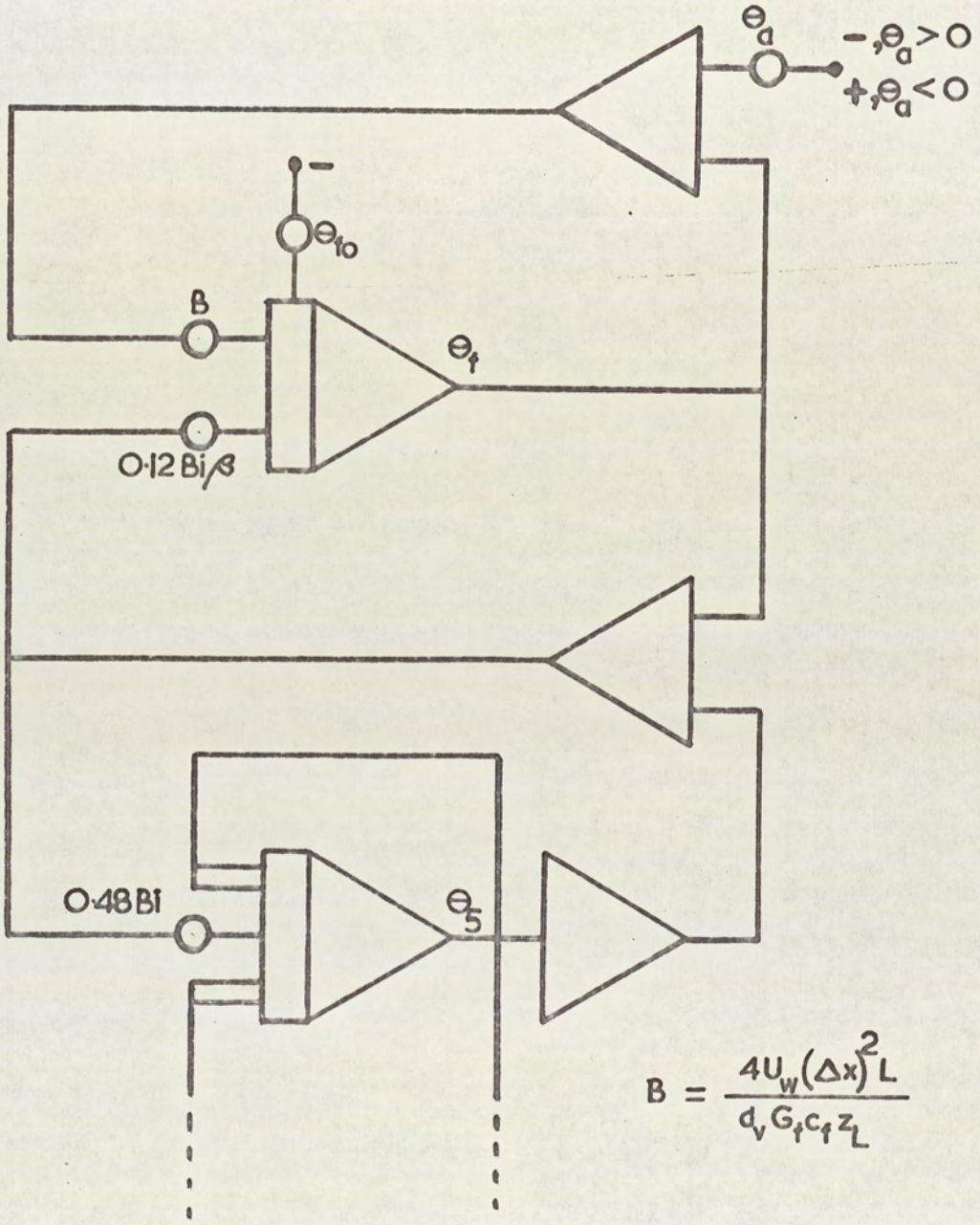

FIGURE 3:4 ANALOGUE COMPUTER CIRCUIT FOR NON-ADIABATIC MOVING BEDS

3.4.4 Moving beds: No intra-particle temperature distribution: Analogue computer solution

The heat balances over the element dy are

$$G_s \cdot c_s \cdot A_x \cdot dT_s = h_f \cdot a \cdot A_x \cdot dy \, (T_f - T_s) \quad \ldots\ldots\ldots\ldots (3{:}2)$$

and

$$G_f \cdot c_f \cdot A_x \cdot dT_f = h_f \cdot a \cdot A_x \cdot dy \, (T_f - T_s) + U_w \cdot \Pi \cdot d_v \cdot dy \, (T_f - T_a) \quad \ldots\ldots\ldots\ldots (3{:}60)$$

On rearranging and substituting for a, A_x and the dimensionless variables z and θ, as in Section 3.3.2, it may be shown that

$$\frac{d\theta_s}{dz} = \frac{3 \cdot Bi (\Delta x)^2 (\theta_f - \theta_s)}{(\Delta x)^2} \quad \ldots\ldots\ldots\ldots\ldots\ldots (3{:}61)$$

and

$$\frac{d\theta_f}{dz} = \frac{3 \cdot Bi \cdot \beta (\Delta x)^2 (\theta_f - \theta_s)}{(\Delta x)^2} + \frac{4 \cdot U_w (\Delta x)^2 L \cdot (\theta_f - \theta_a)}{d_v \cdot G_f \cdot c_f (\Delta x)^2 \cdot z_L} \quad \ldots (3{:}62)$$

The overall heat balance may be obtained by substituting (3:2) in (3:60) and integrating over the whole bed:

$$G_f \cdot c_f \cdot A_x \, (T_{fi} - T_{fo}) = G_s \cdot c_s \cdot A_x \, (T_{so} - T_{si}) + U_w \cdot \Pi \cdot d_v \int_0^L (T_f - T_a) dy \quad \ldots\ldots (3{:}63)$$

On substituting and rearranging this becomes

$$1 - \theta_{fo} - \beta \cdot \theta_{so} - \frac{4 \cdot U_w \cdot (\Delta x)^2 \cdot L}{d_v \cdot G_f \cdot c_f (\Delta x)^2 \cdot z_L} \int_0^{z_L} (\theta_f - \theta_a) dz = 0 \quad \ldots\ldots (3{:}64)$$

The analogue computer circuit for the solution of equations (3:61 and 62) is shown in Figure 3:4.

3.4.5 Moving beds: Intra-particle temperature distribution: Analogue computer solution

It can be readily appreciated that the sphere conduction

equations remain unchanged. Only the relationships for the gas temperature and the overall heat balance differ from the adiabatic case and are exactly as derived in the previous section and given as equations (3:62 and 64).

3.5 Digital Simulation of Analogue Computation

Akers[2] used an E.A.L. TR10 analogue computer to determine moving bed temperature distributions knowing the bed parameters and an E.A.L. TR48 hybrid computer with parallel digital logic for analysis of experimental data. In the present work, the TR10 was fairly satisfactory but iterative solution using the more sophisticated machine proved impossible. The control logic was quite adequate but considerable problems were experienced with the analogue circuitry. The rate of integration was variable and drift was quite noticeable. Servo setting of potentiometers was inaccurate and the read-out devices tended to load the measured outputs. As the problems seemed intractable in the time available, the possibilities of digital computer solutions were considered.

In recent years various digital computer programs have been developed which simulate the operations of analogue computation. Gay and Akers[81] applied the I.C.L. 1900 analogue computer simulation program to a moving bed problem which will be dealt with in Section 3.6.1. They showed that the accuracy of the program compared well with analytical and true analogue solutions. Integration was performed using the Runge-Kutta-Merson[82] fourth order finite difference procedure with automatic adjustment of the step size. The program offered advantages of increased accuracy of multiplication, no necessity for amplitude scaling and considerable improvements in function generation, although the latter is of no

consequence in the present context. However, it adhered rigidly to analogue format and offered few logic facilities. It could only be used to give the temperature distribution knowing the heat transfer coefficient. It could be used with several, successive values of Biot number to obtain the true value by interpolation but this would entail considerable computer time and probably would be inferior to manual operation of the TR10. Gay and Akers[81] suggested that an interactive digital simulation program would prove more powerful for analysis of experimental data. Even that could not approach the efficiency of hybrid computer iterative solutions.

The restrictions imposed by digital simulation programs are quite unnecessary if one does not presuppose a knowledge of analogue techniques. Thus it is more useful to retain the digital nature with its inherent logic facilities and add to this the numerical integration routines. This was the philosophy employed by Franks[83]. He described a set of FORTRAN subroutines which permitted the solution of mathematical models consisting of simultaneous differential and algebraic equations. Two methods of integration were included: the second and fourth order Runge-Kutta methods, both without the option of variable step size. In the present work they have been rewritten as ALGOL procedures and a further alternative added: the simple Euler method. The details are contained in Appendix 1.2. All the normal logic facilities of high level digital languages are retained so both simple analogue and complete hybrid computation can be simulated.

3.6 Comparison of Methods of Solution

3.6.1 The problem of Lovell and Karnofsky: Lime calcination

Their problem was chosen to demonstrate the significance of intra-particle temperature distribution and was stated as

> "Limestone is calcined in a continuous, countercurrent, vertical lime kiln. The calcium carbonate is fed in at the top in 2 in. diameter pieces at a superficial mass velocity of 2230 lb/h ft^2. Flue gas and carbon dioxide from the calcination rise through the bed at a superficial mass velocity of 2500 lb/h ft^2. If the limestone enters at 100°F and the gas leaves at 200°F, at what level in the kiln is the gas temperature 400°F?"

Data: $c_f = 0.25$ Btu/lb deg F
$c_s = 0.28$ Btu/lb deg F
$h_f = 78$ Btu/h ft^2 deg F
$k_s = 1.3$ Btu/h ft deg F
$e = 0.5$

The possibilities of chemical reaction and mass transfer need not be considered. The relevant dimensionless parameters are

$$Bi = \frac{h_f . R}{k_s} = \frac{78 \times 1}{1.3 \times 12} = 5.0$$

$$\beta = \frac{G_s . c_s}{G_f . c_f} = \frac{2230 \times 0.28}{2500 \times 0.25} = 1.0$$

$$\theta_{fo} = \frac{T_{fo} - T_{si}}{T_{fi} - T_{si}} = \frac{200-100}{400-100} = 0.333$$

Munro and Amundson[77] computed the analytical solution as far as $z = 0.2$ and then extrapolated graphically, giving $z_L = 0.245$ as the level at which the gas temperature is 400°F. Inspection of their graph suggests that their extrapolation was in error, z_L being nearer to 0.25. Leung and Quon[78] provided solutions as far as $z = 0.1854$ by Munro and Amundson's analytical method, by the

TABLES 3:1, 2, 3, 4 AND 5. LOVELL AND KARNOFSKY'S PROBLEM

Table 3:1. Analogue Computer Solution: Akers

z	θ_f	θ_{sm}	θ_5	θ_4	θ_3	θ_2	θ_1	θ_0
0.051	0.488	0.155	0.313	0.158	0.069	0.026	0.010	0.006
0.101	0.620	0.287	0.451	0.300	0.190	0.120	0.080	0.070
0.152	0.747	0.413	0.581	0.430	0.316	0.236	0.190	0.173
0.202	0.874	0.536	0.710	0.558	0.440	0.359	0.310	0.294
0.253	0.998	0.667	0.835	0.683	0.566	0.482	0.432	0.419

Table 3:2. Numerical Integration Solution: Gay and Akers

z	θ_f	θ_{sm}	θ_5	θ_4	θ_3	θ_2	θ_1	θ_0
0.05	0.494	0.158	0.314	0.159	0.070	0.028	0.012	0.008
0.1	0.625	0.290	0.454	0.302	0.192	0.121	0.083	0.071
0.15	0.752	0.417	0.584	0.432	0.317	0.237	0.190	0.175
0.2	0.878	0.543	0.710	0.560	0.443	0.360	0.311	0.295
0.25	1.004	0.669	0.836	0.686	0.568	0.485	0.435	0.418

Table 3:3. Numerical Integration Solution: Present Work
Second Order Runge-Kutta, $\Delta z = 0.01$

z	θ_f	θ_{sm}	θ_5	θ_4	θ_3	θ_2	θ_1	θ_0
0.05	0.494	0.157	0.309	0.161	0.070	0.029	0.012	0.008
0.1	0.625	0.290	0.454	0.302	0.192	0.121	0.083	0.072
0.15	0.752	0.417	0.584	0.433	0.317	0.237	0.191	0.176
0.2	0.878	0.543	0.710	0.560	0.443	0.360	0.311	0.295
0.249	1.000	0.665	0.833	0.682	0.565	0.481	0.431	0.415
0.25	1.004	0.669	0.836	0.686	0.568	0.485	0.435	0.418

Table 3:4. Leung and Quon's Solutions

z	θ_f Analytical	θ_f Runge-Kutta-Gill	θ_f Analogue
0.05	0.487	0.486	0.490
0.1	0.617	0.616	0.617
0.15	0.743	0.742	0.740
0.1854	0.833	0.831	0.833

Table 3:5. Summary of Present and Previous Solutions

Workers	Method	z_L	L feet	Computation time	Computer
Lovell & Karnofsky	Furnas	0.133	0.88	-	-
	Schmidt	0.200	1.32	-	-
Munro & Amundson	Furnas	0.135	0.90	-	-
	Analytical, extrapolated	0.245	1.63	~4 h	?
Leung & Quon	Analytical) Extrapolated			?	?
	Runge-Kutta-Gill (in the present	0.253	1.69	28 min	IBM 1620
	Analogue) work			<10 s	Pace 231R
Akers	Analytical	0.253	1.69	?	PDS 1020
	Analogue	0.253	1.69	6.33 s	EAL TR10
Gay & Akers	Runge-Kutta-Merson	0.249	1.66	~10 s	ICL 1905
Wilson	Furnas	0.133	0.89	-	-
	Runge-Kutta-Franks	0.249	1.66	~10 s	ICL 1905
	Resistance equation	0.267	1.78	-	-

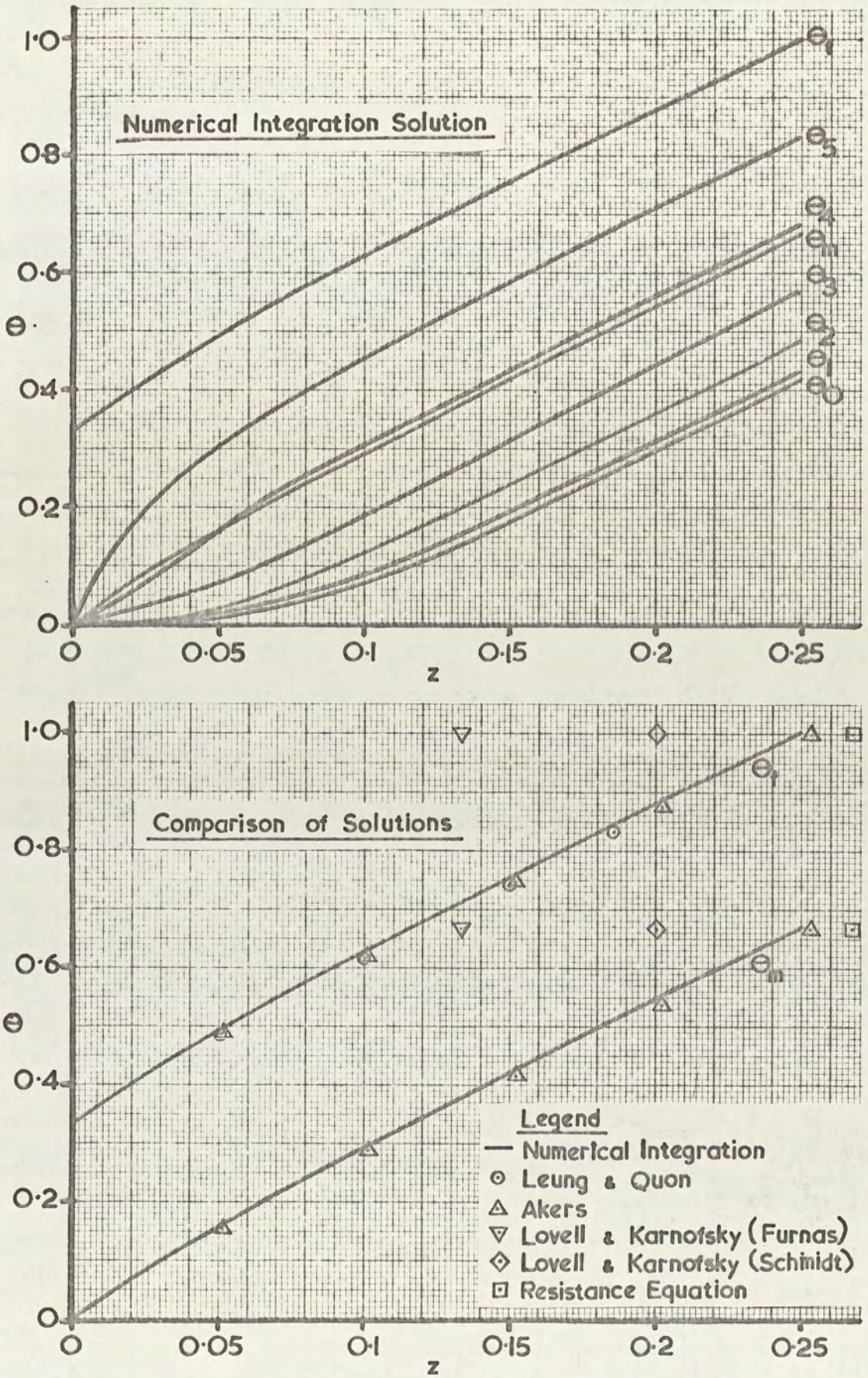

FIGURE 3:5 LOVELL & KARNOFSKY'S PROBLEM

Runge-Kutta-Gill numerical method and by analogue computation. Akers[2] applied the analogue computer technique and also recalculated the analytical solution for the full bed length. Gay and Akers[81] used a digital computer program employing the Runge-Kutta-Merson numerical method to simulate the analogue integration. In the present work, Franks'[83] approach to digital simulation has been employed. It can be seen from Tables 3:1 to 3:5 and Figure 3:5 that the present results are consistent with those of Gay and Akers[81] but differ from those of Leung and Quon[78] and Akers[2]. Gay and Akers suggested that the double use of finite differences (first to reduce the partial differential equations to ordinary differential equations and secondly to integrate) could cause the anomalies with the numerical method and might be overcome by using a larger number of sphere increments. However, the consistency of Leung and Quon's three methods does not support this view.

Although there are slight differences between the various solutions, they are minimal, particularly in comparison with the much more approximate methods. The simple solution of Furnas[35], which assumes no intra-particle temperature distribution (i.e. equation (3:9) for the special case of $\beta = 1$) seriously underestimates the bed length and Lovell and Karnofsky's[76] modified Schmidt method produces an intermediate bed length. The resistance equation (2:10) together with (3:9) provides a reasonable approximation which would suffice for many engineering applications.

The slight error in the overall heat balance with the present numerical method should be noted. Equation (3:29)

$$1 - \theta_{fo} - \beta.\theta_{so} = 0$$

predicts that θ_{so} should be 0.667 at the point where $\theta_f = \theta_{fi} = 1$

TABLES 3:6 AND 7. THE PROBLEM OF KITAEV ET AL.

Table 3:6. Analytical Solution: Kitaev et al.

z	θ_f	θ_{sm}	θ_5				θ_0
0.150	0.459	0.276	0.377				0.120
0.298	0.614	0.469	0.550				0.342
0.447	0.735	0.622	0.685				0.521
0.596	0.831	0.742	0.792				0.662
0.745	0.907	0.836	0.876				0.774
0.893	0.967	0.911	0.942				0.862
0.995	1.000	0.953	0.979				0.910

Table 3:7. Numerical Integration Solution: Present Work
Second Order Runge-Kutta, $\Delta z = 0.01$

z	θ_f	θ_{sm}	θ_5	θ_4	θ_3	θ_2	θ_1	θ_0
0.15	0.464	0.282	0.383	0.293	0.220	0.168	0.137	0.127
0.3	0.619	0.476	0.556	0.485	0.427	0.384	0.357	0.348
0.45	0.741	0.628	0.691	0.635	0.589	0.555	0.534	0.527
0.6	0.836	0.746	0.797	0.753	0.717	0.691	0.674	0.668
0.75	0.912	0.842	0.881	0.846	0.818	0.797	0.784	0.780
0.9	0.971	0.916	0.947	0.920	0.897	0.881	0.870	0.867
0.995	1.002	0.954	0.981	0.958	0.938	0.924	0.915	0.912

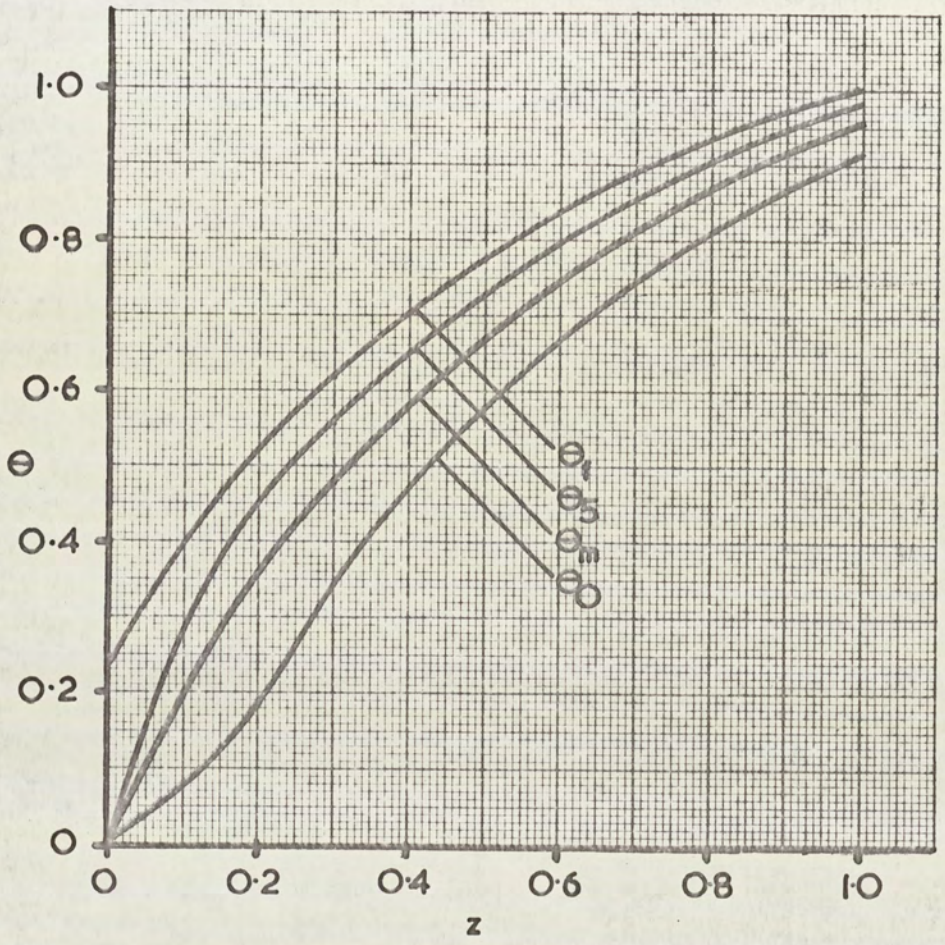

FIGURE 3:6 KITAEV ET AL.'S PROBLEM

whereas only 0.665 has been achieved. Akers'[2] analogue computer solution gave 0.667 at $\theta_f = 0.998$.

3.6.2 The problem of Kitaev et al.: Dry quenching of coke

As the analytical solution of Timofeev[38] differs in appearance from that of Munro and Amundson[77], the numerical simulation was tested against it. Kitaev et al.[38] applied Timofeev's method to the following problem:

> "Find the temperature distribution in the coke chamber of a dry quenching system operating in countercurrent."

Data: $T_{si} = 1000^{\circ}C$
$T_{fi} = 160^{\circ}C$
$T_{fo} = 800^{\circ}C$
$\beta = 0.8$
$Bi = 6.0$

The quenching gas is inert to coke so the possibilities of chemical reaction and mass transfer need not be considered. It was shown in Section 3.3.5 that the cooling of hot solids could be treated in exactly the same manner as the heating of cold solids. Thus

$$\theta_{si} = \frac{1000-1000}{1000-160} = 0$$

$$\theta_{fi} = \frac{1000-160}{1000-160} = 1$$

$$\theta_{fo} = \frac{1000-800}{1000-160} = 0.2381$$

It can be seen from Tables 3:6 and 3:7 and Figure 3:6 that numerical integration does underestimate the bed length very slightly as was shown with the Lovell and Karnofsky problem. Timofeev's solution seems quite satisfactory and should be simpler to apply than that of Munro and Amundson as the roots of the transcendental equation (3:22) and factors of $f(W_j)$ in (3:21) were tabulated by Kitaev et al. The numerical solution required 15 s of computer central processor time.

3.6.3 Single sphere in an infinite isothermal medium

The problems of Lovell and Karnofsky[76] and Kitaev et al.[38] demonstrated that numerical and analogue solutions of the equations describing moving bed heat transfer compared very well with the analytical solutions. However, the Biot numbers and β values in the two problems were similar (Bi: 5.0, 6.0; β: 1.0, 0.8) so there is little knowledge of the range of application of the approximate techniques. What small errors there are presumably stem mainly from the integration of the sphere temperature differential equations. For further testing of the numerical solution, it should be sufficient to restrict the analysis to the transient heating of a single sphere in an infinite isothermal medium. It can be appreciated that the moving bed model can be applied to this situation with the simplification that

$$\theta_f = \text{constant} = 1.$$

The concept of a dimensionless bed length involving solids flow rate is no longer applicable but the time of heating can still be represented by a Fourier number:

$$z = \frac{k_s(1-e)y}{G_s . c_s . R^2} \qquad \ldots\ldots\ldots\ldots\ldots\ldots\ldots\ldots (3:28)$$

$$= \frac{k_s}{c_s . R^2} \; \frac{y(1-e)}{G_s} \; \frac{\rho_s}{\rho_s}$$

$$= \frac{k_s . t}{c_s . \rho_s . R^2}$$

$$= \frac{\alpha_s . t}{R^2} \qquad \ldots\ldots\ldots\ldots\ldots\ldots\ldots\ldots (3:65)$$

Akers[2] solved the single sphere problem at a Biot of 1.0 by analogue computation and he showed that the error was never more

TABLES 3:8 AND 3:9. THE SINGLE SPHERE PROBLEM

Table 3:8. Analytical Solution: Kitaev et al.

Bi / z	0.2	0.4	0.6	0.8	1.0	1.5	2	3	4	5	6	8	10	20	50	∞
	θ_5															
0.2	0.144	0.261	0.358	0.437	0.504	0.627	0.711	0.812	0.866	0.899	0.920	0.945	0.959	0.983	0.997	1
0.4	0.238	0.409	0.534	0.627	0.698	0.811	0.874	0.934	0.960	0.973	0.981	0.988	0.992	0.997	0.999	1
0.6	0.321	0.526	0.662	0.753	0.816	0.904	0.945	0.977	0.988	0.993	0.995	0.997	0.998	0.999	1.000	1
0.8	0.395	0.620	0.754	0.837	0.887	0.951	0.976	0.992	0.996	0.998	0.999	0.999	1.000	1.000	1.000	1
1.0	0.461	0.696	0.822	0.891	0.931	0.975	0.989	0.997	0.999	1.000	1.000	1.000	1.000	1.000	1.000	1
	θ_{sm}															
0.2	0.109	0.201	0.278	0.343	0.398	0.505	0.581	0.678	0.735	0.772	0.797	0.829	0.848	0.884	0.903	0.913
0.4	0.206	0.360	0.475	0.564	0.633	0.748	0.816	0.887	0.921	0.939	0.951	0.963	0.970	0.980	0.986	-
0.6	0.293	0.487	0.619	0.711	0.776	0.872	0.919	0.960	0.976	0.984	0.988	0.992	0.994	0.997	0.998	-
0.8	0.370	0.589	0.723	0.809	0.863	0.935	0.965	0.986	0.993	0.996	0.997	0.998	0.999	0.999	1.000	-
1.0	0.439	0.671	0.799	0.870	0.916	0.967	0.984	0.995	0.998	0.999	0.999	1.000	1.000	1.000	1.000	-
	θ_o															
0.2	0.058	0.107	0.153	0.192	0.227	0.301	0.357	0.437	0.490	0.528	0.556	0.593	0.617	0.669	0.701	0.73
0.4	0.159	0.284	0.382	0.461	0.526	0.641	0.715	0.800	0.846	0.873	0.890	0.911	0.923	0.944	0.955	0.963
0.6	0.251	0.426	0.551	0.643	0.710	0.817	0.875	0.930	0.954	0.966	0.973	0.981	0.985	0.991	0.993	-
0.8	0.332	0.540	0.674	0.764	0.823	0.907	0.945	0.976	0.986	0.991	0.993	0.996	0.997	0.998	0.999	-
1.0	0.405	0.632	0.763	0.839	0.892	0.953	0.976	0.991	0.996	0.998	0.998	0.999	0.999	1.000	1.000	-

Table 3:9. Numerical Integration Solution: Present Work: Second Order Runge-Kutta

z \ Bi	0.2	0.4	0.6	0.8	1.0	1.5	2	3	4	5	6	8	10	20	50	∞
	θ_5															
0.2	0.144	0.261	0.358	0.438	0.505	0.630	0.714	0.814	0.868	0.900	0.921	0.946	0.959	0.983	0.994	1
0.4	0.237	0.409	0.535	0.628	0.699	0.812	0.875	0.935	0.960	0.973	0.981	0.988	0.992	0.997	0.999	1
0.6	0.321	0.526	0.662	0.753	0.816	0.904	0.945	0.977	0.988	0.993	0.995	0.997	0.998	0.999	1.000	1
0.8	0.395	0.621	0.754	0.836	0.888	0.951	0.976	0.992	0.996	0.998	0.999	0.999	1.000	1.000	1.000	1
1.0	0.461	0.696	0.822	0.891	0.931	0.975	0.989	0.997	0.999	1.000	1.000	1.000	1.000	1.000	1.000	1
	θ_{sm}															
0.2	0.109	0.201	0.278	0.343	0.399	0.506	0.582	0.679	0.736	0.772	0.797	0.828	0.846	0.882	0.901	0.913
0.4	0.206	0.360	0.476	0.564	0.633	0.748	0.816	0.887	0.920	0.938	0.949	0.962	0.968	0.979	0.984	0.987
0.6	0.293	0.487	0.619	0.711	0.776	0.872	0.919	0.960	0.976	0.983	0.987	0.991	0.993	0.996	0.998	-
0.8	0.370	0.589	0.723	0.808	0.863	0.935	0.964	0.986	0.993	0.995	0.997	0.998	0.999	0.999	1.000	-
1.0	0.439	0.671	0.799	0.873	0.916	0.967	0.984	0.995	0.998	0.999	0.999	1.000	1.000	1.000	1.000	-
	θ_o															
0.2	0.058	0.109	0.153	0.193	0.228	0.301	0.358	0.437	0.490	0.527	0.554	0.591	0.614	0.664	0.695	0.716
0.4	0.159	0.283	0.382	0.461	0.525	0.640	0.714	0.798	0.843	0.870	0.887	0.908	0.919	0.940	0.951	0.958
0.6	0.250	0.426	0.551	0.642	0.710	0.816	0.874	0.929	0.952	0.965	0.972	0.979	0.983	0.989	0.992	-
0.8	0.332	0.540	0.674	0.763	0.823	0.906	0.944	0.975	0.986	0.990	0.993	0.995	0.997	0.998	0.999	-
1.0	0.405	0.631	0.763	0.842	0.892	0.952	0.976	0.991	0.996	0.997	0.998	0.999	0.999	1.000	1.000	-
Δz	0.01	0.01	0.01	0.01	0.01	0.01	0.01	0.01	0.01	0.01	0.005	0.005	0.005	0.005	0.0025	0.0025

than 2% compared with the analytical solution. Kitaev et al. obtained the analytical solution for Biot numbers from 0.2 to 50 and even ∞. Their solution is similar to that of Gurney and Lurie[84] but the graphical and tabular presentation of the results is more convenient for comparison. For the case

$$Bi = \infty$$

the derivative equations are simplified even further. θ_f disappears from the analysis completely and

$$\theta_5 = \text{constant} = 1$$

Although all the sphere nodal temperatures were calculated, only those which are directly comparable with the results of Kitaev et al. are presented in Table 3:9. Other Biot numbers and greater Z values were also used but these are not included in the table. Comparison of Tables 3:8 and 3:9 shows that the agreement between the analytical and numerical solutions is very close, even at high Biot numbers, and generally the results are indistinguishable for three figure accuracy.

3.6.4 Effect of step length and integration order on accuracy of numerical solution

Reference has already been made to the three levels of sophistication of the numerical solution: the Euler method and the second and fourth order Runge-Kutta methods. These are described in Appendix 1.2. Each involves stepwise progression towards the solution and the accuracy is dependent upon the value chosen for the step length Δz of the independent variable. The effects of step length were investigated and it was found that there was a critical value for each of the three methods below which the solution was stable, convergent and independent of Δz. The approximate critical values for Lovell and Karnofsky's problem were:

TABLES 3:10, 11 AND 12. NUMERICAL SOLUTION OF LOVELL AND KARNOFSKY'S PROBLEM

Table 3:10. Euler Method: $\Delta z = 0.01$.

z	θ_f	θ_{sm}	θ_5	θ_4	θ_3	θ_2	θ_1	θ_0
0.05	0.496	0.159	0.319	0.164	0.067	0.020	0.004	0.000
0.1	0.626	0.291	0.456	0.304	0.192	0.117	0.075	0.062
0.15	0.752	0.417	0.584	0.433	0.317	0.236	0.187	0.172
0.2	0.878	0.543	0.711	0.560	0.443	0.360	0.310	0.293
0.249	1.000	0.665	0.833	0.682	0.565	0.481	0.431	0.414

Table 3:11. Second Order Runge-Kutta: $\Delta z = 0.01$.

z	θ_f	θ_{sm}	θ_5	θ_4	θ_3	θ_2	θ_1	θ_0
0.05	0.494	0.157	0.309	0.161	0.070	0.029	0.012	0.008
0.1	0.625	0.290	0.454	0.302	0.192	0.121	0.083	0.072
0.15	0.752	0.417	0.584	0.433	0.317	0.237	0.191	0.176
0.2	0.878	0.543	0.710	0.560	0.443	0.360	0.311	0.295
0.249	1.000	0.665	0.833	0.682	0.565	0.481	0.431	0.415

Table 3:12. Fourth Order Runge-Kutta: $\Delta z = 0.01$.

z	θ_f	θ_{sm}	θ_5	θ_4	θ_3	θ_2	θ_1	θ_0
0.05	0.494	0.158	0.314	0.159	0.070	0.028	0.012	0.008
0.1	0.625	0.290	0.454	0.302	0.192	0.121	0.083	0.071
0.15	0.752	0.417	0.584	0.433	0.317	0.237	0.191	0.175
0.2	0.878	0.543	0.710	0.560	0.443	0.360	0.311	0.295
0.249	1.000	0.665	0.833	0.682	0.565	0.481	0.431	0.415

TABLE 3:13. AKERS' DATA: CRITICAL STEP LENGTHS FOR NUMERICAL SOLUTION

Run	z_L	Bi_{lm}	β	Critical Δz		
				Euler	Second Runge-Kutta	Fourth Runge-Kutta
21	1.81	0.469	2.443	0.020	0.020	0.028
59	1.21	1.148	0.269	0.019	0.019	0.026
86	0.87	0.828	0.704	0.020	0.020	0.026

Euler	0.015
Second Order Runge-Kutta	0.015
Fourth Order Runge-Kutta	0.018

Solutions were computed from $\Delta z = 0.0025$ up to the critical values and found to be quite consistent. These are shown in Tables 3:10 to 3:12. It can be seen that there are differences between the methods at low z values but all converge to the same final solution. The consequence of this is that although the computed temperature distributions (knowing all bed parameters) may differ, calculation of Biot numbers from experimental data is independent of the method employed provided Δz is less than the critical value. This was verified using the data for Lovell and Karnofsky's problem. The critical values for some data from Akers' work were also determined and are shown in Table 3:13.

As the conclusion that all three methods iterated to the same Biot number was drawn from only one example, it was felt that the Euler method should not be used except, perhaps, for large bed lengths for which the computation time would be excessive. The advantage of the greater critical Δz with the fourth order method was outweighed by the increased computational effort involved in the four derivative evaluations per step. It was decided that the second order method should be used wherevever possible as it seemed the best compromise.

3.6.5 Experimental data of Akers

As a final test of the accuracy of the numerical integration, a selection of Akers'[2] data was recalculated using the second order Runge-Kutta method and compared with his results from hybrid computer analysis. As the experimental Biot numbers were much

TABLE 3:14. RECALCULATION OF AKERS' DATA USING SECOND ORDER RUNGE-KUTTA NUMERICAL SOLUTION

Run	z_L	β	θ_{fo}	Biot Number		
				Akers		Wilson
				Furnas	Analogue	Numerical
26	3.02	2.169	0.4593	0.0465	0.0460	0.0468
28	6.28	1.239	0.4632	0.0448	0.0439	0.0452
30	5.27	1.226	0.2800	0.1091	0.1112	0.1110
31	3.97	0.885	0.3032	0.262	0.276	0.273
32	4.88	0.714	0.4401	0.176	0.181	0.176
34	2.06	1.675	0.4675	0.099	0.110	0.102
35	5.67	0.725	0.3581	0.243	0.288	0.256
39	5.45	0.667	0.3752	0.331	0.360	0.350
41	6.37	0.503	0.5072	0.346	0.496	0.365
43	5.47	0.506	0.4996	0.485	0.586	0.522
46	1.94	0.310	0.6980	0.828	0.846	1.020
51	2.39	0.464	0.6032	0.371	0.416	0.403
53	5.02	0.597	0.4880	0.202	0.216	0.212
54	1.83	0.442	0.5850	0.733	0.870	0.870
55	1.75	0.292	0.7169	0.856	1.110	1.032
57	1.34	0.318	0.6959	1.023	1.104	1.281
59	1.21	0.269	0.7409	1.148	1.200	1.520
62	2.51	0.637	0.4290	0.519	0.552	0.580
63	2.03	0.781	0.4218	0.363	0.394	0.392
65	1.80	0.449	0.5827	0.709	0.670	0.830
66	4.86	0.618	0.4211	0.334	0.435	0.365
69	6.59	0.680	0.3772	0.232	0.274	0.249
73	2.25	1.645	0.4518	0.0895	0.0892	0.0910
78	0.598	0.827	0.5203	0.696	0.793	0.795
79	1.871	0.303	0.7050	0.838	0.793	1.020
80	0.934	0.603	0.5258	0.797	1.170	0.964
81	5.94	1.482	0.5472	0.0278	0.0312	0.0279
82	0.401	1.376	0.4852	0.563	0.602	0.626
83	1.16	0.494	0.5822	0.754	0.796	0.890
84	0.882	0.623	0.5398	0.728	0.796	0.850
85	0.886	0.662	0.5069	0.784	0.882	0.925
86	0.870	0.704	0.4613	0.828	0.996	1.056
88	0.922	0.616	0.5508	0.668	0.718	0.770
89	0.915	0.619	0.5323	0.745	0.773	0.872

lower than for Lovell and Karnofsky's problem, a step length of 0.018 was chosen. Several discrepancies were apparent which, at first, were attributed to instability of the numerical solution. However, reduction of the step length to 0.01 and even 0.005 produced no changes in the Biot numbers. The results are shown together with Akers' data in Table 3:14.

It is suggested that, although potentially superior to the numerical method, the analogue computer method itself may be unstable. Akers did refer to the sensitivity of the solution to the setting of the potentiometers. Alternatively the errors might stem from maloperation of the electronic components of the circuit rather than inherent program instability. Present experience with the TR48 supports the view that the analogue hardware was probably at fault. The numerical method is much less machine oriented than the analogue one so the present results could easily be checked by future workers should this prove necessary.

To conclude this section, it may be stated that the numerical method is of sufficient accuracy for the present work and seems best suited of all the methods available.

SECTION 4

EXPERIMENTAL WORK

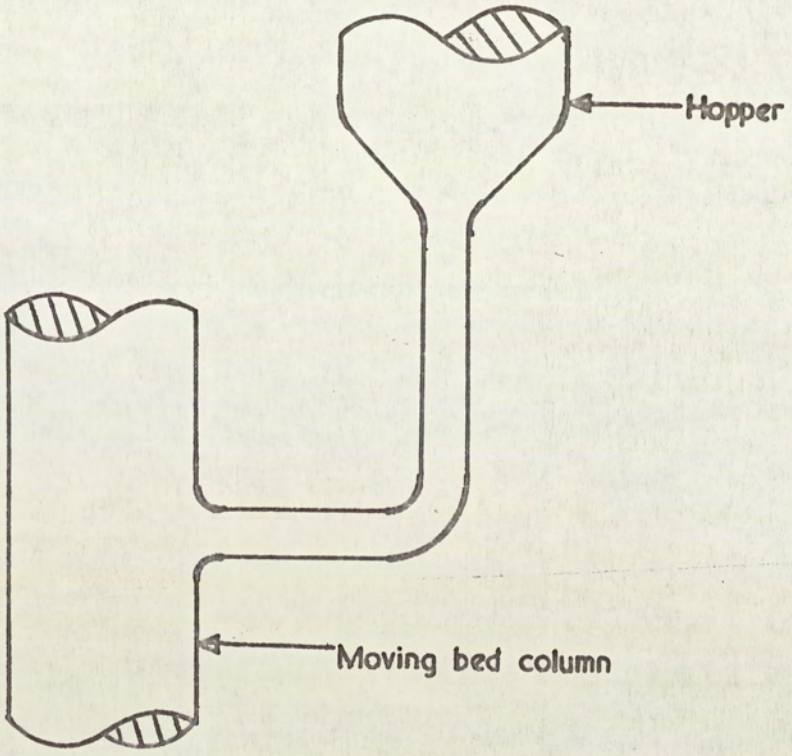

FIGURE 4:1 UNSUCCESSFUL CHARGING ARRANGEMENT

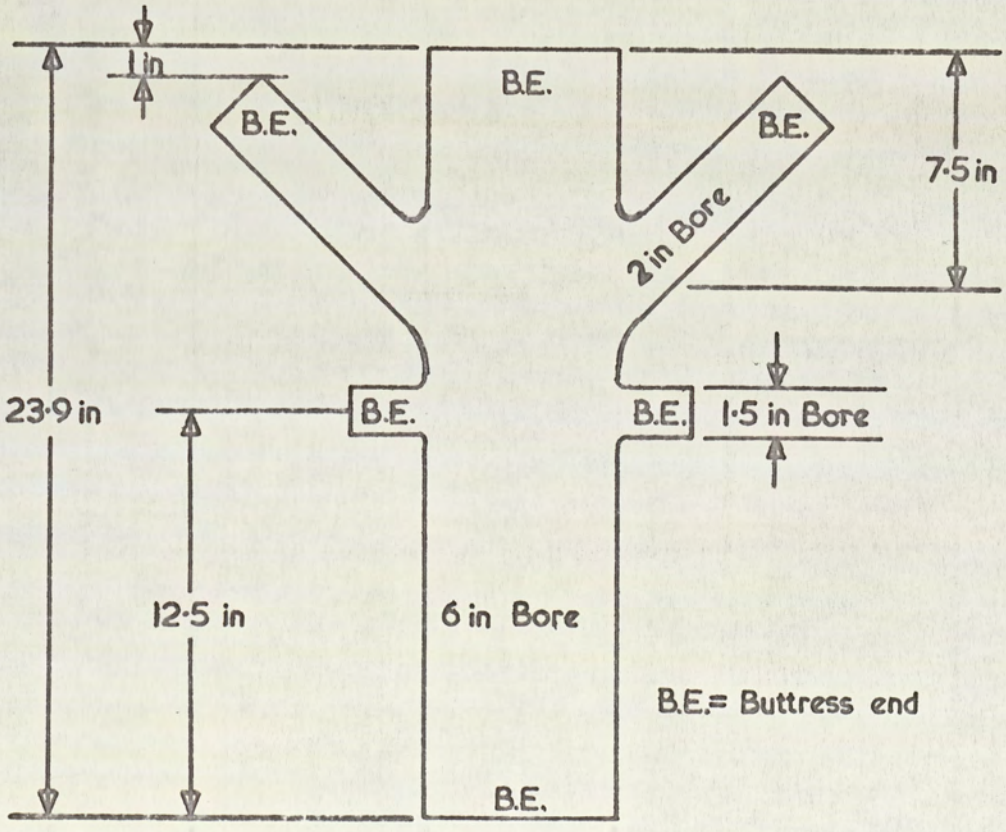

FIGURE 4:2 SHORT MOVING BED COLUMN
(HEAT TRANSFER STUDY)

SECTION 4 - EXPERIMENTAL WORK

4.1 Design of Apparatus

Akers'[2] experimental technique was basically sound but the equipment required refinement in several respects, as indicated in Section 2.2. It was essential that the feeding of fresh solids and the exhaust of spent gas be separated for the gas outlet temperature measurements to be reliable. Variations in bed voidage due to the thermocouple probes and the wall had to be kept to a minimum. Glass was chosen as the material for the moving bed column and associated pipework so that the flow of the solids could be viewed. Standard Q.V.F. borosilicate glass sections were to be used wherever possible.

Details of the equipment and manufacturers are contained in Appendix 2.1.

4.1.1 Flow characteristics of spherical solids

Akers used soda glass ballotini of 6 and 12 mm nominal diameter and high alumina ceramic of $\frac{1}{2}$ in nominal diameter. Tests showed that the solids could not be fed into the bed using the equipment indicated in Figure 4:1 because of interlocking of the particles. The minimum angle of inclination of a $1\frac{1}{2}$ in pipe necessary to disturb the equilibrium was found to be about 10° for the ballotini but 20° for the ceramic due to the greater surface roughness and lack of sphericity. The large particles tended to "hang-up" regardless of the angle of inclination and the 6 mm ballotini behaved similarly in a 1 in pipe. It was inferred that the minimum ratio of pipe bore to particle diameter must be about 4 for steady flow of ballotini under packed bed conditions.

As the thermal conductivity of alumina ceramic is approximately

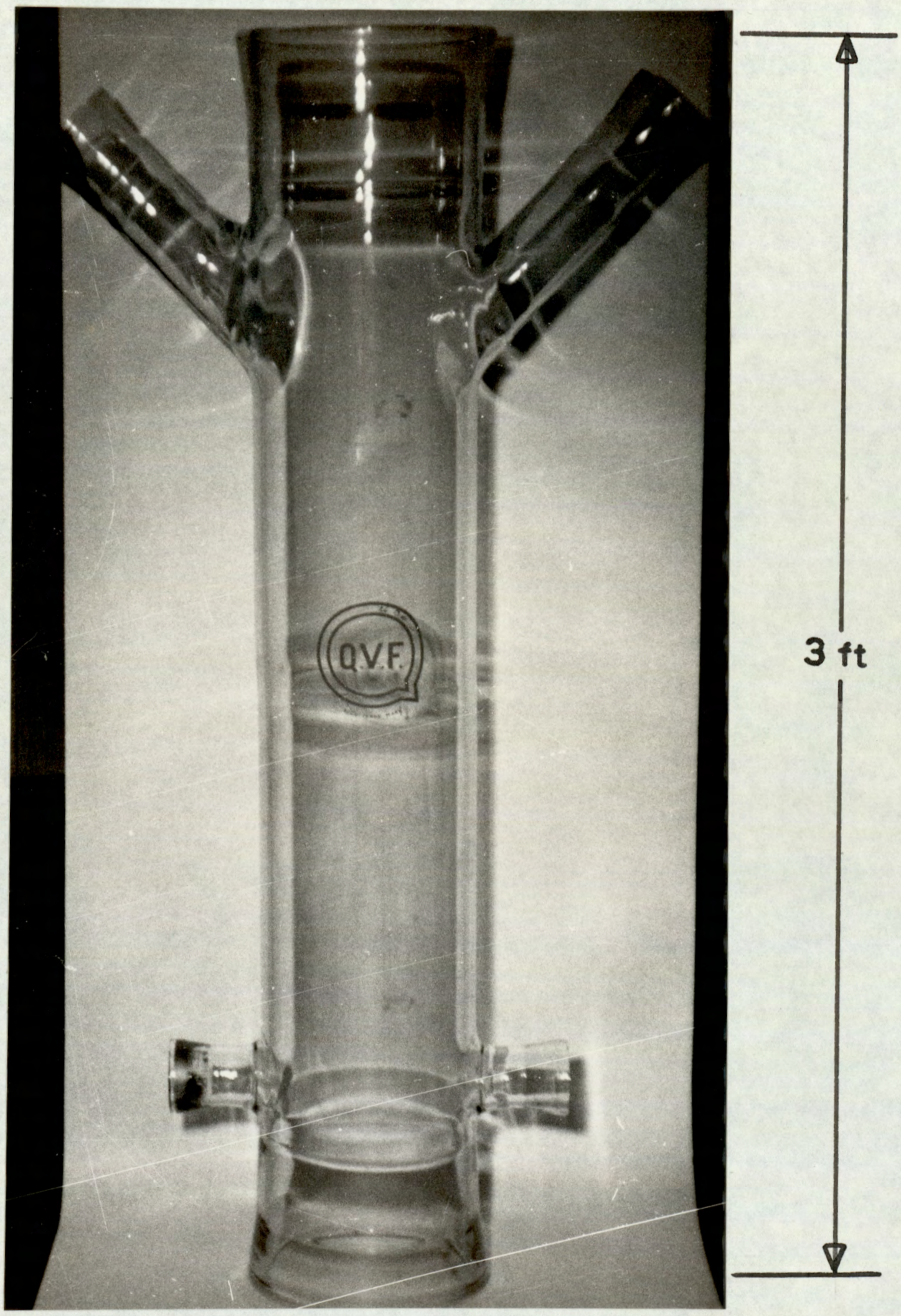

FIGURE 4:3 LONG MOVING BED COLUMN
(BALLOTINI FLOW CHARACTERISTICS)

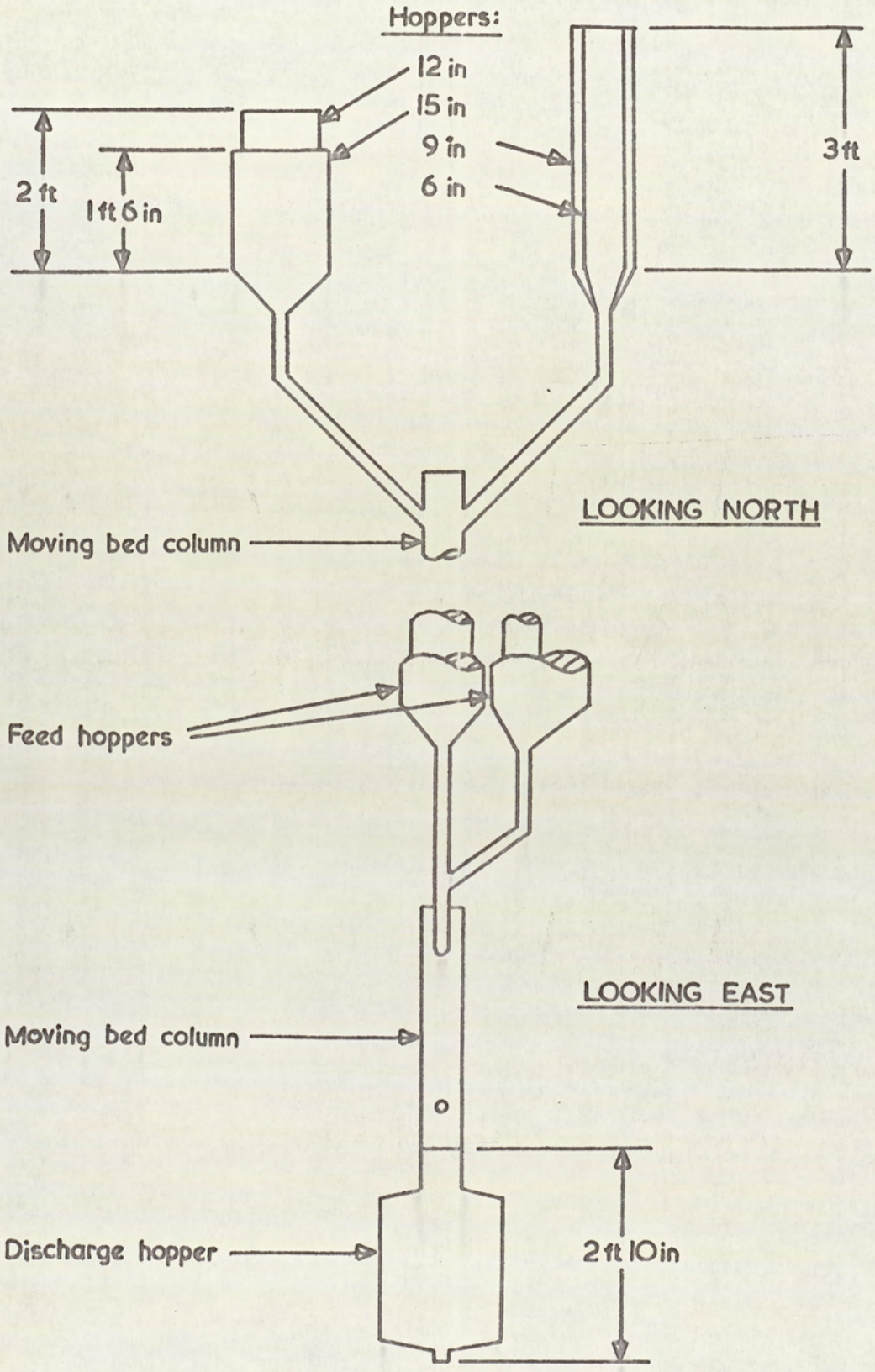

FIGURE 4:4 DIAGRAMMATIC ARRANGEMENT OF BALLOTINI FEED & DISCHARGE HOPPERS

ten times greater than that of ballotini, Biot numbers would be smaller and the model involving intra-particle temperature distribution would not be tested adequately. If it was necessary to use high thermal conductivity materials, metals would be more appropriate. The range of conductivities could then be from about 50 times that of glass (steel) to 200 (aluminium) and even 400 (copper). The flow properties of smooth metallic spheres would be superior to those of alumina ceramic. It was felt that the present work should be restricted to soda glass ballotini of 6, 9 and 12 mm diameter for which solids feed conduits of 2 in bore would be suitable.

The wall effects with small diameter columns were weighed against the required throughputs of solids and gas with large ones and 6 in nominal bore was selected as the most realistic compromise. Two columns were obtained: one for further investigation of the flow characteristics of moving packed beds and the other for the heat transfer study, see Figures 4:2 and 3. The arrangement of the feed and discharge hoppers is shown in Figure 4:4.

4.1.2 Height of column for moving bed heat transfer study

The compactness of moving bed heat exchangers due to the high transfer coefficients and surface area per unit volume was demonstrated by Sissom and Jackson[31], see Section 2.2. Their published temperature distributions illustrated that, although the length of the bed was 13 in, no more than 1.5 in was effectively utilised. In the remaining 11.5 in the gas and solids temperatures were coincident within the sensitivity limits of the thermocouples. They used aluminium granules of 0.027 in mean diameter but Akers[2] used glass and ceramic spheres 10 or 20 times larger and obtained measurable gas-solid temperature differences at both ends of 3 in

deep beds. Both models of moving bed heat transfer become indeterminate if

$$T_{fo} - T_{si} = 0 \quad \text{or} \quad T_{fi} - T_{so} = 0$$

and there is a problem of choice of effective bed length. It has already been pointed out that Sissom and Jackson were forced to superimpose temperature distributions calculated from equation (2:19)[32] before they could calculate transfer coefficients from their data. Thus, moving beds for determination of design data must not be too effective.

The relationship between the maximum bed length with which reliable data could be obtained and the gas and solids flowrates was investigated. The derivation and results are contained in Appendix 2.2. The conclusion was that the bed should be as short as the method of manufacture would permit.

4.1.3 Solids flowrate control

There is a problem with any moving bed equipment of producing the required movement. Norton[26] employed a rotary discharge table feeding an elevator for continuous recycling. Kilpatrick[28] used a pneumatic elevator both for removal of material from the bottom of the bed and for recycling. Akers[2] supported the test materials on a bed of $\frac{1}{4}$ mm mean diameter lead glass ballotini which drained through orifices. As Akers' method seemed quite adequate and required no sophisticated equipment, it was retained for the present work. Kuong[85] and Pilpel[86] showed that the rate of such discharge was independent of the bed height, only the nature of the material and the orifice size being important. It was thought that the orifices could be calibrated so that the solids flowrates would not need to be measured in every run.

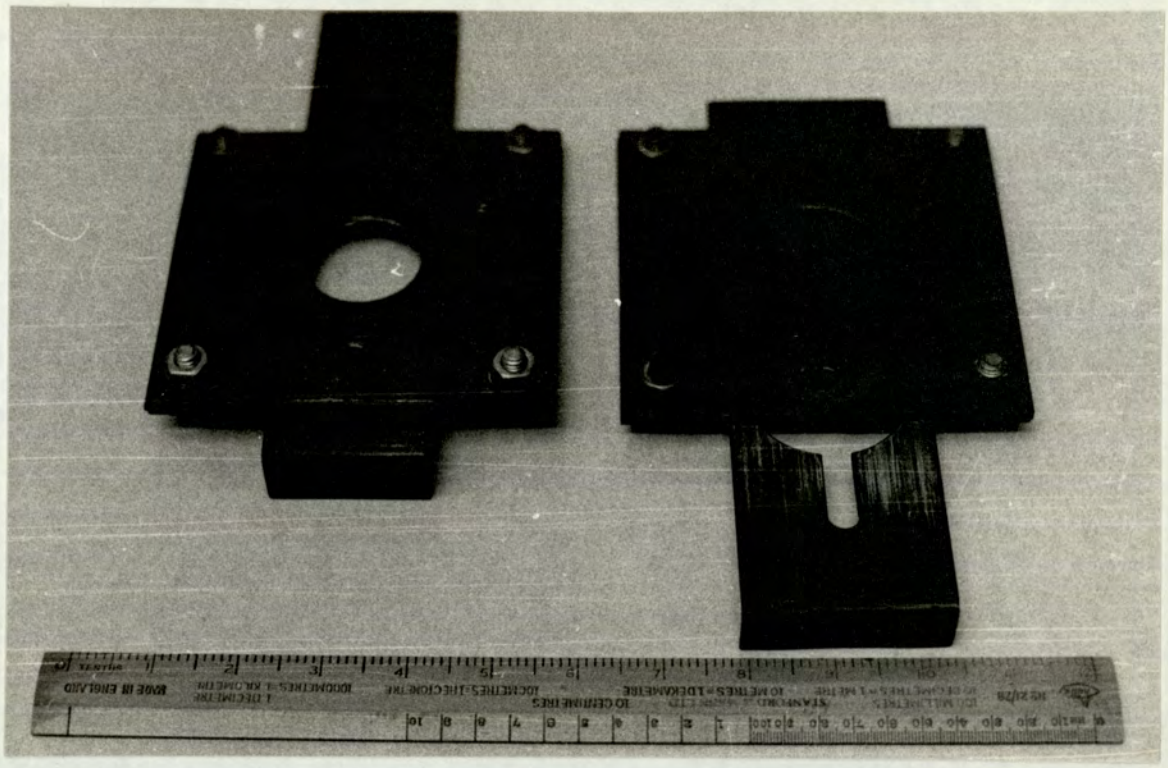

FIGURE 4:5 BALLOTINI FLOW ON-OFF VALVES

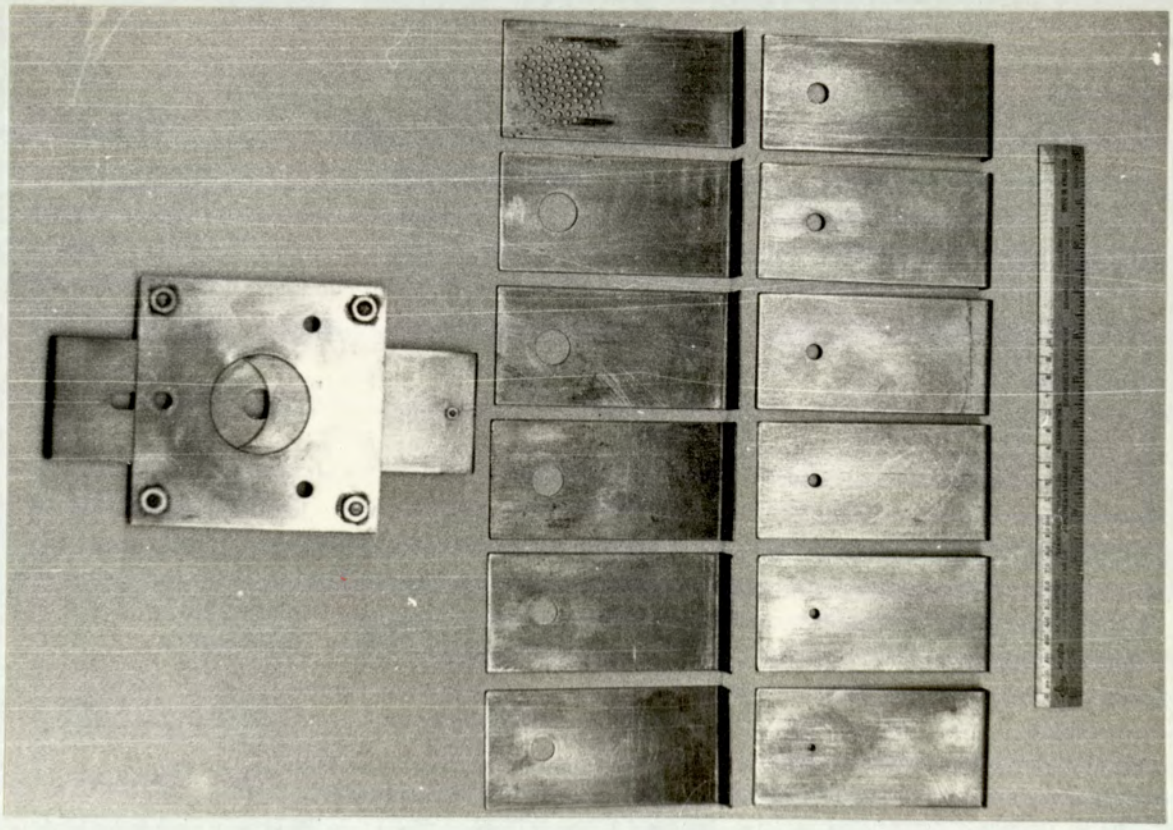

FIGURE 4:6 BALLOTINI FLOW CONTROL VALVE

Solids feed hoppers were fitted above the moving bed column as shown in Figure 4:4. These were 6, 9 and 12 in nominal bore Q.V.F. pipe sections and one 15 in steel drum. The intention was that the glass hoppers would be calibrated in weight of charged material and the flowrates measured for each of the discharge orifices. The various hopper diameters were chosen to give high accuracy over the whole range of flowrates.

The overall height of the rig including the hoppers, solids feed pipes, moving bed column, support ballotini hopper and discharge space was such that access for loading the 6 in and 9 in hoppers was severely restricted. A pneumatic elevator constructed of $1\frac{1}{2}$ in Q.V.F. pipe was installed to overcome the problem.

ON-OFF valves were required at the base of each hopper but it was essential that they should not increase the overall height of the rig significantly. Simple gate valves were made from 1/16 in thick brass sheet, see Figure 4:5. They were clamped between the buttress ends of the 2 in Q.V.F. pipes. Including one gasket, they were less than $\frac{3}{8}$ in thick. Similar valves were fitted in the pneumatic elevator lines. A version with two slides was made for the support ballotini hopper: one permanently attached slide for ON-OFF control and the other a removeable orifice plate for flowrate control. A set of interchangeable plates was made with circular orifices from 1/16 in to 13/16 in, see Figure 4:6.

4.1.4 Air flowrate measurement

Air was chosen as the process fluid because its thermophysical properties were accurately known, a suitable high pressure supply was readily available, cylinder gases would be expensive, there was no physiological danger and to be consistent with most previous workers.

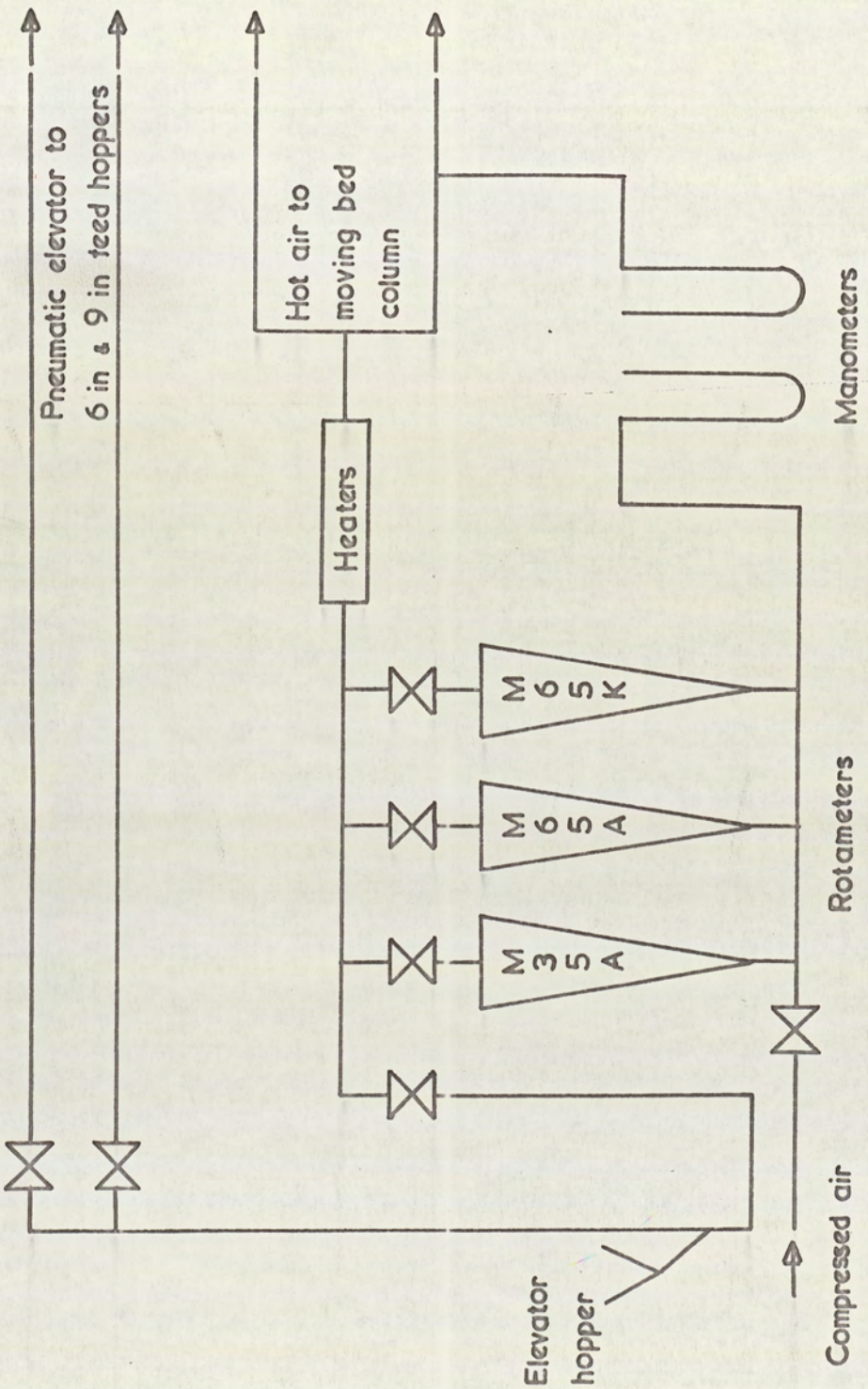

FIGURE 4:7 AIR FLOW DIAGRAMMATIC

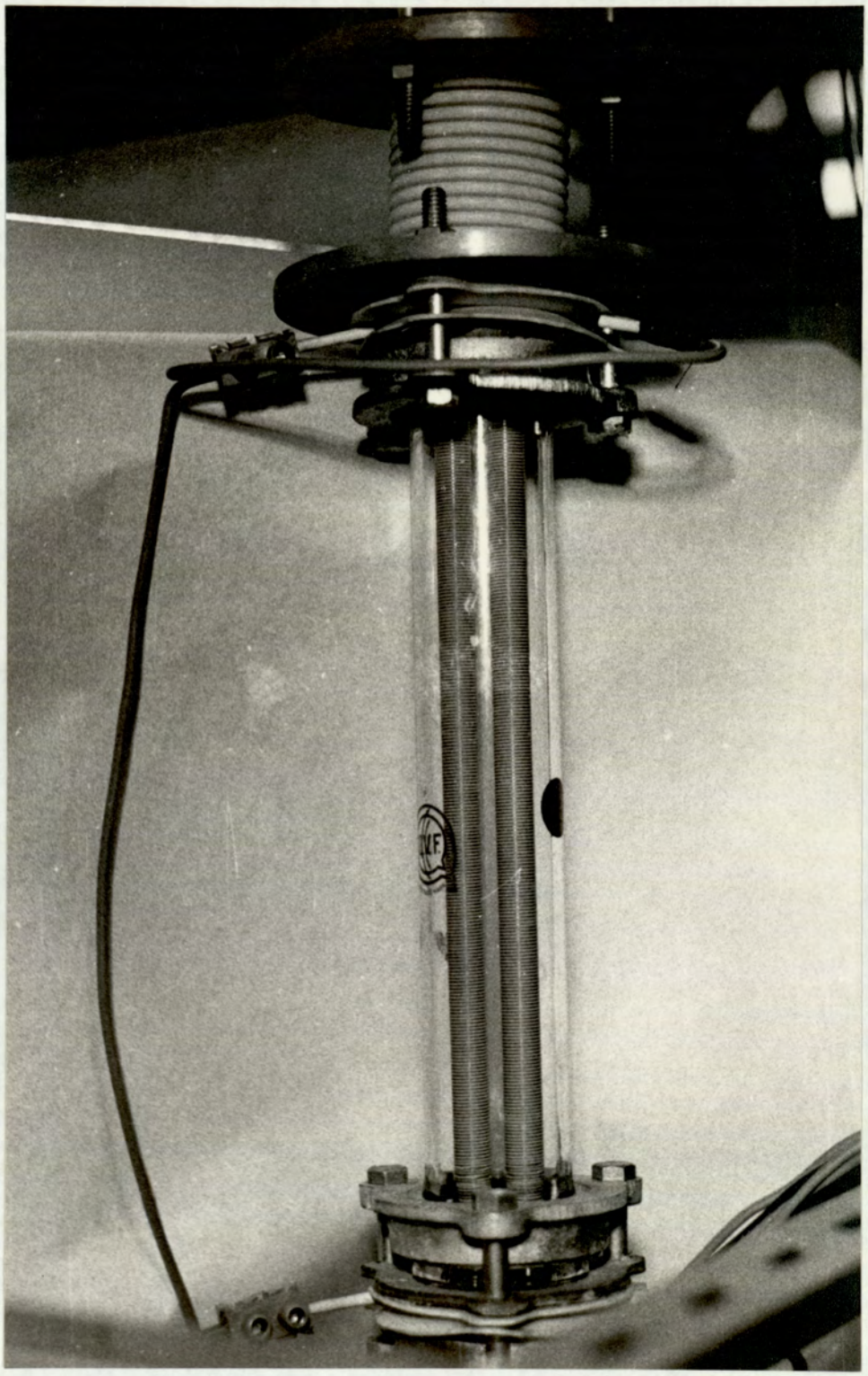

FIGURE 4:8 ONE 2-Kw SECTION OF THE AIR HEATER

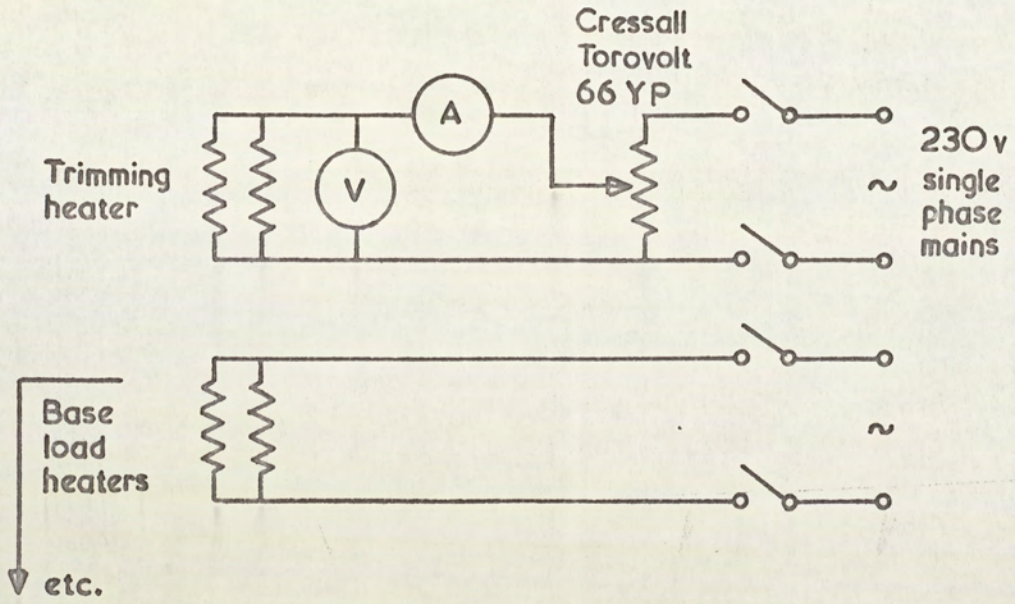

FIGURE 4:9 AIR HEATER ELECTRICAL CIRCUIT

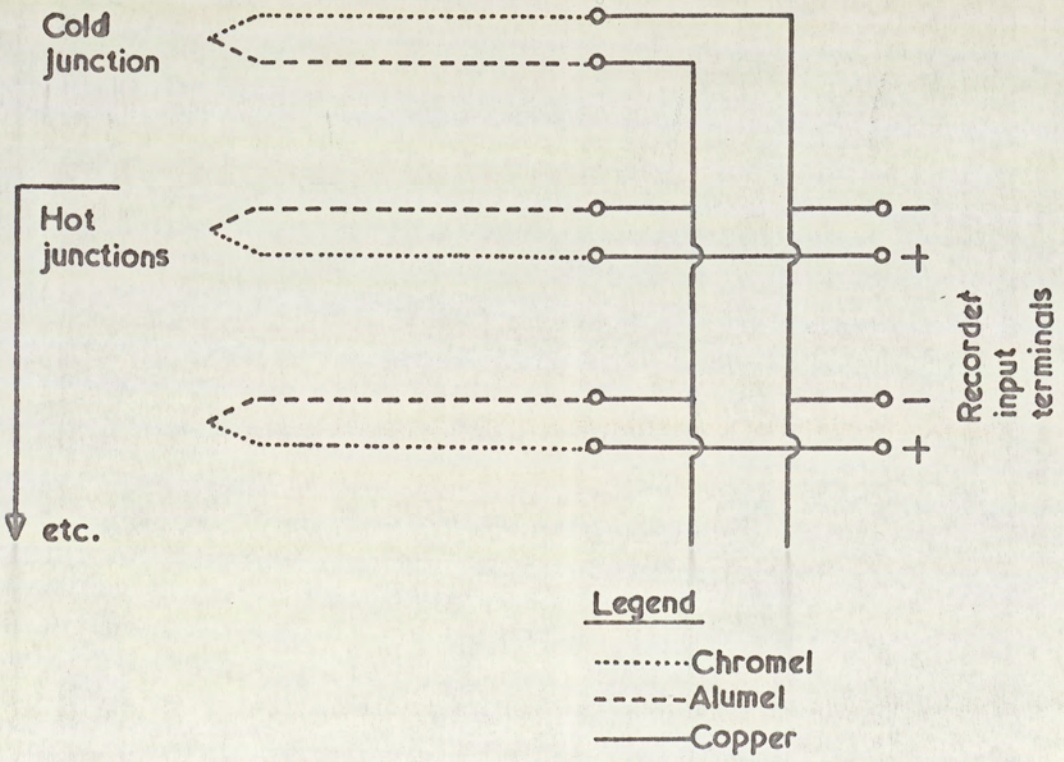

FIGURE 4:10 THERMOCOUPLE CIRCUIT

Metric Series Rotameters M35A, M65A and M65K were chosen for measuring the flowrate. The manufacturers provide two methods of calibration:

(1) Charts for each size of Rotameter specific to particular fluids.

(2) A general calibration handbook.

At low scale readings the two methods give similar results but they tend to diverge as the flowrate increases. Akers checked the calibration of his Rotameters using venturi meters manufactured to the specification set out in B.S. 1042[87] and found that for M35A and larger tubes the handbook gave more accurate results. As Akers' M35A and M65A meters were used in the present work, the handbook method was applied without further calibration tests. As the ranges of the three meters overlapped, it was generally possible to work at low scale readings for which the charts and handbook are consistent anyway. The two methods are described in Appendix 2.3. The air flow is shown diagrammatically in Figure 4:7.

4.1.5 Air heaters

It was intended that the range of investigation should not be narrower than that of Akers, i.e. maximum air loading rate of 3 608 lb/h ft^2 at inlet temperatures of about 100°C. This corresponds to a heat input to a 6 in diameter column of 7.5 kW. At a heater efficiency of, say, 90%, 8.3 kW would be required so 10 kW were installed to accommodate possible higher flowrates and operating temperatures. A pair of domestic 1 kW fire bars was fitted inside each of five 12 in long sections of $1\frac{1}{2}$ in Q.V.F. as shown in Figure 4:8. The electrical supply wires were sandwiched between asbestos gaskets in the pipework joints. The electrical circuit is shown in Figure 4:9.

4.1.6 Temperature measurement

All temperatures were measured with chromel-alumel thermocouples with argon-arc welded junctions. The 1 mm diameter junctions and exposed portions of the wires were coated with a thin layer of lacquer to insulate them electrically without increasing the response time significantly. The remaining lengths of wire were insulated with 1.0 or 1.5 mm internal diameter P.V.C. sleeving.

The calibration of all of the thermocouples was checked at the ice and steam points before installation. The corresponding E.M.F.s from B.S. 1827[88] are: 0°C and 0 mV, 100°C and 4.10 mV (cold junction at 0°C). At the ice point the maximum variation from the standard was -0.02 mV (-0.5 degC) and at the steam point ±0.01 mV (±0.25 degC). The thermocouple outputs were continuously recorded by a 16 point potentiometric recorder with 5s point interval. The calibration of the recorder was checked with a portable potentiometer and found to be better than -0.01 mV over the whole of the 0-6 mV range.

The circuit diagram for the thermocouples is shown in Figure 4:10. Three recorder inputs were connected in parallel for both the air and solids outlet temperatures to reduce the printing intervals to no more than 30s rather than 80s for the full 16 point cycle.

The following temperatures were monitored:

1. Air at Inlet to the Heaters

One thermocouple sandwiched between neoprene gaskets in a $1\frac{1}{2}$ in Q.V.F. pipe joint and extending to the centre line of the pipe.

FIGURE 4:11 INLET AIR MIXERS

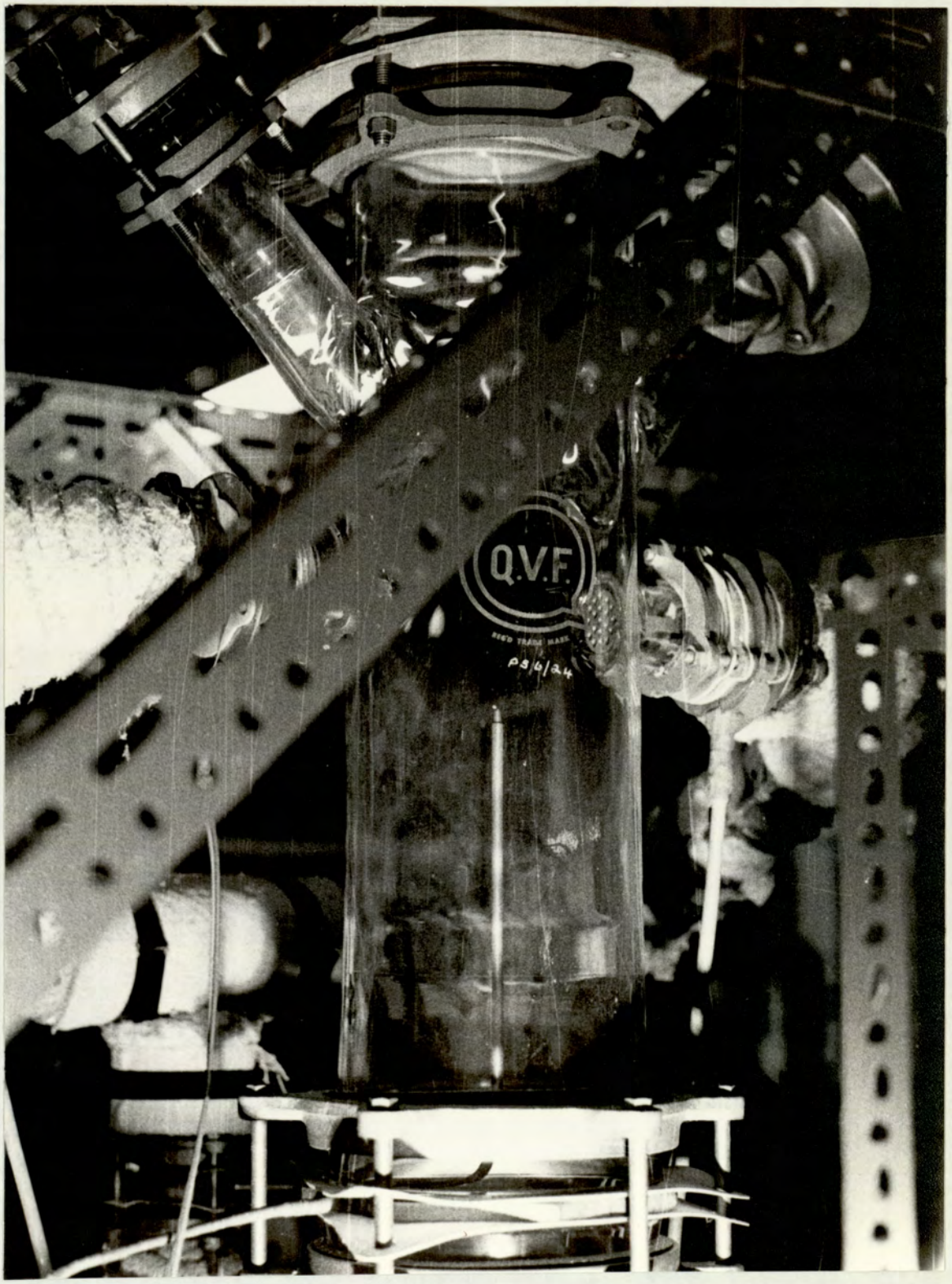

FIGURE 4:12 SHORT MOVING BED COLUMN
(HEAT TRANSFER STUDY)

2. Air at Inlet to the Bed

Akers[2] experienced great difficulty with this measurement as the hot air became stratified in its flow around the bends in the supply pipework. He overcame the radial distribution by using mixers similar to those shown in Figure 4:11. In the present work the thermocouples were fitted inside 1/16 in stainless steel tubes which passed through $\frac{1}{8}$ in thick Q.V.F. asbestos gaskets placed immediately downstream of the mixers so that the radial distributions could be investigated.

3. Solids at Outlet from the Heat Transfer Section of the Moving Bed

A probe was positioned from below the test section so that no dislocations of the packing were introduced. The probe was a $\frac{1}{4}$ in O.D. stainless steel pipe surrounding a spring steel coil pipe with a thermocouple on the inside, see Figure 4:12. Thus limited axial temperature scans could be carried out. The stainless steel pipe was silver soldered to a $\frac{3}{8}$ in thick brass ring clamped between gaskets in the joint at the bottom of the column.

4. Solids at Inlet to the Bed

Thermocouples were fitted between the P.T.F.E. expansion bellows and 2 in side arms on each side of the column. They protruded into the pipe by about $\frac{1}{8}$ in.

5. Air at Outlet from the Bed

A probe for radial scans was mounted horizontally in the joint at the top of the column. It consisted of a thermocouple sleeved with P.V.C. up to the junction and sheathed with $\frac{1}{4}$ in O.D. stainless steel to within 2 in of the junction.

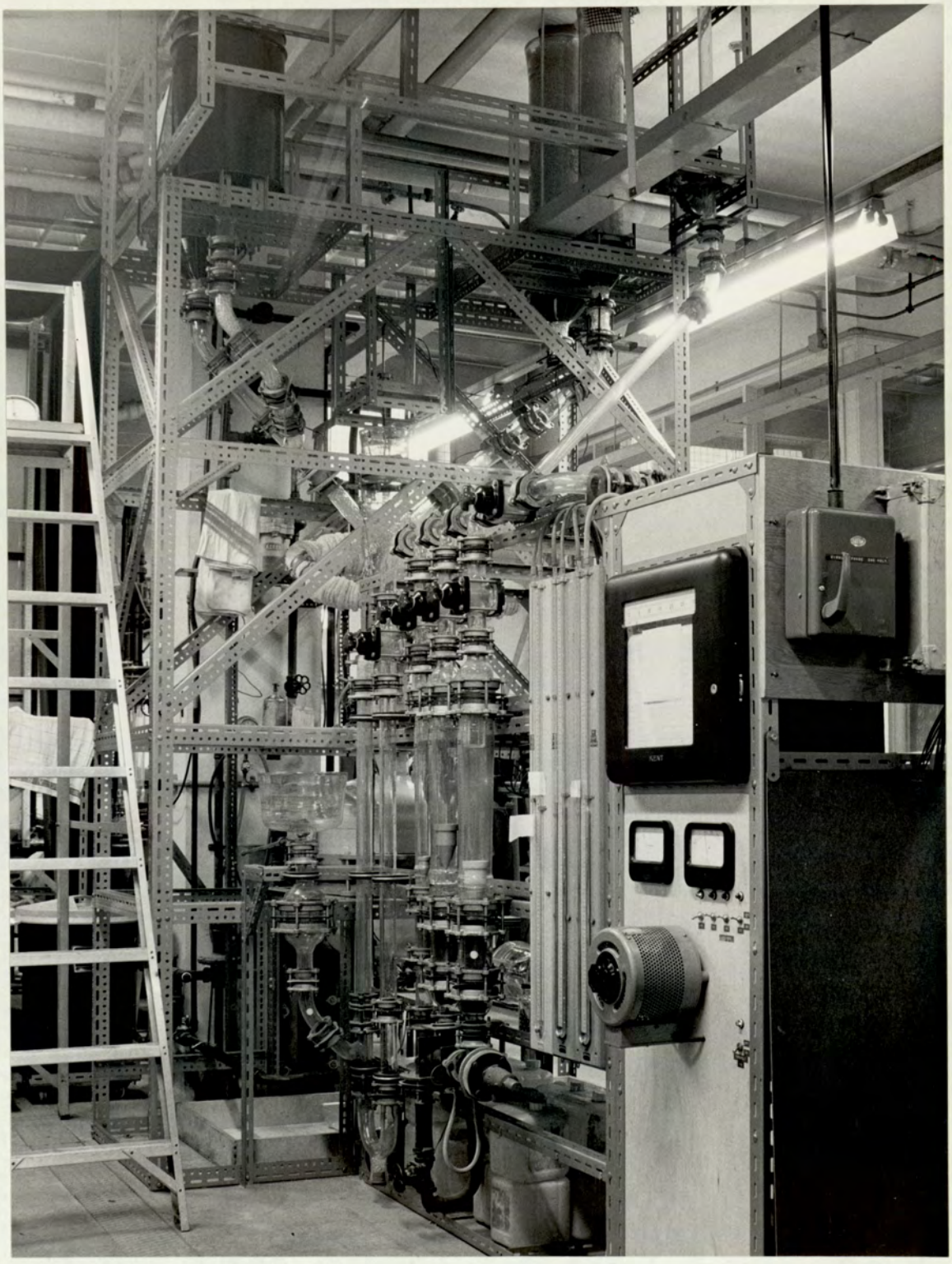

FIGURE 4:13 GENERAL VIEW OF WEST SIDE OF RIG

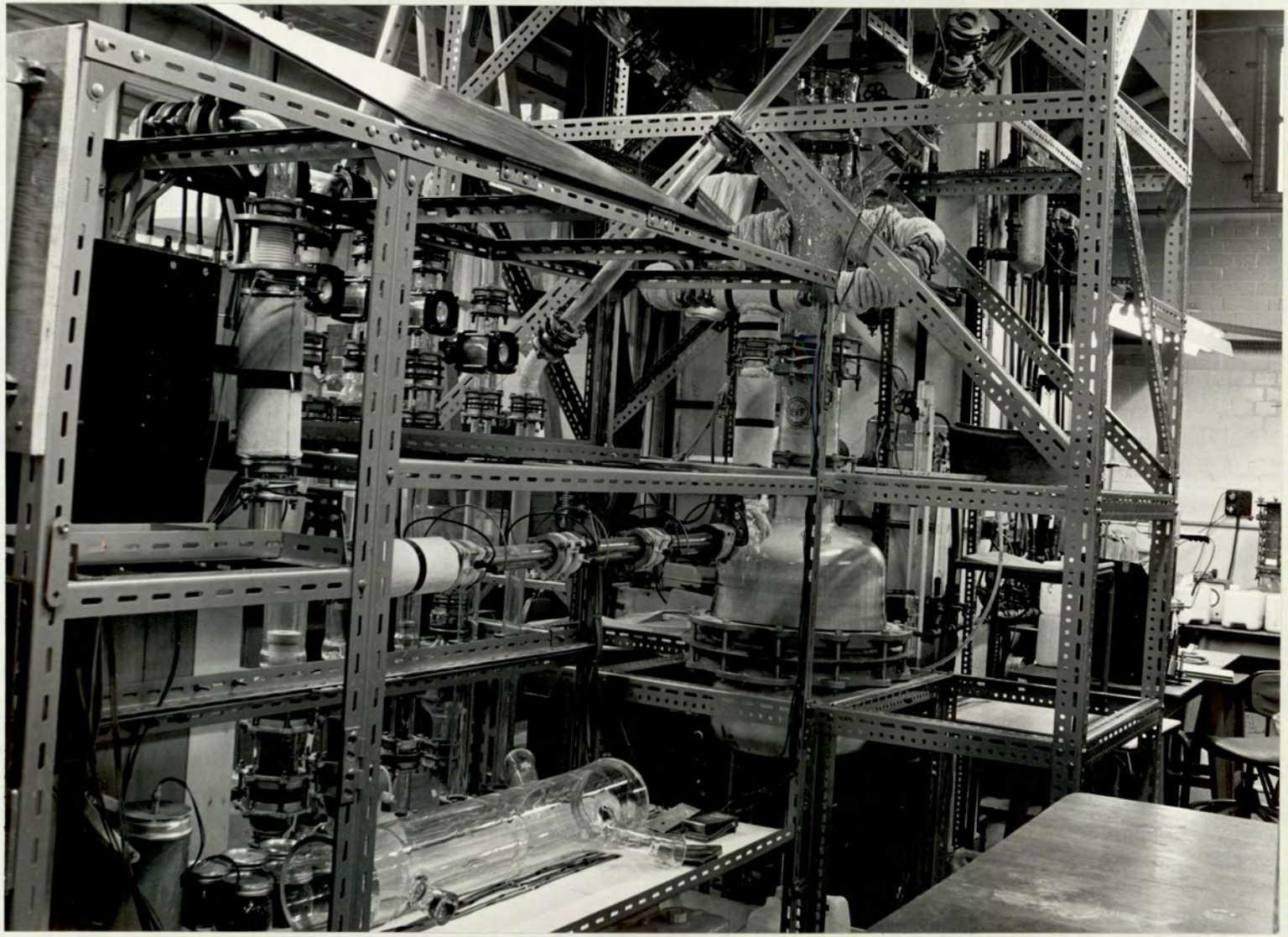

FIGURE 4:14 GENERAL VIEW OF EAST SIDE OF RIG

6. Ambient Air

Thermocouples were attached to the framework at ground, mean and ceiling level.

7. Cold Junction

This was immersed in liquid paraffin contained in a sealed polythene tube to prevent corrosion by ice-water[89].

4.1.7 Miscellaneous features

A pressure relief valve set at 20 lbf/in^2 gauge was fitted to the inlet side of the Rotameters.

Neoprene rubber gaskets were used on all Q.V.F. joints operating at ambient but for higher temperatures compressed asbestos fibre gaskets were used. These were fairly satisfactory for simple joints but were insufficiently pliable for sandwiching thermo-couples or heater connections. The maximum working temperature for neoprene is only 120°C and for butyl rubber 150°C. As it was possible that Akers' range of operation might be extended, gaskets were made from 1/16 in silicone rubber sheet which would be suitable up to 220°C.

Thermal expansion was accommodated by fitting P.T.F.E. bellows between the side arms and the feed hoppers. The air heater pipework was suspended on spring-loaded hangers and a bellows was fitted at the cold end.

Perforated plate baffles were fitted in both air inlets to prevent ballotini entering the side arms.

Figures 4:13 and 14 are general views of the apparatus.

4.2 Preliminary Tests of Apparatus at Ambient Temperature

4.2.1 Discharge hopper flow characteristics

On opening the discharge hopper valve, the support material

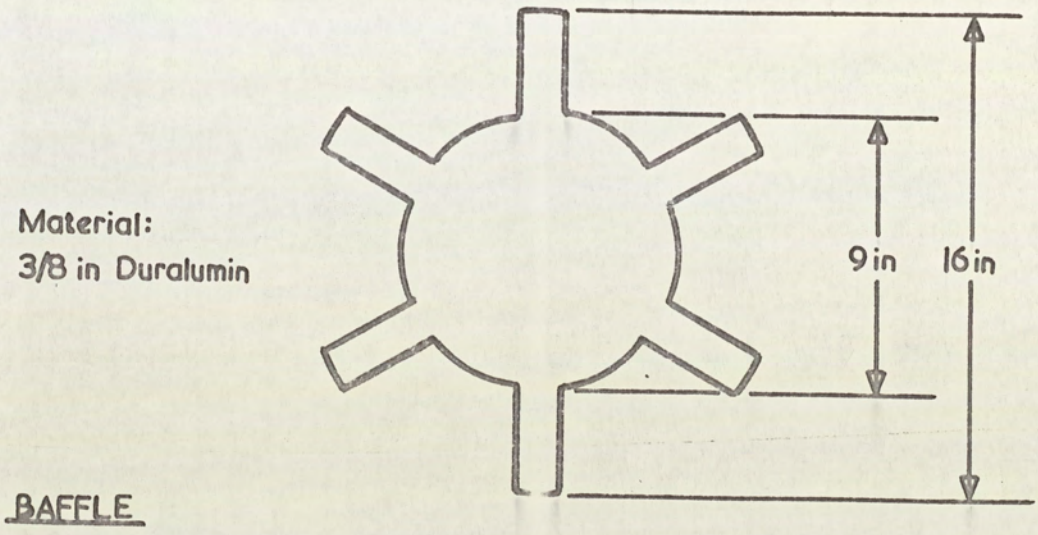

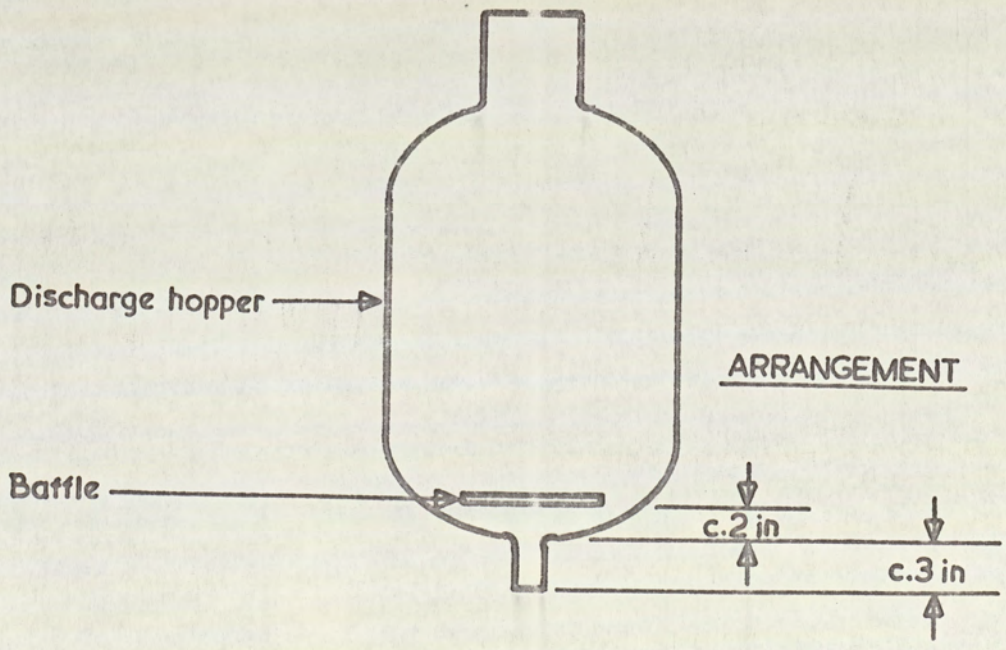

FIGURE 4:15 BALLOTINI DISCHARGE HOPPER BAFFLE

drained out, the bed descended and fresh material ran in from the hoppers. However, after approximately 10% of the 336 lb of lead glass support ballotini had been discharged, soda glass test spheres appeared in the discharge. This was attributed to the formation of a "rat hole" due to the large ratio of hopper to orifice diameters, i.e. flow was confined to the centre portion of the hopper, the extremeties remaining static. Richards[90] described a method for the design of baffles which would induce "mass flow" (flow distributed over the whole cross section) in hoppers subject to "rat holing". A baffle was designed accordingly and is shown in Figure 4:15. Flow was then much more satisfactory and at least 80% of the support material could be utilised before mixing of the two grades of ballotini was apparent. The quantity of support material was later increased to about 390 lb and then all test spheres (260 lb) passed through the heat transfer section before any appeared in the discharge.

4.2.2 Rotameter float instability

Above scale heights of 15 cm, the Rotameter floats became very unstable. It was consequently difficult to estimate the flow-rate and there was a danger of breakage of the tubes and the korranite float. The manufacturers suggested[91] the phenomenon was due to disturbances in the inlet pipework and could be overcome by increasing the length of straight pipe and fitting flow straighteners. Simple straighteners comprising two 1/16 in thick sheets of copper intersecting at right angles were fitted in additional 6 in lengths of Q.V.F. pipe. Thereafter, the floats were quite stable up to the maximum throughput of each Rotameter.

4.2.3 Fixed and moving bed pressure drops

It was noticed that the bed pressure drop decreased as the

discharge valve was opened and the bed started to move. At first this was attributed to the decrease in bed height from that achieved by rapid loading to that maintained under flow conditions but calculation showed that this was not the complete explanation. It appeared that the bed gradually expanded as it moved. The measurement of voidage in relation to particle size, vessel size and movement will be discussed in Section 4.4.

4.2.4 Solids flowrate measurement

The support ballotini was seen to be draining out much faster with air flowing through the bed than without. The column and discharge hopper were pressurised. Thus the solids flowrate was a function of the air flowrate and bed material as well as the orifice size. Calibration of the orifices was felt to be possible but inadvisable as subsequent calculation of heat transfer coefficients would be dependent on the accuracy of pressure drop measurements as well as the calibration itself. Two methods were proposed for measurement of the solids flowrates during runs:

(1) Weighed charge method in which a known quantity of material is loaded into the hopper and timed from the start of movement until the supply is exhausted.

(2) Calibrated hopper method in which the transparent hoppers are graduated in terms of weight of ballotini and the fall of the material past the graduations is timed.

It was proposed that the supply of ballotini during the period of bed expansion referred to in Section 4.2.3 should be taken from a hopper other than that in which the flowrate would be determined due to the transient nature of the period both from solids flow and heat transfer considerations.

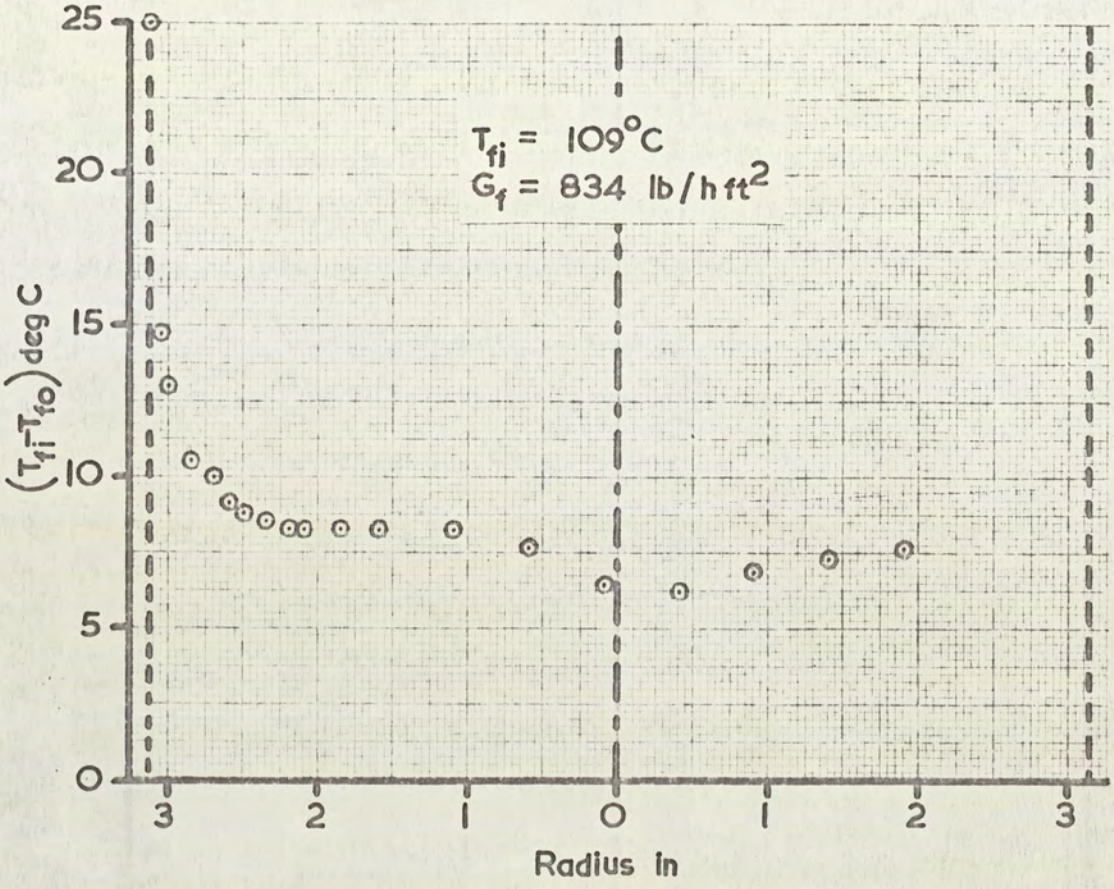

FIGURE 4:16 RADIAL T_{fo} SCAN : HORIZONTAL PROBE : FIXED BED

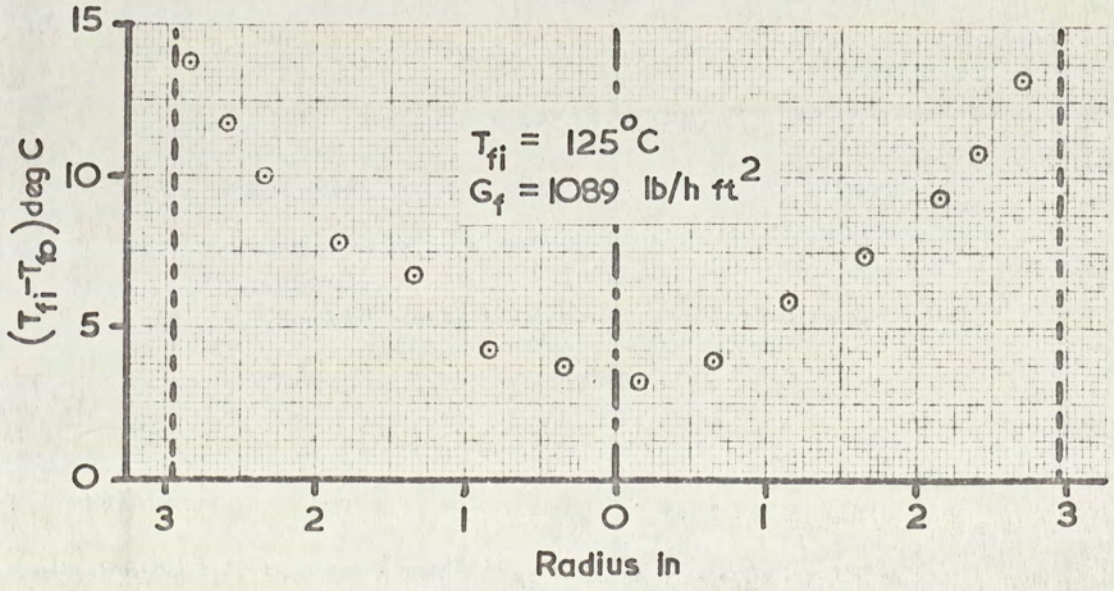

FIGURE 4:17 RADIAL T_{fo} SCAN : VERTICAL PROBE : FIXED BED

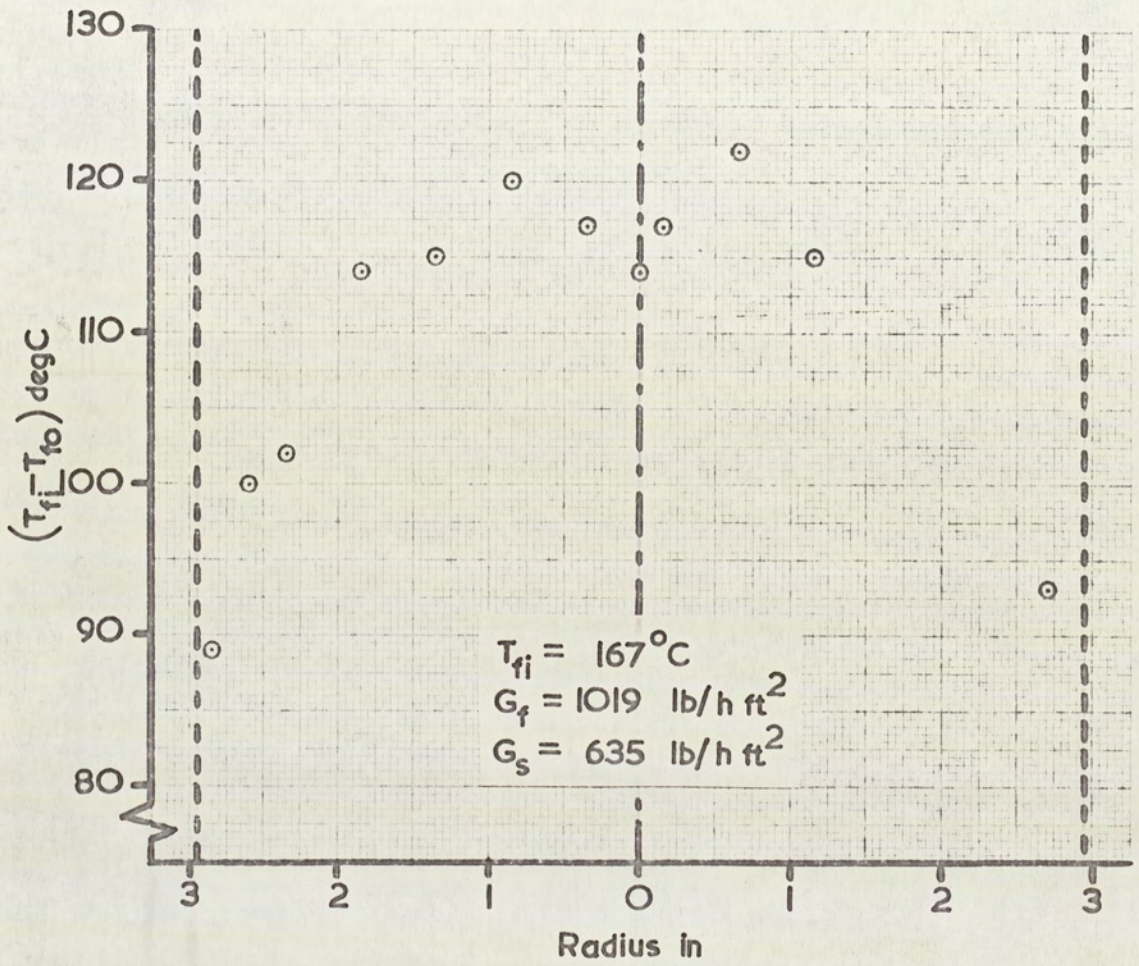

FIGURE 4:18 RADIAL T_{fo} SCAN : VERTICAL PROBE: MOVING BED

4.3 Preliminary Tests of Apparatus at Elevated Temperatures

4.3.1 Air outlet temperature measurement

The horizontal probe was used to scan across the diameter of the long column to investigate the temperature profile for fixed beds at steady state, i.e. only heat transfer was through the wall to the surroundings. On moving the probe it was found that there was a time lag of about two minutes before the thermocouple registered the new steady state value. This was attributed to the conduction lag in the P.V.C. sleeving. The time lag was reduced to about 5s by removing 1 in of sleeving adjacent to the thermocouple junction.

Except very close to the walls, the temperature profile was fairly flat as illustrated in Figure 4:16. However, the effect of the sleeving had demonstrated the importance of conduction along the thermocouple wires so, ideally, both the junction and the wire adjacent to it should be at isothermal conditions. Axial temperature variations were unlikely to be significant so the closest approach to isothermal conditions for the bead and wires would be obtained by mounting the thermocouple vertically. The stainless steel sheath was replaced with a longer $\frac{1}{4}$ in I.D. copper one suspended parallel to the column axis. With this probe the temperature profile was shown to be parabolic and much steeper, see Figure 4:17. The profile shown in Figure 4:18 was obtained under moving bed conditions. It can be seen that the air temperatures adjacent to the walls were higher than on the axis, whereas the reverse was true for fixed beds. Steady state appeared to have been achieved but the profile in Figure 4:18 could have been due to heat flowing into the bed from the walls and two layers of

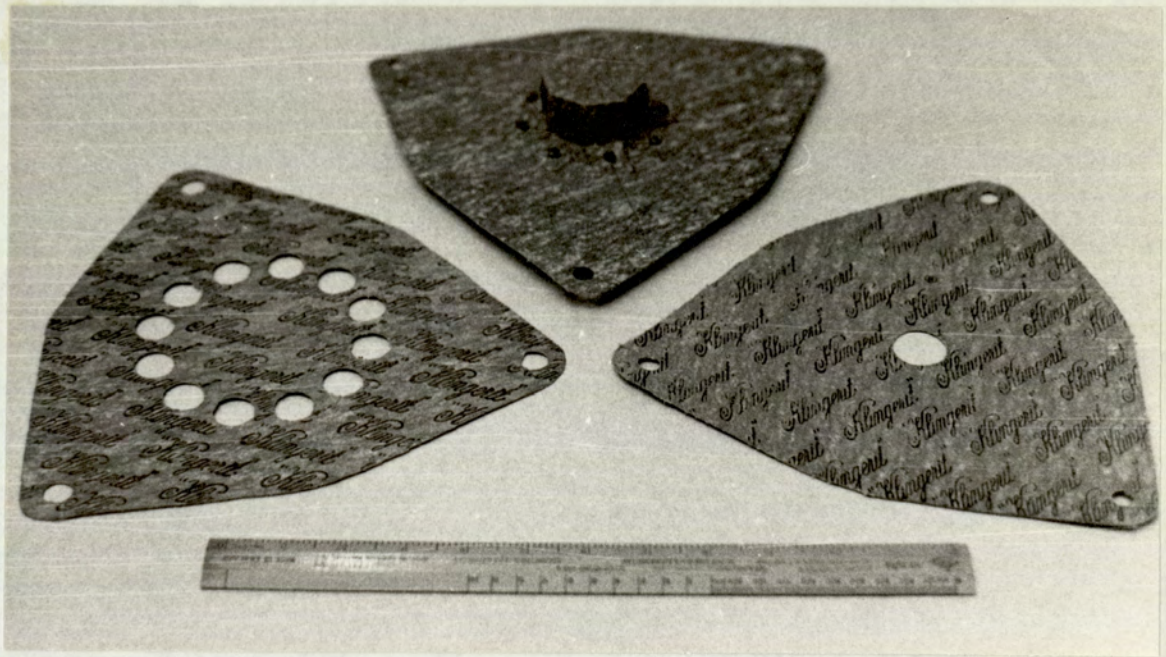

FIGURE 4:19 OUTLET AIR MIXERS

1 in diameter asbestos rope lagging. Another possible reason is that dislocations of the bed packing arrangement near the walls increased the local voidage so there was preferential air flow in that region. To be certain that the bed and column achieved steady state in an acceptable time, it was felt that the heat capacity and conduction resistance of the column should be reduced by dispensing with the lagging. However, the greater heat losses would then tend to increase the radial air temperature distribution so some method of measuring the mean value was required.

It is conceivable that the mean could be obtained by integration of point values of temperature and velocity but this would introduce considerable practical problems. The velocities would be too low for accurate Pitot tube measurements so other methods, such as hot wire anemometry[46] at ambient temperature, would have to be employed. The simplest solution seemed to be the use of a mixing device so that only one measurement of the outlet air temperature and none of velocity would be required. A low pressure drop baffle was made of 1/16 in Klingerit with twelve $\frac{3}{4}$ in diameter holes on a pitch circle of 4 in diameter as shown in Figure 4:19. Scans at each of the holes showed that there were no significant temperature distributions so it would suffice to measure the outlet air temperature in later work at only one hole.

4.3.2 Solids inlet temperature measurement

The thermocouples fitted in the joints between the 2 in side arms and the P.T.F.E. expansion bellows became heated by conduction through the side arms so they were moved to the joints at the opposite ends of the bellows. The conduction effect was still appreciable under fixed bed conditions but, once the ballotini

TABLE 4:1. BALLOTINI DENSITIES AND DIAMETERS

Nominal diameter mm	Actual diameter mm	Density g/cm^3
6	5.97	2.45
9	8.90	2.49
12	11.88	2.50

TABLE 4:2. VESSEL DIAMETERS AND VESSEL: PARTICLE DIAMETER RATIOS

Column	d_v		$d_v : d_p$		
	in	mm	Nominal particle diameter mm		
			6	9	12
Long (Ballotini flow characteristics)	5.88	149.4	25.0	16.8	12.6
Short (Moving bed heat transfer)	6.07	154.3	25.8	17.3	13.0

started flowing, the indicated temperature rapidly approached values near to ambient, generally slightly above but sometimes even below.

4.3.3 Air inlet and solids outlet thermocouple probes

These probes were intended to be used for radial (air) and axial (solids) scanning but the insulating lacquer proved to be too brittle for this application and flaked off. The couples then shorted out on the steel sheaths. The problem was overcome by inserting the individual wires in P.T.F.E. sleeving. The stainless steel sheaths of the gas inlet probes were dispensed with completely.

4.3.4 Air heater efficiency

At low flowrates, much of the heat seemed to be transferred directly from the elements to the pipe by radiation as softening of the borosilicate glass (softening point 600°C) occurred on one occasion despite the air temperature at the column inlet being only 140°C. Quantitative measurements of the efficiency will be described in Section 4.4.6.

4.4 Important Parameters of Equipment and Heat Transfer Materials

4.4.1 Ballotini density and particle size

The mean density and particle diameter of the test ballotini were determined simultaneously by a specific gravity bottle method. The results are shown in Table 4:1.

4.4.2 Internal diameters of moving bed columns

Measurements with internal calipers were unsatisfactory due to variations in the bore so the mean diameter was obtained by weighing the quantity of water in a known length of the column. The results together with the corresponding values of $d_v : d_p$ are shown in Table 4:2.

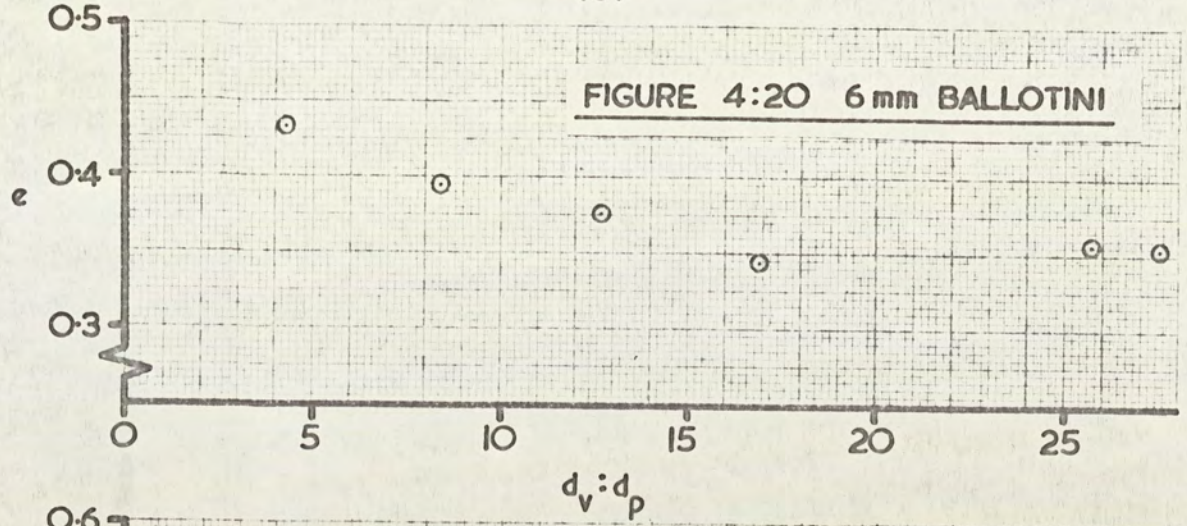

FIGURE 4:20 6 mm BALLOTINI

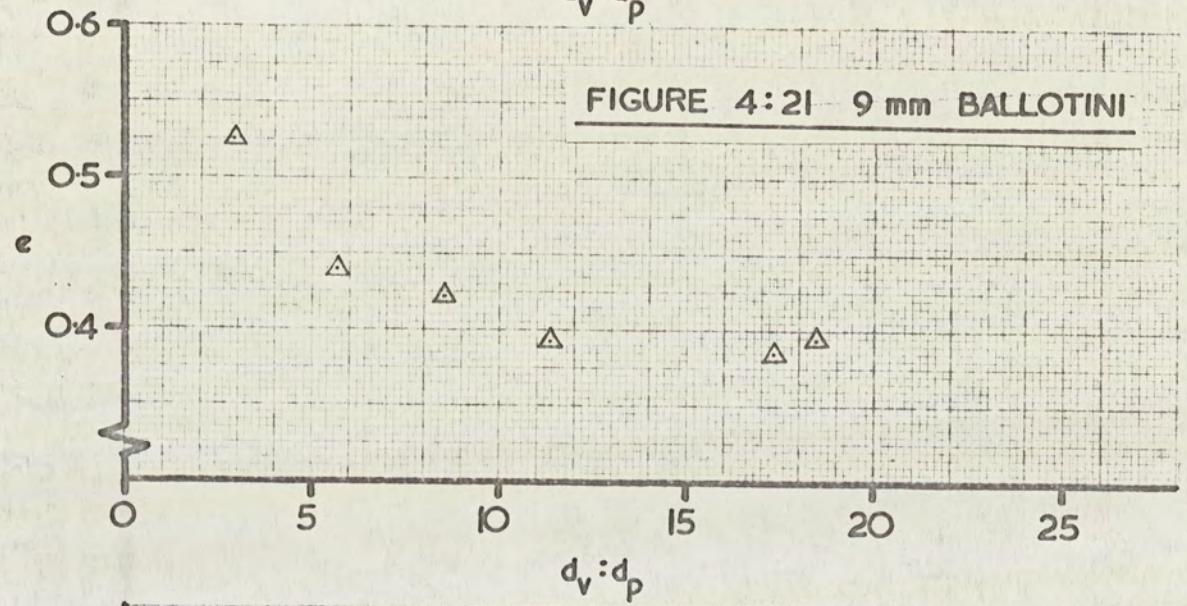

FIGURE 4:21 9 mm BALLOTINI

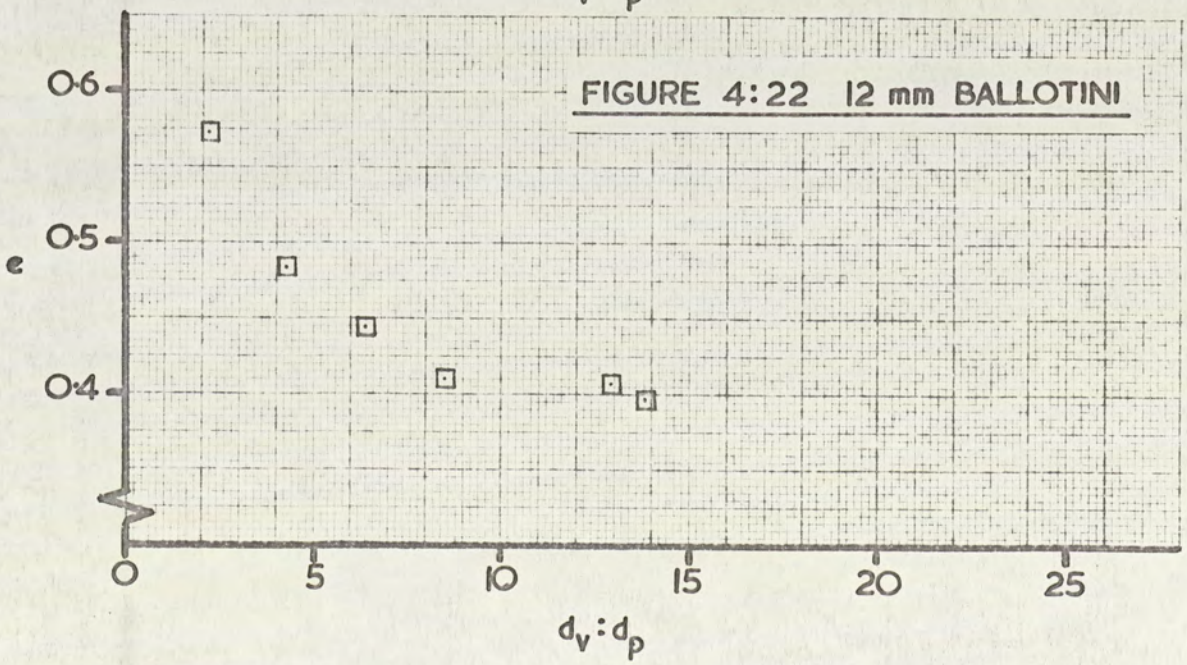

FIGURE 4:22 12 mm BALLOTINI

FIGURES 4:20, 4:21 & 4 22 WALL EFFECTS : e v. $d_v : d_p$

4.4.3 Relationship between voidage, particle size and vessel diameter

As a preliminary to measurements in the moving bed columns, the voidage was measured for the three sizes of test ballotini in containers ranging from 1.0 to 6.46 in I.D. to determine the magnitude of the wall effect and perhaps draw some qualitative conclusions about the heat transfer aspects. The containers were tapped to produce close, random packing. The results are expressed graphically in Figures 4:20, 21 and 22. It can be seen that wall effect rapidly decreased as $d_v : d_p$ increased and was virtually zero at the values of the ratio to be used in the present work. It was reasonable to conclude that any further increases in $d_v : d_p$ would not result in appreciable increases in heat transfer. This was fairly consistent with the findings of Denton[39,40] viz. no increase in heat transfer provided $d_v : d_p > 17.5$. Even for the 12 mm ballotini ($d_v : d_p = 13$) the errors seemed likely to be small.

4.4.4 Moving bed voidage

Although the information presented in the previous section seemed adequate, it was felt that the voidage should be measured under actual moving bed conditions because there was no certainty of close packing of the particles and because preliminary work had suggested that a voidage change occurred as the bed began to move. At first a visual method of measuring the bed expansion was employed in which coloured ballotini tracers were placed at the wall of the long column 9 in height apart. The separation was measured after the bed had descended a further 9 in. The indicated change in voidage of about 1% was less than the preliminary pressure drop measurements had suggested and the space velocity of the tracers was less than that calculated from the mean solids mass

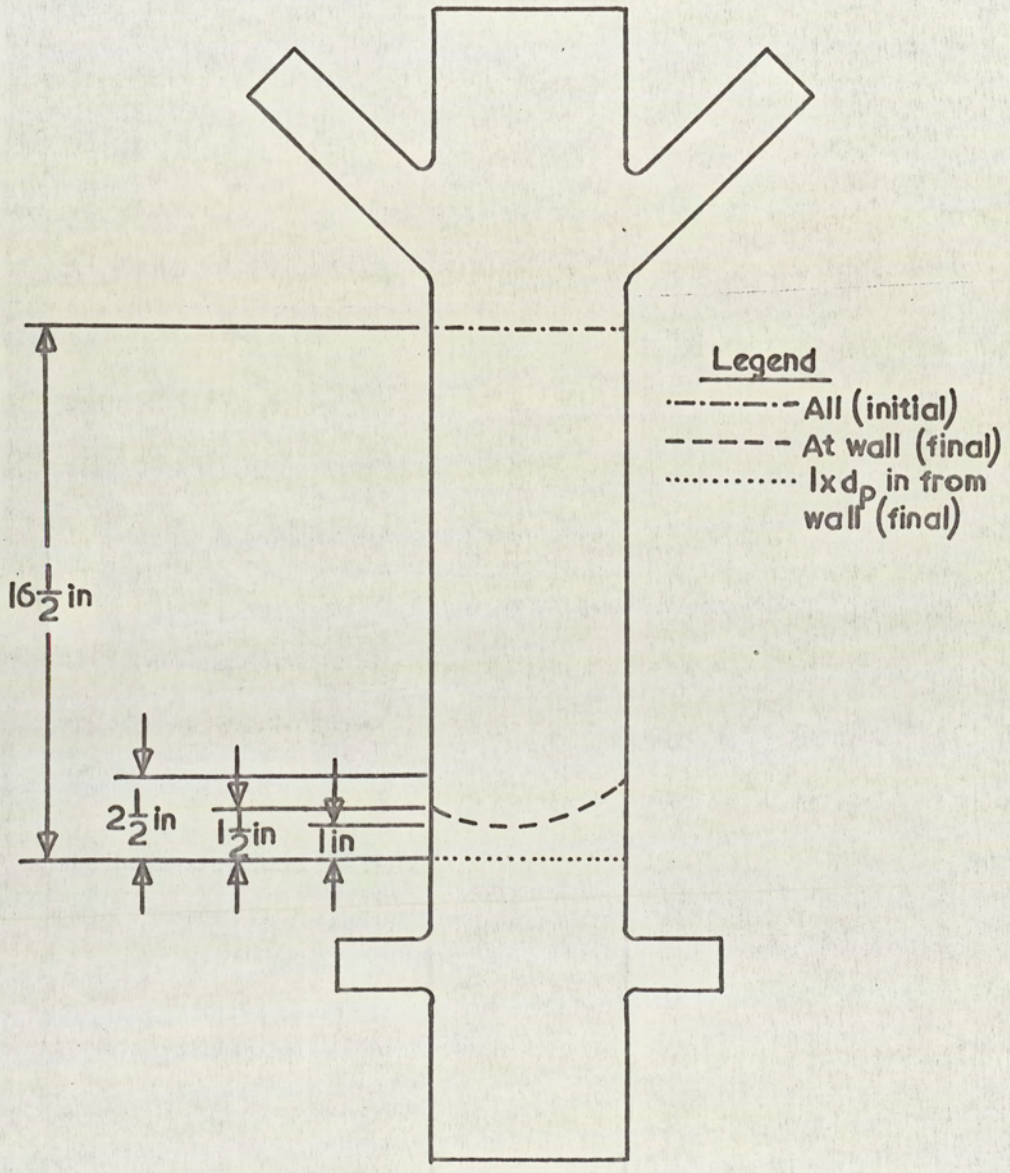

FIGURE 4:23 DEMONSTRATION OF SOLIDS VELOCITY PROFILE WITH COLOURED BALLOTINI

flowrate. It was concluded that there was a radial solids velocity profile. This was confirmed by placing a ring of tracers around the whole circumference extending two particles into the bed. After allowing the bed to descend, separation of those in contact with the wall from those further in occurred. There was some scatter but the separation was clearly visible and, from the pattern shown in Figure 4:23, was largely attributable to the conditions at the air feed side arms. Although the inlet baffles prevented gross penetration of the side arms by the ballotini, they did not present a smooth surface continuous with the column wall so some outward movement, hold-up and consequent dislocation of the matrix must have occurred. As the bed was not sufficiently transparent, it proved impossible to investigate the velocity profile further in. It is pertinent to note that both Denton[92] and Akers[2] reported that beds of spheres moved in plug flow but the present findings were confirmed by Brinn et al[74] with sand of mean diameter 0.025 in moving down a 1 in copper pipe. They demonstrated the presence of plug flow over much of the cross section but a velocity profile near the walls. Although the use of tracers provided useful information on the mechanism of the solids flow, it did not yield the voidage. Sissom and Jackson[31] described a direct method which involved trapping the bed between gate valves but this was not possible in the present equipment and probably would not work with large ballotini anyway. It was felt that the mean values of moving bed voidage would be obtained most easily from pressure drop measurements.

The voidage under the static conditions produced by rapidly loading the column was calculated from the weight of material charged, bed depth, column diameter and ballotini density. The

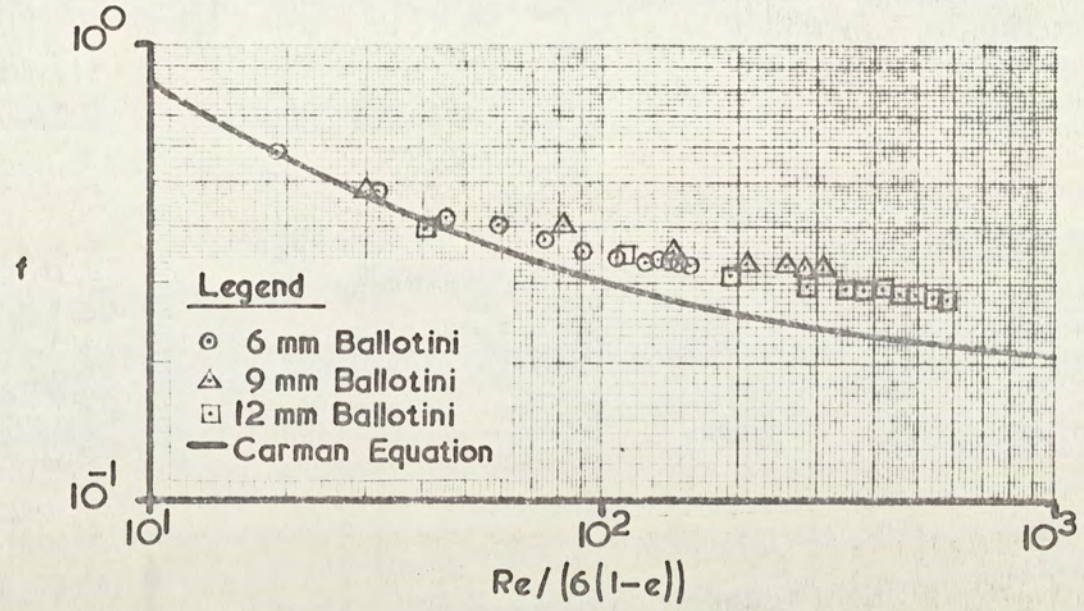

FIGURE 4:24 COMPARISON OF FRICTION FACTORS WITH CARMAN'S EQUATION

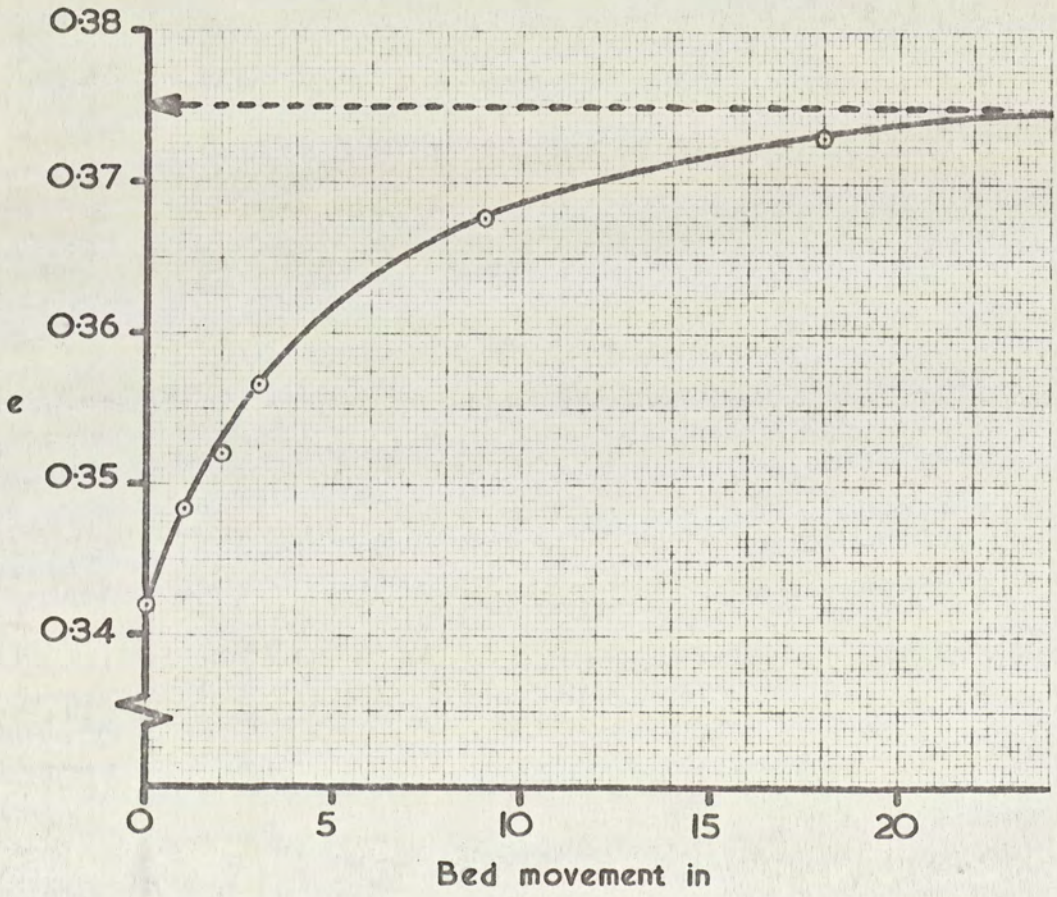

FIGURE 4:25 VOIDAGE CHANGE DURING BED MOVEMENT: 6 mm BALLOTINI

pressure drop through the bed was measured over a range of air flowrates. The ballotini gate valves were not designed to be air-tight so the discharge valve leaked even when closed. The leakage could be eliminated by sealing with P.V.C. tape when the bed was stationary but then the moving bed voidage could not be measured. However, although expansion of the bed could be detected visually when movement started, there was no evidence of the bed compacting once movement stopped. Therefore, the procedure was to allow the bed to descend a measured distance, shut the discharge valve, seal it with tape and then determine the pressure drops again. This was repeated until there was no further change in the voidage as indicated by the pressure drops becoming independent of the bed movement.

It was thought that it might be possible to match the data for the freshly loaded static beds to the Carman equation[93]

$$f = 5\left(\frac{Re}{6(1-e)}\right)^{-1} + 0.4\left(\frac{Re}{6(1-e)}\right)^{-0.1} \quad \ldots\ldots\ldots\ldots (4:1)$$

where the friction factor f is

$$f = \frac{\Delta P . e^3 . d_p}{L . 6(1-e)\rho_f . V^2}$$

and the superficial velocity V is

$$V = \frac{G_f}{\rho_f}$$

and then solve for the moving bed voidage but, as shown in Figure 4:24, the data did not fit equation (4:1). Attempts were made to improve the fit by modifying the constants 5 and 0.4 but without success. A more satisfactory approach was to fit polynomials to the fixed bed data using a computer library curve

TABLE 4:3. FRICTION FACTOR V. REYNOLDS NUMBER POLYNOMIALS

Coefficient	Nominal particle diameter mm		
	6	9	12
C_{13}	9.31×10^{-1}	5.40×10^{-1}	4.28×10^{-1}
C_{14}	-2.77×10^{-2}	-2.33×10^{-3}	-8.05×10^{-4}
C_{15}	5.98×10^{-4}	9.57×10^{-6}	-5.95×10^{-8}
C_{16}	-6.67×10^{-6}	-2.24×10^{-8}	9.50×10^{-9}
C_{17}	3.63×10^{-8}	4.64×10^{-11}	-2.23×10^{-11}
C_{18}	-7.57×10^{-11}	-6.20×10^{-14}	1.53×10^{-14}
Range of $\frac{Re}{6(1-e)}$	20 - 155	35 - 320	45 - 625

fitting program[94]. Polynomials from degree 1 to 6 were tried and degree 5 was considered most suitable. The general form of the equations was

$$f = C_{13} + C_{14}\left(\frac{Re}{6(1-e)}\right) + C_{15}\left(\frac{Re}{6(1-e)}\right)^2$$

$$+ C_{16}\left(\frac{Re}{6(1-e)}\right)^3 + C_{17}\left(\frac{Re}{6(1-e)}\right)^4 + C_{18}\left(\frac{Re}{6(1-e)}\right)^5 \quad \ldots\ldots (4:2)$$

The range of application of each of the equations and the values of the coefficients are shown in Table 4:3.

The moving bed voidage was determined from the static bed polynomials in the following manner. It was assumed that the relationship expressed in equation (4:2) would be the same during movement, the only change being that in the mean voidage. The voidage was obtained from (4:2) by an iterative, algorithmic method. Substituting for f in (4:2) and rearranging gives

$$e^3 = \frac{6(1-e)\rho.V^2.L}{\Delta P.d_p}\left(C_{13} + C_{14}\left(\frac{Re}{6(1-e)}\right) + \ldots\ldots C_{18}\left(\frac{Re}{6(1-e)}\right)^5\right)$$

For a particular test the term

$$\frac{6\rho.V^2.L}{\Delta P.d_p} = C_{19}$$

is a constant so

$$e = \left[(1-e)C_{19}\left(C_{13} + C_{14}\left(\frac{Re}{6(1-e)}\right) + \ldots\ldots C_{18}\left(\frac{Re}{6(1-e)}\right)^5\right)\right]^{\frac{1}{3}}$$

$\ldots\ldots\ldots$ (4:3)

which may be used as an algorithm by putting voidage on the right hand side as e_o, the first estimate, and on the left as e_1, the

value calculated on the assumption of e_o. The iteration proceeds until the difference between e_1 and e_o becomes less than some predetermined figure (0.0001). In this way the voidages were calculated at each air flowrate for each distance moved by the bed. The relationship between voidage and bed movement for the 6 mm ballotini is clearly shown in Figure 4:25. Unfortunately the tests were suspended before the true steady state voidage was achieved but extrapolation seems justified. It was not possible to obtain similar relationships for the 9 and 12 mm ballotini because the beds were fluidised during the wall heat loss calibrations which followed the measurements of the freshly loaded, static pressure drops. However, the consistency of the results at bed movements from 4 to 38 in (9 mm) and 1 to 13 in (12 mm) indicated that steady state voidages had been achieved, which was all that was required for analysis of moving bed heat transfer data. The results of these tests are contained in Appendix 2.4.

All of the tests described above were carried out using a 5/16 in discharge orifice, i.e. a mass flowrate of about 500 lb/h ft^2. No systematic attempt was made to investigate the effect of solids flowrate on the voidage but some preliminary tests with 6 mm ballotini were carried out using a $\frac{3}{4}$ in orifice (3 000 lb/h ft^2) as well as the 5/16 in one and no differences were detected.

4.4.5 Heat losses through the column walls

The theory on which the measurement of the heat losses was based was dealt with in Section 3.4.1 and equation (3:49) was derived for fixed beds at steady state conditions:

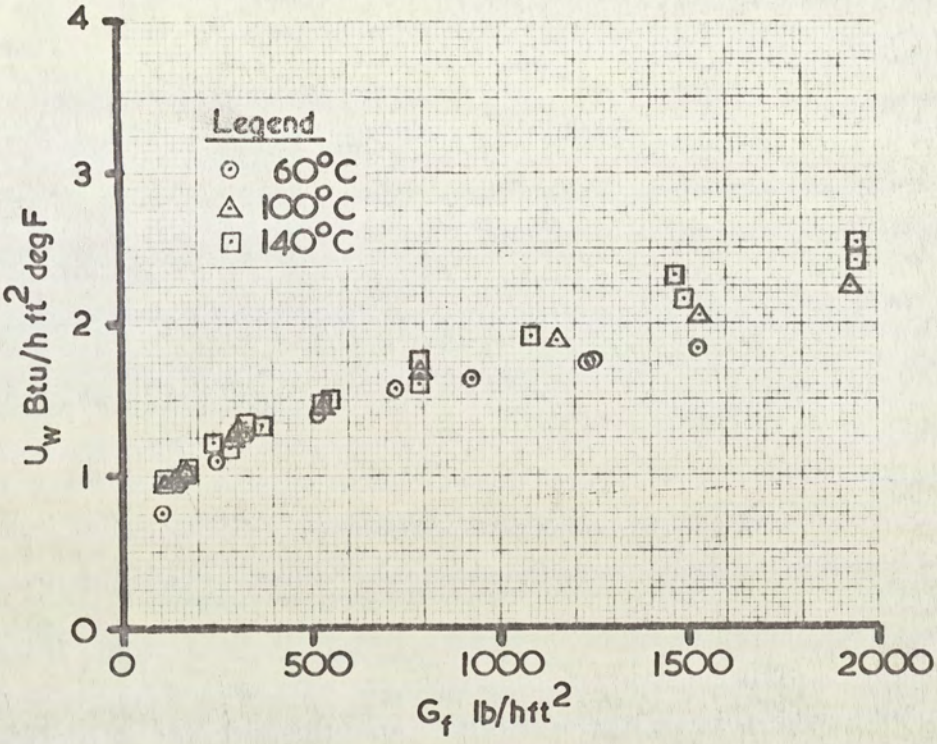

FIGURE 4:26 U_w v. G_f :LONG COLUMN:UNLAGGED: EMPTY

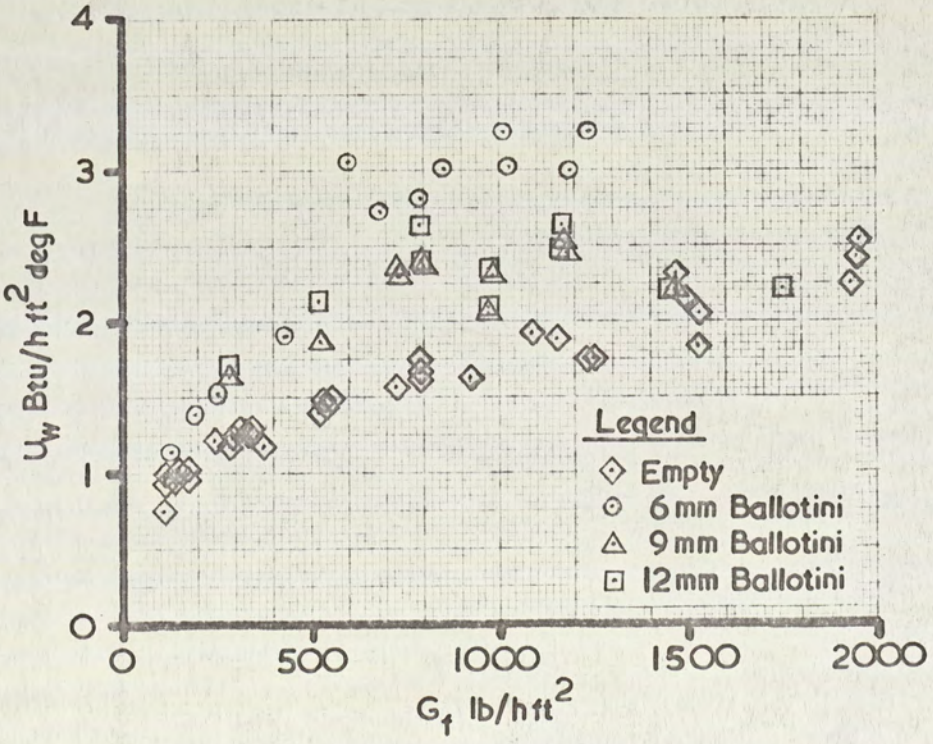

FIGURE 4:27 U_w v. G_f : LONG COLUMN: UNLAGGED: EMPTY & PACKED

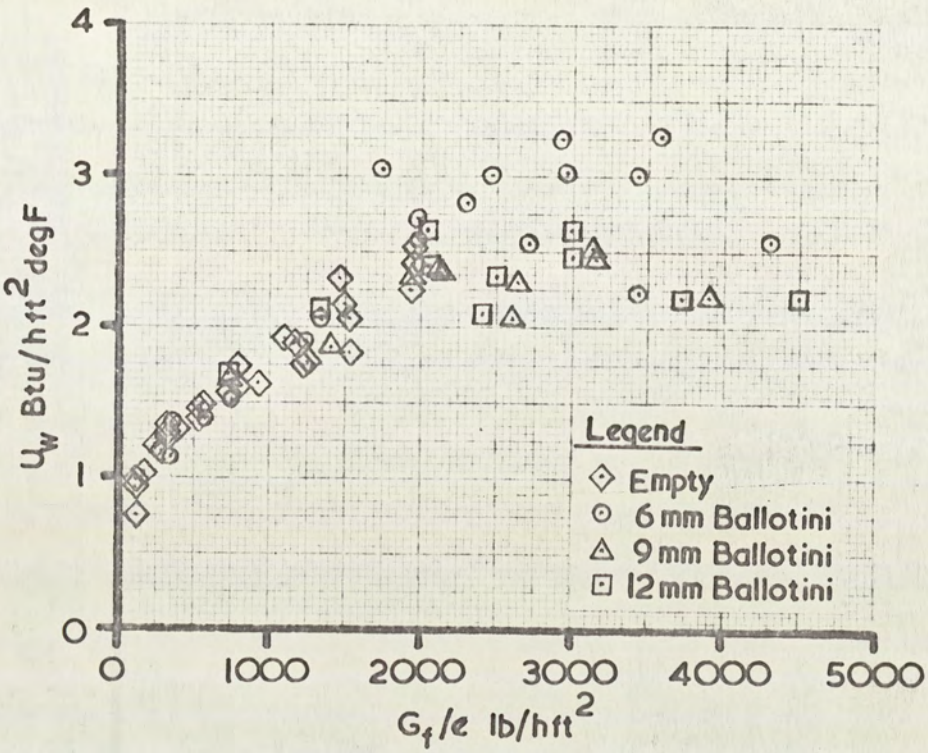

FIGURE 4:28 U_w v. G_f/e : LONG COLUMN : UNLAGGED : EMPTY & PACKED

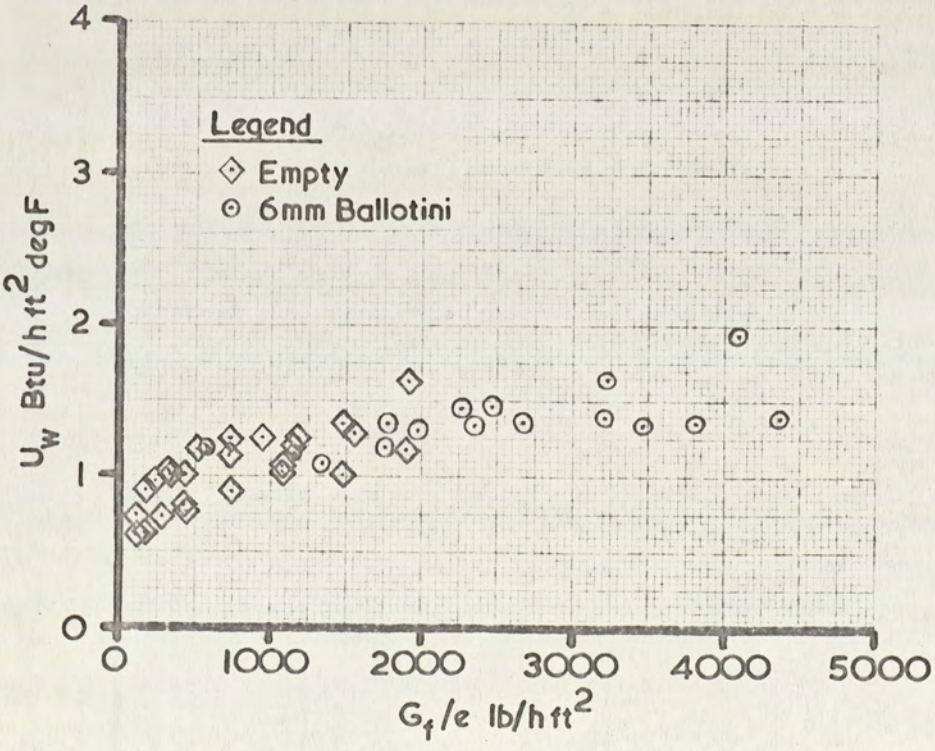

FIGURE 4:29 U v. G /e : LONG COLUMN : ONE LAYER OF LAGGING : EMPTY & PACKED

$$U_w = \frac{d_v \cdot G_f \cdot c_f}{4L} \log_e \left(\frac{T_{fi} - T_a}{T_{fo} - T_a} \right) \quad \ldots\ldots\ldots\ldots\ldots \quad (3:49)$$

where L is the length over which the temperature drop $(T_{fi}-T_{fo})$ occurs. This could have been the bed length but it was more convenient to measure T_{fo} at the outlet air mixing baffle in the joint at the top of the column. The ambient temperature used in (3:49) was that indicated by the thermocouple sited midway between floor and ceiling levels approximately 3 ft from the column. The conditions investigated were empty column, fixed beds of each size of soda glass test ballotini, unlagged column, lagged with one or two layers of 1 in diameter asbestos rope and air inlet temperatures of 60, 100 and 140°C. As the temperature drops were small, particularly at high flowrates, inlet temperatures of 60 and 100°C were used to simulate the conditions likely to be met during moving bed operation, i.e. the values of logarithmic mean temperature difference would be more realistic.

The first tests were carried out with the empty, unlagged column and the results are presented graphically in Figure 4:26. The dependence of the overall wall heat transfer coefficient U_w on the air flowrate G_f and, to a lesser extent, temperature T_{fi} is obvious. Strictly, U_w is probably dependent upon $(T_{fi}-T_a)$ or ΔT_{lmw} rather than T_{fi}. Inclusion of fixed bed data led to a much less satisfactory correlation, see Figure 4:27. However, it was realised that the space velocity of the air was higher in fixed beds than in the empty column by the factor $\frac{1}{e}$. Although there is still some considerable scatter, Figure 4:28 demonstrates the relationship between U_w and G_f/e. A similar but flatter relationship was obtained with the results for one layer of lagging, see

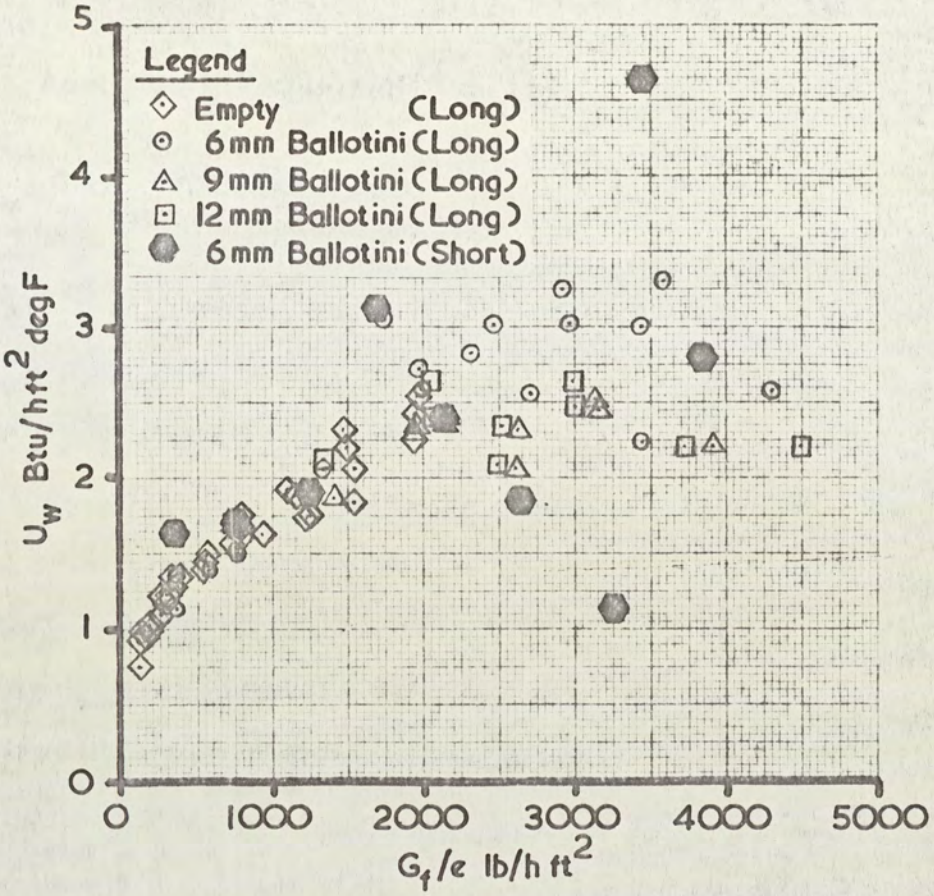

FIGURE 4:30 U_w v. G_f/e : LONG & SHORT COLUMNS UNLAGGED : EMPTY & PACKED

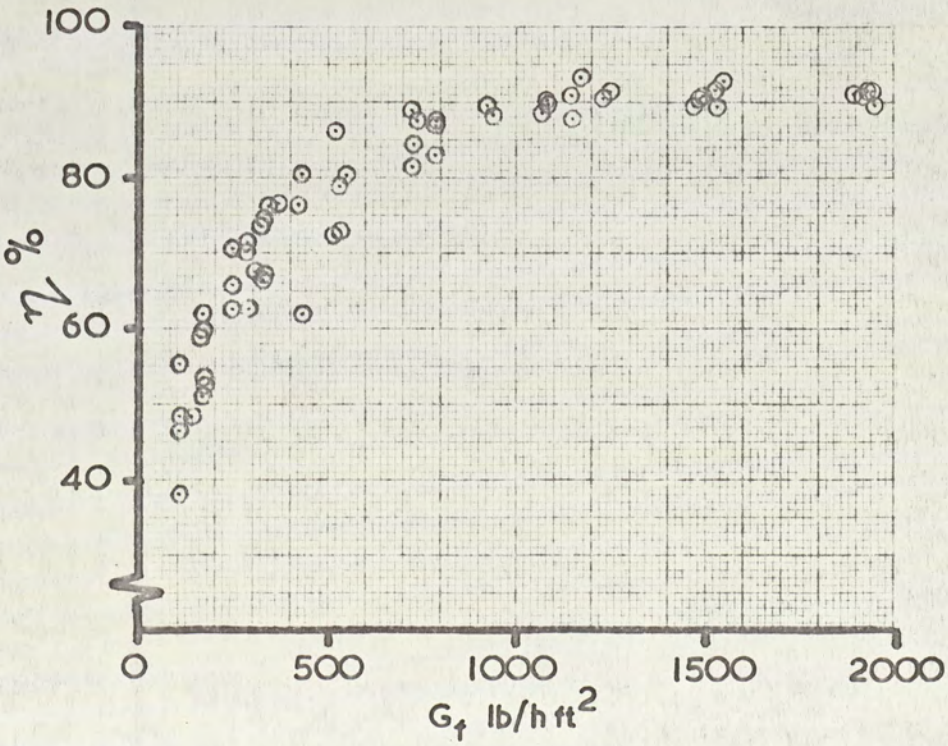

FIGURE 4:31 AIR HEATER EFFICIENCY

Figure 4:29. Data for two layers of lagging were obtained only with beds of 6 mm ballotini.

The scatter of the results can be seen to increase with the flowrate. As G_f increases, so does U_w but the quantity of heat lost as a proportion of that supplied decreases and T_{fo} approaches T_{fi}. The consequent relative error in measuring the difference $(T_{fi}-T_{fo})$ is probably a major factor in the scatter. It may also be that the measurements taken and the method of analysis were not sophisticated enough. Having established the dependence of U_w on G_f, the combination of empty column and fixed bed results could be criticised in that the region above the bed where e = 1 has been treated as if it also contained ballotini, i.e. U_w was assumed to be constant over the whole length of the column. There is probably a sharp discontinuity in the rate of heat transfer at the inside wall as the air emerges from the bed, but it is considered that no great change in the natural convection currents on the outside wall would occur and that constant U_w is a reasonable first approximation.

In view of the extra time taken to achieve steady state with lagging on the column and also because of the need to measure the bed height in each run, it was considered that moving bed heat transfer in the short column should be carried out without lagging. Measurements of U_w for the short column were therefore restricted to a static bed of 6 mm ballotini without lagging. The scatter of the results was worse than with the long column, no doubt due to the greater relative errors in measuring the smaller differences between T_{fi} and T_{fo}, but the coefficients were of similar magnitudes as shown in Figure 4:30. Again it was assumed that U_w was constant over the whole length of the bed. This is perhaps more approximate

than for the long column as the length of empty tube between the top of the bed and the T_{fo} probe is comparable with the bed height.

The combined results for the two columns were correlated by the following equation using a three factor, least mean squares analysis:

$$U_w = 0.201 \left(\frac{G_f}{e}\right)^{0.310} \Delta T_{lmw}^{0.067} \quad \ldots\ldots\ldots\ldots (4:4)$$

where the units are

U_w: Btu/h ft^2 degF

G_f: lb/h ft^2

e : dimensionless

ΔT_{lmw}: equivalent chromel-alumel thermocouple output in mV

The detailed results of the wall heat loss measurements are given in Appendix 2:5.

4.4.6 Air heater efficiency

While carrying out the work described in the previous section, the electrical power consumption by the air heaters was noted and the efficiency η calculated using the temperature of the air entering the column T_{fi} as the final conditions:

$$\eta = \frac{G_f . A_x . c_f \, (T_{fi} - T_{hi}) \, 100}{I.v} \quad \ldots\ldots\ldots\ldots (4:5)$$

where T_{hi} is the temperature of the air entering the heater, I is the current taken by the heaters, v is the voltage drop across the heaters.

The efficiency is shown as a function of the air flowrate in Figure 4:31. It can be seen that the efficiency decreases rapidly below 500 lb/h ft^2 (expressed per unit cross section area of the long column; approximately equivalent to 8 000 lb/h ft^2 of

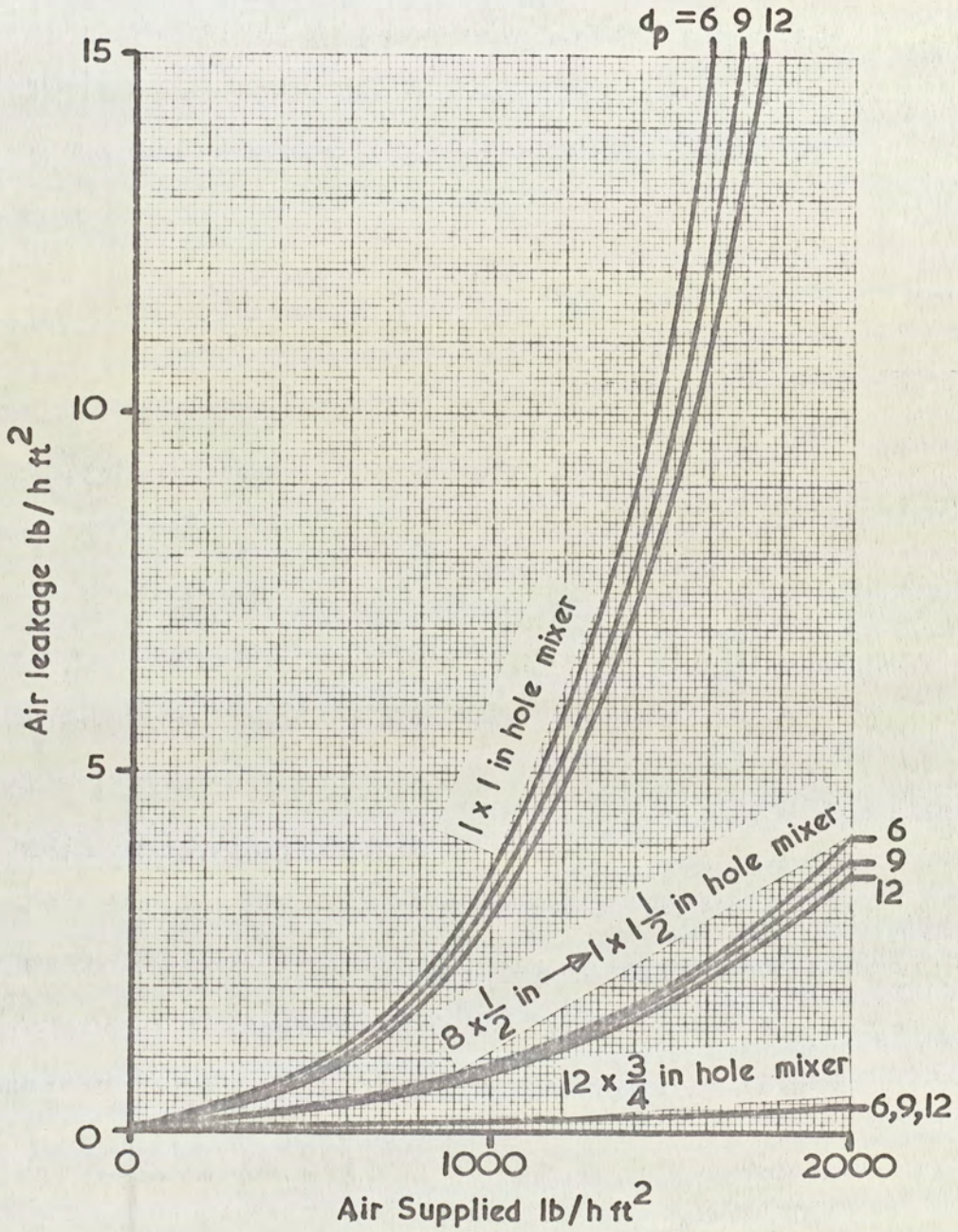

N.B. Flowrates expressed per unit cross sectional area of the moving bed.

FIGURE 4:32 AIR LEAKAGE THROUGH BALLOTINI DISCHARGE VALVE

the heater pipe cross section) as demonstrated by the softening of the borosilicate glass, see Section 4.3.4.

4.4.7 Air leaks

The leakage of air through the ballotini discharge valve and orifice was referred to in Section 4.4.4. Obviously such leakage reduced the quantity of air flowing upwards through the bed so must not be included in the heat balance when calculating transfer coefficients. The driving force for the leakage was the pressure in the bed at the air inlet and was dependent on the pressure drops across the bed and gas outlet mixing baffle. These pressure drops were measured separately and the pressure at the inlet point obtained as graphical functions of flowrate with ballotini size and mixer type as parameters. The top of the column was then blanked off and air supplied via an additional Rotameter, type M10K. With the discharge valve open and the bed moving, air was admitted to the column at a rate just sufficient to maintain the internal pressure at selected values. Thus the relationship between pressure and leakage was obtained. Hence, by eliminating pressure between the two calibrations, the relationship between air supplied to the column and leakage was determined, see Figure 4:32. The correction for leakage was quite small in all cases. It was thought that the leakage would be dependent on the discharge orifice size and possibly on the position of the interface between the test ballotini and the smaller support material. However, no relationship was detected for orifices from $\frac{1}{8}$ to $\frac{1}{2}$ in diameter nor for interface positions from 48 to 12 in above the orifice.

4.4.8 Thermophysical properties of air and ballotini

Air

The specific heat, viscosity and thermal conductivity of

TABLE 4:4. THERMOPHYSICAL PROPERTIES OF AIR

Temperature			C_f	μ_f	k_f
°F	°C	mV Chromel-Alumel	$\frac{Btu}{lb\,degF}$	$\frac{lb}{hft}$	$\frac{Btu}{hft\,degF}$
40.3	4.6	0.189	0.2396	0.04248	0.0143
90.3	32.4	1.328	0.2399	0.04536	0.0156
140.3	60.2	2.467	0.2403	0.04860	0.0168
190.3	87.9	3.606	0.2409	0.05148	0.0180
240.3	115.7	4.745	0.2416	0.05436	0.0191
290.3	143.5	5.884	0.2424	0.05688	0.0202
340.3	171.3	7.022	0.2434	0.05976	0.0213

air were required as functions of temperature which could either be used directly for point values or integrated to obtain means over specified ranges. Polynomials were fitted to the data[95] shown in Table 4:4 using the curve fitting computer program[94]. The properties were obtained as functions of the equivalent millivoltage outputs by chromel-alumel thermocouples rather than actual temperatures to avoid errors in converting to degrees when processing experimental data. Second degree expressions were found to be quite adequate:

$$c_f = 0.2396 + 0.0001778.T_f + 0.00005232.T_f^2 \quad \ldots\ldots (4:6)$$

$$\mu_f = 0.04190 + 0.002767.T_f - 0.00003304.T_f^2 \quad \ldots\ldots (4:7)$$

$$k_f = 0.01410 + 0.001132.T_f - 0.00001560.T_f^2 \quad \ldots\ldots (4:8)$$

where the units are

c_f: Btu/lb degF

μ_f: lb/h ft

k_f: Btu/h ft degF

T_f: equivalent millivoltage, chromel-alumel

These were then integrated as

$$\frac{\int_{T_{fo}}^{T_{fi}} f(T_f)\, dT_f}{(T_{fi}-T_{fo})}$$

to give the mean properties:

$$c_{fm} = 0.2396 + 0.0000889(T_{fi}+T_{fo}) + 0.00001744\,((T_{fi}+T_{fo})^2 - T_{fi}.T_{fo}) \quad \ldots\ldots (4:9)$$

TABLE 4:5. COEFFICIENTS IN SHARPE AND GINTHER'S EQUATION

Component	Weight fraction	Coefficient C_{20}		Coefficient C_{21}	
		Factor x 10^6	Component x 10^6	Factor x 10^4	Component x 10^4
SiO_2	0.7178	468	336	1 657	1 190
CaO	0.0460	410	18.85	1 709	78.7
Na_2O	0.1348	829	111.7	2 229	300.6
K_2O	0.0439	335	14.7	2 019	88.7
BaO	0.0402	-	-	-	-
MgO	0.0020	514	1.028	2 142	4.284
Fe_2O_3, Al_2O_3, TiO_2	0.0039	453	1.766	1 765	6.89
SO_3	0.0048	830	3.98	1 890	9.08
SbO_2	0.0048	-	-	-	-
Defficiency	0.0018	-	-	-	-
Total	1.0000		488.024		1 678.254
Weight fraction for which no factors available = 0.0468					
Correction = ÷ (1.0000 - 0.0468)					
Coefficients		C_{20} = 513 x 10^{-6}		C_{21} = 1 762 x 10^{-4}	

$$\mu_{fm} = 0.04190 + 0.001384\ (T_{fi}+T_{fo})$$

$$- 0.00001101\ ((T_{fi}+T_{fo})^2 - T_{fi}.T_{fo}) \quad \ldots\ldots\ (4:10)$$

$$k_{fm} = 0.01410 + 0.000566\ (T_{fi}+T_{fo})$$

$$- 0.00000520\ ((T_{fi}+T_{fo})^2 - T_{fi}.T_{fo}) \quad \ldots\ldots\ (4:11)$$

Ballotini

The English Glass Co. Limited[96] gave the following for the mean specific heat of soda glass ballotini between a datum of 20°C and T_s °C:

$$c_{sm,s-20} = \frac{0.00051.T_s + 0.1749}{0.00146.T_s + 1} \quad \ldots\ldots\ (4:12)$$

where T_s is expressed in °C.

A similar equation to this, but relative to a datum of 0°C, is that of Sharpe and Ginther[97]:

$$c_{sm,s-o} = \frac{C_{20}.T_s + C_{21}}{0.00146.T_s + 1} \quad \ldots\ldots\ (4:13)$$

It seems likely that (4:12) was derived from (4:13). The constants C_{20} and C_{21} are dependent upon the glass composition and have been calculated from tabulated factors[97] using a chemical analysis of the glass obtained by Akers[98], see Table 4:5. Substituting for C_{20} and C_{21}, (4:13) becomes

$$c_{sm,s-o} = \frac{0.000153.T_s + 0.1762}{0\ 00146.T_s + 1}$$

Although the solids temperature at inlet to the bed was about 20°C, a general equation relating to any two temperatures T_{si} and T_{so} would be preferable to (4:12):

$$c_{sm,so-si} = \frac{c_{sm,so-o}(T_{so}-0) - c_{sm,si-o}(T_{si}-0)}{(T_{so}-T_{si})} \quad \ldots\ (4:14)$$

Substituting (4:13):

$$c_{sm,so-si} = \frac{\left(\frac{0.000513.T_{so} + 0.1762}{0.00146.T_{so} + 1}\right)T_{so} - \left(\frac{0.000513.T_{si} + 0.1762}{0.00146.T_{si} + 1}\right)T_{si}}{(T_{so} - T_{si})} \quad \ldots\ldots\ldots\ldots (4:15)$$

This is the equation used for analysis of experimental data in the present work. However, it conflicts with that used by Akers[2] in which the value for C_{21} was 0.1697. It seems that this value was obtained by applying both (4:12) and (4:13) to the temperature range 0 to 20°C. While this is acceptable for (4:13), it is rather doubtful for (4:12):

$$(4:12): \quad c_{sm,0-20} = \frac{0.00051 \times 0 + 0.1749}{0.00146 \times 0 + 1}$$

$$= 0.1749$$

$$(4:13): \quad c_{sm,20-0} = \frac{0.000513 \times 20 + C_{21}}{0.00146 \times 20 + 1}$$

Equating the two and solving gives $C_{21} = 0.1697$. The error in the use of this value by Akers is likely to have been quite small and could not explain the gross discrepancies between his results and those of other workers (see Section 2.4).

The other property of the solid required is the thermal conductivity. Akers calculated it at -100, 0 and +100°C using the chemical composition of the glass and Ratcliffe's[99] addition formula:

$-100°C: \quad k_s = 0.426$ Btu/h ft degF

$0°C: \quad k_s = 0.541$ Btu/h ft degF

$+100°C: \quad k_s = 0.623$ Btu/h ft degF

A quadratic was fitted to the data using the curve fitting

program[94]:

$$k_s = 0.541 + 0.0240.T_s - 0.000982.T_s^2 \quad \ldots\ldots\ldots (4:16)$$

which, on integration, gave

$$k_{sm} = 0.541 + 0.0120(T_{so}+T_{si}) - 0.000327[(T_{so}+T_{si})^2 - T_{so}.T_{si}] \quad \ldots\ldots\ldots (4:17)$$

where the temperatures are expressed as equivalent millivoltage outputs from chromel-alumel thermocouples.

4.5 Moving Bed Runs

4.5.1 Procedure

The $\frac{1}{4}$ mm nominal diameter lead glass support ballotini were poured through a 22 mesh sieve during loading to prevent the discharge orifice becoming blocked with extraneous matter, particularly the larger test ballotini which might remain from the previous run. 6 and 9 mm diameter ballotini were generally loaded into the 6 and 9 in hoppers but sometimes into the other two. 12 mm ballotini were always loaded into the two large hoppers to avoid damage to the glass conveyor pipe. Some material was loaded into each of the hoppers on one side of the column: some to be fed during the initial transient period when large changes in bed height, voidage, pressure drop and temperatures occurred and the remainder to be used for measurement of the solids flowrate under steady state conditions. Although hoppers might be changed during a run, feed side arms were not as radical changes in the profile of the top of the bed would then occur.

After loading, air was admitted to the bed at the required flowrate, the heaters switched on and the heat input gradually increased until the gas inlet temperature reached about 140°C, i.e. chromel-alumel output of about 5.8 mV. For large terminal

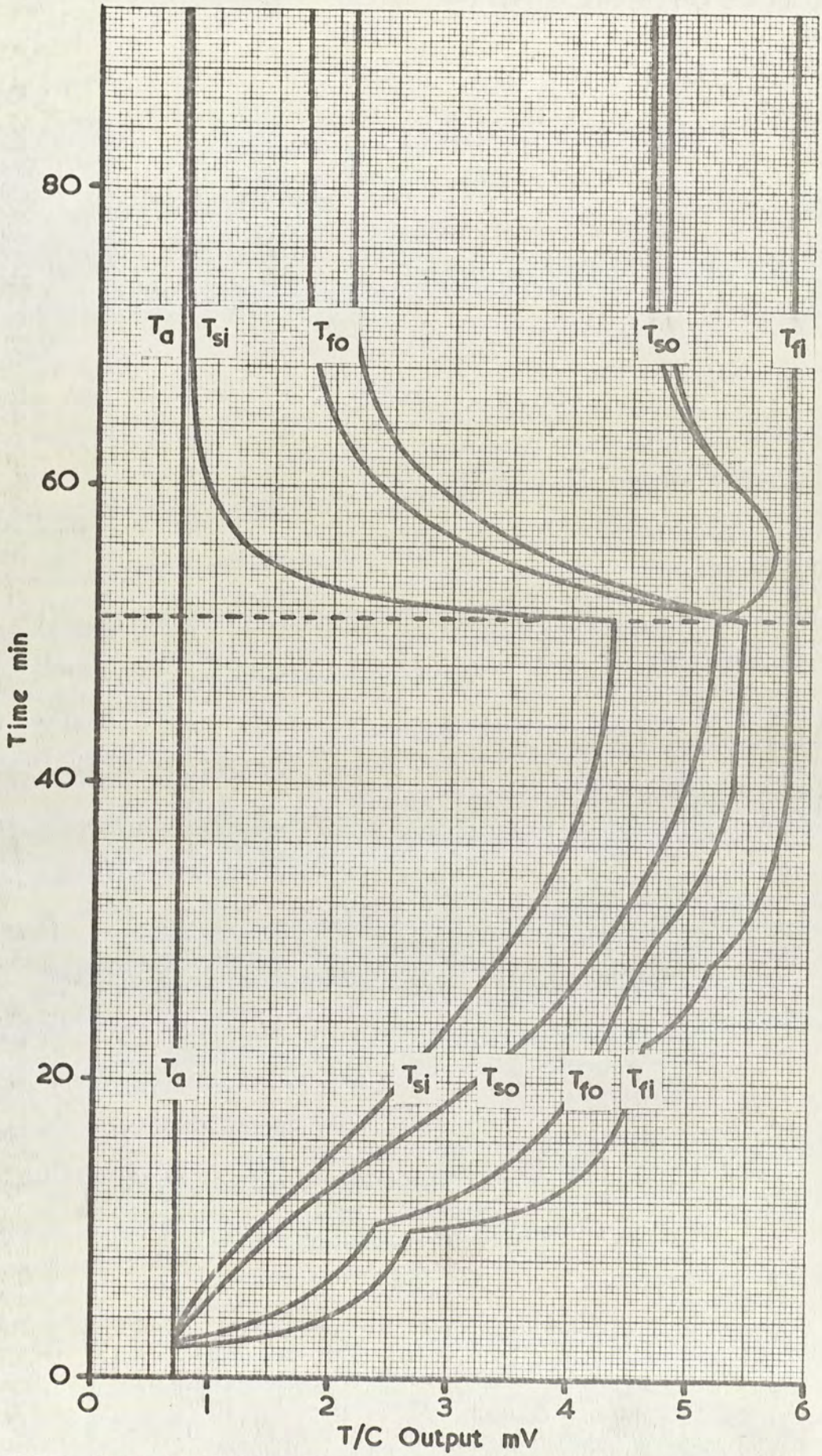

FIGURE 4:33 MOVING BED RUN 43 : TEMPERATURE TRACE

temperature differences, the gas inlet temperature needed to be as high as possible compatible with the working range of the silicone rubber gasket material. For accuracy in measuring the temperatures, full use needed to be made of the recorder span. The possible ranges were 0-3 mV, 0-6 mV and 0-15 mV. Thus a gas inlet temperature of about 140°C measured on the 0-6 mV range represented the most satisfactory combination. It was necessary to use inlet temperatures of about 100°C in a few runs at low air flowrates to avoid problems of the heater pipework overheating as described in Section 4.3.4.

When the inlet air conditions, both flowrate and temperature, had stabilised, the discharge valve was opened, the fine ballotini drained through the discharge orifice and the bed began to move. After the initial transient period, the solids feed hopper was changed and the flowrate determined by either the weighed charge or calibrated hopper method. Inlet air conditions were maintained constant until the bed had achieved steady state. A typical temperature trace is shown in Figure 4:33.

The ranges of the air and solids flowrates were dependent on a number of factors. First, the terminal temperature differences should be large enough to be measured accurately, as explained in Section 4.1.2. Initially it was expected that the data would be analysed with the TR48 hybrid analogue computer. As this would involve setting the dimensionless gas outlet temperature on a potentiometer, it was felt that T_{fo} should be maintained at least 0.5 mV above the solids inlet temperature, i.e. dimensionless gas outlet temperature θ_{fo} of about 0.1. Although the solids outlet temperature would not be set on a potentiometer, the criterion

that ($T_{fi}-T_{so}$) should not be less than 0.1 mV ($\theta_{so} \doteq 0.98$) was chosen to avoid doubts about the effective bed length. Secondly, fluidisation of the bed material had to be avoided, particularly with the 6 and 9 mm ballotini. With the 12 mm the upper limit of gas flowrate was actually determined by the capacity of the compressed air system. Thirdly, the solids flowrate could not be so high that steady state would not be achieved with the available ballotini (280 lb of any one size). The range of air and solids flowrates widened with increase in particle size, i.e. decrease in surface area for heat transfer.

On completion of a run, separation of the support and test material remaining in the apparatus was accomplished by draining through 3/16, $\frac{1}{4}$ or $\frac{3}{8}$ in mesh sieves, as appropriate.

4.5.2 Discussion of the measured variables

Solids outlet temperature

The thermocouple junction was sited 2 in below the centre line of the air inlets as recommended by Akers[2]. It can be deduced from the temperature history shown in Figure 4:33 that the probe was not in the air stream. The temperature lagged well behind that of the inlet air so the probe can have received heat only by conduction from the surrounding ballotini. The stagnant air in the voids would be at virtually the same temperature as the surface of the solids due to the much greater mass and consequent thermal capacity of the solids. Once the bed started moving, the probe temperature rose almost to that of the inlet air due to the passage of the initial charge of ballotini but, thereafter, it dropped towards the moving bed steady state value. The temperature was recorded at 25 or 30s intervals and, even at steady state, was

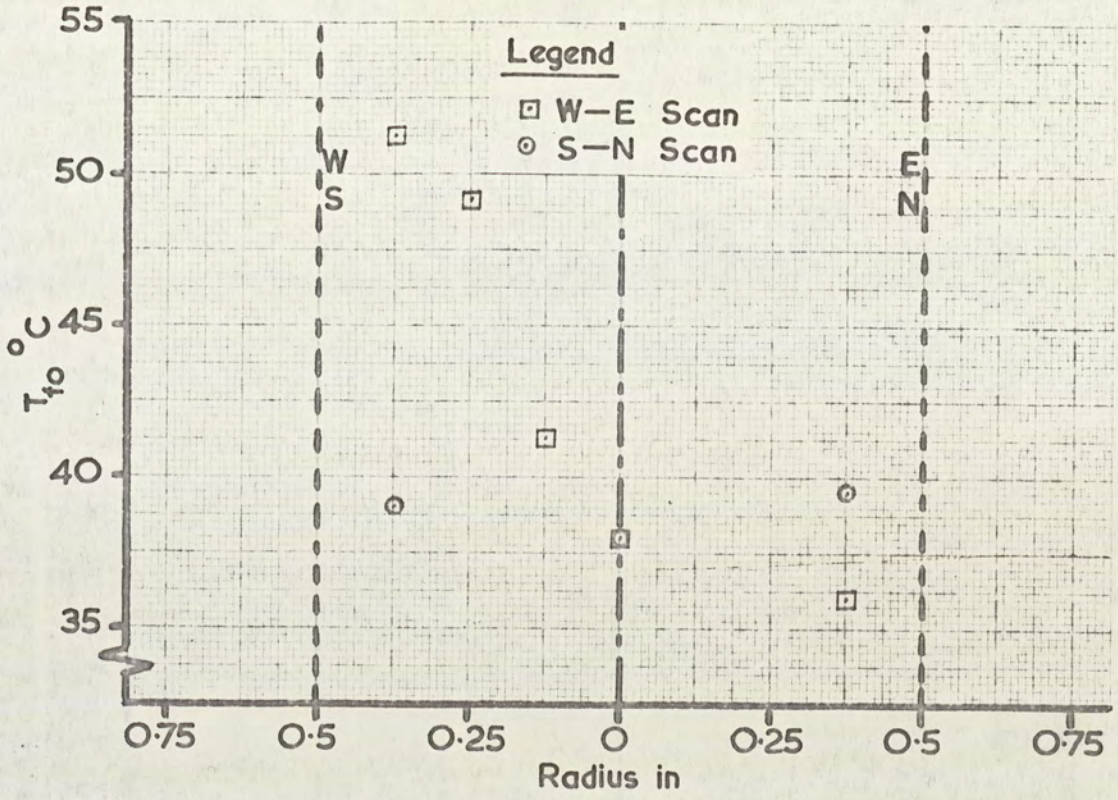

FIGURE 4:34 RADIAL T_{fo} SCAN : MOVING BED RUN 28 : BALLOTINI FED FROM EAST: 1x1 in HOLE MIXER

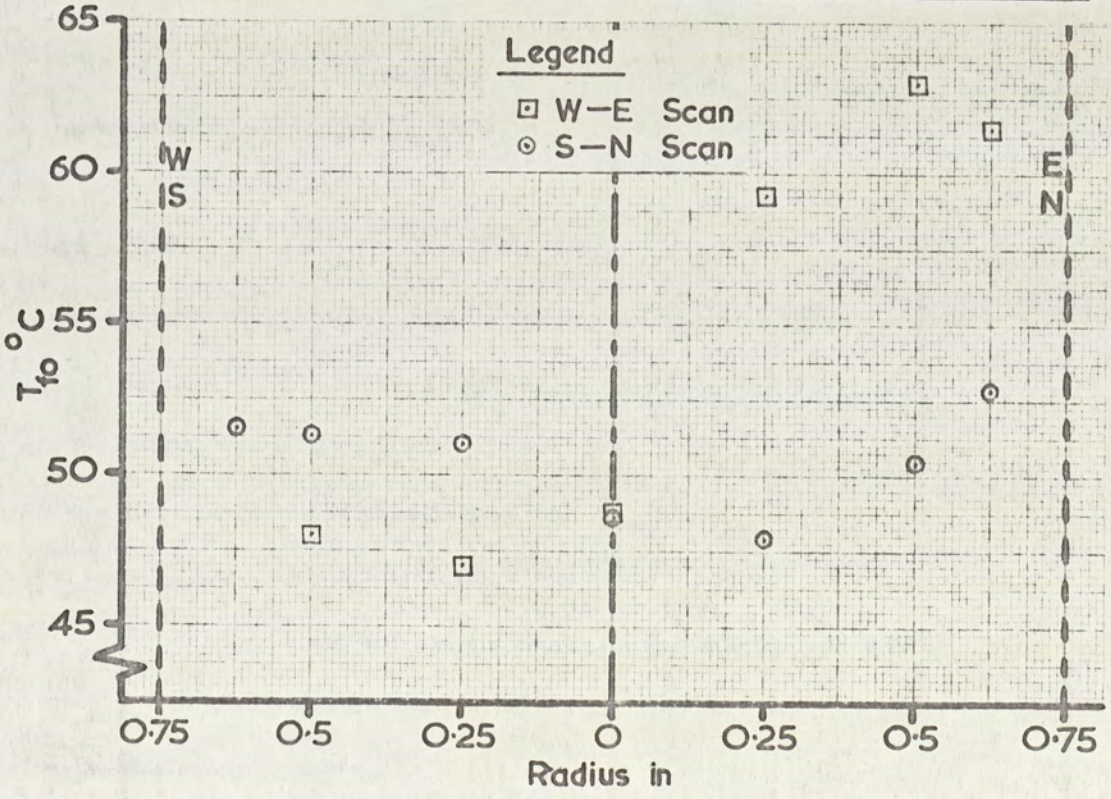

FIGURE 4:35 RADIAL T_{fo} SCAN : MOVING BED RUN 31 : BALLOTINI FED FROM WEST : $8 \times \frac{1}{2}$ in $\longrightarrow$ $1 \times 1\frac{1}{2}$ in HOLE MIXER

subject to scatter ranging from $\pm$6% of the mean at high solids flowrates to nil at low rates. The scatter was attributed to fluctuations in the solids feed rate.

Air outlet temperature

The need for a mixing baffle was explained in Section 4.3.1 and the design with twelve $\frac{3}{4}$ in holes was described. The outlet temperature was taken at a hole on the diameter of the column perpendicular to the air and solids feed side arms so that conditions at the thermocouple corresponded to those at the mean bed height. While this was satisfactory for wall heat loss measurements in the long column, it was felt that a more positive attempt should be made to obtain the mean temperature for the whole cross section for moving bed runs in the short column as the temperature profiles were likely to be more pronounced. A mixer with one central 1 in diameter hole was used in five runs but the pressure drop across it was very high. Another baffle was made of a pattern similar to that of the inlet air mixers. It had eight $\frac{1}{2}$ in diameter holes arranged on a 2 in diameter circle with axes perpendicular to that of the column. The air temperature was measured in the plane of a $1\frac{1}{2}$ in diameter hole on the same axis as the column. All three outlet mixers are shown in Figure 4:19. Radial temperature profiles were detected across the mixer orifices as shown in Figures 4:34 and 35 at low air flowrates (194 and 259 lb/h ft^2). The effect of the profile of the top of the bed due to the solids feed can also be seen. It seems likely that the mixers were more effective at high flowrates but the scatter prevented reliable radial scans being made. Even after steady state had been achieved, the outlet air temperature was subject to

scatter in the same manner as the solids outlet but more pronounced, even as much as $\pm$15% on one occasion.

Because of the considerable scatter of the air and solids outlet temperatures, all temperatures used for calculation of moving bed heat transfer coefficients were obtained as averages over periods of not less than four minutes, but generally twelve.

Solids flowrate

Which of the two methods described in Section 4.2.4 was used in a particular run was merely a matter of convenience. Where both were used the discrepancy was generally less than 3%. The weighed charge method was taken to be the more precise of the two because:

(1) The time increments were greater.

(2) The velocity of the ballotini past the reference point (in the feed pipe rather than the hopper) was greater.

Bed height

The upper and lower limits of the moving bed heat transfer section were defined respectively as:

(1) The intersection of the surface of the bed and the axis of the column. This took account of the inclination of the surface due to the method of feeding the solids.

(2) The axis of the air feed side arms.

The bed height was measured without parallax error by aligning scales marked on each side of the glass column. The solids feed side arms were joined to the column at different heights due to manufacturing problems, the one giving bed heights between 3.0 and 3.7 in and the other between 3.9 and 4.5 depending on the flowrates. There was some variation in the bed height during each run due to the spasmodic nature of the solids flow. It seemed that the bed

surface had to drop sufficiently below the mean height to overcome the interlocking of the particles in the feed side arm. Once the equilibrium was disturbed, ballotini flowed into the column.

SECTION 5

ANALYSIS AND DISCUSSION OF PRESENT MOVING BED HEAT TRANSFER DATA

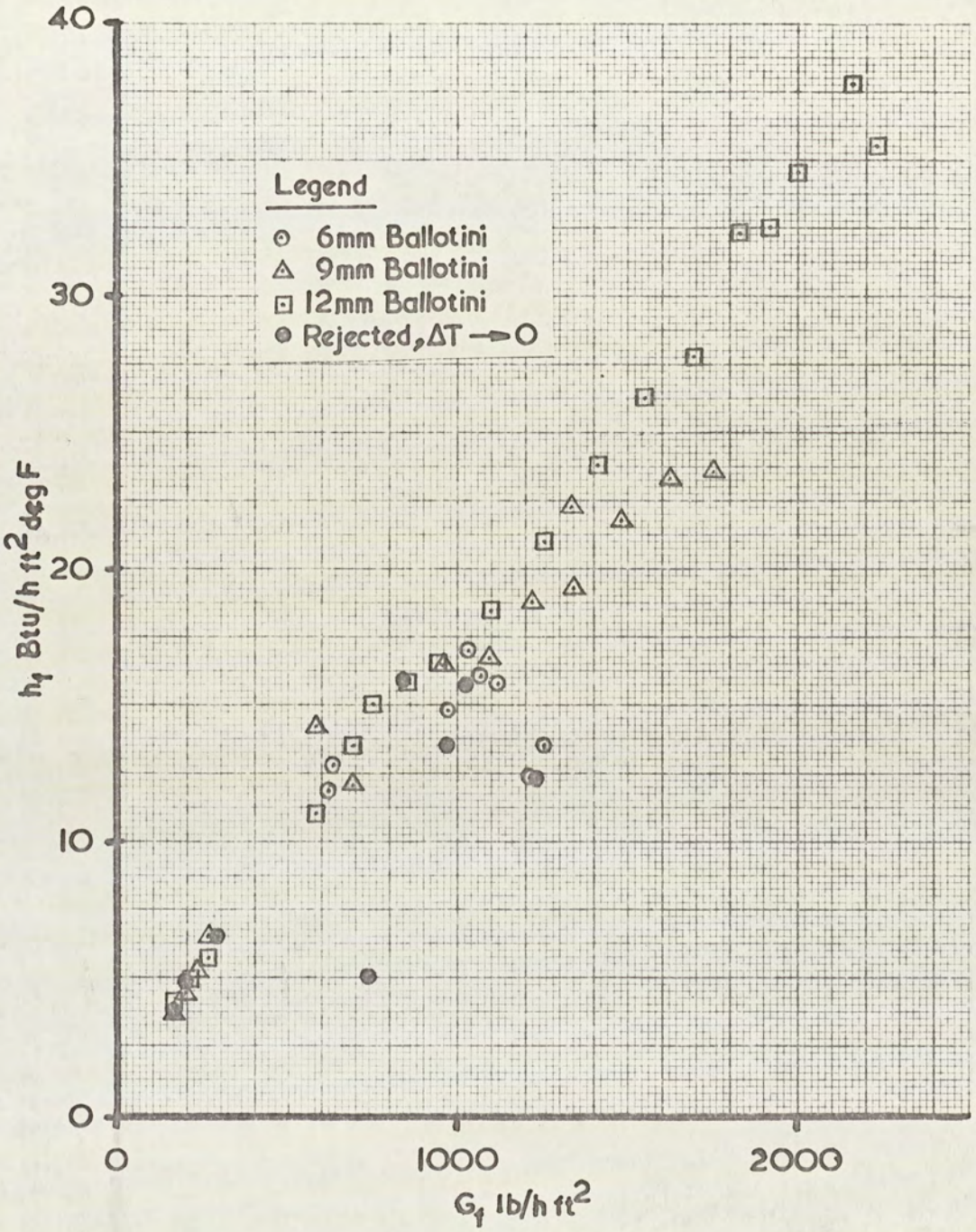

FIGURE 5:1 h_f v. G_f : h_f BASED ON MEAN Q: L.M.T.D. SOLN.: NO I.P.T.D.

SECTION 5 - ANALYSIS AND DISCUSSION OF PRESENT MOVING BED HEAT TRANSFER DATA

5.1 Preliminary Calculations and Logarithmic Mean Temperature Difference Solutions: Non-Adiabatic Enclosure: No Intra-Particle Temperature Distribution

Calculation of heat transfer coefficients, Biot, Nusselt and Reynolds numbers, preparation of parameters for the analogue computer or numerical integration solutions and conversion of observed and derived data to units of the International system were all carried out on the I.C.L. 1905 computer using the program ZMOVBEDHTC described in Appendix 3.1. The program solves the approximate equation (3:59) for a non-adiabatic, counterflow heat exchanger with no intra-particle temperature distribution, see Section 3.4.3:

$$Q = h_f.a.L.A_x.\Delta T_{lm} \quad \ldots\ldots\ldots\ldots \quad (3:59)$$

where $Q = Q_s = Q_f - Q_w$

Now, the overall heat balance is:

$$Q_f - Q_w - Q_s = 0 \quad \ldots\ldots\ldots\ldots\ldots\ldots \quad (5:1)$$

However, there were deficiencies in the heat balances ranging from -26% to +39%, although generally between -4% and +18%, defined as:

$$\text{Deficiency} = 100 - \frac{(Q_w+Q_s).100}{Q_f} \quad \ldots\ldots\ldots\ldots \quad (5:2)$$

i.e. generally $Q_f > (Q_w+Q_s)$. Undoubtedly all experimental results were subject to error and the mathematical model was a simple one but the gross deficiencies were probably due to errors in measuring the air and solids outlet temperatures. As a preliminary to further analysis, (3:59) was solved using the mean of (Q_f-Q_w) and Q_s. The relationship between the resulting heat transfer coefficients and the air flowrate is shown in Figure 5:1. The generalised results in terms of Nusselt and Reynolds numbers are

presented in Figure 5:2. The correlations of Coppage and London[41] and Malling and Thodos[59] (no dispersion) for fixed beds and those of Akers[2] and Norton[26] for moving beds are superimposed to illustrate the spread of previous data. Those runs for which the terminal temperature differences did not fulfil the conditions set out in Section 4.5.1 are also included to illustrate the deviations which can occur as:

$$(T_{fo}-T_{si}) \rightarrow 0$$

$$\text{or } (T_{fi}-T_{so}) \rightarrow 0$$

The satisfactory data were correlated by the following equation using the computer library least mean squares analysis program ZUA03[100]:

$$Nu = 0.115 \times Re^{0.864} \quad \ldots\ldots\ldots\ldots\ldots \quad (5:3)$$

Correlation coefficient = 0.969

Akers[2] was unable to measure T_{fo} as explained in Section 2.2 so he was forced to calculate it from the heat balance on the assumption that T_{so} was reliable. In the present work the solids feed and air outlet were separated and attempts made to measure the mean value of T_{fo} by using mixers. As this was considered to be more reliable than the measurement of T_{so} at a single point on the axis of the column and as intra-particle temperature distribution might be significant, the mean value of T_{so} was calculated from the heat balance, equation (5:1) using the measured value of T_{fo}. The corresponding Nusselt numbers are shown in Figure 5:3 and are generally a little greater than those in Figure 5:2, consistent with:

$$Q_f > (Q_w+Q_s)_{measured}$$

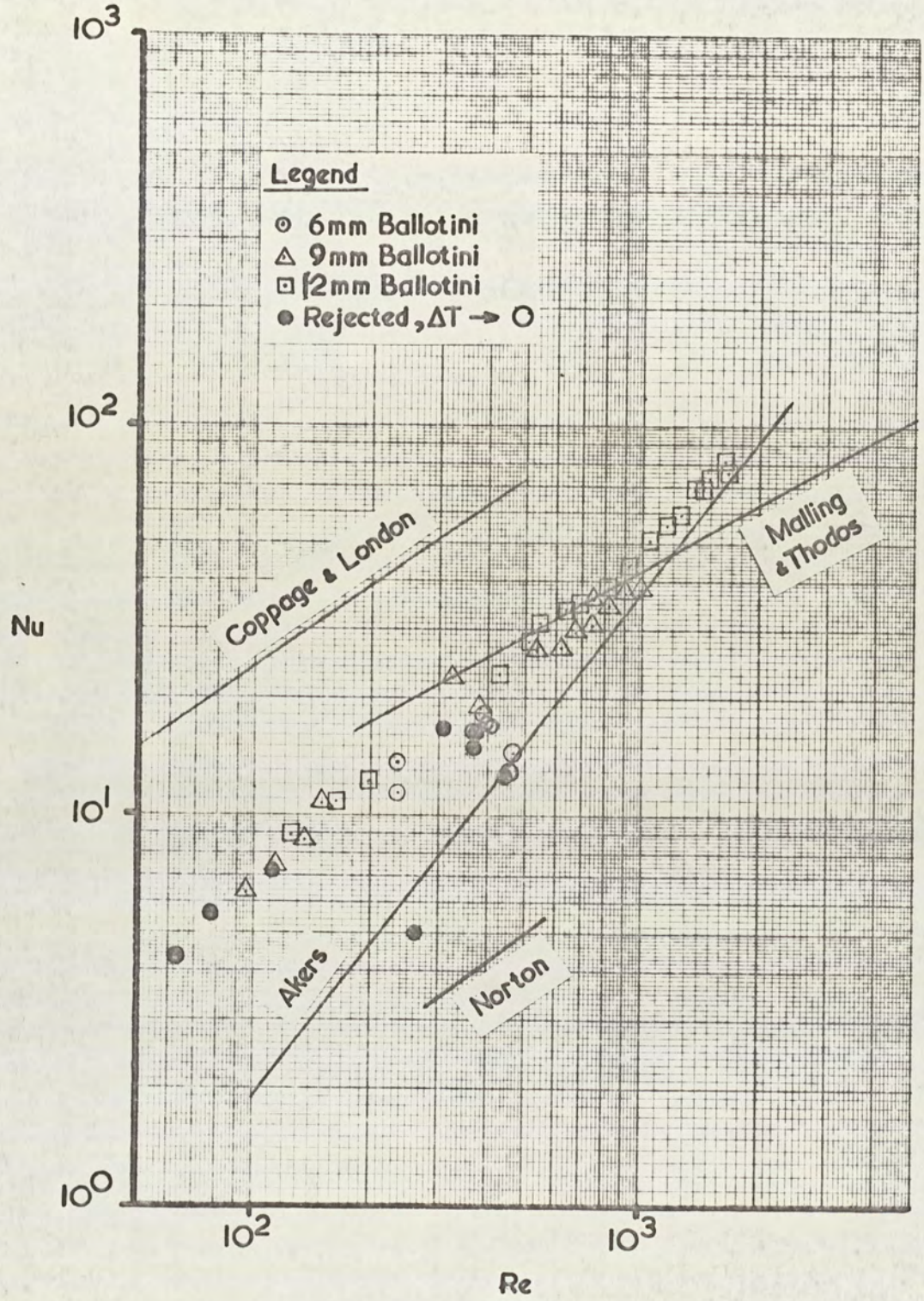

FIGURE 5:2 Nu v. Re : Nu BASED ON MEAN Q : L.M.T.D. SOLN. : NO I.P.T.D.

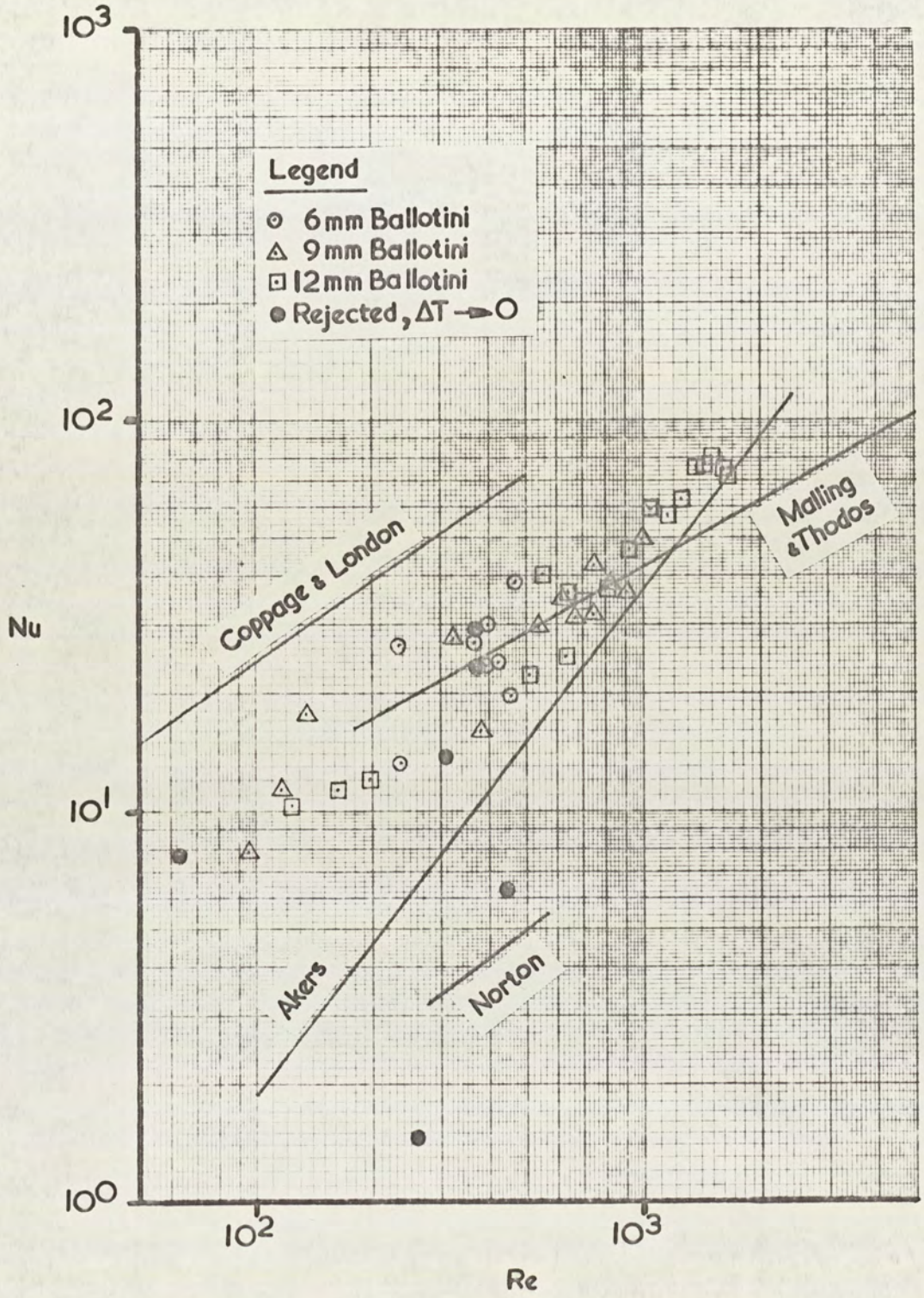

FIGURE 5:3 Nu v. Re : Nu BASED ON Q_f : L.M.T.D. SOLN. : NO I.P.T.D.

presented in Figure 5:2. The correlations of Coppage and London[41] and Malling and Thodos[59] (no dispersion) for fixed beds and those of Akers[2] and Norton[26] for moving beds are superimposed to illustrate the spread of previous data. Those runs for which the terminal temperature differences did not fulfil the conditions set out in Section 4.5.1 are also included to illustrate the deviations which can occur as:

$$(T_{fo}-T_{si}) \rightarrow 0$$

$$\text{or } (T_{fi}-T_{so}) \rightarrow 0$$

The satisfactory data were correlated by the following equation using the computer library least mean squares analysis program ZUA03[100]:

$$Nu = 0.115 \times Re^{0.864} \quad \ldots\ldots\ldots\ldots\ldots \quad (5:3)$$

Correlation coefficient = 0.969

Akers[2] was unable to measure T_{fo} as explained in Section 2.2 so he was forced to calculate it from the heat balance on the assumption that T_{so} was reliable. In the present work the solids feed and air outlet were separated and attempts made to measure the mean value of T_{fo} by using mixers. As this was considered to be more reliable than the measurement of T_{so} at a single point on the axis of the column and as intra-particle temperature distribution might be significant, the mean value of T_{so} was calculated from the heat balance, equation (5:1) using the measured value of T_{fo}. The corresponding Nusselt numbers are shown in Figure 5:3 and are generally a little greater than those in Figure 5:2, consistent with:

$$Q_f > (Q_w+Q_s)_{measured}$$

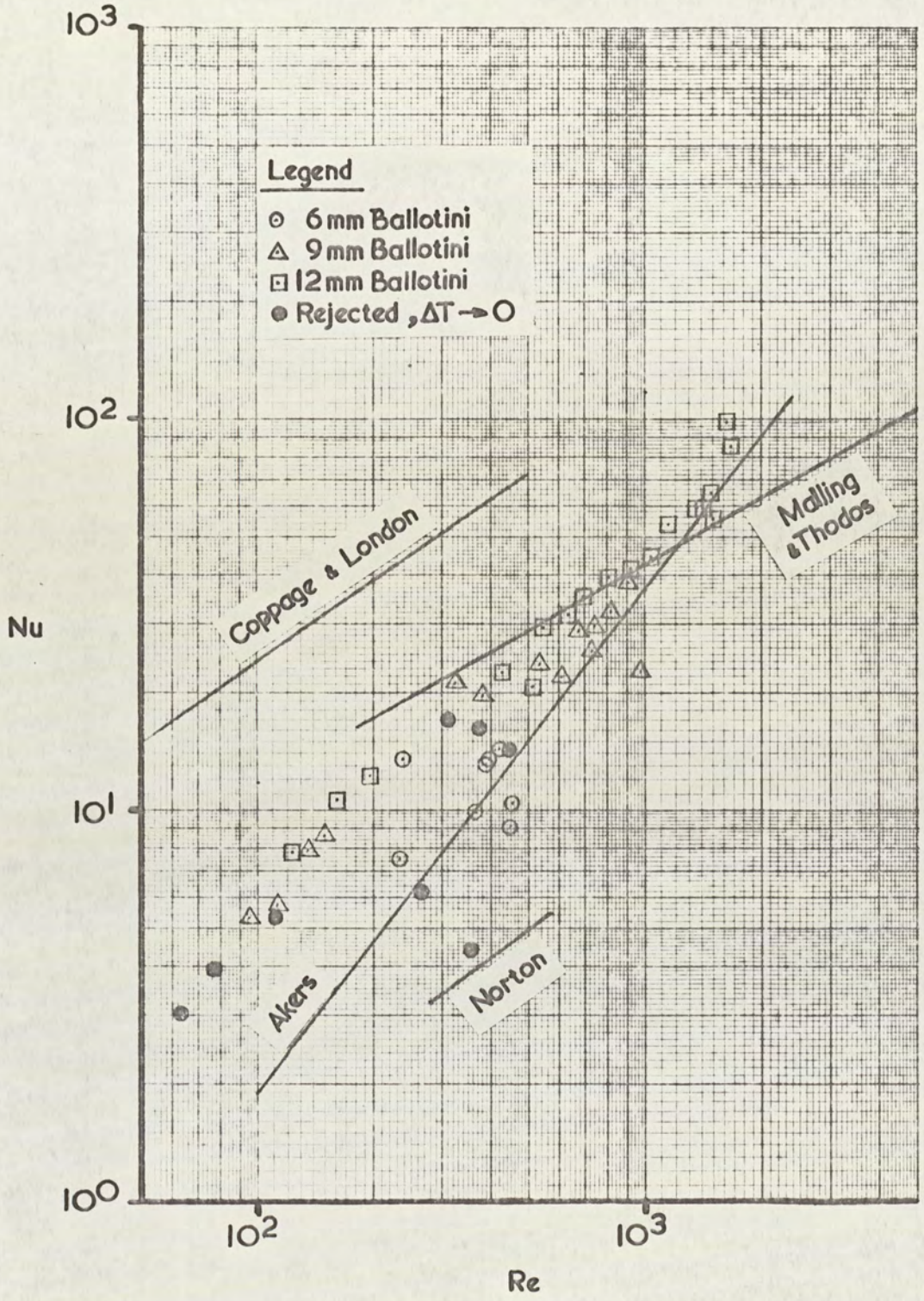

FIGURE 5:4 Nu v. Re: Nu BASED ON Q_s: L.M.T.D. SOLN.: NO I.P.T.D.

However, in Runs 21, 25 and 31 at air flowrates of 289, 197 and 259 lb/hft^2 respectively, the calculated values of T_{so} were greater than T_{fi} indicating that the outlet air mixers were inadequate at such low air flowrates. The temperature profile across the mixer in Run 31 was presented in Figure 4:35, Section 4.5.2. The data based on the measured T_{fo} and the calculated T_{so} were correlated by:

$$Nu = 0.296 \times Re^{0.741} \quad \ldots\ldots\ldots\ldots \quad (5:4)$$

Correlation coefficient = 0.944

The runs for which the terminal temperature differences were suspect were again ignored.

The data were also analysed using the measured value of T_{so} and the value of T_{fo} calculated from it. It can be seen in Figure 5:4 that the Nusselt numbers are generally lower than those in either 5:2 or 5:3. The data were correlated by:

$$Nu = 0.0752 \times Re^{0.914} \quad \ldots\ldots\ldots\ldots \quad (5:5)$$

Correlation coefficient = 0.928

The differences between the three methods are small in comparison with the gross discrepancies between previous fixed and moving bed data. It was felt that the use of the measured value of T_{fo} and the calculated value of T_{so}, as in Figure 5:3, was the most reliable approach and would form the best basis for the subsequent, more sophisticated analyses.

5.2 Numerical Integration Solution: Non-Adiabatic Enclosure: No Intra-Particle Temperature Distribution

Calculation of Biot numbers, heat transfer coefficients and Nusselt numbers by numerical integration was carried out on the

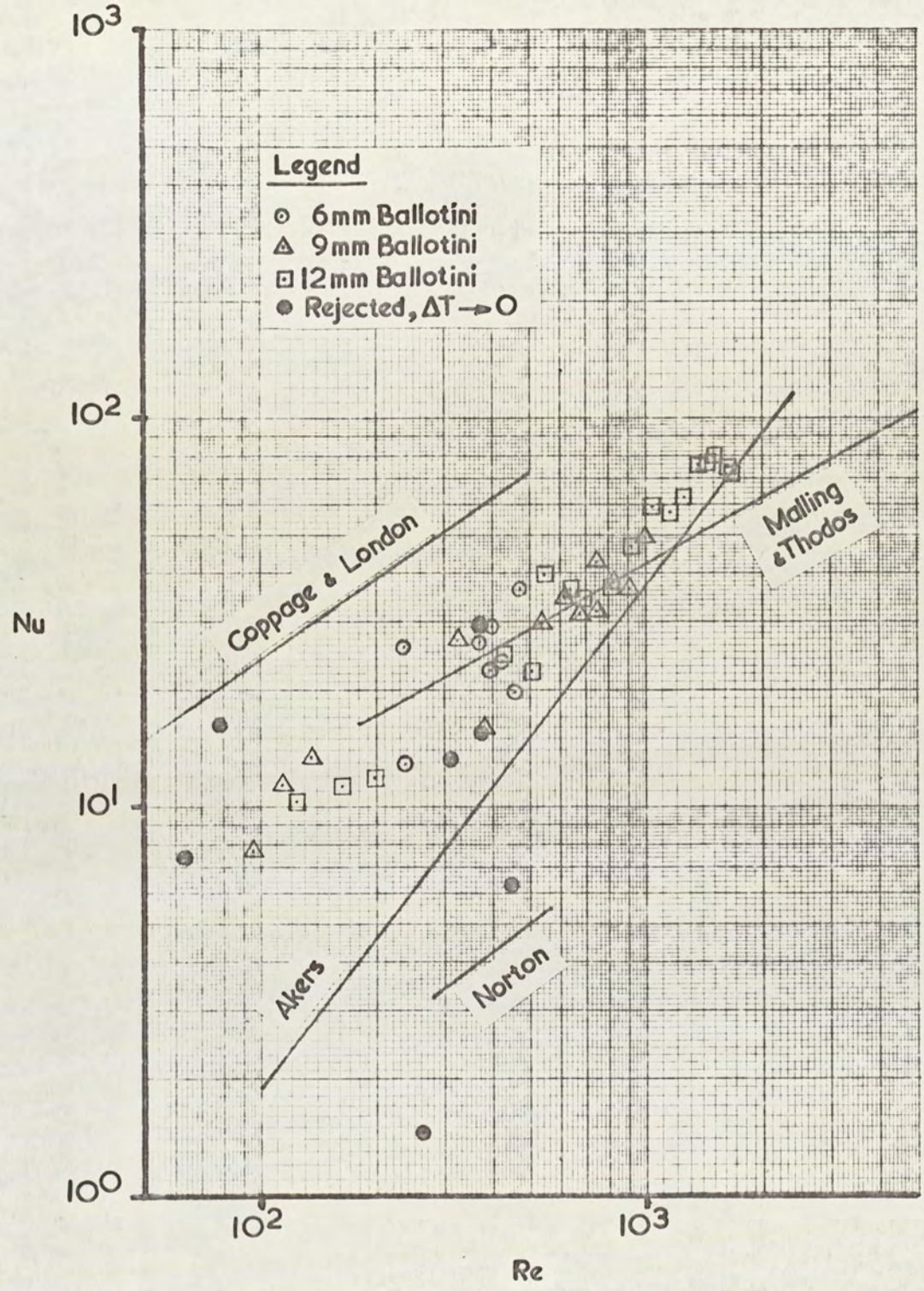

FIGURE 5:5 Nu v. Re : Nu BASED ON Q_f : NUM. INT. SOLN. : NO I.P.T.D.

I.C.L. 1905 using the program ZFRAWRWEXPT given in Appendix 1.2. The input parameters were taken from the version of ZMOVBEDHTC based on the measured value of T_{fo} and the calculated value of T_{so}. The results are presented in Figure 5:5 and are almost indistinguishable from those in Figure 5:3. For runs with dimensionless bed lengths z_L greater than 2.9, ZFRAWRWEXPT gave lower Biot numbers than ZMOVBEDHTC. The differences were generally not more than 2% but for runs 20 and 44 they were 33 and 25%, respectively. It seems that this was connected with the error in the overall heat balance for the numerical integration solution. This was discussed in Section 3.6.1 in connection with the problem of Lovell and Karnofsky[76]. In Runs 20 and 44 the bottom temperature difference $(\theta_{fi}-\theta_{so})$ calculated by ZMOVBEDHTC was very small (20, 0.0005; 44, 0.0042) so errors of the magnitude generated by numerical integration produced results wildly different from the logarithmic mean temperature difference solution. Evidence that the heat balances are in error is provided by Run 25. This was one of the three for which the calculated value of T_{so} was greater than T_{fi} so no solution should be possible. However, the error in the heat balance is sufficient to give a real solution for which T_{so} is less than T_{fi}. This was not the case with Runs 21 and 31 for which the difference $(T_{so}-T_{fi})$ was greater.

Alternatively, the differences could be due to the approximations in the allowance for the wall losses in ZMOVBEDHTC. Unfortunately no quantitative estimate of the heat balance error is possible as the heat loss to the surroundings was not specifically calculated in ZFRAWRWEXPT. The wall loss term in the

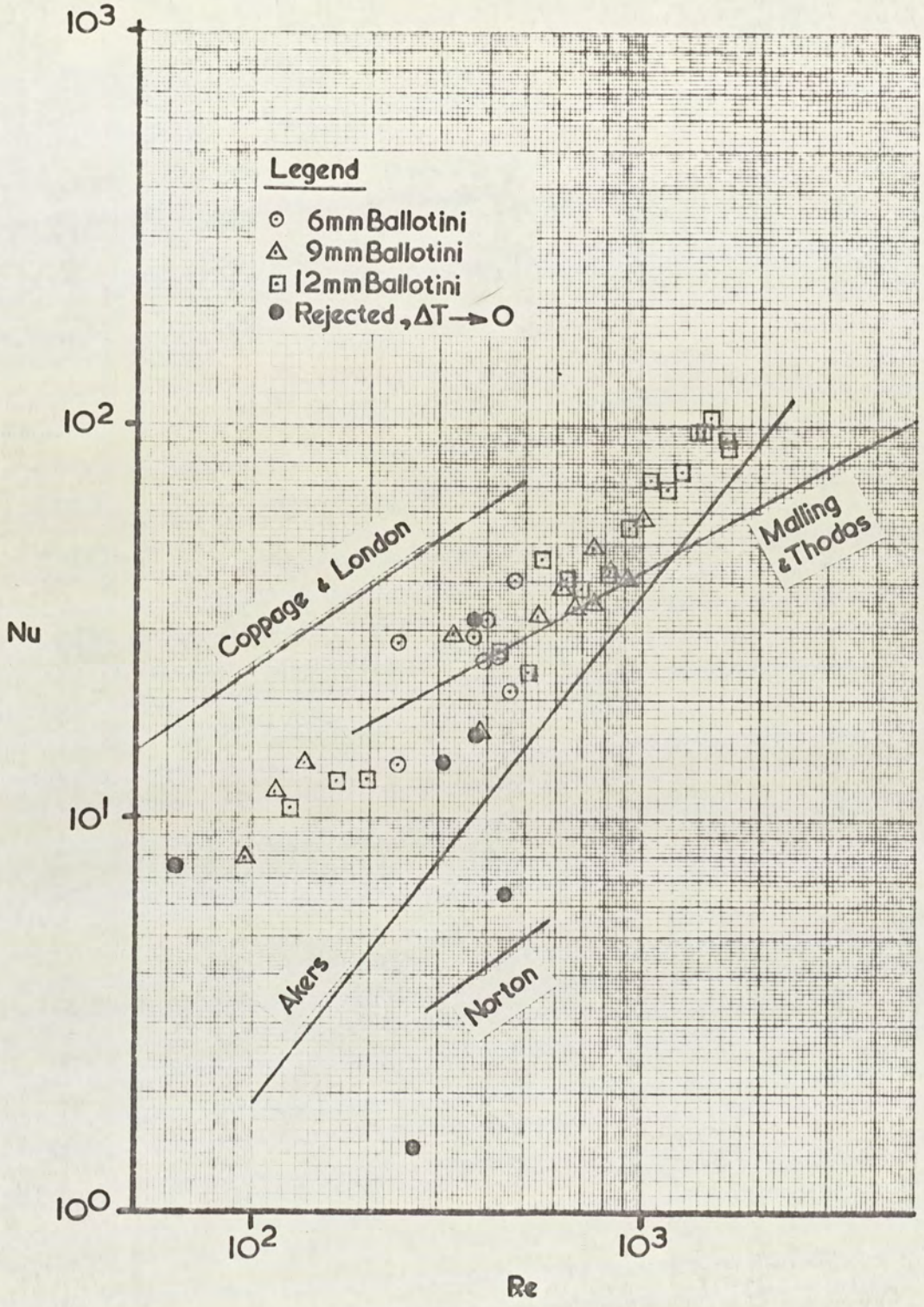

FIGURE 5:6 Nu v. Re : Nu BASED ON Q_f :
NUM. INT. SOLN. : I.P.T.D.

overall heat balance equation (3:64):

$$S = \frac{4.U_w.(\Delta x)^2.L.}{d_v.G_f.c_f.(\Delta x)^2 z_L} \int_o^{z_L} (\theta_f - \theta_a)dz$$

could have been evaluated as:

$$\frac{4.U_w.(\Delta x)^2.L.}{d_v.G_f.c_f.(\Delta x)^2 z_L} \sum_o^{z_L} \left(\frac{(\theta_{f,z} + \theta_{f,z+\Delta z})}{2} - \theta_a \right).\Delta z$$

but this was not considered at the time.

Insert between lines 4 and 5:

or a further differential equation could have been included in the derivative section and integrated numerically:

$$\frac{dS}{dz} = \frac{4.U_w.(\Delta x)^2.L}{d_v.G_f.c_f.(\Delta x)^2.z_L} .(\theta_f - \theta_a)$$

$S = 0$ at $z = 0$

5.3 Numerical Integration Solution: Non-Adiabatic Enclosure: Intra-Particle Temperature Distribution

The data were finally processed using the complete model involving wall heat loss and intra-particle temperature distribution. The input parameters were again obtained from the version of ZMOVBEDHTC based on the measured value of T_{fo} and the calculated value of T_{so}. The results are presented in Figure 5:6 and it can be seen that the points are generally displaced above those shown in Figures 5:3 and 5:5, which demonstrates the effect of the conduction lag within the individual particles. There are three exceptions: Runs 20 and 44 which were discussed in the previous section and Run 23. All three may be explained by the

overall heat balance equation (3:64):

$$S = \frac{4.U_w.(\Delta x)^2.L.}{d_v.G_f.c_f.(\Delta x)^2 z_L} \int_o^{z_L} (\theta_f - \theta_a)dz$$

could have been evaluated as:

$$\frac{4.U_w.(\Delta x)^2.L.}{d_v.G_f.c_f.(\Delta x)^2 z_L} \sum_o^{z_L} \left(\frac{(\theta_{f,z} + \theta_{f,z+\Delta z})}{2} - \theta_a \right).\Delta z$$

but this was not considered at the time.

Another contributory factor in the differences between the two methods may be the latitude on the control test in the numerical solution:

$$1 \leq \theta_{fi} < 1.001$$

The data from the numerical solution were correlated by:

$$Nu = 0.252 \times Re^{0.765} \quad \ldots\ldots\ldots\ldots\ldots \quad (5:6)$$

Correlation coefficient = 0.954

5.3 Numerical Integration Solution: Non-Adiabatic Enclosure: Intra-Particle Temperature Distribution

The data were finally processed using the complete model involving wall heat loss and intra-particle temperature distribution. The input parameters were again obtained from the version of ZMOVBEDHTC based on the measured value of T_{fo} and the calculated value of T_{so}. The results are presented in Figure 5:6 and it can be seen that the points are generally displaced above those shown in Figures 5:3 and 5:5, which demonstrates the effect of the conduction lag within the individual particles. There are three exceptions: Runs 20 and 44 which were discussed in the previous section and Run 23. All three may be explained by the

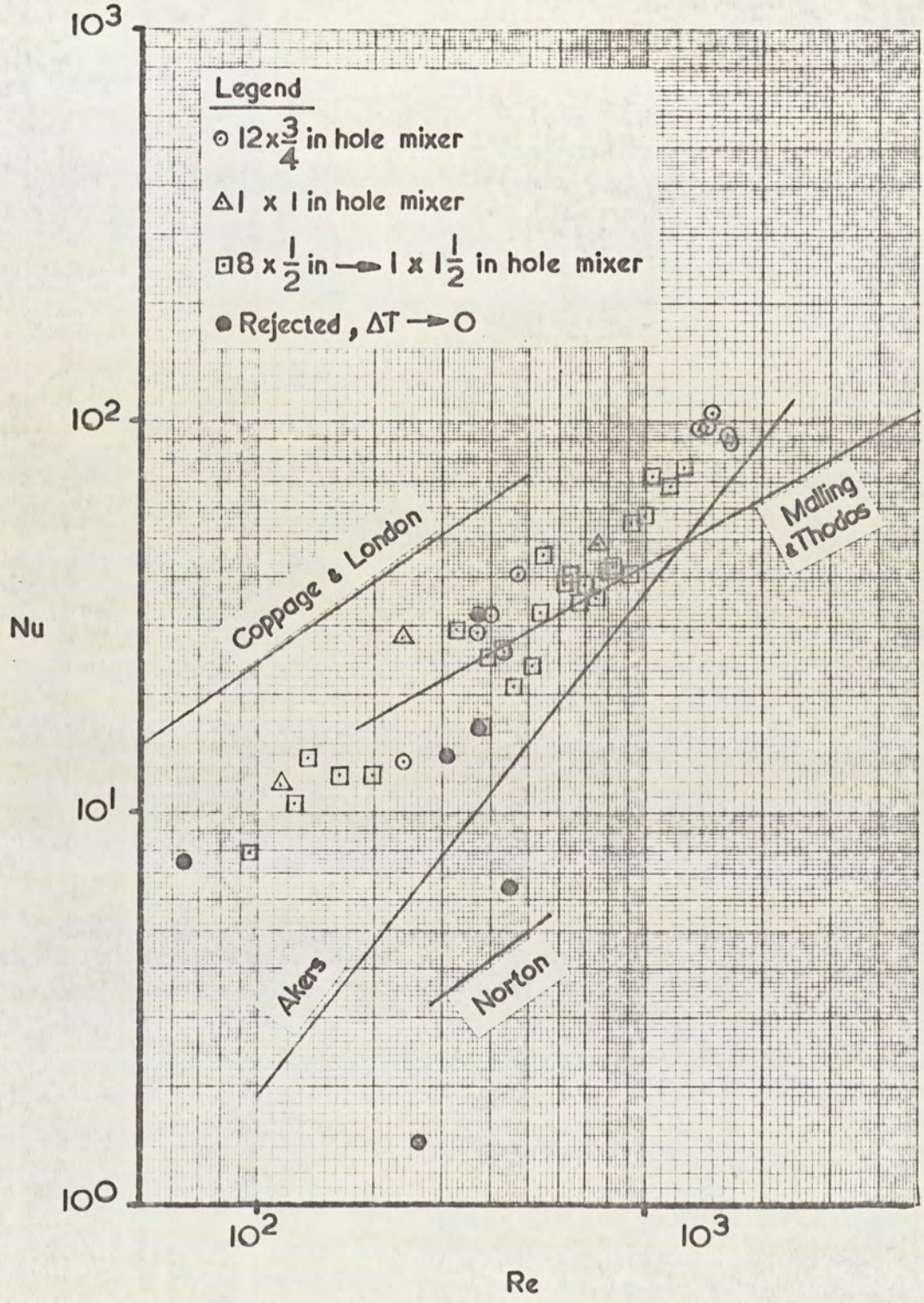

FIGURE 5:7 Nu v. Re : Nu BASED ON Q_f :
NUM. INT. SOLN. : I.P.T.D.
OUTLET AIR MIXERS AS PARAMETER

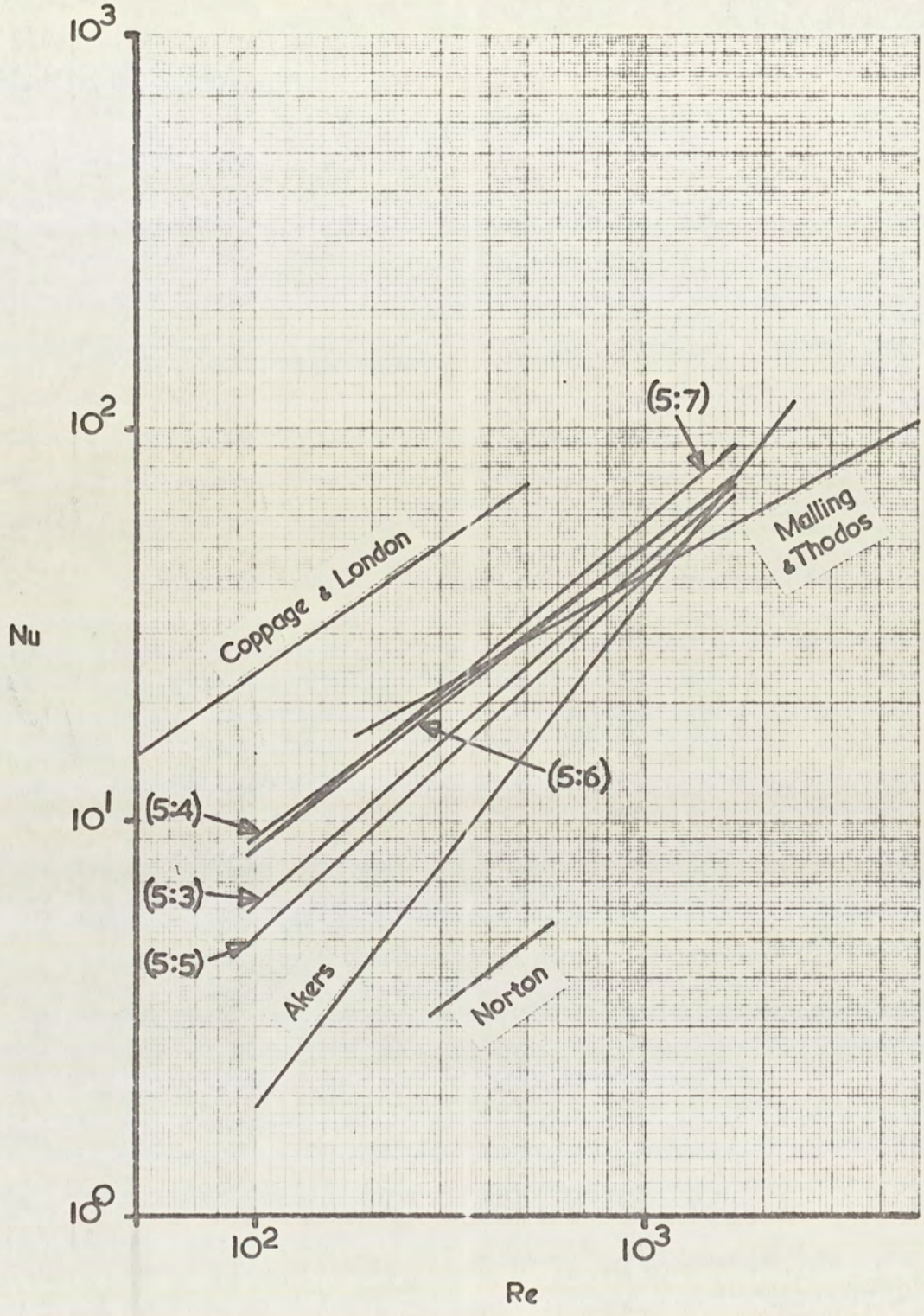

FIGURE 5:8 SUMMARY & COMPARISON OF PRESENT & PREVIOUS DATA

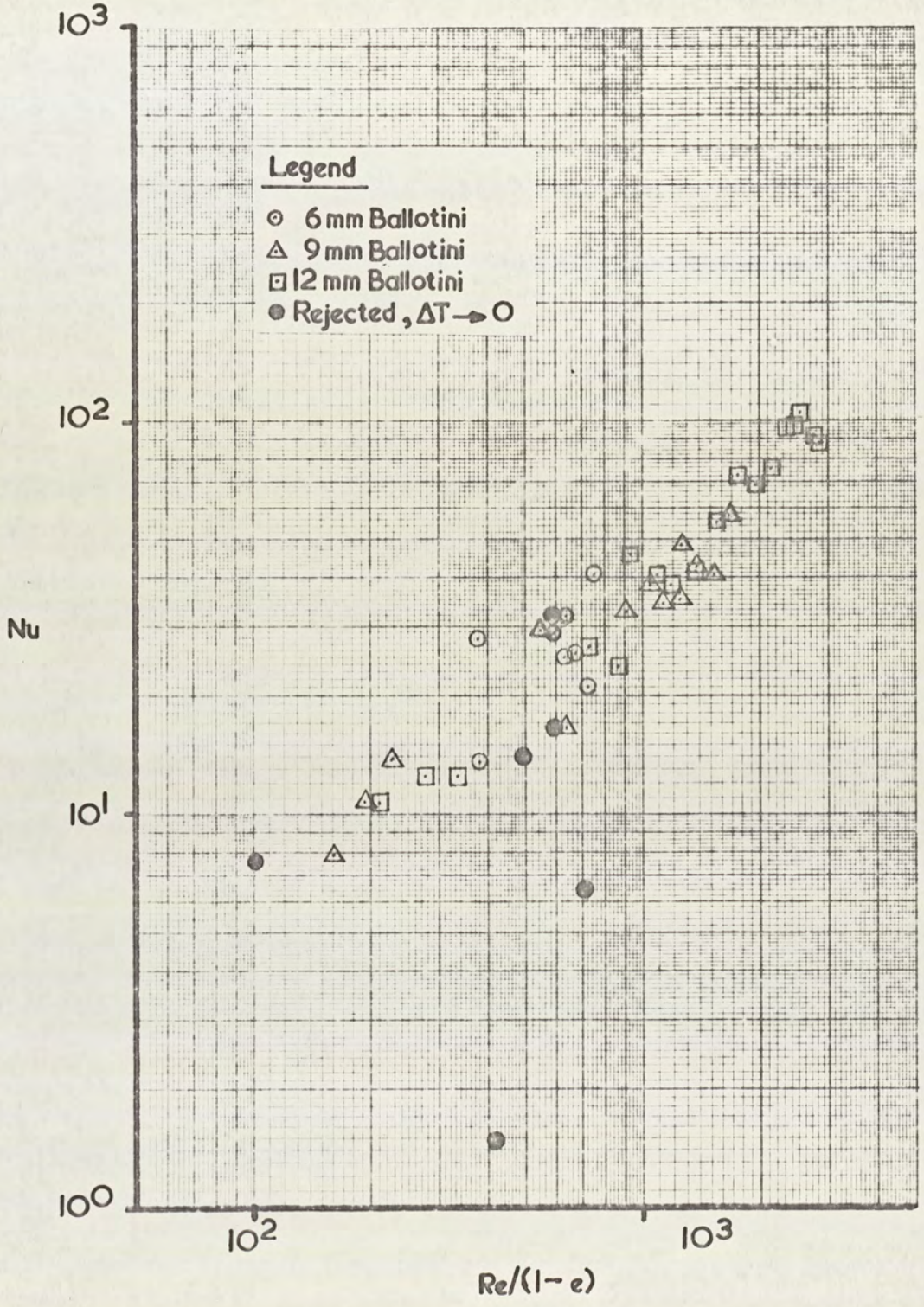

FIGURE 5:9 Nu v. Re/(1−e): Nu BASED ON Q_f: NUM. INT. SOLN.: I.P.T.D.

small values of the terminal temperature differences. The same data is also plotted in Figure 5:7 with the outlet air mixers as the parameter. Only two reliable points are available for the mixer with one 1 in hole but there is no evidence of any inconsistency between the three designs of mixer. The data were correlated by:

$$Nu = 0.183 \times Re^{0.834} \quad \ldots\ldots\ldots\ldots \quad (5:7)$$

Correlation coefficient = 0.953

Equations (5:3) to (5:7) are summarised in Figure 5:8.

The data are presented as:

$$Nu \text{ v. } \frac{Re}{(1-e)}$$

in Figure 5:9 to determine whether voidage is a significant factor but, as the range of voidage is very narrow (0.375 to 0.412), any possible effects are far outweighed by the experimental scatter, as demonstrated by the minimal difference in correlation coefficient between equations (5:7) and (5:8):

$$Nu = 0.126 \times \left(\frac{Re}{1-e}\right)^{0.826} \quad \ldots\ldots\ldots\ldots \quad (5:8)$$

Correlation coefficient = 0.952

It can be argued that Nusselt numbers for moving beds should be greater than for comparable fixed beds at the same fluid rates due to the greater relative velocity of the fluid and solids. Reynolds numbers based on the relative velocity were calculated with a view to testing this hypothesis but the maximum increase over the simple Reynolds number was not more than 0.06%, solids space velocities ranging from 0.1 to 4.6 mm/s compared with air space velocities from 522 to 7290 mm/s. The correlation of the

data was indistinguishable from equation (5:8). The solids velocity may be important but for most practical moving beds it can be ignored, particularly in comparison with the reduction in heat transfer due to dislocations of the matrix during movement.

Akers[2] and Gliddon and Cranfield[42] also accounted for voidage in the manner of equation (5:8), viz.

$$Nu \text{ v. } \frac{Re}{(1-e)}$$

However, this leads to the conclusion that the heat transfer coefficient decreases as the voidage decreases and, therefore, as the fluid velocity increases, which is contrary to expectations.

$$j_H \text{ v. } \frac{Re}{(1-e)}$$

$$\text{or } Nu \text{ v. } \frac{Re}{e}$$

seem to be more realistic. Correlation of the data in the latter form yielded:

$$Nu = 0.0794 \times \left(\frac{Re}{e}\right)^{0.845} \quad \ldots\ldots\ldots\ldots \quad (5:9)$$

with the same correlation coefficient as (5:8), 0.952. Thus, voidage has not been shown to be a significant variable in the present work. However, the experiments were not set up to investigate voidage specifically. Both mean voidage and the ranges of air and solids flowrates were dependent upon particle size. The voidages, numbers of runs and ranges of Re for each size of ballotini were:

6 mm: $e = 0.375$, 8 runs, $236 < Re < 469$

9 mm: $e = 0.406$, 13 runs, $95 < Re < 995$

12 mm: $e = 0.412$, 18 runs, $124 < Re < 1662$

Visual examination of Figure 5:6 does not reveal any clear distinction between the three sizes. The most satisfactory correlation of the present data is that provided by equation (5:7) which does not include a voidage term.

The details of the observed and derived moving bed heat transfer data are contained in Appendix 3.2.

SECTION 6

DISCUSSION OF PREVIOUS MOVING BED DATA

SECTION 6 - DISCUSSION OF PREVIOUS MOVING BED DATA

One of the principle objectives of the present work was to reconcile the differences between the fixed and moving bed heat transfer data in the literature. It was shown in Section 2.4 that moving bed heat transfer coefficients of an order of magnitude less than for fixed beds have been reported. Any differences ought to be in the opposite direction due to the greater relative velocities in moving beds than in fixed beds for given fluid rates as demonstrated by the pressure drop measurements of Happel[101].

It can be seen from Figure 5:6 that the present results are much more consistent with published fixed bed correlations than are those of Akers[2] and Norton[26]. Let us consider the comparison with Akers' results first. Preliminary determinations of packed bed voidage demonstrated that significant wall effects must have been present in the 3 in and 4 in columns used by Akers (d_v:d_p from 6 to 16), see Figures 4:20 and 4:22. Consequently, channelling of the air at the walls and reduction in the overall heat transfer must have occurred.

Investigations of the flow characteristics of beds of ballotini demonstrated radial solids velocity profiles and increased voidage during movement. As the present equipment featured the same type of air inlets as those used by Akers, it seems certain that profiles were present in his work and were probably more pronounced in the smaller diameter columns despite his reported observations of plug flow. This would have tended to increase the channelling effect above that in fixed beds. Comparison of Figures 5:3 and 5:4 illustrates that $(Q_f - Q_w) > Q_s$, generally. Akers was forced to calculate T_{fo} from the heat balance using the measured point value

of T_{so}. However, that value was probably lower than the average for the cross section due to the air and solids velocity profiles so the calculated heat transfer coefficients would have been low, although Akers did report that there was little radial variation in the solids temperature. The terminal temperature differences were very small in a number of Akers' runs so the calculations of the transfer coefficients may have suffered from the same errors as some of the present results. Instability of the hybrid analogue computer solution was referred to in Section 3.6.5 although this probably gave random variations rather than a general decrease in the transfer coefficients. Another possible source of error was the use by Akers of the fixed bed voidage in the moving bed calculations. This would have increased the dimensionless bed length z and specific surface area for heat transfer a:

$$z = \frac{k_s(1-e)L}{G_s \cdot c_s \cdot R^2}$$

$$a = \frac{6(1-e)}{d_p}$$

so both analogue computer and logarithmic mean temperature difference solutions would have generated low values of h_f.

Let us now consider Norton's[26] results. It is difficult to draw conclusions about the air and solids velocity profiles as the equipment was so different from that in the present work but with $d_v:d_p$ ratios of not less than 38 it seems unlikely that wall effects and dislocations of the matrix would have been significant. Use of the static bed voidage would have overestimated the heat transfer surface area again and so reduced the coefficients but

this would not have been a large effect. Comparison of Figures 5:5 and 5:6 shows that the correction for intra-particle temperature distribution with glass spheres from 6 to 12 mm diameter is small. Norton used ceramic spheres of similar size but higher thermal conductivity so the correction would have been even smaller. However, his bed depths were much greater than in the present work or that of Akers, 3 to 5 ft compared with 3 to 4.5 in. The combination of the greater conductivity and bed depth must have caused one or other of the terminal temperature differences to tend to zero. Measurement accuracy would have been inadequate and calculated heat transfer coefficients would have been subject to the same errors as several of the present results for 6 mm ballotini as shown in Figure 5:6. He may have used the arithmetic mean temperature difference which would have been greater than the logarithmic mean even if the measurement accuracy were adequate. Thus the calculated heat transfer coefficients would have been too small.

SECTION 7

DESIGN OF MOVING BED HEAT EXCHANGERS

SECTION 7 - DESIGN OF MOVING BED HEAT EXCHANGERS

Consider a design situation in which the following data might be specified:

(1) Solids flowrate M_s

(2) Solids inlet temperature T_{si}

(3) Mean solids outlet temperature T_{smo}

(4) Particle size d_p

(5) Some information regarding the fluid outlet temperature T_{fo}. Possibly the actual temperature but, for direct fired furnaces such as non-ferrous metal melters, the thermal efficiency would be more likely.

(6) The fluid inlet temperature T_{fi} for direct fired applications would be fixed once the fuel was chosen.

Overall heat balance assuming negligible losses to the surroundings:

$$M_s \cdot c_s \cdot (T_{so} - T_{si}) = M_f \cdot c_f \cdot (T_{fi} - T_{fo}) \quad \ldots\ldots\ldots \quad (7:1)$$

$$\therefore M_f = \frac{M_s \cdot c_s \cdot (T_{so} - T_{si})}{c_f \cdot (T_{fi} - T_{fo})} \quad \ldots\ldots\ldots\ldots\ldots \quad (7:2)$$

Thermal efficiency:

$$\eta = \frac{M_s \cdot c_s \cdot (T_{so} - T_{si})}{M_f \cdot c_f \cdot (T_{fi} - T_{si})} \quad \ldots\ldots\ldots\ldots\ldots \quad (7:3)$$

Substituting (7:1) in (7:3):

$$\eta = \frac{M_f \cdot c_f \cdot (T_{fi} - T_{fo})}{M_f \cdot c_f \cdot (T_{fi} - T_{si})} \quad \ldots\ldots\ldots\ldots\ldots \quad (7:4)$$

Assuming c_f is the same for both temperature ranges, then:

$$T_{fo} = T_{fi} - \eta(T_{fi} - T_{si}) \quad \ldots\ldots\ldots\ldots\ldots \quad (7:5)$$

The choice of column diameter d_v would depend on:

(1) Flow characteristics of the solids.

(2) Bypassing of fluid at the walls.

(3) Bed pressure drop: costs of fans, compressors etc. (probably involves iteration as pressure drop dependent on bed length which would not be known at this stage).

(4) Fluidisation of the solids.

Having chosen d_v, the fluid loading rate G_f and the Reynolds number Re could be calculated. Depending on the $d_v:d_p$ ratio and the likely packing arrangement of the solids, the significance of wall effects could be determined and the Nusselt number Nu corresponding to Re could then be obtained from one of the fixed or moving bed correlations given in Sections 2.4 and 5.3. Once the Biot number Bi and the heat capacity rate ratio β had been calculated, the necessary bed length could be obtained by either the logarithmic mean temperature difference solution of Furnas[35] or the full intra-particle temperature distribution solution by analogue computation or numerical integration.

It was shown in Section 3.6.1 by reference to the problem of Lovell and Karnofsky[76] that the simple Furnas solution ignoring intra-particle temperature distribution can seriously underestimate the bed length viz. 0.89 ft compared with 1.66 ft, an underestimation of 46.4%. However, comparison of Figures 5:5 and 5:6 given in Section 5 shows that the correction for the conduction lag is very small at low Reynolds numbers but reaches about 30% of the Nusselt number with the 12 mm ballotini at high air flowrates. Various opinions have been expressed as to the threshold value of the Biot number at which conduction becomes significant. Meek[45] suggested

1.0 whereas Kitaev[38] gave 0.25 and Akers[2] demonstrated the effects even at Biot numbers as low as 0.05. If analogue computers or digital machines with simulation languages are available to designers, the safest solution is to take account of intra-particle temperature distribution whatever the Biot number. However, in the absence of such facilities or when the number of calculations does not justify the program preparation or when high accuracy is not required it would be quicker and simpler to use the Furnas solution provided that some estimate of the error could be made. Thus a general relationship is required between the bed lengths predicted by each of the two methods for the same input data of Bi, β and T_{fo}.

Consider the simple Furnas solution: The heat transfer rate is given by:

$$Q = h_f . a . A_x . y . \Delta T_m \quad \ldots\ldots\ldots\ldots\ldots\ldots \quad (7:6)$$

(see equation (3:59), Section 3.4.3).

Now:

$$Bi = \frac{h_f . d_p}{2 . k_s} ,$$

$$z = \frac{4 . k_s . (1-e) . y}{G_s . c_s . d_p^{\,2}} \quad \ldots\ldots\ldots\ldots\ldots\ldots \quad (3:28)$$

and

$$a = \frac{6 . (1-e)}{d_p} \quad \ldots\ldots\ldots\ldots\ldots\ldots \quad (3:6)$$

Substituting Bi, z and a in (7:6):

$$Q = \frac{2 . k_s . Bi}{d_p} \cdot \frac{6 . (1-e)}{d_p} \cdot \frac{G_s . c_s . d_p^{\,2} . z}{4 . k_s . (1-e)} \cdot A_x . \Delta T_m$$

$$= 3 . Bi . G_s . c_s . z . A_x . \Delta T_m \quad \ldots\ldots\ldots\ldots \quad (7:7)$$

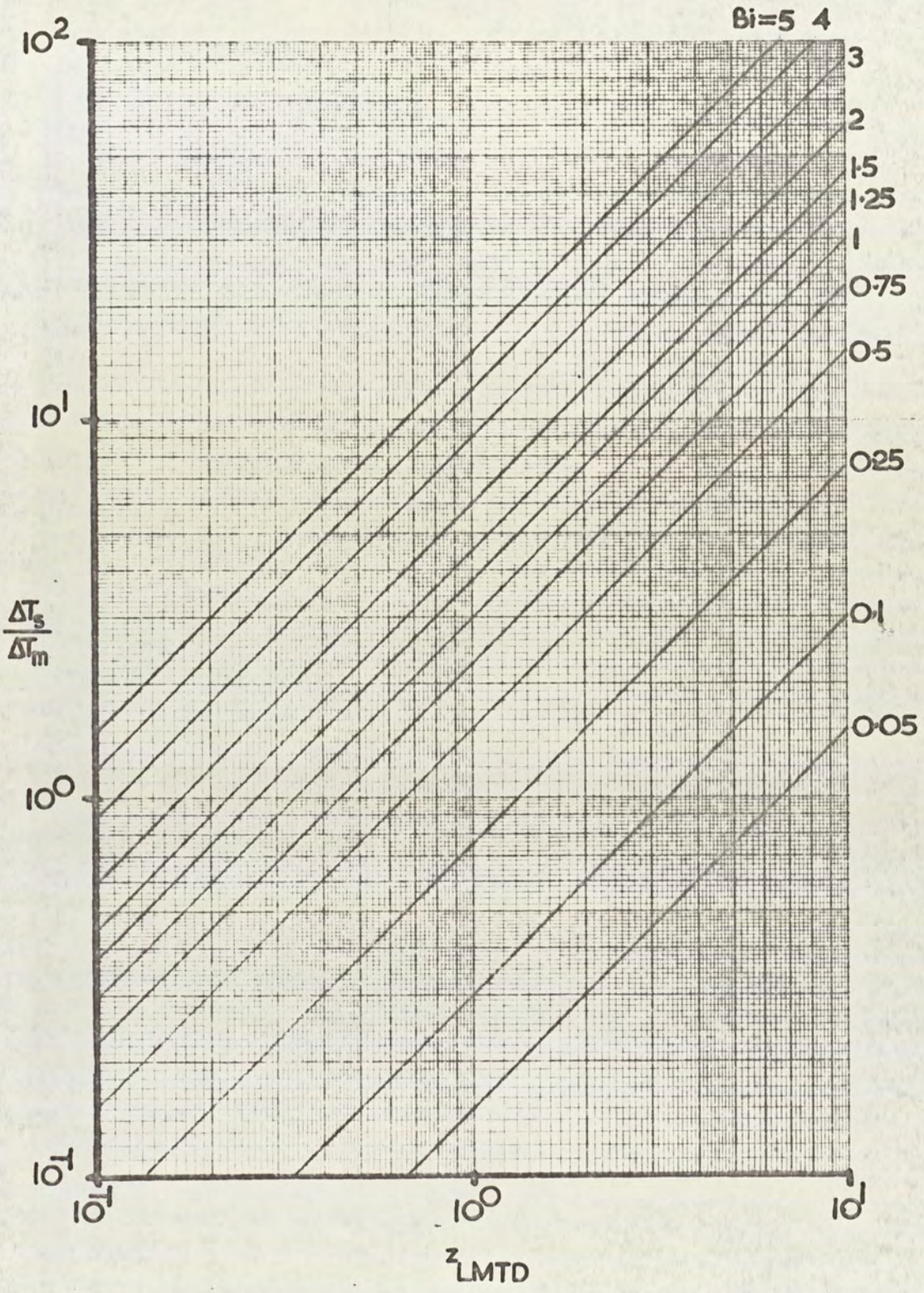

FIGURE 7:1 GENERAL DESIGN DATA:

L.M.T.D. SOLN.: NO I.P.T.D.

Now:

$$Q = Q_f \cdot c_f \cdot A_x \cdot \Delta T_f$$

$$= G_s \cdot c_s \cdot A_x \cdot \Delta T_s \quad \ldots\ldots\ldots\ldots\ldots\ldots \quad (7:8)$$

where $\Delta T_f = T_{fi} - T_{fo}$

$\Delta T_s = T_{so} - T_{si}$

Dividing (7:8) by (7:7)

$$z = \frac{\Delta T_s}{\Delta T_m} \cdot \frac{1}{3.Bi} \quad \ldots\ldots\ldots\ldots\ldots\ldots \quad (7:9)$$

where $\Delta T_m = \dfrac{\Delta T_o - \Delta T_L}{\log_e\left(\dfrac{\Delta T_o}{\Delta T_L}\right)}$, for $\beta < 1$

$\Delta T_m = \Delta T_L = \Delta T_o$, for $\beta = 1$

$\Delta T_m = \dfrac{\Delta T_L - \Delta T_o}{\log_e\left(\dfrac{\Delta T_L}{\Delta T_o}\right)}$, for $\beta > 1$

$\Delta T_o = T_{fo} - T_{si}$

$\Delta T_L = T_{fi} - T_{so}$

The general solution of (7:9) is represented in Figure 7:1 for all values of β as:

$$\frac{\Delta T_s}{\Delta T_m} \text{ v. } z$$

with Bi as parameter.

The numerical integration solution for intra-particle temperature distribution for a range of values of β and Bi was run on the I.C.L. 1905 computer with the program ZFRAGENDES given in Appendix 1.2. The values of $\Delta T_s/\Delta T_m$ were calculated at appropriate values of z using the mean solids temperature T_{sm} given by equation (3:42), see Appendix 1.1. The corresponding values of z

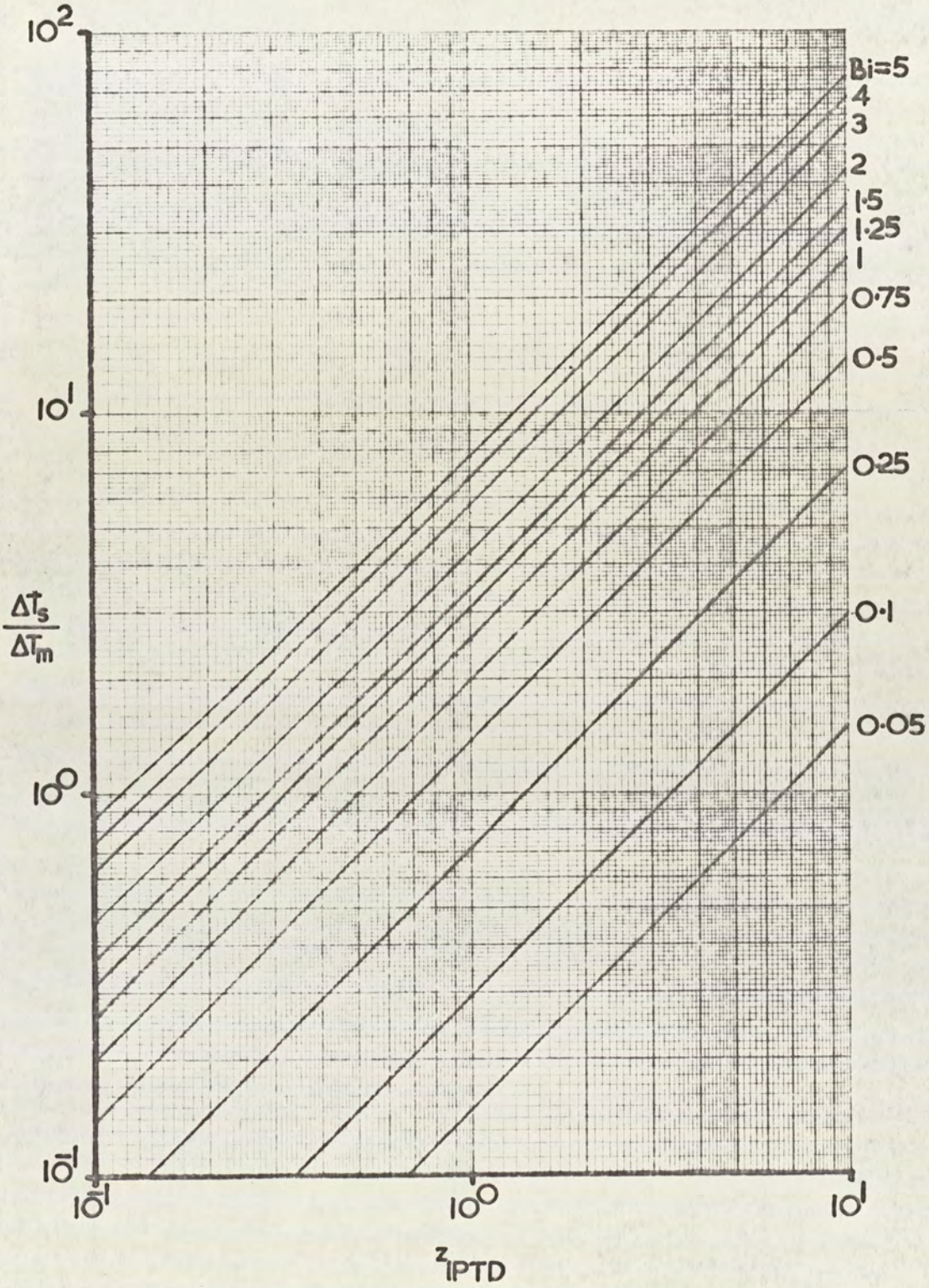

FIGURE 7:2 GENERAL DESIGN DATA:

NUM. INT. SOLN. : I.P.T.D.

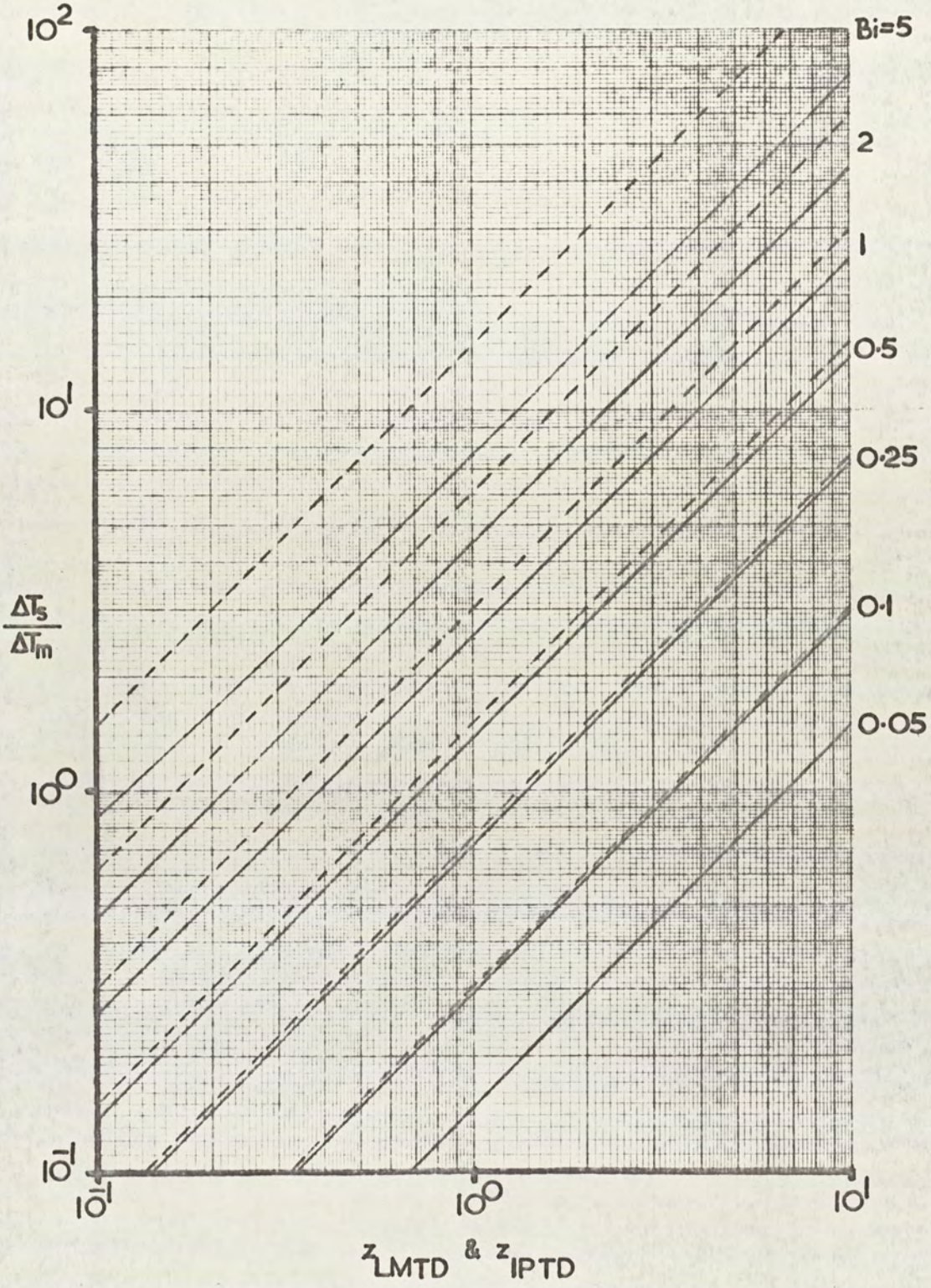

FIGURE 7:3 GENERAL DESIGN DATA:

COMPARISON OF SOLUTIONS

from equation (7:9) were compared and the extent of the under-estimation by the simple solution determined as:

$$\text{Percentage Underestimation} = \frac{z_{IPTD} - z_{LMTD}}{z_{IPTD}} \cdot 100 \quad \ldots\ldots \quad (7:10)$$

where z_{IPTD} is the bed length for intra-particle temperature distribution by numerical integration

z_{LMTD} is the bed length for the Furnas logarithmic mean temperature difference solution.

The detailed results of the numerical integrations are tabulated in Appendix 4 and it can be seen that the variation in $\Delta T_s/\Delta T_m$ with β at the same z and Bi is negligible except at high values of z and Bi ($z>5$, $Bi>1.5$) where T_f and T_s are almost equal. The divergence may be due to round off error in the calculations but is of little importance as it is outside the range of practical values of z_L because:

$$z_L = \frac{k_s.(1-e).L.4}{G_s.c_s.d_p^2}$$

$$Bi = \frac{h_f.d_p}{2k_s}$$

i.e. high Bi generally implies high d_p/k_s and consequently low z_L. Figure 7:2 shows:

$$\frac{\Delta T_s}{\Delta T_m} \text{ v. } z_{IPTD}$$

for $\beta = 1$ with Bi as parameter. Figure 7:3 compares the two methods of solution to demonstrate the increasing effect of the conduction lag as the Biot number is increased. Clearly there is no threshold value of Bi as the effect is always present to some extent.

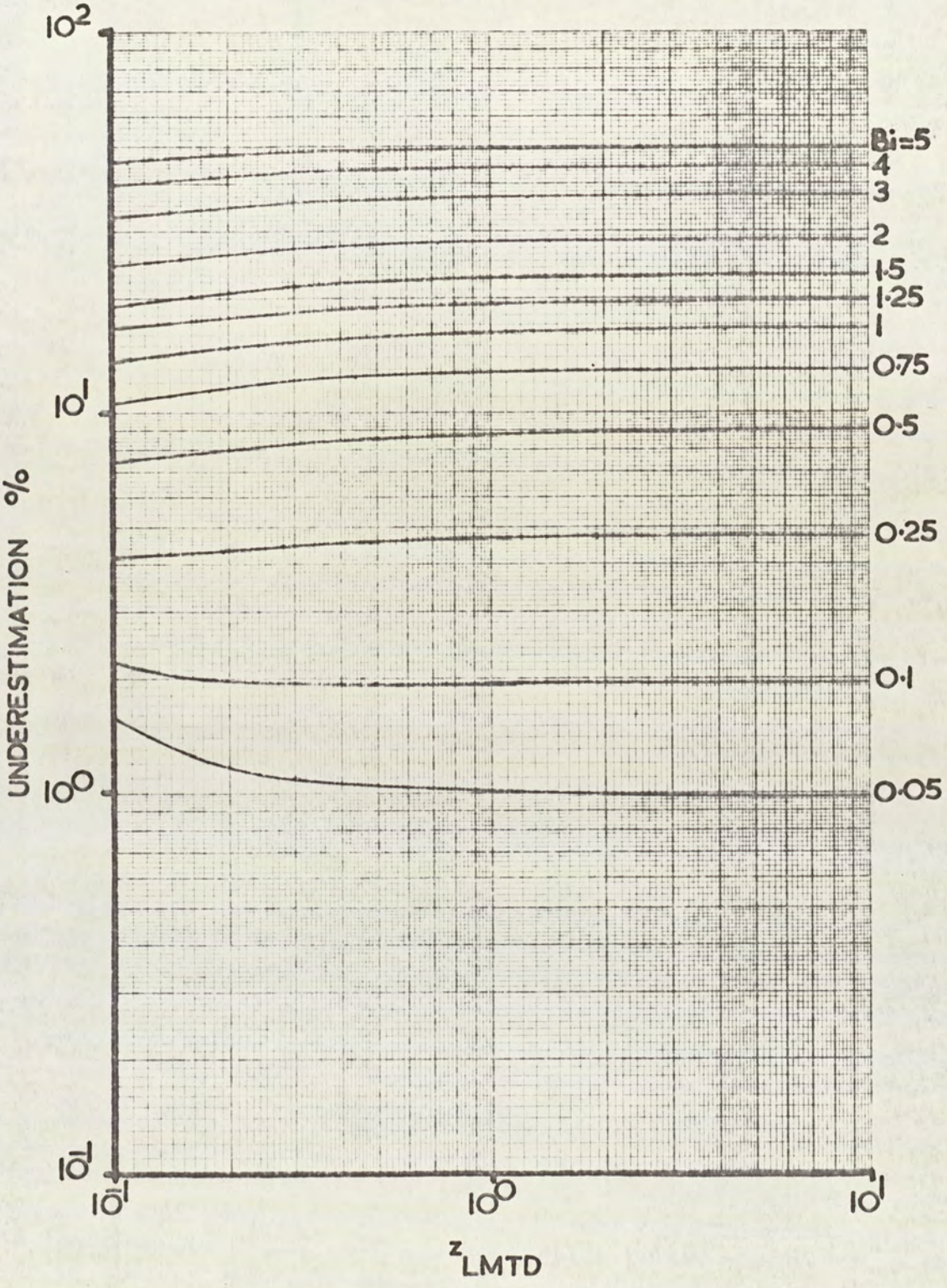

FIGURE 7:4 GENERAL DESIGN DATA :

UNDERESTIMATION BY L.M.T.D. SOLUTION

Figure 7:4 shows:

Percentage Underestimation v. z_{LMTD}

for $\beta = 1$ with Bi as parameter.

As Figures 7:1 to 7:4 cover most of the ranges of values of Bi, β and z likely to be met in practice, it is suggested that they could be used directly for design purposes where the axial fluid and solid temperature distributions are not required. There are two possible approaches:

(1) Calculate the bed length using the Furnas solution and then apply a correction using the percentage underestimation from Figure 7:4.

(2) Calculate $\Delta T_s/\Delta T_m$ and obtain z directly from Figure 7:2. This method seems to be the better of the two.

As regards the design of melting bed equipment, it was shown in the literature survey, Section 2.1, that little information is available. It should suffice for the present to design melters simply as heat exchangers in which change of phase occurs without change in physical shape, i.e. the sensible heat plus the latent heat is supplied through a constant heat transfer area equal to the original surface area of the charge. At worst this should only overestimate the bed length required as in a practical melter the surface area would generally be increased by the phase change.

SECTION 8

SUGGESTIONS FOR FUTURE WORK

SECTION 8 - SUGGESTIONS FOR FUTURE WORK

Explanations of the discrepancies between published fixed and moving bed data have been suggested in Section 6 but even the present results are not completely satisfactory. There is some scatter and at Reynolds numbers below 200 the correlating line diverges from the fixed bed lines. While experimental error is inevitable, it seems likely that gross errors stem from inadequacies of the model and equipment.

It has been shown that the basic assumptions of uniform fluid and solid velocity profiles are unjustified although no quantitative measurements of the deviations from ideality have been made. The solids flow could be made more uniform by blending the air inlets into the inside wall of the column so that a smooth surface would be presented to the descending solids. Improvement in the solids flow pattern by preventing dislocations of the matrix would inevitably flatten the air velocity profile and the radial temperature profiles in both streams. Further improvement in the latter could be achieved by lagging the column to reduce wall heat losses or balancing such losses as in the SCICE equipment[48]. However, this would introduce problems of bed height measurement and approach to steady state conditions. The present profile of the bed surface also leads to radial temperature and velocity distributions. It could be improved by feeding solids from both sides of the column or possibly around the whole circumference, although the latter would again increase the difficulty of bed height measurement. Although the top of the bed is well defined, the bottom is more vague. It was taken as the centre line of the air feed side arms but these were 1.5 in

diameter compared with the maximum bed height of only 4.5 in. A narrow slit around the whole column would be better. If it was filled in with some porous material the requirements for plug flow of solids could also be met. The entrance-exit effects demonstrated by Malling and Thodos[59] should be considered. A layer of stationary spheres could be placed just above the bed surface. The air entrance effect is probably negligible anyway due to the small area of the feed side arms compared with the bed cross section.

All of the above are improvements which could be incorporated but there are other deficiencies in the equipment which probably cannot be overcome. Cross flow heat transfer is inevitable at both ends of the bed. It might be possible to introduce the air stream through an internal distributor but this would cause dislocations of the descending matrix and heat transfer through the walls of the distributor pipe to the ballotini. Similar distribution of the feed ballotini would suffer from solids flow problems as well as preheating. Although cross flow cannot be eliminated, the effects could be minimised by using longer beds but then one or other of the terminal temperature differences would tend to zero. This could be avoided by using larger particles but the consequent increase in the wall effects would require the column diameter to be increased. The whole scale of operation would need to be increased.

Development of a model to fit the behaviour of the present equipment would be very difficult and, even if possible, would require a considerable increase in the amount of input data, viz. air and solids radial and axial temperature and velocity

distributions. It is doubtful whether the effort could be justified.

The philosophy of conducting experimental measurements of packed bed heat transfer coefficients under moving bed conditions should be questioned before extending the use of the technique. Although the present results are not in complete agreement with published fixed bed data, they have served to explain the discrepancies in previous moving bed work and proved, or at least provided strong evidence, that there are no differences between the heat transfer processes in the two types of equipment. The apparent differences stemmed from velocity profiles, measurement errors and analytical errors. Accepting the evidence, it seems logical that heat transfer should be divorced from bed movement in future experimental basic research. However, to serve the needs of designers, the fluid and solids flow characteristics of particular types of equipment must be studied and related to the heat transfer characteristics. Fixed bed work should be directed towards the measurement of wall effects as d_p approaches d_v as this is a feature of several tower melters. The use of non-spherical particles in laboratory scale moving beds would introduce solids flow problems but shape factors for the types of material likely to be met in practice might be obtained from existing pressure drop data or by direct fixed bed heat transfer measurements.

As regards the theoretical and computational aspects of moving bed heat transfer, a number of factors are worthy of investigation. As digital computers are more generally available than analogue machines, the numerical integration technique is particularly

useful both for design purposes and analysis of experimental data. However, it has been shown in Section 3.6.1 that the heat balance is subject to error. The reasons for this and the magnitude and variation of the error should be determined and improvements made, if possible. Gay and Akers[81] suggested that the error stemmed from the double use of finite differences, first to reduce the partial differential equations to ordinary differential equations and secondly to integrate, and might be overcome by using a larger number of sphere increments. If the heat balance check suggested in Section 5.2 were incorporated into the version of the program ZFRAWRWEXPT which ignores intra-particle temperature distribution, their suggestion could be verified. The quadrature formula for T_{sm}, equation (3:42), might not be adequate. Third order correct finite differences might be more appropriate for the present application than second order. The error might be concerned with the step length but Gay and Akers discounted this factor. Although $\Delta z = 0.018$ does not produce wild instability, small errors might develop where large changes of gradient occur. It is not advisable to reduce the fixed value of Δz due to the computation time required but the facility of variable step length would be very valuable. Third order differences, more sphere increments and fourth order integration would then be feasible. Variable step length procedures have been developed by Merson[82] and Zonneveld[102].

The present model involving intra-particle temperature distribution and wall heat loss could be made more sophisticated by including the effects of axial dispersion in the fluid phase and axial conduction between the particles. A similar approach

to that in Section 7 for the conduction lag could be used to determine the errors in the simple model over ranges of various parameters. Reference has been made already to the models of Littman et al.[43] and Malling and Thodos[59]. Those of Kunii and Smith[103], Amundson[104,105] and Siegmund et al.[106] might also prove useful. It might be possible to apply the channelling model of Kunii and Suzuki[71] to large scale wall effects.

Much work needs to be done on the application of the moving bed principle to melting. Owing to the problems inherent in industrial scale research, high wall effects and non-spherical particles, it is not surprising that Watson and Glen[10] and Glen[11] were unable to obtain a satisfactory correlation of their data. In view of the observations of Knight et al.[14] on the different mechanisms of melting of copper and aluminium and the significance of the solid phase thermal conductivity and melt surface tension recognised by Standish[25], the analysis of melting bed data must inevitably be system orientated. Scaffold formation and upward transport of melt by combustion gases are also worthy of investigation.

SECTION 9

CONCLUSIONS

SECTION 9 - CONCLUSIONS

The literature survey demonstrated that heat transfer data for moving beds differed by as much as an order of magnitude from those obtained using fixed bed techniques. Moreover, the moving bed data of different workers were much less consistent as a group than were those for fixed beds. As previous workers were unable to correlate melting results satisfactorily and as the preheating zones of tower melters are essentially moving beds, the present work was aimed primarily at resolving the differences between fixed and moving bed heat transfer as a first step towards understanding the complete melting process.

As the experimental tower was constructed of glass it was possible to observe the movement of the spherical solid particles. It was discovered that, contrary to the opinions of most other workers, the bed did not move in plug flow. Expansion at the start of movement and radial solids velocity profiles were detected. The change in mean voidage from fixed to moving bed conditions was determined from pressure drop measurements. The dislocations of the bed matrix near the wall of the present 6-in diameter column caused bypassing of the air in the regions of high voidage and consequently reduced the overall heat transfer rate. It is considered that this effect must have been even more marked in the 3 and 4 in columns used in previous moving bed work[2] and was responsible for much of the reported disagreement between fixed and moving bed heat transfer data.

Other aspects of the flow characteristics of spherical solids were investigated to obtain data for the design of the present

equipment and to overcome difficulties encountered during its commissioning. It was found that the minimum value of the $d_v:d_p$ ratio for the steady flow of glass ballotini under packed bed conditions was about 4, but this figure was exceeded for particles of greater surface roughness and lower degree of sphericity.

The equipment was not lagged for two reasons: first, so that the variations in the bed height could be observed; secondly, so that the time taken to achieve steady state thermal equilibrium would not be excessive. This necessitated measurement of the heat losses, the transfer coefficients being correlated by:

$$U_w = 0.201 \times \left(\frac{G_f}{e}\right)^{0.310} \times \Delta T_{lmw}^{0.067} \quad \ldots\ldots\ldots \quad (4:4)$$

where the units are:

U_w: Btu/hft^{2}degF

G_f: lb/hft^2

e: dimensionless

ΔT_{lmw}: equivalent chromel-alumel thermocouple output in mV.

The wall heat losses were incorporated into the mathematical model of moving bed heat transfer.

Outlet air mixing baffles were fitted to reduce the temperature and velocity profiles prior to temperature measurement but the outlet solids temperature was only measured at one point on the axis of the bed. Consideration of the heat balance showed that this solids temperature was lower than the mean outlet value so heat transfer coefficients calculated from it were too low. It is likely that this error occurred in previous work[2]. Transfer coefficients in the present work were based on the measured air

outlet temperature.

It was shown that large bed lengths produced errors in previous moving bed work, particularly in that of Norton[26]. As the bed length increases so does the number of transfer units and one or other or both of the terminal temperature differences tends to zero. This effect has been demonstrated even with beds as short as 3 in. After rejection of runs subject to this error and correction of the heat transfer coefficients for intra-particle temperature distribution, the present results were seen to be in close agreement with previous fixed bed data and were correlated by:

$$Nu = 0.183 \times Re^{0.834} \quad \ldots\ldots\ldots\ldots\ldots\ldots \quad (5:7)$$

for $95 \leqslant Re \leqslant 1662$.

The effect of the relative velocity of the air and solids streams was investigated but shown to be insignificant. It may be concluded that there are no differences between the heat transfer processes occurring in fixed and moving beds. The apparent differences reported in the literature stemmed from the use of non-ideal experimental systems, measurement errors and analytical errors. However, the possibilities of dislocations of the bed matrix, fluid and solids velocity and temperature profiles and consequential reductions in overall heat transfer rates should not be neglected in the design of moving bed equipment.

As the range of voidage in the present work was very narrow (0.375 to 0.412), any possible effects were far outweighed by the experimental scatter but if wide variations are encountered in design work, equation (5:7) could be replaced by:

$$Nu = 0.0794 \times \left(\frac{Re}{e}\right)^{0.845} \quad \ldots\ldots\ldots\ldots\ldots\ldots \quad (5:9)$$

for $235 \leqslant \frac{Re}{e} \leqslant 4034$.

A digital computer technique[83] was applied to the analysis of the heating of spherical particles, both in moving beds and in isolation. It could be developed further but, even in its present form, it is superior to previous analogue computer methods.

The effect of the conduction lag within the solids ranged from 1 to 30% in the present investigation. To simplify design work, correction factors have been calculated by digital numerical integration which enable the simple logarithmic mean temperature difference solutions for two-fluid heat exchangers to be applied to moving beds.

APPENDIX 1

AMPLIFICATION OF THE THEORY

APPENDIX 1 - AMPLIFICATION OF THE THEORY

A1.1 Derivation of the Mean Solids Temperature

Consider a sphere in terms of the dimensionless radius and temperature variables. For an elementary shell of radius x and thickness δx:

Volume $= 4.\Pi.x^2.\delta x$

Heat content $= 4.\Pi.x^2.\delta x.\rho_s.c_s.\theta_x$

The mean temperature of the whole sphere is given by:

$$\theta_m = \frac{\sum_{x=o}^{x=1} 4.\Pi.x^2.\delta x.\rho_s.c_s.\theta_x}{\sum_{x=o}^{x=1} 4.\Pi.x^2.\delta x.\rho_s.c_s}$$

$$= \frac{\int_{x=o}^{x=1} 4.\Pi.x^2.\rho_s.c_s.\theta_x.dx}{\frac{4}{3}.\Pi.(1)^3.\rho_s.c_s}$$

$$= 3.\int_{x=o}^{x=1} x^2.\theta_x.dx \quad \ldots\ldots\ldots\ldots\ldots\ldots \quad (A1:1)$$

Using a 6-point, closed end, Newton-Coates quadrature[79], it may be shown that:

$$\int_{q_o}^{q_5} s.dq = \frac{5.\Delta q}{288}\left[19.s_o+75.s_1+50.s_2+50.s_3+75.s_4+19.s_5\right]$$

$\ldots\ldots\ldots\ldots\ldots$ (A1:2)

As the mean solids temperature is to be obtained from the 6 nodal temperatures θ_o to θ_5, equation (A1:1) may be evaluated as:

$$\theta_m = \frac{3.5.\Delta x}{288}\left[19.(x_o^2.\theta_o) + 75.(x_1^2.\theta_1) \ldots\ldots\right.$$
$$\left. \ldots\ldots + 19.(x_5^2.\theta_5)\right]$$
$\ldots\ldots\ldots\ldots\ldots\ldots$ (A1:3)

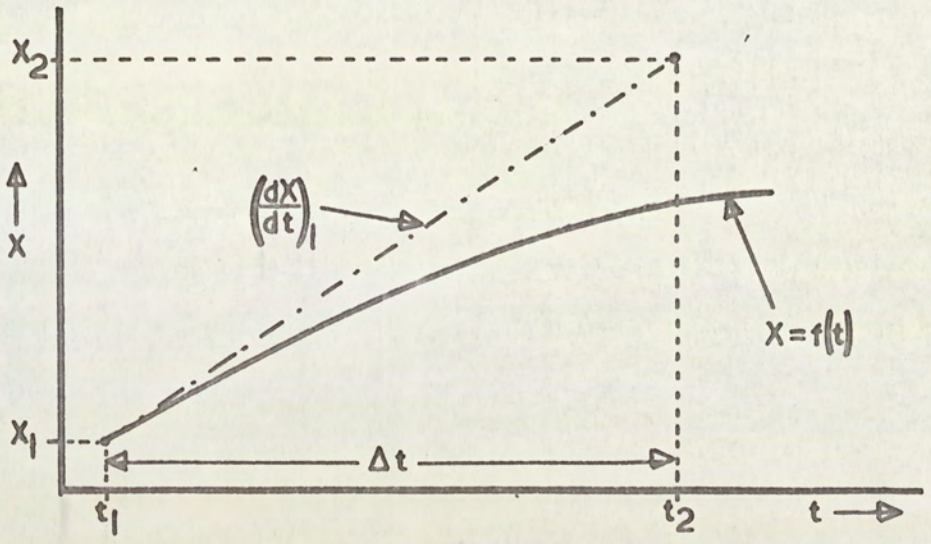

FIGURE A1:1 EULER METHOD

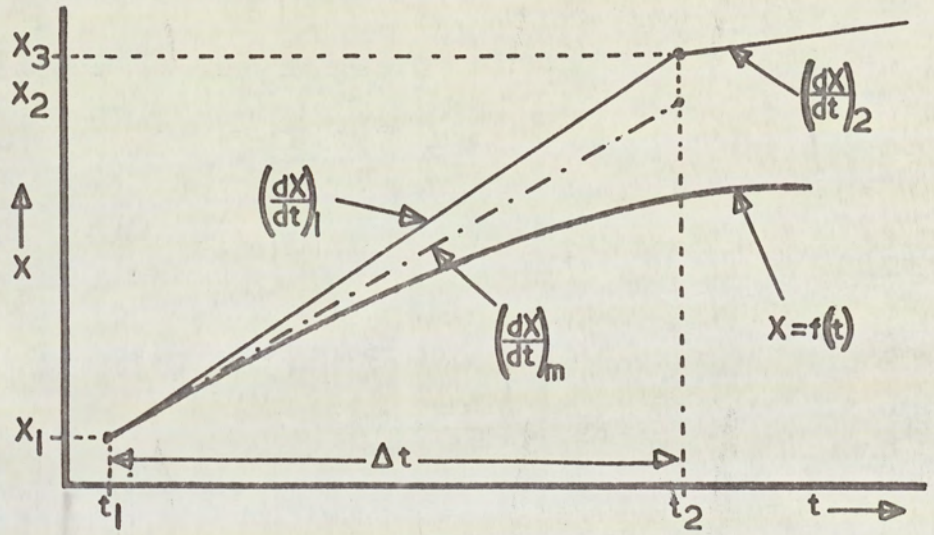

FIGURE A1:2 SECOND ORDER RUNGE-KUTTA METHOD

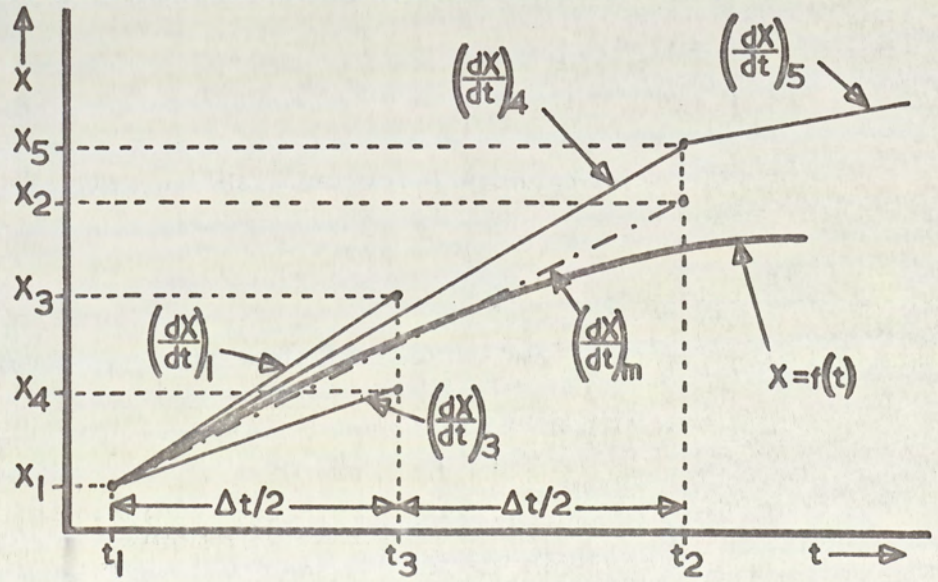

FIGURE A1:3 FOURTH ORDER RUNGE-KUTTA METHOD

Now,

$$\Delta x = 0.2$$

$$x_n = n.\Delta x.$$

Substituting in (A1:3):

$$\theta_m = \frac{57.\theta_5}{288} + \frac{\theta_4}{2} + \frac{3.\theta_3}{16} + \frac{\theta_2}{12} + \frac{\theta_1}{32} \quad \ldots\ldots\ldots \quad (3:42)$$

or, if the coefficients are to be set on the potentiometers of an analogue computer,

$$\theta_m = 0.1979.\theta_5 + 0.5.\theta_4 + 0.1875.\theta_3 + 0.0833.\theta_2 + 0.0312.\theta_1$$

A1.2 Numerical Integration

There are three levels of sophistication of the numerical integration: the Euler method and the Second and Fourth Order Runge-Kutta methods. Franks[83] considered only the latter two but the simple Euler solution has been shown to be quite useful in the present work.

The following descriptions of the methods relate to the variables X and t where X is any dependent variable and t is an independent one, usually time but not necessarily so. In the present work t was the dimensionless bed length z and X represented the various air and solids temperatures.

Euler Method

Referring to Figure A1:1, knowing the value of the function X_1 and the gradient $\left(\frac{dX}{dt}\right)_1$ at t_1, the Euler approximation to X at t_2 is:

$$X_2 = X_1 + \left(\frac{dX}{dt}\right)_1 . \Delta t \quad \ldots\ldots\ldots\ldots\ldots \quad (A1:4)$$

Thus the relationship between X and t may be obtained by successive applications of equation (A1:4).

Second Order Runge-Kutta Method

This is an extension of the simple Euler method in which the error is reduced by evaluating the derivative at both t_1 and t_2 and using the average to obtain X_2, see Figure A1:2.

$$X_3 = X_1 + \left(\frac{dX}{dt}\right)_1 \cdot \Delta t \quad \ldots\ldots\ldots\ldots\ldots\ldots \quad (A1:5)$$

Substitution of X_3 in the differential equation gives:

$\left(\frac{dX}{dt}\right)_2$ then

$$\left(\frac{dX}{dt}\right)_m = \frac{1}{2}\left[\left(\frac{dX}{dt}\right)_1 + \left(\frac{dX}{dt}\right)_2\right] \quad \ldots\ldots\ldots\ldots\ldots\ldots \quad (A1:6)$$

and

$$X_2 = X_1 + \left(\frac{dX}{dt}\right)_m \cdot \Delta t \quad \ldots\ldots\ldots\ldots\ldots\ldots \quad (A1:7)$$

which is a better approximation to the true value of X at t_2 than is that given by equation (A1:4).

Fourth Order Runge-Kutta Method

This is the third level of sophistication in which a further reduction in the integration error is achieved by evaluating the derivative in the middle of the interval as well as at t_1 and t_2, as indicated in Figure A1:3.

$$X_3 = X_1 + \left(\frac{dX}{dt}\right)_1 \cdot \frac{\Delta t}{2} \quad \ldots\ldots\ldots\ldots\ldots\ldots \quad (A1:8)$$

The derivative at t_3 is calculated by substitution of X_3 in the differential equation. X at t_3 is then recalculated as X_4:

$$X_4 = X_1 + \left(\frac{dX}{dt}\right)_3 \cdot \frac{\Delta t}{2} \quad \ldots\ldots\ldots\ldots\ldots\ldots \quad (A1:9)$$

This is used to give another value of the derivative at t_3 and from it a value of X at t_2 is obtained:

$$X_5 = X_1 + \left(\frac{dX}{dt}\right)_4 \cdot \Delta t \quad \ldots\ldots\ldots\ldots\ldots\ldots \quad (A1:10)$$

the corresponding value of the derivative being $\frac{dX}{dt}_5$. The four

```
        'COMMENT' DEPENDENT VARIABLE INTEGRATION PROCEDURE
                  --------- -------- ----------- ---------;
        'PROCEDURE' INT(X,DX,DT);
        'REAL' X,DX,DT;
        'BEGIN'
        JN:=JN+1;
        'IF' IO=1 'THEN' 'GOTO' D1;
        'IF' IO=4 'THEN' 'GOTO' D3;
        'IF' JS=1 'THEN' 'GOTO' D1 'ELSE' 'GOTO' D2;
    D1:DXA[JN]:=DX;
        X:=X+DX*DT;
        'GOTO' GOBACK;
    D2:X:=X+(DX-DXA[JN])*DT/2;
        'GOTO' GOBACK;
    D3:'IF' JS4=1 'THEN' 'GOTO' D4;
        'IF' JS4=2 'THEN' 'GOTO' D5;
        'IF' JS4=3 'THEN' 'GOTO' D5 'ELSE' 'GOTO' D7;
    D4:XA[JN]:=X;
        DXA[JN]:=DX;
        X:=X+DX*DT;
        'GOTO' GOBACK;
    D5:DXA[JN]:=DXA[JN]+2*DX;
        X:=XA[JN]+DX*DT;
        'GOTO' GOBACK;
    D7:DXA[JN]:=(DXA[JN]+DX)/6;
        X:=XA[JN]+DXA[JN]*DT;
GOBACK:'END';
```

FIGURE A1:4 THE PROCEDURE INT

derivatives are then combined as:

$$\left(\frac{dX}{dt}\right)_m = \frac{1}{6}\left[\left(\frac{dX}{dt}\right)_1 + 2.\left(\frac{dX}{dt}\right)_3 + 2.\left(\frac{dX}{dt}\right)_4 + \left(\frac{dX}{dt}\right)_5\right] \quad \ldots\ldots\ldots \text{(A1:11)}$$

and the best approximation to X at t_2 calculated as:

$$X_2 = X_1 + \left(\frac{dX}{dt}\right)_m . \Delta t \quad \ldots\ldots\ldots\ldots\ldots\ldots \text{(A1:12)}$$

Equations (A1:4) to (A1:12) are contained in the ALGOL procedure INT shown in Figure A1:4. Manipulation of the variables X and $\frac{dX}{dt}$ within the interval Δt (represented in the procedure by X, DX and DT respectively) is dependent upon the levels of the following integers:

(1) IO - Integration Order

1: Euler

2: Second Order Runge-Kutta

4: Fourth Order Runge-Kutta

(2) JS - Pass Counter (Second Order Runge-Kutta)

0: First pass through derivative equations at start of computation with initial condition of X and t.

1: t_1 incremented to $t_2 = (t_1 + \Delta t)$, first approximation to X calculated from equation (A1:5), first pass through derivative equations for this increment.

2: Second approximation to X calculated from equation (A1:7), second pass through the derivative equations for this increment ready for next increment.

(3) JS4 - Pass Counter (Fourth Order Runge-Kutta)

0: First pass with initial conditions.

1: t_1 incremented to $t_3 = (t_1 + \Delta t/2)$, equation (A1:8), first pass for this increment.

2: Equation (A1:9), second pass.

3: t_1 incremented to $t_2 = (t_1 + \Delta t)$, equation (A1:10), third pass.

4: Final approximation to X_2 calculated from equation (A1:12), fourth pass ready for next increment.

```
        'COMMENT' INDEPENDENT VARIABLE INTEGRATION PROCEDURE
                  ---------- -------- ---------- ---------;
        'PROCEDURE' INTI(T,DT);
        'REAL' T,DT;
        'BEGIN'
        JN:=0;
        'IF' IO=1 'THEN' 'GOTO' I3;
        'IF' IO=4 'THEN' 'GOTO' I1;
        JS:=JS+1;
        'IF' JS=3 'THEN' JS:=1;
        'IF' JS=2 'THEN' 'GOTO' RETURN;
    I3:T:=T+DT;
        'GOTO' RETURN;
    I1:JS4:=JS4+1;
        'IF' JS4=5 'THEN' JS4:=1;
        'IF' JS4=1 'THEN' 'GOTO' I2;
        'IF' JS4=3 'THEN' 'GOTO' I4 'ELSE' 'GOTO' RETURN;
    I2:DT:=DT/2;
        'GOTO' I3;
    I4:T:=T+DT;
       DT:=2*DT;
RETURN:'END';
```

FIGURE AI:5 THE PROCEDURE INTI

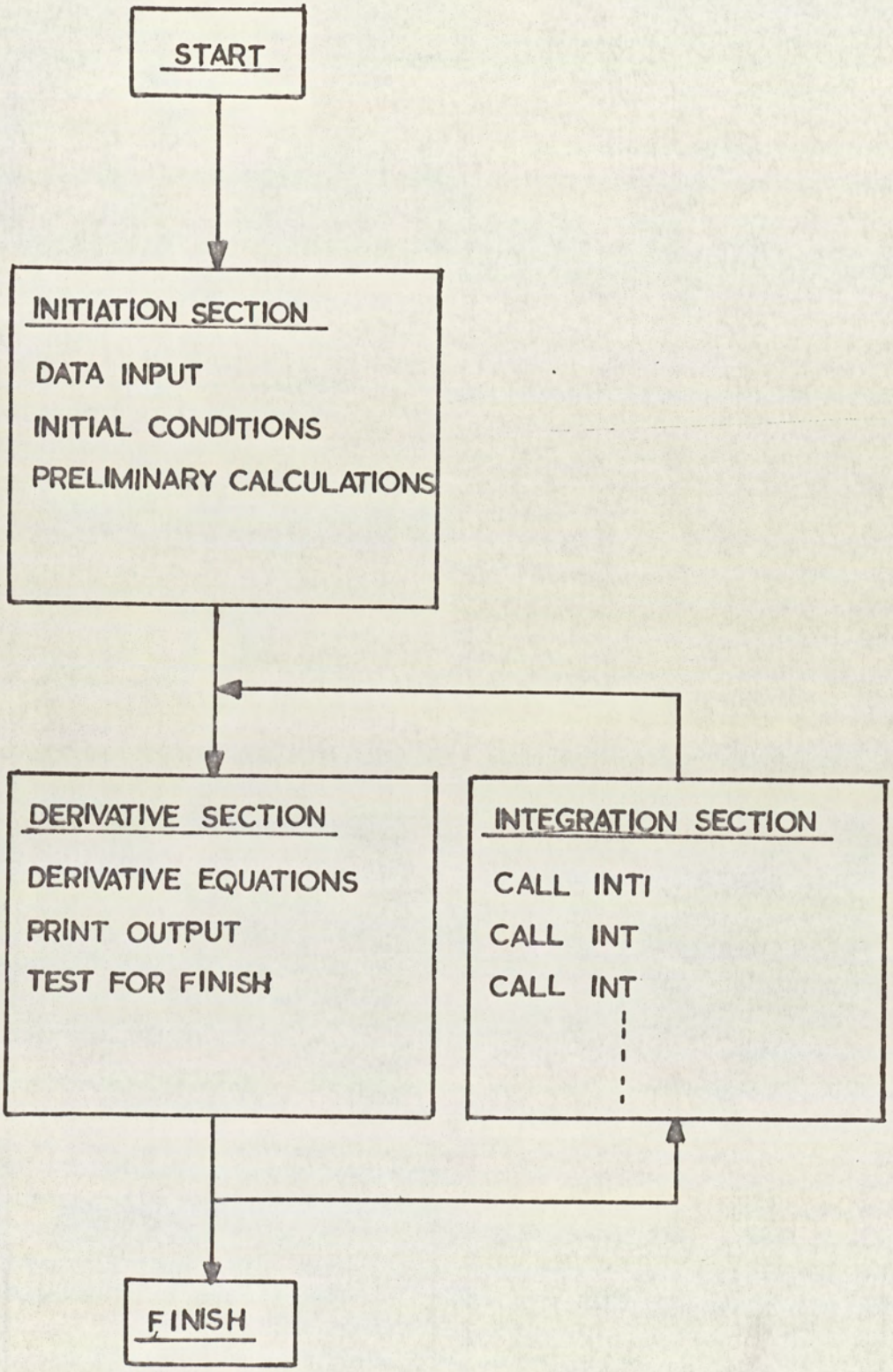

FIGURE A1:6 BASIC PROGRAM STRUCTURE FOR NUMERICAL INTEGRATION

FIGURE A1:7 THE PROGRAM ZFRANKSLK

```
04/09/72          COMPILED BY XALE MK.  5C

'SEND TO' ( ED,ASTD-DEFAULT(0),.PROGRAM)
'WORK' (ED,WORK FILE    )
'TRACE' 2
'BEGIN' 'COMMENT' CEPSF015,                                                    FRA  100
                  WILSON,                                                      FRA  200
                  ZFRANKSLK,                                                   FRA  300
DIGITAL SIMULATION OF HYBRID-ANALOG SIMULATION                                 FRA  400
------- ---------- -- ------------ ----------                                 FRA  500
OF THE LOVELL & KARNOFSKY PROBLEM                                              FRA  600
-- --- ------ - --------- ------- ;                                           FRA  700
      'BEGIN' 'REAL' BIOT,BETA,Z,ZL,TS0,TS1,TS2,TS3,TS4,TS5,TG,TGO,            FRA  750
                     DTS0,DTS1,DTS2,DTS3,DTS4,DTS5,DTG,TSM,DZ;                 FRA  800
              'INTEGER' IO,JN,JS,JS4,RUNS,COUNTER;                             FRA  900
              'REAL' 'ARRAY' XA,DXA[1:7];                                      FRA  950
      'COMMENT' INDEPENDENT VARIABLE INTEGRATION PROCEDURE                     FRA 1005
                ----------- -------- ----------- ---------;                   FRA 1010
      'PROCEDURE' INTI(T,DT);                                                  FRA 1015
      'REAL' T,DT;                                                             FRA 1017
      'BEGIN'                                                                  FRA 1020
      JN:=0;                                                                   FRA 1025
      'IF' IO=1 'THEN' 'GOTO' I3;                                              FRA 1027
      'IF' IO=4 'THEN' 'GOTO' I1;                                              FRA 1030
      JS:=JS+1;                                                                FRA 1035
      'IF' JS=3 'THEN' JS:=1;                                                  FRA 1040
      'IF' JS=2 'THEN' 'GOTO' RETURN;                                          FRA 1045
   I3:T:=T+DT;                                                                 FRA 1050
      'GOTO' RETURN;                                                           FRA 1055
   I1:JS4:=JS4+1;                                                              FRA 1060
      'IF' JS4=5 'THEN' JS4:=1;                                                FRA 1065
      'IF' JS4=1 'THEN' 'GOTO' I2;                                             FRA 1070
      'IF' JS4=3 'THEN' 'GOTO' I4 'ELSE' 'GOTO' RETURN;                        FRA 1075
   I2:DT:=DT/2;                                                                FRA 1080
      'GOTO' I3;                                                               FRA 1085
   I4:T:=T+DT;                                                                 FRA 1090
      DT:=2*DT;                                                                FRA 1095
RETURN:'END';                                                                  FRA 1100
      'COMMENT' DEPENDENT VARIABLE INTEGRATION PROCEDURE                       FRA 1105
                --------- -------- ----------- ---------;                     FRA 1110
      'PROCEDURE' INT(X,DX,DT);                                                FRA 1115
      'REAL' X,DX,DT;                                                          FRA 1118
      'BEGIN'                                                                  FRA 1122
      JN:=JN+1;                                                                FRA 1125
      'IF' IO=1 'THEN' 'GOTO' D1;                                              FRA 1127
      'IF' IO=4 'THEN' 'GOTO' D3;                                              FRA 1130
      'IF' JS=1 'THEN' 'GOTO' D1 'ELSE' 'GOTO' D2;                             FRA 1135
   D1:DXA[JN]:=DX;                                                             FRA 1140
      X:=X+DX*DT;                                                              FRA 1145
      'GOTO' GOBACK;                                                           FRA 1150
   D2:X:=X+(DX-DXA[JN])*DT/2;                                                  FRA 1155
      'GOTO' GOBACK;                                                           FRA 1160
   D3:'IF' JS4=1 'THEN' 'GOTO' D4;                                             FRA 1165
      'IF' JS4=2 'THEN' 'GOTO' D5;                                             FRA 1170
      'IF' JS4=3 'THEN' 'GOTO' D5 'ELSE' 'GOTO' D7;                            FRA 1175
   D4:XA[JN]:=X;                                                               FRA 1180
      DXA[JN]:=DX;                                                             FRA 1185
      X:=X+DX*DT;                                                              FRA 1190
      'GOTO' GOBACK;                                                           FRA 1195

   D5:DXA[JN]:=DXA[JN]+2*DX;                                                   FRA 1200
      X:=XA[JN]+DX*DT;                                                         FRA 1205
      'GOTO' GOBACK;                                                           FRA 1210
   D7:DXA[JN]:=(DXA[JN]+DX)/6;                                                 FRA 1215
      X:=XA[JN]+DXA[JN]*DT;                                                    FRA 1220
GOBACK:'END';                                                                  FRA 1225
      'COMMENT' INITIATION SECTION                                             FRA 1300
                ---------- --------;                                          FRA 1400
      RUNS:=READ;                                                              FRA 1430
      'FOR' COUNTER:=1 'STEP' 1 'UNTIL' RUNS 'DO' 'BEGIN'                      FRA 1470
      COPYTEXT('('S')');                                                       FRA 1500
      WRITETEXT('('2C1S')'BIOT'('6S')'BETA'('5S')'DZ'('10S')'TGO'('6FRA 1600
      S')'IO'('1C')'')');                                                      FRA 1700
      BIOT:=5.0;BETA:=1.0;SPACE(17);                                           FRA 1800
      DZ:=READ;PRINT(DZ,2,6);                                                  FRA 2200
      TGO:=1/3;PRINT(TGO,1,6);                                                 FRA 2350
      IO:=READ;PRINT(IO,1,0);                                                  FRA 2400
      ZL:=0.25;                                                                FRA 2425
 FIVE:TS0:=0;                                                                  FRA 2500
      TS1:=0;                                                                  FRA 2550
      TS2:=0;                                                                  FRA 2600
      TS3:=0;                                                                  FRA 2700
      TS4:=0;                                                                  FRA 2800
      TS5:=0;                                                                  FRA 2900
      TG:=TGO;                                                                 FRA 3000
      Z:=0;                                                                    FRA 3500
      JS:=0;                                                                   FRA 3600
      WRITETEXT('('2C1S')'TG'('9S')'Z'('10S')'TSM'('6S')'TS5'('6S')'FRA 3700
      TS4'('6S')'TS3'('6S')'TS2'('6S')'TS1'('6S')'TS0'('1C')'')');             FRA 7300
      'COMMENT' DERIVATIVE SECTION                                             FRA 7400
                ---------- -------;                                           FRA 3800
THREE:DTS0:=150*(TS1-TS0);                                                     FRA 3900
      DTS1:=50*(TS2-TS1);                                                      FRA 3970
      DTS2:=(1.2*TS5-2*TS2+0.5*TS1)*25;                                        FRA 4040
      DTS3:=(4*TS4/3-2*TS3+2*TS2/3)*25;                                        FRA 4100
      DTS4:=(1.25*TS5-2*TS4+0.75*TS3)*25;                                      FRA 4200
      DTS5:=12*BIOT*(TG-TS5)-50*(TS5-TS4);                                     FRA 4300
      DTG:=3*BETA*BIOT*(TG-TS5);                                               FRA 4400
      'IF' IO =1 'THEN' 'GOTO' SEVEN ;                                         FRA 4500
      'IF' JS =2 'THEN' 'GOTO' SEVEN ;                                         FRA 4700
      'IF' JS4=4 'THEN' 'GOTO' SEVEN ;                                         FRA 4800
      'COMMENT' INTEGRATION SECTION                                            FRA 4900
                ----------- -------;                                          FRA 5000
  ONE:INTI(Z,DZ);                                                              FRA 5100
      INT(TG,DTG,DZ);                                                          FRA 5200
      INT(TS5,DTS5,DZ);                                                        FRA 5300
      INT(TS4,DTS4,DZ);                                                        FRA 5400
      INT(TS3,DTS3,DZ);                                                        FRA 5500
      INT(TS2,DTS2,DZ);                                                        FRA 5600
      INT(TS1,DTS1,DZ);                                                        FRA 5700
      INT(TS0,DTS0,DZ);                                                        FRA 5800
      'GOTO' THREE;                                                            FRA 5850
SEVEN:TSM:=57*TS5/288+TS4/2+3*TS3/16+TS2/12+TS1/32;                            FRA 5900
      PRINT(TG,1,6);                                                           FRA 7200
      PRINT(Z,1,6);                                                            FRA 7500
      PRINT(TSM,1,4);                                                          FRA 7700
      PRINT(TS5,1,4);                                                          FRA 7800
      PRINT(TS4,1,4);                                                          FRA 7900
      PRINT(TS3,1,4);                                                          FRA 8000
      PRINT(TS2,1,4);                                                          FRA 8100

      PRINT(TS1,1,4);                                                          FRA 8200
      PRINT(TS0,1,4);                                                          FRA 8300
      'IF' Z=ZL 'THEN' 'GOTO' FINISH ;                                         FRA 8370
      NEWLINE(1);                                                              FRA 8400
      'IF' (Z+DZ) 'GE' ZL 'THEN' DZ:=(ZL-Z);                                   FRA 8500
      'GOTO' ONE ;                                                             FRA 8600
 FINISH:NEWLINE(2);                                                            FRA 8700
      'END';'END';'END';                                                       FRA 8800
USED    25                                                                     FRA 8900
XXX         EC


4992
```

(4) JN - Call Counter

As several differential equations may need to be solved simultaneously, the values of X and $\frac{dX}{dt}$ are retained in arrays XA[JN] and DXA[JN] so that they are available when required. Each successive call of procedure INT causes JN to be incremented.

Control over the levels of the above integers and incrementing of the independent variable t is achieved by the procedure INTI shown in Figure A1:5. This sets JN to zero prior to each pass through the series of INT calls, sets JS and JS4 to the values corresponding to the particular pass through the derivative equations and increments t by either Δt or $\Delta t/2$, as appropriate.

The basic program structure incorporating procedures INTI and INT is shown in Figure A1:6. The application of the technique to the problems of moving bed heat transfer is illustrated by the following programs:

(1) ZFRANKSLK (see Figure A1:7)

This is suitable for the solution of problems in which all parameters are known and the axial and intra-particle temperature distributions are required, i.e. it is comparable with the analogue computer program shown in Figure 3.2. It was used for the problems posed by Lovell and Karnofsky[76] and Kitaev et al.[38], see Sections 3.6.1 and 3.6.2. After simplification of the derivative equations as indicated in Section 3.6.3 it was also applied to the case of a single sphere in an infinite isothermal medium.

(2) ZFRAGENDES

This was referred to in Section 7. It is essentially the same as ZFRANKSLK but with some modifications to generate the general design parameters. It is essential that problems be

amplitude scaled for analogue computer solutions but, for most practical purposes, this is unnecessary for digital computation although the use of dimensionless temperature variables with maxima of 1.0 has been found very convenient in the present work. ZFRAGENDES was run from an initial condition of $\theta_{fo} = 0.01$ until terminated by one of the following:

$$\theta_f = 10$$

$$\frac{\Delta\theta_s}{\Delta\theta_m} = \frac{\Delta T_s}{\Delta T_m} = 100$$

$$z = 10$$

(3) ZFRAWRWEXPT (see Figure A1:8)

This is the program used for calculation of heat transfer coefficients from experimental results. The logic is equivalent to that in the hybrid-analogue computer solution of Akers[2] shown in Figure 3:3. The version given in Figure A1:8 takes account of wall heat losses and intra-particle temperature distribution. The wall heat loss term in the air temperature derivative equation was not included when Akers[2] results were re-calculated and the solids equations were simplified as set out in Section 3.4.4 for the case of no intra-particle temperature distribution.

It can be seen that the sphere centre temperature derivative equation (3:38) is not included in the program listing. The nodal temperature equations generally involve θ_{n+1}, θ_n and θ_{n-1} as given by equation (3:34):

$$\frac{d\theta_n}{dz} = \frac{\theta_{n+1}.(1+\frac{1}{n}) - 2.\theta_n + \theta_{n-1}.(1-\frac{1}{n})}{(\Delta x)^2}$$

However, for n = 1, this simplifies to:

$$\frac{d\theta_1}{dz} = \frac{2.\theta_2 - 2.\theta_1}{(\Delta x)^2}$$

Also the expression for θ_{sm} does not include θ_o:

$$\theta_{sm} = \frac{57.\theta_5}{288} + \frac{\theta_4}{2} + \frac{3.\theta_3}{16} + \frac{\theta_2}{12} + \frac{\theta_1}{32} \quad \ldots\ldots\ldots\ldots \quad (3:42)$$

Thus θ_o is not essential to the solution so the computation time may be reduced by eliminating equation (3:38).

After the procedure calls, the absolute values of the dimensionless temperatures are tested to determine whether they have exceeded 2.0. This situation would arise if the integration step length were too large and the solution became wildly unstable. Δz is decreased at label TWELVE. However, the test will not detect small errors. The figure 2.0 could not be reduced safely to, say, just greater than 1.0 as the test might then interact with the control of the Biot number. It can be seen from the program listing that the calculation is first run with the input value of Bi (from the logarithmic mean temperature difference solution) until z_L is reached. As θ_f has not reached 1.0, Bi is increased by $\Delta Bi = Bi_{LMTD} \times 0.1$, initial conditions are re-established and the calculation is run again. This process is repeated until θ_f reaches 1.0 before z reaches z_L. At z_L, θ_f is somewhat greater than 1.0. Bi is decreased to (Bi - 0.9 x ΔBi) and ΔBi to ΔBi x 0.1. Iteration continues until the value of Bi is such that $\theta_f = 1.0$ and $z = z_L$ are achieved simultaneously. However, if the absolute value test is made too stringent, it is conceivable that the value of θ_f at z_L will cause Δz to be decreased whereas Bi should be. Instability was not detected with any of the present results.

Nomenclature

The identifiers used in the programs do not always coincide with the nomenclature used elsewhere in the thesis due to the requirements of the I.C.L. 1905 compiler. The following will assist in the interpretation of the program listings:

TSM = θ_{sm}, TSO = θ_o, TSI = θ_1, etc.

TG = θ_f, TGO = θ_{fo}

TA = θ_a

DTSO = $\frac{d\theta_o}{dz}$, DTSI = $\frac{d\theta_1}{dz}$ etc.

DTG = $\frac{d\theta_f}{dz}$

BIOT = Bi, DELBI = ΔBi

BETA = β

Z = z, ZL = z_L, DZ = Δz

HG = h_f, HGA = $h_f.a$

POTB = $\frac{4.U_w.(\Delta x)^2.L}{d_v.G_f.c_f.z_L}$

KSMEAN = k_{sm}, between T_{si} and T_{so}

KGMEAN = k_{fm}, between T_{fo} and T_{fi}

NU = Nu

DP = d_p

EM = e, moving bed voidage

APPENDIX 2

AMPLIFICATION OF THE EXPERIMENTAL WORK

APPENDIX 2 - AMPLIFICATION OF THE EXPERIMENTAL WORK

A2.1 The Equipment

1 Pipework, columns and hoppers

Except for the two moving bed columns, all items of glassware were standard Q.V.F. borosilicate sections.

Q.V.F. Ltd.,
Duke Street,
Fenton,
Stoke-on-Trent,
Staffordshire.

2 Spherical solids

The 6, 9 and 12-mm nominal diameter soda glass test ballotini and $\frac{1}{4}$-mm nominal diameter lead glass support ballotini, all of West German manufacture, were supplied by:

English Glass Co. Ltd.,
Scudamore Road,
Leicester.

Regalox high alumina ceramic spheres were manufactured by:

Royal Worcester Industrial Ceramics Ltd.,
Tonyrefail,
Glamorgan.

and supplied by:

P.E. Hines & Sons Ltd.,
York House,
Wharf Street,
Stoke-on-Trent,
Staffordshire.

3 Air heaters

Type 32441, 1 kW fire bars were manufactured by:

Heating Elements Ltd.,
Wigston Magna,
Leicester.

Plysu silicone rubber sheet for gaskets was manufactured by:

Woodville Rubber Co. Ltd.,
Alton Lane,
Ross-on-Wye.

4 Temperature measurement

Chromel and alumel 28 s.w.g. (0.0148 in diameter) thermocouple wire was manufactured by:

British Driver-Harris Co. Ltd.,
Cheadle Heath,
Stockport,
Cheshire.

Thermocouple junctions were welded with a Model 125 SRL Dynatech argon arc welder supplied by:

S.T.P.,
Sittingbourne,
Kent.

Thermocouple e.m.f.s were recorded with a Kent Mk.3, 16-point, potentiometric recorder manufactured by:

George Kent Ltd.,
Luton,
Bedfordshire.

P.T.F.E. sleeving of 0.020 in I.D., 0.032 in O.D. was manufactured by:

Polypenco Ltd.,
Gate House,
Welwyn Garden City,
Herts.

5 Air flowrate measurement

Metric series Rotameters M10K, M35A, M65A and M65K were manufactured by:

Rotameter Mfg. Co. Ltd.,
330, Purley Way,
Croydon,
Surrey,
CR9 4PG

A2.2 Selection of Length of Moving Bed

It was pointed out in Section 4.1.2 that, if the heat transfer effectiveness of a moving bed is too great, then one or other of the terminal temperature differences tends to zero. The

effectiveness is dependent upon the number of transfer units (N.T.U.). Kays and London[107] suggested that N.T.U. was less than 5 for most industrial heat exchangers. The relationship between the bed length for 5 transfer units and the air and solids flowrates was investigated to determine the optimum length of the column for the present work.

$$N.T.U. = \frac{h_f . A_x . L . a}{(M.c)_{min}} \quad \ldots\ldots\ldots\ldots\ldots\ldots \quad (A2:1)$$

For simplicity, it was assumed that there was a linear relationship between h_f and G_f. Inspection of Akers'[2] results suggested that the following co-ordinates would suffice:

$h_f = 0$ Btu/hft^{2}degF at $G_f = 0$ lb/hft^2

$h_f = 45$ Btu/hft^{2}degF at $G_f = 3000$ lb/hft^2

i.e. $h_f = \frac{45}{3000} . G_f \quad \ldots\ldots\ldots\ldots\ldots\ldots \quad (A2:2)$

Assume $(M.c)_{min} = M_s . c_s$

Substituting in (A2:1) and rearranging:

$$L = \frac{1000}{18} . \frac{d_p . G_s . c_s}{(1-e) . G_f} \quad \ldots\ldots\ldots\ldots\ldots\ldots \quad (A2:3)$$

Taking $e = 0.4$ and $c_s = 0.18$ Btu/lbdegF this becomes:

$$L = 3.94 \frac{G_s}{G_f} \text{ in, for } d_p = 6 \text{ mm}$$

$$L = 5.91 \frac{G_s}{G_f} \text{ in, for } d_p = 9 \text{ mm}$$

$$L = 7.88 \frac{G_s}{G_f} \text{ in, for } d_p = 12 \text{ mm}$$

If $(M.c)_{min} = M_f . c_f$, (A2:3) is replaced by:

$$L = \frac{1000}{18} . \frac{d_p . c_f}{(1-e)} \quad \ldots\ldots\ldots\ldots\ldots\ldots \quad (A2:4)$$

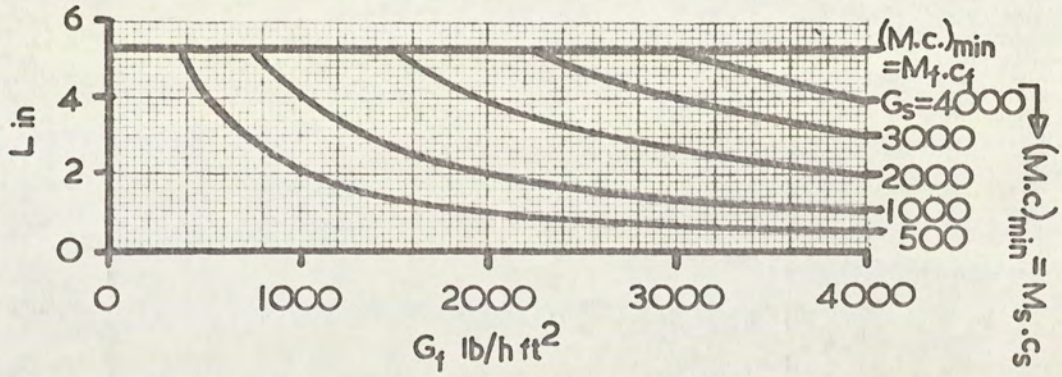

FIGURE A2:1 BED LENGTH FOR N.T.U.=5:6mm BALLOTINI

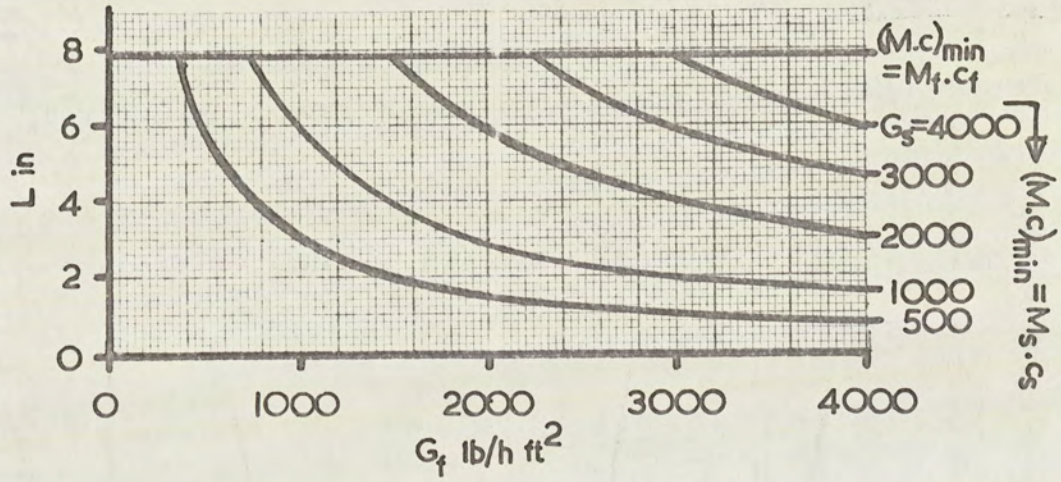

FIGURE A2:2 BED LENGTH FOR N.T.U.=5: 9mm BALLOTINI

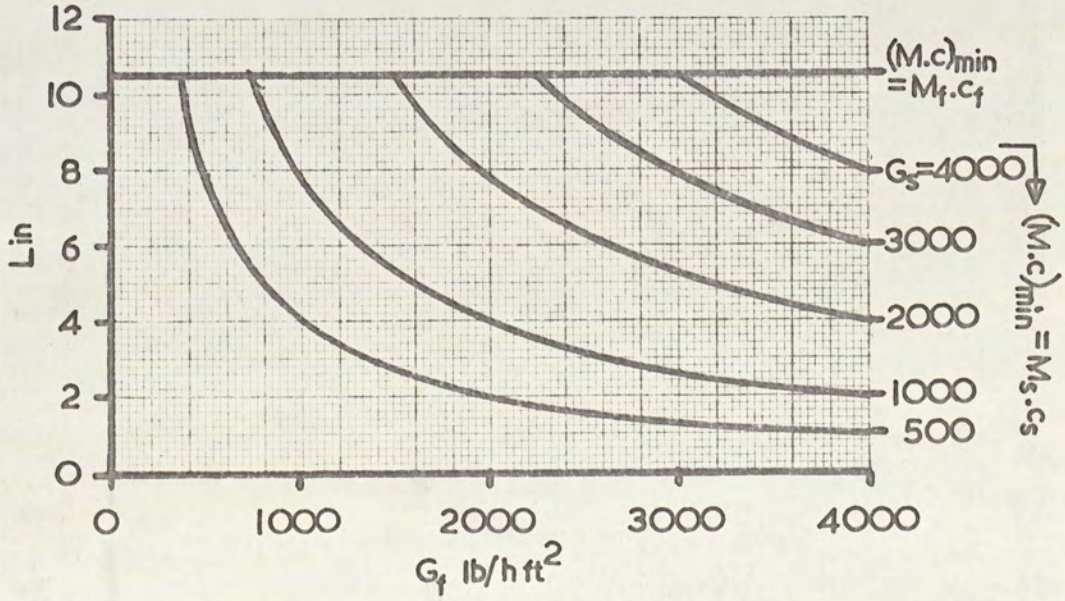

FIGURE A2:3 BED LENGTH FOR N.T.U.=5:12mm BALLOTINI

Taking e = 0.4 and c_f = 0.24 Btu/lbdegF this becomes:

$L = 5.25$ in, for $d_p = 6$ mm

$L = 7.87$ in, for $d_p = 9$ mm

$L = 10.5$ in, for $d_p = 12$ mm

If $M_s \cdot c_s = M_f \cdot c_f$

then $G_f = 0.75 \cdot G_s$ . . . . . (A2:5)

The solution of equations (A2:3) and (A2:4) is shown in Figures (A2:1), (A2:2) and (A2:3). It can be seen that the bed must be short for a wide range of operation.

A2.3 Rotameter Calibrations

The manufacturers publish calibration charts[108] for air at 15°C and 76 cmHg Abs. If changes in viscosity and flow pattern are neglected, the flowrate F at a given scale reading but different conditions of temperature T and pressure P may be obtained from:

$$F_2 = F_1 \sqrt{\frac{P_1 \cdot T_2}{P_2 \cdot T_1}} \quad \text{. . . . . (A2:6)}$$

where subscript 1 refers to chart calibration conditions, i.e. 76 cmHg Abs, 288°K, subscript 2 refers to operating conditions.

The general calibration handbook[109] takes account of both viscosity and flow pattern. It contains charts of the dynamic characteristics of each size of Rotameter:

I^1 v. Scale Reading

for values of a parameter f^1 from 0.1 to 1.0

where $I^1 = \log_{10}\left(\frac{K_1 \cdot 10^4 \cdot \mu_f}{\rho_f} \sqrt{\frac{\rho_s \cdot \rho_f}{w_s \cdot (\rho_s - \rho_f)}}\right)$ . . . . . (A2:7)

ρ_s = float density,

w_s = float weight,

K_1 = constant for a particular Rotameter size, physical properties of the fluid are evaluated at the operating conditions.

Having calculated I, the relationship between f^1 and scale reading may be read off the chart and the flowrate F at the working conditions determined from:

$$F = f^1 \cdot F_T \quad \ldots\ldots\ldots\ldots\ldots\ldots \quad (A2:8)$$

where $$F_T = K_2 \cdot \sqrt{\frac{w_s \cdot (\rho_s - \rho_f)}{\rho_s \cdot \rho_f}} \quad \ldots\ldots\ldots\ldots \quad (A2:9)$$

K_2 = constant for a particular Rotameter size.

A2.4 MOVING BED VOIDAGE MEASUREMENTS

TABLE A2:1 FIXED BED DATA

Table A2:1.1 6 mm Ballotini: Voidage = 0.342

G_f lb/hft^2	ΔP cmH_2O	$\frac{Re}{6(1-e)}$	f
1 379.13	92.00	156.12	0.328
1 311.47	84.20	148.46	0.331
1 242.18	76.85	140.62	0.335
1 177.16	69.55	133.26	0.337
1 104.05	60.65	124.98	0.332
947.32	46.10	107.24	0.341
798.79	34.15	90.42	0.353
658.96	24.75	74.59	0.374
521.84	16.85	59.07	0.404
399.53	10.25	45.23	0.419
279.76	5.75	31.67	0.479
166.62	2.50	18.86	0.582

Table A2:1.2 9 mm Ballotini: Voidage = 0.374

G_f lb/hft^2	ΔP cmH_2O	$\frac{Re}{6(1-e)}$	f
1 728.34	68.55	307.34	0.324
1 576.88	57.50	280.41	0.325
1 433.12	48.25	254.84	0.329
1 177.72	33.05	209.43	0.331
796.45	16.30	141.63	0.353
460.08	6.20	81.81	0.402
167.23	1.00	29.74	0.479

Table A2:1.3 12 mm Ballotini: Voidage = 0.388

G_f lb/hft^2	ΔP cmH_2O	$\frac{Re}{6(1-e)}$	f
165.89	0.55	40.34	0.396
456.02	3.50	110.88	0.348
787.99	10.40	191.60	0.312
1 163.63	19.35	282.94	0.296
1 413.85	28.05	343.79	0.292
1 554.66	33.60	378.03	0.290
1 700.82	40.40	413.57	0.293
1 860.14	47.00	452.31	0.285
2 022.92	55.20	491.89	0.285
2 198.97	63.80	534.70	0.280
2 386.39	74.20	580.27	0.277

TABLE A2:2 MOVED BED DATA

Table A2:2.1 6 mm Ballotini

Bed movement in	G_f lb/hft^2	ΔP cmH_2O	e
1	1 306.47	78.15	0.3499
	1 237.06	71.30	0.3490
	1 172.92	65.05	0.3475
	1 100.96	56.65	0.3487
	944.91	43.50	0.3474
	796.24	31.80	0.3498
	657.65	23.15	0.3487
	520.47	15.90	0.3457
	398.86	9.80	0.3476
	279.28	5.35	0.3484
2	1 304.16	74.85	0.3543
	1 235.88	68.50	0.3533
	1 171.46	62.15	0.3523
	1 099.58	54.60	0.3526
	943.43	41.65	0.3514
	795.94	31.20	0.3514
	657.00	22.45	0.3519
	519.95	15.25	0.3499
	398.46	9.45	0.3512
	279.00	5.20	0.3513
3	1 302.67	72.35	0.3575
	1 234.44	66.25	0.3567
	1 170.07	60.05	0.3557
9	1 300.37	64.65	0.3682
	1 231.89	59.05	0.3681
	1 167.95	53.75	0.3669
18	1 298.22	61.40	0.3730
	1 229.81	55.70	0.3739
	1 165.95	50.80	0.3726

Table A2:2.2 9 mm Ballotini

Bed movement in	G_f lb/hft^2	ΔP cmH_2O	e
18	456.11	4.55	0.4073
	788.41	11.80	0.4087
	1 136.64	24.40	0.4022
	1 417.44	36.35	0.4051
	1 558.11	42.90	0.4067

Table A2:2.3 12 mm Ballotini

Bed movement in	G_f lb/hft^2	ΔP cmH_2O	e
13	457.83	2.70	0.4147
	790.11	7.35	0.4133
	1 164.52	15.25	0.4124
	1 279.52	18.80	0.4093
	1 414.06	22.55	0.4106
	1 552.97	26.70	0.4121
	1 698.75	31.55	0.4125
	1 855.26	37.00	0.4130
	2 014.94	43.20	0.4124
	2 188.10	49.60	0.4134
	2 374.54	57.50	0.4142

Note

Many measurements of the moved bed voidage of 9 and 12 mm ballotini were made as explained in Section 4.4.4 but Tables A2:2.2 and A2:2.3 are typical examples.

TABLE A2:3 SUMMARY OF VOIDAGES

d_p mm	e Fixed	e Moved
6	0.342	0.375
9	0.374	0.406
12	0.388	0.412

A2.5 WALL HEAT LOSS DATA

TABLE A2:4 UNLAGGED LONG COLUMN

Bed	Nominal T_{fi} °C	G_f $\frac{lb}{hft^2}$	G_f/e $\frac{lb}{hft^2}$	ΔT_{lmw} mV	U_w $\frac{Btu}{hft^2 degF}$
Empty	140	1 949		4.44	2.53
		1 465		4.54	2.32
		1 944		4.62	2.42
		1 493		4.55	2.16
		1 085		4.53	1.92
		791		4.50	1.61
		531		4.34	1.48
		283		4.10	1.18
		791		4.41	1.75
		553		4.40	1.49
		370		4.29	1.34
		166		3.72	1.02
		325		4.07	1.35
		243		4.03	1.22
		170		3.71	1.04
		106		3.39	0.98
	100	1 927		3.03	2.25
		1 534		2.98	2.06
		1 148		2.93	1.89
		785		3.15	1.67
		533		2.69	1.45
		288		2.57	1.23
		305		2.55	1.29
		166		2.37	1.01
		167		2.37	1.00
		137		2.21	0.95
		104		2.13	0.93
	60	103		1.07	0.75
		169		1.18	0.95
		245		1.23	1.10

TABLE A2:4 UNLAGGED LONG COLUMN (CONTD.)

Bed	Nominal T_{fi} °C	G_f $\frac{lb}{hft^2}$	G_f/e $\frac{lb}{hft^2}$	ΔT_{lmw} mV	U_w $\frac{Btu}{hft^2 degF}$
		327		1.30	1.27
		337		1.31	1.30
		517		1.35	1.40
		725		1.36	1.57
		925		1.40	1.63
		1 247		1.41	1.76
		1 233		1.41	1.75
		1 525		1.47	1.83
6 mm	140	1 188	3 434	4.24	3.00
		1 023	2 958	4.23	3.02
		855	2 470	4.17	3.01
		682	1 972	4.11	2.72
	100	1 239	3 581	2.72	3.26
		1 007	2 910	2.77	3.25
		799	2 310	2.67	2.82
		603	1 742	2.53	3.06
		427	1 233	2.60	1.91
		259	749	2.45	1.52
		196	568	2.41	1.39
		121	350	2.25	1.14
	60	1 491	4 309	1.57	2.57
		1 186	3 428	1.56	2.23
		937	2 708	1.55	2.56
		685	1 980	1.46	2.59
		464	1 341	1.43	2.06
		261	754	1.33	1.50
		122	352	1.07	1.36
9 mm	Various	973	2 602	1.45	2.06
		281	752	2.53	1.63
		523	1 398	2.76	1.87
		796	2 128	2.81	2.39
		982	2 626	2.80	2.31
		727	1 944	3.43	2.35

TABLE A2:4 UNLAGGED LONG COLUMN (CONTD.)

Bed	Nominal T_{fi} °C	G_f $\frac{lb}{hft^2}$	G_f/e $\frac{lb}{hft^2}$	ΔT_{lmw} mV	U_w $\frac{Btu}{hft^2 degF}$
12 mm	Various	1 177	3 146	3.68	2.45
		727	1 943	3.42	2.30
		798	2 134	4.16	2.37
		1 174	3 139	4.39	2.52
		1 461	3 906	4.43	2.21
		967	2 492	1.47	2.09
		280	722	2.55	1.70
		520	1 341	2.75	2.13
		794	2 046	2.84	2.40
		973	2 508	2.89	2.33
		1 158	2 986	3.64	2.47
		792	2 042	4.14	2.64
		1 161	2 993	4.30	2.64
		1 442	3 716	4.52	2.21
		1 746	4 499	4.65	2.21

TABLE A2:5 LONG COLUMN WITH ONE LAYER OF 1 in ASBESTOS ROPE LAGGING

Bed	Nominal T_{fi} °C	G_f $\frac{lb}{hft^2}$	G_f/e $\frac{lb}{hft^2}$	ΔT_{lmw} mV	U_w $\frac{Btu}{hft^2 degF}$
Empty	140	1 898		4.76	1.17
		1 475		4.63	1.01
		1 071		4.52	1.03
		734		4.42	0.90
		428		4.13	0.76
	100	102		2.36	0.74
		171		2.56	0.90
		241		2.61	0.97
		323		2.65	1.03
		328		2.67	1.01
		513		2.78	1.17
		723		2.84	1.23
		939		2.89	1.26
		1 171		2.84	1.26
		1 150		2.82	1.20
		1 550		2.83	1.29
	60	1 918		1.51	1.64
		1 469		1.40	1.35
		1 080		1.37	1.07
		734		1.42	1.25
		420		1.43	0.81
		431		1.45	1.01
		280		1.35	0.73
		166		1.26	0.62
		164		1.25	0.63
		106		1.19	0.61
6 mm	140	1 319	3 813	4.69	1.36
		1 110	3 208	4.60	1.39
		924	2 671	4.56	1.36
		781	2 259	4.51	1.45
		611	1 767	4.47	1.35

TABLE A2:5 LONG COLUMN WITH ONE LAYER OF 1 in ASBESTOS ROPE LAGGING (CONTD.)

Bed	Nominal T_{fi} °C	G_f $\frac{lb}{hft^2}$	G_f/e $\frac{lb}{hft^2}$	ΔT_{lmw} mV	U_w $\frac{Btu}{hft^2 degF}$
	100	1 411	4 077	3.08	1.94
		1 114	3 220	3.11	1.64
		851	2 460	3.14	1.46
		604	1 747	2.92	1.19
		398	1 151	2.83	1.13
		196	567	2.57	1.18
	60	1 507	4 357	1.65	1.39
		1 198	3 462	1.59	1.33
		929	2 346	1.56	1.33
		686	1 983	1.54	1.31
		465	1 343	1.52	1.08

TABLE A2:6 LONG COLUMN WITH TWO LAYERS OF 1 in ASBESTOS ROPE LAGGING

Bed	Nominal T_{fi} °C	G_f lb/hft^2	G_f/e lb/hft^2	ΔT_{lmw} mV	U_w Btu/hft^2/degF
6 mm	140	1 122	3 490	4.89	0.92
		958	2 980	4.88	0.88
		804	2 500	4.84	0.78
		661	2 050	4.78	0.81
		518	1 610	4.74	0.76
	100	1 159	3 600	3.19	0.64
		167	519	2.67	0.83
		400	1 243	2.89	1.06
		660	2 050	2.98	0.96
		913	2 840	3.00	0.82
	60	167	519	1.39	0.72
		399	1 240	1.50	0.78
		658	2 045	1.55	0.80
		911	2 830	1.57	0.75
		1 268	3 940	1.63	0.73
	120	660	2 050	3.87	0.90

TABLE A2:7 UNLAGGED SHORT COLUMN

Bed	Nominal T_{fi} °C	G_f lb/hft^2	G_f/e lb/hft^2	ΔT_{lmw} mV	U_w Btu/hft^2/degF
6 mm	Various	427	1 248	1.50	1.91
		900	2 630	1.56	1.85
		1 313	3 840	1.50	2.80
		257	752	2.94	1.71
		732	2 140	3.12	2.41
		1 179	3 447	3.10	4.65
		116	338	3.15	1.64
		579	1 691	4.42	3.12
		1 113	3 255	4.75	1.13

APPENDIX 3

MOVING BED HEAT TRANSFER CALCULATIONS

APPENDIX 3 - MOVING BED HEAT TRANSFER CALCULATIONS

A3.1 The Program ZMOVBEDHTC

The ALGOL program listed in Figure A3:1 is the version in which both the air and solids outlet temperatures are assumed to be reliable. It can be seen that it is comprised of seven sections with looping within each so that all runs are processed to the same extent before passing on to the next section. The input data and results of the calculations are stored by means of subscripted variables e.g. HG[J].

To reduce the labour of punching d_p, e and ρ_s onto data cards, only the nominal particle diameter is input. The appropriate values of the three parameters are selected from the arrays DPP, EMM and RHOSS.

The air flowrate through the bed is corrected for the leakage through the ballotini discharge orifice using the data shown in Figure 4:32.

After calculation of the wall heat loss transfer coefficient in the heat balance section, the air outlet temperature measured above the bed, T^1_{fo}, is corrected for wall losses to obtain the value as the air emerges from the ballotini, T_{fo}.

Two other versions of the program were also used: one in which T_{fo} was calculated in the heat balance section from the measured value of T_{so} and another in which T_{so} was calculated from the value of T_{fo} obtained by correction of the measured T^1_{fo}. In the former case, the mean air specific heat was unknown because the temperature T_{fo} was unknown so an iterative loop was included to find the temperature and specific heat which satisfied the heat balance. The other version involved similar iteration to find T_{so}.

Nomenclature

The identifiers which conflict with the nomenclature used elsewhere in the thesis are:

TA = T_a, TSI = T_{si}, TGODASH = T^1_{fo}, TGO = T_{fo}, TSO = T_{so}, TGI = T_{fi}

DA = θ_a, DGO = θ_{fo}, DSO = θ_{so}

KGMEAN = k_{fm}, MUGMEAN = μ_{fm}, RHOGMEAN = ρ_{fm}, CPMEAN = c_{fm}

KSMEAN = k_{sm}, RHOS = ρ_s, CSMEAN = c_{sm}

QW = Q_w, QS = Q_s, QG = Q_f

UW = U_w

HGGW = h_f based on $(Q_f - Q_w)$

HGS = h_f based on Q_s

HG = h_f mean

RECARMAN = $\frac{Re}{6(1-e)}$, RERELCAR = $\frac{Re}{6(1-e)}$ based on relative velocity.

REAKERS = $\frac{Re}{(1-e)}$, REP = Re

UGSPACE = air space velocity

USSPACE = solids space velocity

POTA = air temperature potentiometer setting

POTB = wall heat loss potentiometer setting

INLETP = air pressure at bed inlet

PA = atmospheric pressure

P4 = mean air pressure in bed

BEDHT = L

EM = e, moving bed voidage

DP = d_p

GG = G_f

DLGG = air leakage rate expressed per unit cross section area of moving bed.

A3.2 Moving Bed Heat Transfer Data

Notes

(1) Runs which were rejected because one or other of the terminal temperature differences was too small:

11, 12, 19, 20, 21, 22, 23, 25.

(2) Runs which were rejected because the value of T_{so} calculated from the measured T_{fo} using the heat balance was greater than T_{fi}:

21, 25, 31.

(3) Explanation of Tables A3:7, 8 and 9:

Column 1. h_f, Bi and Nu based on the mean of the heat transfer rates calculated from the measured air temperature (after correction for the heat lost through the walls between the measuring point and the top of the bed) and the measured solids temperature. Logarithmic mean temperature difference solution. Plotted in Figures 5:1 and 2.

Column 2. Based on T_{fo} calculated from the heat balance and T_{so} measured. L.M.T.D. solution. Plotted in Figure 5:4.

Column 3. Based on measured T^1_{fo} corrected to the top of the bed and T_{so} calculated from the heat balance. L.M.T.D. solution. Plotted in Figure 5:3.

Column 4. Based on measured T^1_{fo} corrected to the top of the bed. Numerical integration solution, no intra-particle temperature distribution. Plotted in Figure 5:5.

Column 5. Based on measured T^1_{fo} corrected to the top of the bed. N.I. solution, I.P.T.D. Plotted in Figures 5:6, 7 and 9.

TABLE A3:1 MEASURED TEMPERATURES

Table A3:1.1 6 mm Ballotini

Run	T_a °C	T_{si} °C	T^1_{fo} °C	T_{so} °C	T_{fi} °C
11	24.4	24.4	90.2	142.0	143.4
12	24.1	26.8	31.5	79.3	144.1
13	23.4	24.4	39.0	111.0	141.5
14	22.9	23.9	49.3	128.5	144.6
15	19.5	21.5	47.1	123.4	139.3
17	22.9	22.9	57.6	131.5	135.1
18	22.9	23.2	53.2	120.7	140.0
19	24.1	22.9	70.0	138.3	139.8
20	20.5	21.2	79.0	139.8	140.2
21	21.7	21.5	47.6	105.6	106.8
22	23.9	22.9	104.9	140.5	141.0
23	22.4	22.7	31.5	93.2	106.8
24	21.5	24.6	36.6	113.9	137.1
25	22.0	21.7	32.0	97.6	105.9
53	22.2	23.2	47.8	107.8	138.5
54	22.4	22.0	35.4	112.7	141.7

Table A3:1.2 9 mm Ballotini

Run	T_a °C	T_{si} °C	T^1_{fo} °C	T_{so} °C	T_{fi} °C
27	22.2	22.4	43.9	73.2	142.4
28	21.7	22.4	37.6	92.2	106.6
29	20.0	22.0	56.1	100.2	138.3
30	20.5	24.9	42.2	74.4	141.5
31	20.2	21.2	46.3	101.2	105.6
33	20.5	20.5	68.8	132.4	138.3
34	21.5	21.2	58.0	132.2	140.5
43	16.8	18.3	47.3	115.4	142.0
44	16.6	17.8	44.4	103.2	107.8
45	18.0	17.3	31.5	89.3	105.6
50	21.7	22.0	57.6	118.3	139.8
51	20.7	21.7	57.6	114.9	139.5
58	21.7	22.2	57.8	116.8	138.5
59	21.2	22.0	49.5	105.9	134.4

Table A3:1.3 12 mm Ballotini

Run	T_a °C	T_{si} °C	T^1_{fo} °C	T_{so} °C	T_{fi} °C
35	21.5	22.7	53.4	86.3	137.1
36	23.9	26.3	70.7	111.0	136.6
37	24.4	25.4	64.4	105.6	137.1
38	22.4	22.0	68.3	122.0	137.3
39	22.9	22.0	74.4	125.6	136.6
40	22.4	22.2	57.1	105.1	112.7
41	20.2	24.9	61.2	92.7	134.4
42	21.5	21.5	40.0	88.5	111.5
46	22.7	22.0	51.7	84.1	139.5
47	22.9	23.7	60.5	90.5	133.9
48	21.7	22.4	48.0	96.3	108.5
49	19.8	22.0	50.5	72.2	135.6
52	23.9	23.9	53.4	71.5	137.1
55	20.7	22.0	50.5	84.6	138.0
56	21.7	21.5	73.2	131.2	141.0
57	22.7	21.5	55.9	100.5	136.3
60	21.2	23.4	69.5	114.1	139.5
61	22.2	22.0	64.9	109.5	139.5

TABLE A3:2 OTHER MEASURED DATA

Table A3:2.1 6 mm Ballotini

Run	G_s lb/hft^2	G_f lb/hft^2	Bed height in	Bed inlet pressure cmH_2O
11	641.26	1 232.69	4.4	17.60
12	1 494.28	970.02	4.1	15.30
13	1 088.65	972.56	4.1	15.30
14	972.33	1 066.09	4.2	17.10
15	1 046.89	1 118.20	4.4	17.50
17	492.13	635.61	3.8	8.40
18	1 046.89	1 253.27	4.4	16.30
19	548.80	840.53	3.8	12.80
20	551.78	1 024.59	4.4	16.50
21	178.66	288.97	3.7	2.05
22	254.42	735.80	4.2	10.80
23	168.52	160.54	3.5	1.30
24	653.19	619.19	4.1	14.40
25	189.40	196.92	4.0	1.80
53	1 228.83	1 209.62	4.4	22.40
54	1 249.71	1 029.29	4.5	21.50

Table A3:2.2 9 mm Ballotini

Run	G_s lb/hft^2	G_f lb/hft^2	Bed height in	Bed inlet pressure cmH_2O
27	2 568.02	1 332.01	3.0	44.50
28	184.62	193.73	3.9	1.25
29	1 989.40	1 622.42	3.6	33.50
30	3 236.12	1 768.81	4.1	39.00
31	174.78	258.90	3.6	1.15
33	468.57	691.47	4.2	8.20
34	454.25	585.44	3.7	5.80
43	1 000.07	958.99	4.3	14.70
44	170.31	233.18	4.2	1.00
45	170.31	161.54	4.1	0.55
50	1 139.35	1 214.54	4.2	22.20
51	1 303.40	1 339.20	4.2	26.10
58	1 366.03	1 475.88	4.3	30.50
59	1 124.44	1 094.53	4.2	18.00

Table A3:2.3 12 mm Ballotini

Run	G_s lb/hft^2	G_f lb/hft^2	Bed height in	Bed inlet pressure cmH_2O
35	2 854.35	2 001.94	3.6	25.00
36	960.40	1 098.39	3.4	15.30
37	963.38	947.62	3.5	11.40
38	418.46	584.93	3.6	4.50
39	472.74	695.69	3.5	6.50
40	175.38	295.97	3.6	1.00
41	1 876.06	1 552.74	3.3	28.00
42	170.01	159.87	3.5	0.45
46	2 916.98	1 915.10	3.7	23.00
47	2 052.03	1 688.08	3.3	32.00
48	175.38	210.00	3.6	0.70
49	4 787.08	2 158.89	3.6	27.00
52	4 966.03	2 226.64	3.7	29.00
55	2 773.82	1 834.70	3.7	22.00
56	468.27	751.73	3.7	7.70
57	948.47	857.51	3.6	9.80
60	1 034.96	1 254.67	3.5	19.00
61	1 240.76	1 410.62	3.5	23.50

TABLE A3:3 HEAT BALANCE

Table A3:3.1 6 mm Ballotini

Run	Q_w Btu/h	Q_s Btu/h	Q_f Btu/h	Deficiency %
11	257.4	5 767	5 433	-10.88
12	94.2	5 683	9 506	39.22
13	120.7	7 025	8 627	17.17
14	158.8	7 694	8 761	10.37
15	170.0	8 018	8 879	7.78
17	131.6	4 406	4 165	- 0.30
18	180.1	7 668	9 365	16.20
19	164.9	4 822	4 922	- 1.33
20	231.2	4 980	5 231	0.38
21	75.8	1 112	1 409	15.75
22	232.0	2 282	1 996	-25.99
23	39.9	869	1 028	11.51
24	102.8	4 358	5 360	16.78
25	49.7	1 055	1 239	10.84
53	165.6	7 719	9 457	16.62
54	126.6	8 442	9 489	9.70

Table A3:3.2 9 mm Ballotini

Run	Q_w Btu/h	Q_s Btu/h	Q_f Btu/h	Deficiency %
27	108.6	9 347	11 281	16.18
28	56.6	941	1 121	10.94
29	168.7	11 466	11 437	- 1.73
30	162.2	11 540	15 192	22.97
31	70.2	1 030	1 256	12.46
33	173.7	3 967	4 012	- 3.21
34	129.8	3 814	4 071	3.11
43	166.1	7 219	7 791	5.21
44	85.0	1 069	1 211	4.76
45	54.1	888	1 009	6.61
50	179.6	8 213	8 549	1.82
51	187.8	9 057	9 404	1.69
58	194.1	9 663	10 223	3.58
59	153.2	6 981	7 979	10.58

Table A3:3.3 12 mm Ballotini

Run	Q_w Btu/h	Q_s Btu/h	Q_f Btu/h	Deficiency %
35	167.3	13 211	14 441	7.35
36	154.1	6 069	6 087	-2.24
37	141.4	5 739	5 829	-0.89
38	136.1	3 141	3 345	2.02
39	145.8	3 690	3 562	-7.68
40	82.3	1 076	1 153	-0.45
41	157.2	9 327	9 686	2.09
42	53.4	830	945	6.50
46	164.1	13 152	14 521	8.30
47	152.4	10 021	10 598	4.00
48	67.0	951	1 030	1.17
49	168.6	17 229	15 862	-9.68
52	169.3	16 942	16 092	-6.34
55	164.1	12 611	13 862	7.84
56	162.2	3 886	4 236	4.42
57	130.7	5 516	5 877	3.91
60	172.3	7 011	7 425	3.26
61	167.8	8 066	8 967	8.18

TABLE A3:4 AIR OUTLET TEMPERATURES

Table A3:4.1 6 mm Ballotini

Run	Measured at air mixer T^1_{fo} °C	Corrected to top of bed T_{fo} °C	Top of bed calculated from measured T_{so} T_{fo} °C
11	90.2	93.0	87.5
12	31.5	31.8	76.0
13	39.0	39.8	57.3
14	49.3	50.5	60.3
15	47.1	48.3	55.4
17	57.6	60.1	59.9
18	53.2	54.4	68.3
19	70.0	72.8	71.9
20	79.0	81.9	82.1
21	47.6	50.9	59.7
22	104.9	110.0	101.9
23	31.5	33.3	41.7
24	36.6	37.6	54.4
25	32.0	33.5	41.4
53	47.8	48.9	63.8
54	35.4	36.0	46.3

Table A3:4.2 9 mm Ballotini

Run	Measured at air mixer T^{1}_{fo} °C	Corrected to top of bed T_{fo} °C	Top of bed calculated from measured T_{so} T_{fo} °C
27	43.9	44.9	60.7
28	37.6	40.1	47.4
29	56.1	57.5	56.0
30	42.2	42.9	65.6
31	46.3	49.9	56.9
33	68.8	71.9	69.7
34	58.0	60.8	63.3
43	47.3	48.8	53.7
44	44.4	48.2	51.0
45	31.5	33.9	38.6
50	57.6	59.1	60.6
51	57.6	59.0	60.4
58	57.8	59.1	62.0
59	49.5	50.8	59.7

Table A3:4.3 12 mm Ballotini

Run	Measured at air mixer T^{l}_{fo} °C	Corrected to top of bed T_{fo} °C	Top of bed calculated from measured T_{so} T_{fo} °C
35	53.4	54.4	60.5
36	70.7	73.1	71.7
37	64.4	66.6	66.0
38	68.3	71.8	73.2
39	74.4	78.0	73.5
40	57.1	61.8	61.6
41	61.2	62.9	64.4
42	40.0	43.6	48.1
46	51.7	52.7	59.0
47	60.5	61.9	64.8
48	48.0	52.2	52.9
49	50.5	51.4	43.2
52	53.4	54.3	49.0
55	50.5	51.5	58.3
56	73.2	76.5	79.3
57	55.9	57.8	60.9
60	69.5	71.7	73.9
61	64.9	66.7	72.6

TABLE A3:5 PARAMETERS INPUT TO NUMERICAL INTEGRATION

Table A3:5.1 6 mm Ballotini

Run	θ_a	θ_{fo}	β	z_L	POTB
11	0.0000	0.5768	0.4507	10.7913	0.000097
12	-0.0229	0.0426	1.3189	4.3373	0.000251
13	-0.0083	0.1317	0.9698	5.9295	0.000186
14	-0.0081	0.2204	0.7972	6.7788	0.000159
15	-0.0166	0.2278	0.8112	6.6159	0.000165
17	0.0000	0.3311	0.6715	12.1496	0.000115
18	-0.0021	0.2674	0.7288	6.6003	0.000153
19	0.0104	0.4265	0.5684	10.8788	0.000107
20	-0.0061	0.5094	0.4691	12.5215	0.000094
21	0.0029	0.3444	0.5318	32.6978	0.000071
22	0.0083	0.7376	0.2951	26.0856	0.000055
23	-0.0029	0.1256	0.8905	32.9598	0.000097
24	-0.0282	0.1157	0.9186	9.8733	0.000153
25	0.0029	0.1406	0.8184	33.4825	0.000095
53	-0.0085	0.2229	0.8767	5.6460	0.000183
54	0.0041	0.1170	1.0452	5.6828	0.000204

Table A3:5.2 9 mm Ballotini

Run	θ_a	θ_{fo}	β	z_L	POTB
27	-0.0020	0.1872	1.6078	0.7972	0.000805
28	-0.0087	0.2100	0.8070	14.3333	0.000216
29	-0.0168	0.3052	1.0339	1.2287	0.000552
30	-0.0377	0.1546	1.5331	0.8622	0.000835
31	-0.0116	0.3400	0.5764	13.9327	0.000170
33	0.0000	0.4361	0.5852	6.0350	0.000238
34	0.0020	0.3322	0.6743	5.4733	0.000258
43	-0.0118	0.2469	0.8928	2.9044	0.000400
44	-0.0136	0.3375	0.6186	16.7249	0.000178
45	0.0083	0.1873	0.8821	16.3956	0.000224
50	-0.0021	0.3152	0.8058	2.4870	0.000389
51	-0.0083	0.3168	0.8333	2.1764	0.000416
58	-0.0042	0.3174	0.7954	2.1238	0.000407
59	-0.0065	0.2565	0.8791	2.5239	0.000408

Table A3:5.3 12 mm Ballotini

Run	θ_a	θ_{fo}	β	z_L	POTB
35	-0.0107	0.2776	1.1930	0.4766	0.001220
36	-0.0221	0.4242	0.7466	1.3291	0.000631
37	-0.0087	0.3692	0.8641	1.3660	0.000697
38	0.0042	0.4325	0.6160	3.2198	0.000426
39	0.0085	0.4887	0.5822	2.7755	0.000428
40	0.0027	0.4380	0.5720	7.7265	0.000306
41	-0.0423	0.3469	1.0171	0.6636	0.000964
42	0.0000	0.2464	0.8921	7.7784	0.000407
46	0.0062	0.2612	1.2714	0.4797	0.001282
47	-0.0066	0.3469	1.0215	0.6070	0.000991
48	-0.0085	0.3462	0.7039	7.7429	0.000351
49	-0.0193	0.2593	1.8116	0.2865	0.001925
52	0.0000	0.2684	1.8274	0.2835	0.001952
55	-0.0105	0.2544	1.2624	0.5045	0.001257
56	0.0020	0.4603	0.5413	2.9482	0.000404
57	0.0106	0.3162	0.9356	1.4295	0.000731
60	-0.0189	0.4161	0.7072	1.2678	0.000623
61	0.0021	0.3804	0.7532	1.0581	0.000686

TABLE A3:6 DIMENSIONLESS BALLOTINI OUTLET TEMPERATURES

Table A3:6.1 6 mm Ballotini

Run	Measured θ_{so}	Calculated from corrected value of T_{fo}		
		Heat balance θ_{so}	Numerical integration	
			No I.P.T.D. θ_{so}	I.P.T.D. θ_{smo}
11	0.9877	0.8945	0.8915	0.8914
12	0.4470	0.7187	0.7181	0.7179
13	0.7396	0.8828	0.8794	0.8795
14	0.8667	0.9601	0.9539	0.9539
15	0.8654	0.9337	0.9286	0.9284
17	0.9674	0.9647	0.9563	0.9562
18	0.8351	0.9858	0.9795	0.9784
19	0.9875	0.9753	0.9683	0.9680
20	0.9959	0.9995	0.9900	0.9900
21	0.9857	1.1665	-	-
22	0.9959	0.7857	0.7824	0.7844
23	0.8377	0.9438	0.9284	0.9286
24	0.7939	0.9442	0.9372	0.9368
25	0.9014	1.0079	0.9818	-
53	0.7336	0.8709	0.8673	0.8676
54	0.7576	0.8336	0.8303	0.8309

Table A3:6.2 9 mm Ballotini

Run	Measured θ_{so}	Calculated from corrected value of T_{fo}		
		Heat balance θ_{so}	Numerical integration	
			No I.P.T.D. θ_{so}	I.P.T.D. θ_{smo}
27	0.4228	0.5006	0.5006	0.4998
28	0.8290	0.9295	0.9156	0.9155
29	0.6730	0.6622	0.6614	0.6608
30	0.4247	0.5455	0.5454	0.5447
31	0.9480	1.0811	-	-
33	0.9503	0.9220	0.9155	0.9154
34	0.9305	0.9587	0.9509	0.9516
43	0.7850	0.8256	0.8227	0.8221
44	0.9485	0.9958	0.9739	0.9740
45	0.8149	0.8719	0.8597	0.8594
50	0.8178	0.8320	0.8301	0.8291
51	0.7909	0.8036	0.8020	0.8012
58	0.8134	0.8418	0.8400	0.8391
59	0.7462	0.8295	0.8275	0.8263

Table A3:6.3 12 mm Ballotini

Run	Measured θ_{so}	Calculated from corrected value of T_{fo}		
		Heat balance θ_{so}	Numerical integration	
			No I.P.T.D. θ_{so}	I.P.T.D. θ_{smo}
35	0.5565	0.5985	0.5981	0.5971
36	0.7677	0.7517	0.7501	0.7501
37	0.7183	0.7123	0.7109	0.7104
38	0.8668	0.8838	0.8786	0.8796
39	0.9043	0.8423	0.8395	0.8384
40	0.9164	0.9124	0.9025	0.9036
41	0.6192	0.6317	0.6309	0.6305
42	0.7453	0.7969	0.7892	0.7893
46	0.5290	0.5745	0.5740	0.5734
47	0.6062	0.6302	0.6297	0.6288
48	0.8584	0.8684	0.8591	0.8599
49	0.4421	0.4045	0.4043	0.4032
52	0.4203	0.3961	0.3961	0.3945
55	0.5399	0.5836	0.5834	0.5821
56	0.9184	0.9588	0.9534	0.9533
57	0.6879	0.7146	0.7129	0.7124
60	0.7815	0.8065	0.8047	0.8055
61	0.7448	0.8073	0.8058	0.8055

TABLE A3:7 HEAT TRANSFER COEFFICIENTS

Table A3:7.1 6 mm Ballotini

Run	h_f Btu/hft^{2}degF				
	1	2	3	4	5
11	12.324	13.840	6.163	6.165	6.288
12	13.635	4.232	26.769	26.783	29.259
13	14.825	9.352	24.663	24.592	26.689
14	16.049	12.736	27.802	27.300	29.913
15	15.762	13.269	22.216	22.039	23.705
17	12.730	12.802	12.386	12.066	12.549
18	13.375	9.920	35.867	34.075	38.021
19	15.909	16.236	13.144	12.752	13.278
20	15.734	15.657	22.531	14.987	15.771
21	6.457	4.839	-	-	-
22	4.990	6.092	1.454	1.453	1.467
23	3.810	2.652	6.725	6.475	6.616
24	11.527	6.986	24.030	23.670	25.593
25	4.874	3.462	-	14.061	-
53	11.883	8.559	18.443	18.387	19.548
54	16.608	12.206	21.440	21.374	22.961

Table A3:7.2 9 mm Ballotini

Run	h_f Btu/hft^{2}degF				
	1	2	3	4	5
27	22.339	16.184	26.483	26.498	30.113
28	4.370	3.415	6.890	6.732	6.959
29	23.321	23.998	22.740	22.74	25.469
30	23.568	14.467	30.698	30.714	35.672
31	6.453	5.203	-	-	-
33	12.038	12.589	10.123	10.044	10.550
34	14.204	13.448	17.381	17.031	18.595
43	16.436	14.806	18.667	18.649	20.460
44	5.181	4.760	10.626	7.890	8.310
45	3.713	3.145	4.597	4.544	4.645
50	18.750	18.182	19.632	19.632	21.634
51	19.341	18.808	20.084	20.085	22.194
58	21.702	20.448	23.810	23.810	26.834
59	16.681	13.712	21.363	21.364	23.757

Table A3:7.3 12 mm Ballotini

Run	h_f Btu/hft^{2}degF				
	1	2	3	4	5
35	34.509	30.556	37.799	37.818	48.761
36	18.396	18.924	17.647	17.647	19.888
37	16.543	16.752	16.302	16.303	18.178
38	11.015	10.728	11.755	11.708	12.695
39	13.452	14.726	10.655	10.655	11.412
40	5.639	5.673	5.528	5.473	5.694
41	26.273	25.500	27.009	27.008	32.409
42	3.992	3.512	4.624	4.610	4.753
46	32.544	28.234	35.901	35.902	45.596
47	27.848	26.309	29.346	29.360	35.801
48	4.941	4.849	5.130	5.098	5.282
49	37.799	45.409	34.733	34.749	42.894
52	35.544	39.763	33.656	33.690	41.229
55	32.301	28.150	35.515	35.534	44.999
56	15.055	14.231	19.430	19.236	21.956
57	15.871	14.921	16.927	16.926	18.958
60	20.952	20.089	22.480	22.481	26.303
61	23.928	21.394	28.372	28.371	34.613

TABLE A3:8 BIOT NUMBERS

Table A3:8.1 6 mm Ballotini

Run	Bi				
	1	2	3	4	5
11	0.1979	0.2223	0.0996	0.0996	0.1016
12	0.2269	0.0704	0.4367	0.4369	0.4773
13	0.2423	0.1528	0.3992	0.3980	0.4319
14	0.2597	0.2061	0.4471	0.4391	0.4811
15	0.2562	0.2157	0.3595	0.3566	0.3856
17	0.2058	0.2070	0.2003	0.1951	0.2029
18	0.2175	0.1613	0.5776	0.5487	0.6123
19	0.2562	0.2615	0.2119	0.2055	0.2140
20	0.2535	0.2522	0.3629	0.2414	0.2541
21	0.1061	0.0795	0.1668	-	-
22	0.0803	0.0980	0.0237	0.0237	0.0239
23	0.0630	0.0439	0.1106	0.1065	0.1088
24	0.1880	0.1139	0.3882	0.3824	0.4134
25	0.0805	0.0571	0.2829	0.2308	-
53	0.1947	0.1403	0.2994	0.2985	0.3174
54	0.2716	0.1996	0.3487	0.3477	0.3735

Table A3:8.2 9 mm Ballotini

Run	Bi				
	1	2	3	4	5
27	0.5585	0.4046	0.6580	0.6583	0.7482
28	0.1079	0.0843	0.1692	0.1653	0.1709
29	0.5730	0.5897	0.5592	0.5592	0.6263
30	0.5877	0.3608	0.7584	0.7588	0.8813
31	0.1586	0.1278	0.3658	-	-
33	0.2905	0.3038	0.2448	0.2428	0.2551
34	0.3427	0.3244	0.4185	0.4101	0.4478
43	0.4012	0.3614	0.4543	0.4539	0.4979
44	0.1274	0.1171	0.2607	0.1958	0.2039
45	0.0922	0.0781	0.1138	0.1124	0.1149
50	0.4557	0.4419	0.4767	0.4767	0.5253
51	0.4711	0.4581	0.4888	0.4888	0.5401
58	0.5278	0.4973	0.5780	0.5780	0.6514
59	0.4085	0.3358	0.5202	0.5202	0.5785

Table A3:8.3 12 mm Ballotini

Run	Bi				
	1	2	3	4	5
35	1.1415	1.0108	1.2465	1.2471	1.6080
36	0.5977	0.6149	0.5740	0.5740	0.6469
37	0.5396	0.5464	0.5320	0.5320	0.5932
38	0.3567	0.3474	0.3802	0.3787	0.4106
39	0.4347	0.4758	0.3457	0.3457	0.3702
40	0.1844	0.1855	0.1808	0.1790	0.1862
41	0.8642	0.8388	0.8876	0.8876	1.0651
42	0.1320	0.1161	0.1524	0.1519	0.1567
46	1.0786	0.9358	1.1858	1.1858	1.5060
47	0.9181	0.8674	0.9658	0.9663	1.1783
48	0.1624	0.1594	0.1685	0.1675	0.1736
49	1.2630	1.5172	1.1639	1.1645	1.4374
52	1.1865	1.3273	1.1256	1.1267	1.3789
55	1.0703	0.9327	1.1729	1.1735	1.4861
56	0.4851	0.4586	0.6244	0.6182	0.7058
57	0.5207	0.4896	0.5543	0.5543	0.6208
60	0.6809	0.6528	0.7293	0.7293	0.8533
61	0.7805	0.6978	0.9214	0.9214	1.1241

TABLE A3:9 NUSSELT NUMBERS

Table A3:9.1 6 mm Ballotini

Run	Nu				
	1	2	3	4	5
11	12.557	14.185	6.280	6.281	6.407
12	14.869	4.388	29.191	29.207	31.907
13	16.063	9.930	26.723	26.646	28.917
14	17.114	13.431	29.648	29.112	31.899
15	16.952	14.154	23.893	23.702	25.494
17	13.569	13.649	13.203	12.861	13.376
18	14.272	10.420	38.273	36.360	40.570
19	16.633	16.993	13.743	13.333	13.883
20	16.279	16.195	23.311	15.505	16.321
21	7.187	5.329	-	-	-
22	5.008	6.165	1.459	1.458	1.473
23	4.334	2.984	7.650	7.366	7.526
24	12.584	7.479	26.235	25.841	27.940
25	5.549	3.902	-	16.009	-
53	12.782	9.050	19.838	19.778	21.027
54	18.073	13.123	23.330	22.295	24.986

Table A3:9.2 9 mm Ballotini

Run	Nu				
	1	2	3	4	5
27	35.842	25.500	42.493	42.518	48.318
28	7.353	5.694	11.592	11.326	11.708
29	37.052	38.188	36.128	36.128	40.464
30	37.945	22.695	49.424	49.450	57.433
31	10.740	8.585	-	-	-
33	18.818	19.727	15.824	15.700	16.492
34	22.425	21.172	27.441	26.890	29.360
43	26.266	23.529	29.832	29.804	32.698
44	8.618	7.890	17.675	13.274	13.822
45	6.304	5.307	7.805	7.714	7.886
50	29.686	28.738	31.083	31.082	34.252
51	30.633	29.742	31.809	31.811	35.151
58	34.405	32.311	37.746	37.746	42.540
59	26.823	21.824	34.351	34.353	38.201

Table A3:9.3 12 mm Ballotini

Run	Nu				
	1	2	3	4	5
35	73.548	64.671	80.560	80.601	103.923
36	38.409	39.574	36.845	36.845	41.524
37	34.773	35.237	34.267	34.269	38.210
38	23.012	22.381	24.559	24.460	26.523
39	27.937	30.735	22.128	22.128	23.699
40	12.249	12.326	12.007	11.888	12.368
41	55.624	53.895	57.182	57.179	68.615
42	8.876	7.767	10.280	10.248	10.567
46	69.315	59.640	76.467	76.467	97.113
47	59.054	55.608	62.231	62.260	75.919
48	10.909	10.697	11.326	11.255	12.368
49	80.975	98.212	74.406	74.442	91.890
52	75.768	85.280	71.745	71.818	87.889
55	69.003	59.667	75.868	75.911	96.132
56	31.169	29.373	40.227	39.825	45.457
57	33.723	31.593	35.968	35.966	40.282
60	43.675	41.774	46.861	46.862	54.829
61	50.160	44.550	59.477	59.473	72.559

TABLE A3:10 REYNOLDS NUMBERS

Table A3:10.1 6 mm Ballotini

Run	T_{fo} calculated from observed T_{so} Re	T_{fc} calculated from observed T^{1}_{fo}	
		Re	Re/(1-e)
11	444.90	442.63	708.20
12	353.70	369.53	591.26
13	362.04	368.46	589.53
14	394.50	398.33	637.33
15	417.93	420.91	673.46
17	237.46	237.41	379.86
18	462.17	468.54	749.67
19	308.98	308.71	493.94
20	372.80	372.88	596.61
21	111.04	112.07	179.30
22	262.63	260.70	417.13
23	62.79	63.36	101.38
24	231.69	235.66	377.05
25	77.12	77.78	124.44
53	448.23	454.94	727.90
54	387.00	391.07	625.72

Table A3:10.2 9 mm Ballotini

Run	T_{fo} calculated from observed T_{so} Re	T_{fo} calculated from observed T^{1}_{fo}	
		Re	Re/(1-e)
27	732.43	744.06	1 252.63
28	112.35	113.22	190.61
29	903.39	902.12	1 518.73
30	972.53	994.74	1 674.64
31	148.95	150.03	252.58
33	380.18	379.40	638.71
34	323.25	324.05	545.53
43	533.65	536.25	902.78
44	134.67	135.07	227.39
45	94.74	95.23	160.31
50	672.56	673.54	1 133.91
51	741.82	742.82	1 250.53
58	816.91	819.21	1 379.15
59	609.85	615.29	1 035.84

Table A3:10.3 12 mm Ballotini

Run	T_{fo} calculated from observed T_{so} Re	T_{fo} calculated from observed T^{1}_{fo}	
		Re	Re/(1-e)
35	1 485.19	1 494.21	2 541.18
36	805.79	804.67	1 368.49
37	698.81	698.38	1 187.72
38	428.36	428.91	729.45
39	509.65	507.44	862.99
40	197.30	197.25	335.46
41	1 149.26	1 150.96	1 957.41
42	123.19	123.76	210.48
46	1 418.36	1 428.58	2 429.56
47	1 249.32	1 252.89	2 130.77
48	161.49	161.60	274.83
49	1 631.99	1 618.52	2 752.58
52	1 670.96	1 662.15	2 826.79
55	1 362.87	1 372.16	2 333.60
56	545.32	546.81	929.95
57	636.03	637.98	1 085.00
60	915.78	917.75	1 560.79
61	1 030.76	1 036.76	1 763.19

APPENDIX 4

GENERAL DESIGN DATA FOR MOVING BED HEAT EXCHANGERS WITH INTRA-PARTICLE TEMPERATURE DISTRIBUTION

Table A4:1 General Design Data

Bi	z	$\Delta T_s/\Delta T_m$		
		$\beta = 1/3$	$\beta = 1$	$\beta = 3$
0.05	0.1	0.015	0.015	0.015
	0.2	0.030	0.030	0.030
	0.5	0.074	0.074	0.074
	1.0	0.148	0.148	0.148
	2.0	0.297	0.297	0.297
	5.0	0.743	0.743	0.743
	10.0	1.485	1.485	1.485
0.1	0.1	0.029	0.029	0.029
	0.2	0.059	0.059	0.059
	0.5	0.147	0.147	0.147
	1.0	0.294	0.294	0.294
	2.0	0.584	0.584	0.584
	5.0	1.471	1.471	1.471
	10.0	2.941	2.942	2.941
0.25	0.1	0.072	0.072	0.072
	0.2	0.143	0.144	0.144
	0.5	0.358	0.358	0.358
	1.0	0.715	0.715	0.716
	2.0	1.429	1.430	1.431
	5.0	3.571	3.574	
	10.0	7.141	7.147	
0.5	0.1	0.139	0.139	0.139
	0.2	0.276	0.276	0.277
	0.5	0.684	0.686	0.688
	1.0	1.364	1.368	1.374
	2.0	2.725	2.733	2.745
	5.0	6.808	6.828	6.856
	10.0	13.612	13.652	13.708

Table A4:1 - Continued

Bi	z	$\Delta T_s/\Delta T_m$		
		$\beta = 1/3$	$\beta = 1$	$\beta = 3$
0.75	0.1	0.201	0.202	0.202
	0.2	0.398	0.399	0.401
	0.5	0.982	0.987	0.995
	1.0	1.955	1.966	1.985
	2.0	3.902	3.925	
	5.0	9.744	9.803	
	10.0	19.480	19.598	
1.0	0.1	0.260	0.261	0.262
	0.2	0.510	0.513	0.518
	0.5	1.254	1.264	1.283
	1.0	2.493	2.517	2.557
	2.0	4.972	5.021	
	5.0	12.410	12.533	
	10.0	24.809	25.054	
1.25	0.1	0.315	0.316	0.319
	0.2	0.614	0.619	0.629
	0.5	1.503	1.521	1.554
	1.0	2.984	3.024	3.094
	2.0	5.946	6.030	
	5.0	14.834	15.048	
	10.0	29.715	30.078	
1.5	0.1	0.366	0.369	0.373
	0.2	0.710	0.718	0.734
	0.5	1.731	1.759	1.801
	1.0	3.432	3.494	
	2.0	6.834	6.964	
	5.0	17.041	17.372	
	10.0	34.111	34.720	

Table A4:1 - Continued

Bi	z	$\Delta T_s/\Delta T_m$		
		$\beta = 1/3$	$\beta = 1$	$\beta = 3$
2.0	0.1	0.459	0.464	0.471
	0.2	0.881	0.898	0.929
	0.5	2.133	2.188	2.287
	1.0	4.217	4.337	
	2.0	8.387	8.635	
	5.0	20.896	21.529	
	10.0	34.880	43.019	
3.0	0.1	0.613	0.627	0.653
	0.2	1.157	1.196	1.273
	0.5	2.765	2.891	3.122
	1.0	5.442	5.714	
	2.0	10.798	11.360	
	5.0	26.872	28.299	
	10.0	35.384	56.530	
4.0	0.1	0.734	0.759	0.808
	0.2	1.366	1.435	1.570
	0.5	3.233	3.444	3.843
	1.0	6.342	6.793	
	2.0	12.559	13.489	
	5.0	31.264	33.578	
	10.0	35.719	67.060	
5.0	0.1	0.831	0.869	0.946
	0.2	1.530	1.629	1.832
	0.5	3.590	3.891	
	1.0	7.022	7.660	
	2.0	13.887	15.198	
	5.0	35.384	37.811	
	10.0	36.759	75.499	

APPENDIX 5

NOMENCLATURE

APPENDIX 5 - NOMENCLATURE

Symbol	Description	Dimensions
a	heat transfer area per unit volume of bed $= \frac{6(1-e)}{d_p}$, for spheres.	L^{-1}
A_x	cross sectional area of bed	L^2
Bi	Biot number $= \frac{h_f.R}{k_s}$, for spheres	1
c	specific heat	$H.M^{-1}.T^{-1}$
C	coefficient	-
d	diameter	L
e	voidage	1
f	friction factor $= \frac{\Delta P.e^3.d_p}{L.6.(1-e).V^2}$	1
f^1	Rotameter calibration parameter	1
F	volumetric flowrate	$L^3.t^{-1}$
G	mass flowrate per unit cross section area of bed	$M.t^{-1}.L^{-2}$
h	film heat transfer coefficient	$H.t^{-1}.L^{-2}.T^{-1}$
H_e	liquid hold-up per unit volume of bed	1
I^1	Rotameter calibration parameter	-
I.v	electric power consumption by air heaters	$H.t^{-1}$
j_D	mass transfer factor $= Sh.Sc^{\frac{2}{3}}$	1
j_H	heat transfer factor $= St.Pr^{\frac{2}{3}} = Nu.Re^{-1}.Pr^{-\frac{1}{3}}$	1

Symbol	Description	Dimensions
k	thermal conductivity	$H.t^{-1}.L^{-1}.T^{-1}$
K	Rotameter constant	-
L	bed length (height)	L
m	index	-
M	mass flowrate	$M.t^{-1}$
n	reference number of spherical shell = $\frac{x}{\Delta x}$	1
Nu	Nusselt number = $\frac{h_f \cdot d_p}{k_f}$	1
Pe	Péclet number = $\frac{d_p \cdot c_f \cdot G_f}{k_f}$ = Re.Pr	1
Pr	Prandtl number = $\frac{c_f \cdot \mu_f}{k_f}$	1
q	variable	-
Q	heat transfer rate	$H.t^{-1}$
r	radius of spherical shell	L
R	radius of sphere	L
Re	Reynolds number = $\frac{G_f \cdot d_p}{\mu_f}$	1
s	variable	-
Sc	Schmidt number	1
Sh	Sherwood number	1
St	Stanton number = $\frac{h_f}{G_f \cdot c_f}$	1
t	time	t
T	temperature	T
U	overall heat transfer coefficient	$H.t^{-1}.L^{-2}.T^{-1}$

Symbol	Description	Dimensions
V	superficial velocity	$L.t^{-1}$
w	Rotameter float weight	M
W	root of transcendental equation	1
x	dimensionless sphere radius = $\frac{r}{R} = n.\Delta x$	1
X	variable	-
y	distance down from top of bed	L
z	Fourier number, dimensionless bed length	1
	$= \frac{k_s.(1-e).y}{G_s.c_s.R^2} = \frac{\alpha_s.t}{R^2}$	

Greek Symbols

α	thermal diffusivity = $\frac{k}{\rho.c}$	$L^2.t^{-1}$
β	ratio of the heat capacity rates = $\frac{G_s.c_s}{G_f.c_f}$	1
ΔP	pressure drop	$M.L^{-1}.t^{-2}$
ΔT	temperature difference	T
Δx	increment of dimensionless sphere radius	1
Δz	integration step length	1
η	percentage heater efficiency	1
θ	dimensionless temperature $\frac{T-T_{si}}{T_{fi}-T_{si}}$	1
λ	latent heat of fusion	$H.M^{-1}$
μ	viscosity	$M.L^{-1}.t^{-1}$
ρ	density	$M.L^{-3}$

Dimensions

H	heat
L	length
M	mass
t	time
T	temperature
1	dimensionless
-	various

Subscripts

a	ambient
c	channel
ef	effective turbulent property
f	fluid
h	heaters
i	inlet
IPTD	intra-particle temperature distribution solution
j	reference number of a term in an infinite series
l	logarithmic
L	bottom of bed
LMTD	logarithmic mean temperature difference solution
m	mean
M	melt
n	reference number of spherical shell
o	outlet
p	particle
s	solid
v	vessel
w	wall

APPENDIX 6

BIBLIOGRAPHY

APPENDIX 6 - BIBLIOGRAPHY

* Actual references not consulted.

(1) Ross, T.K. Int. Dev. Heat Transfer, Amer. Soc. Mech. Engrs. (5), 919-925 (1961).

(2) Akers, J.B. "Heat transfer by convection to a moving bed", Ph.D. Thesis, University of Aston in Birmingham, Jan (1967).

(3) Evans, F.C. Found. Tr.J., 99, 177-180 (1955).

(4) de Winton, C.J.P. Gas J., Oct. 16 (1963).

(5) Harvey, F. "High pressure at Coleshill", Inst. Gas. Engrs., Midland Sectn., Mar. 5 (1965).

(6) I.C.I. Ltd., Agricultural Divn., Billingham, Co. Durham. "The I.C.I. steam-naptha process", (1964).

(7) Shelmerdine, A.B. J. Inst. Fuel, 40 (2), 48-53 (1967).

(8) Ayres, E., Lawrie, W.B. Found. Tr. J. 109, 195-198 (1960).

(9) Lawrie, W.B., Ayres, E. Brit. Foundryman, 55 (2), 74-79 (1962).

(10) Watson, D., Glen, C.G. Inst. Gas Engrs. J., 3, 17-40 (1963).

(11) Glen, C.G. Inst. Gas Engrs. J., 4, 27-45 (1964).

(12) Martins, G.P., Glen, C.G. Brit. Pat. 1 074 261, July 5(1967).

(13) Glen, C.G. Gas J. (Gas in Industry), 8 (88), 194-198 (1965).

(14) Knight, S.J., Manuel, K., Randle, R.G. "Non-ferrous metal melting", Midland Junior Gas Ass., Feb. 9 (1965).

(15) Manuel, K. Brit. Pat. 1 144 561, Mar. 5 (1969).

(16) Randle, R.G., Knight, S.J. Brit. Pat. 1 143 745, Feb. 26 (1969).

(17) Higgs, A., Lashley, H., Thompson, G.R. Brit. Pat. 1 172 863, Dec. 3 (1969).

(18) Laidlaw, R.A., Church, B.J. "Modern methods of aluminium melting, with particular reference to tower melting furnaces", London & Southern Junior Gas Ass., Mar. (1967).

(19) Keating, J.H. U.S. Pat. 3 247 555, Apr. 26 (1966).

(20) Mantle, E.C. Brit. Non-Ferrous Met. Res. Ass., Conf. "Maximising the yield of non-ferrous metals processes", Liége, Belg., "The impact of new processes on production methods", 205-216, Oct. (1971).

(21) Anon. Found. Tr. J. 132, 203-208 (1972).

(22) Westofen G.m.b.H. French Pat. 1 435 545, June 1 (1965).

(23) Hills, A.W.D. Chem. Process Engng., 50 (2), 69-77 (1969).

*(24) Glen, C.G., Royal School of Mines, Imperial College, London. Communication to Akers, J.B., Oct 31 (1966).

(25) Standish, N. Trans. Met. Soc. Amer. Inst. Min. Engrs., 242, 1733-1740 (1968).

(26) Norton, C.L. J. Amer. Ceram. Soc., 29, 187-193 (1946).

(27) Bowers, T.G., Reintjes, H. Chem. Engng. Progr. Symp. Series, 53 (32), 69-74 (1961).

(28) Kilpatrick, M.O., Dean, L.E., Hall, D.S., Seed, K.W. Petrol. Refin. 33 (4), 171-174 (1954).

(29) Gamson, B.W., Thodos, G., Hougen, O.A. Trans. Amer. Inst. Chem. Engrs. 39, 1-35 (1943).

(30) Löf, G.O.G., Hawley, R.W. Industr. Engng. Chem., 40 (6), 1061-1070 (1948).

(31) Sissom, L.E., Jackson, T.W. Trans. Amer. Soc. Mech. Engrs. Series C, J. of Heat Transfer, 89 (1), 1-6 (1967).

(32) Frantz, J.F. Chem. Engng. Progr., 57 (7), 35-42 (1961).

*(33) Schumann, T.E.W. J. Franklin Inst., 208, 405-416 (1929).

*(34) Young, P.A. Symp. Chem. Engng. in Metallurgical Ind., Inst. Chem. Engrs., 33 (1963).

(35) Furnas, C.C. Trans. Amer. Inst. Chem. Engrs., 24, 142-193 (1930).

(36) Furnas, C.C. Industr. Engng. Chem., 22, 26-31 (1930).

(37) Saunders, O.A., Ford, H. J. Iron St. Inst., 142 (1), 291p-328p (1940).

(38) Kitaev, B.I., Yaroshenko, Yu.G., Suchov, V.D. (Eng. Edn. edited by Young P.A.). "Heat exchange in shaft furnaces", Pergamon Press, London (1967).

*(39) Denton, W.H. Proc. Gen. Disc. Heat Transfer, Inst. Mech. Engrs., 370 (1951).

*(40) Denton, W.H., Robinson, C.H., Tibbs, R.S. A.E.R.E., R4346 (1963).

(41) Coppage, J.E., London, A.L. Chem. Engng. Progr., 52, 57-63 (1956).

(42) Gliddon, B.J., Cranfield, R.R. Brit. Chem. Engng., 15 (4), 481-482 (1970).

(43) Littman, H., Barile, R.G., Pulsifer, A.H. Industr. Engng. Chem. Fund., 7 (4), 554-561 (1968).

(44) Handley, D., Heggs, P.J. Trans. Inst. Chem. Engrs., 46, T251-T264 (1968).

(45) Meek, R.M.G. Int. Dev. Heat Transfer, Amer. Soc. Mech. Engrs., (4), 770-780 (1961).

(46) Lindauer, G.C. Amer. Inst. Chem. Engrs. J., 13 (6), 1181-1187 (1967).

(47) Johnson, A. J. Iron St. Inst., 206, 671-688 (1968).

(48) Bradshaw, A.V., Johnson, A., McLachlan, N.H., Chiu, Y-T. Trans. Inst. Chem. Engrs., 48, T77-T84 (1970).

(49) Wadsworth, J. Int. Dev. Heat Transfer, Amer. Soc. Mech. Engrs., (4), 760-769 (1961).

(50) Martin, J.J., McCabe, W.L., Monrad, C.C. Chem. Engng. Progr., 47, 91-94 (1951).

(51) Rowe, P.N., Claxton, K.T. Trans. Inst. Chem. Engrs., 43, T321-T331 (1965).

(52) Cornish, A.R.H. Trans. Inst. Chem. Engrs., 43, T332-T333 (1965).

(53) Gillespie, B.M., Crandall, E.D.[V] Amer. Inst. Chem. Engrs. J., 14 (3), 483-490 (1968). Carberry, J.J.

(54) Schwartz, C.E., Smith, J.M. Industr. Engng. Chem., 45 (6), 1209-1218 (1953).

(55) Baldwin, D.E., Beckman, R.B., Rothfus, R.R., Kermode, R.I. Industr. Engng. Chem. Proc. Des. Dev., 5 (3), 281-284 (1966).

*(56) Eichorn, J., White, R.R. Chem. Engng. Progr. Symp. Series., 48 (4), 11-18 (1952).

*(57) Baumeister, E.B., Bennett, C.O. Amer. Inst. Chem. Engrs. J., 4, 69-74 (1958).

(58) Wilke, C.R., Hougen, O.A. Trans. Amer. Inst. Chem. Engrs., 41, 445-451 (1945).

(59) Malling, G.F., Thodos, G. Int. J. Heat Mass Transfer, 10, 489-498 (1967).

(60) Chu, J.C., Kalil, J., Wetteroth, W.A. Chem. Engng. Progr. 49 (3), 141-149 (1953).

(61) Hicks, R.E., Mandersloot, W.G.B. Chem. Engng. Sci., 23, 1201-1210 (1968).

(62) Rowe, P.N. Chem. Engr., Lond., 41, CE69-CE76 (1963).

*(63) Engel, F.V.A. Engineer, Lond., 206, 479 (1958).

*(64) Engel, F.V.A. Engineer, Lond., 198, 637 (1954).

(65) Yeh, G.C. J. Chem. Engng. Data, 6 (4), 526-530 (1961).

(66) Freund, J., Pinon, R. Rev. Gen. Therm., 6 (64), 343-352 (1967).

(67) Yagi, J., Muchi, I. Trans. Iron St. Inst. Jap., 10, 181-187 (1970).

(68) Ranz, W.E. Chem. Engng. Progr., 48, 247-253 (1952).

(69) Bird, R.B., Stewart, W.E., Lightfoot, E.N. "Transport phenomena", John Wiley and Sons Inc. (1963).

(70) Hougen, O.A., Watson, K.M., Ragatz, R.A. "Chemical process principles charts", John Wiley and Sons Inc. (1964).

(71) Kunii, D., Suzuki, M. Int. J. Heat Mass Transfer, 10, 845-852 (1967).

(72) Barker, J.J. Industr. Engng. Chem. 57 (4), 43-51 (1965).

(73) Mayhew, Y.R., Rogers, G.F.C. "Thermodynamic properties of fluids and other data", Basil Blackwell, Oxford (1964).

(74) Brinn, M.S., Friedman, S.J., Gluckert, F.A., Pigford, R.L. Industr. Engng. Chem., 40 (6), 1050-1060 (1948).

(75) Brittingham, G.J. Aust. Pat 273 006 Feb. 7 (1967).

(76) Lovell, C.L., Karnofsky, G. Industr. Engng. Chem., 35, 391-397 (1943).

(77) Munro, W.D., Amundson, N.R. Industr. Engng. Chem. 42, 1481-1488 (1950).

(78) Leung, P.K., Quon, D. Can. J. Chem. Engng., 43, 45-48 (1965).

(79) Lapidus, L. "Digital computation for chemical engineers", McGraw Hill, New York (1962).

(80) Wartmann, R., Mertes, H. Arch. Eisenhüttenw., 37 (3), 201-207 (1966).

(81) Gay, B., Akers, J.B. Europ. Fed. Chem. Engng. Conf., "The use of computers in studies preceding the design of chemical plants", Florence, It., "Analogue computer analysis of moving bed heat transfer data". Apr. (1970).

*(82) Fox, L. "Numerical solution of ordinary and partial differential equations", Chapter 2, Pergamon Press (1962).

(83) Franks, R.G.E., Du Pont Chemical Co., Wilmington, U.S.A. Private communication to Gay, B. April 10 (1970), Du Pont report "A digital computer program for simulating differential and algebraic equations".

(84) Gurnie, H.P., Lurie, J. Industr. Engng. Chem., 15 (11), 1170-1172 (1923).

(85) Kuong, J.F. Brit. Chem. Engng., 8, 572 (1963).

(86) Pilpel, N. Brit. Chem. Engng., 11, 699-702 (1966).

(87) British Standards Institution, London. B.S. 1042:1943, "Flow measurement".

(88) British Standards Institution, London. B.S. 1827:1952, "Reference tables for thermocouples (nickel/aluminium v. nickel/chromium)".

*(89) Roeser, W.F., Dahl, A.I., Gowens, G.J. J. Res. Nat. Bur. Stand., 14 (3), 242 (1935).

(90) Richards, J.C. "The storage and recovery of particulate solids", Inst. Chem. Engrs., London (1966).

(91) Latter, J.C., Rotameter Mfg. Co. Ltd., 330, Purley Way, Croydon, CR9 4PG. Personal communication to Wilson, W.R. June 20 (1969).

*(92) Denton, W.H. "The packing and flow of spheres", A.E.R.E., E/R 1095 (1957).

(93) Coulson, J.M., Richardson, J.F. "Chemical engineering", Vol. 2, Pergamon Press Ltd., Oxford and London (1962).

(94) University of Aston. User application program ZUA01, I.C.L. 1905 Library.

(95) Keenan, J.H., Kaye, J. "Gas tables", Wiley and Sons Inc., N.Y. (1945).

*(96) Abbott, J.S., English Glass Co. Ltd., Scudamore Road, Leicester. Communication to Akers, J.B., June 29 (1966).

(97) Sharp, D.E., Ginther, L.B. J. Amer. Ceram. Soc., 34, 260-271 (1951).

*(98) Bastick, R.E., Chance Bros. Ltd., Glassworks, Smethwick, 40. Communication to Akers, J.B., Aug. 9 (1966).

(99) Ratcliffe, E.H. Glass Technology, 4, (4), 113-128 (1963).

(100) University of Aston. User application program. ZUA03, I.C.L. 1905 Library.

(101) Happel, J. Industr. Engng. Chem., 41, 1161-1174 (1949).

*(102) Zonneveld, J.A. "Automatic numerical integration", Mathematisch Centrum: Amsterdam (1964).

*(103) Kunii, D., Smith, J.M. Amer. Inst. Chem. Engrs. J., 7, 29-34 (1961).

*(104) Amundson, N.R. Industr. Engng. Chem., 48, 26-35 (1956).

*(105) Amundson, N.R. Industr. Engng. Chem., 48, 35-43 (1956).

*(106) Siegmund, C.W., Munro, W.D., Amundson, N.R. Industr. Engng. Chem., 48, 43-50 (1956).

(107) Kays, W.M., London, A.L. "Compact heat exchangers", 2nd. edn., McGraw Hill Book Co. (1964).

(108) Rotameter Mfg. Co. Ltd., 330 Purley Way, Croydon, CR9 4PG. Publication numbers: RP 2319, 2321, 2322-A.

(109) Rotameter Mfg. Co. Ltd. Publication number: RP 3000.